Synthesis and characterisation of zeolites, their application in catalysis and subsequent rationalisation : methanol-to-olefins (MTO) process with designed ZSM-5 zeolites

Pit Losch

UNIVERSITÉ DE STRASBOURG

ÉCOLE DOCTORALE DES SCIENCES CHIMIQUES
Institut de Chimie, UMR 7177

THÈSE

présentée par :

Pit LOSCH

soutenue le : **30 septembre 2016**

pour obtenir le grade de :
Docteur de l'université de Strasbourg

Discipline / Spécialité : Chimie / Catalyse Hétérogène

Synthesis and **C**haracterisation of Zeolites, their **A**pplication in Catalysis and Subsequent **R**ationalisation
Methanol-To-Olefins (MTO) Process with Designed ZSM-5 Zeolites

THÈSE dirigée par :

Mr. LOUIS Benoît	Directeur de Recherche CNRS, Université de Strasbourg
Mr. PALE Patrick	Professeur, Université de Strasbourg

RAPPORTEURS :

Mr. LERCHER Johannes A.	Professeur, Technische Universität München (TUM)
Mme. MINTOVA Svetlana	Directeur de Recherche CNRS, École Nationale Supérieure d'Ingénieurs de Caen (ENSICaen)

AUTRES MEMBRES DU JURY :

Mr. BRAUNSTEIN Pierre	Directeur de Recherche CNRS, Université de Strasbourg
Mme. CHIZALLET Céline	Docteur, Institut Français du Pétrole, Énergies Nouvelles (IFPEN) Lyon
Mr. HUEBSCH Eric	Docteur, DuPont Chemicals, Luxembourg
Mme. KIWI-MINSKER Lioubov	Professeur, École Polytechnique Fédérale de Lausanne (EPFL)

I) Acknowledgements

I am expressing, first of all a deep gratitude for my PhD-supervisor's guidance, his patience and advice has led me to accomplish this work. We already found each other before this PhD, since I owe him my PhD-funding (AFR-grant: 5898454) from the national research fund Luxembourg (NRFL). Over the last three years, Dr. **Benoît Louis** has in fact become much more than a PhD-supervisor to me. Our scientific, politics and sports related discussions allowed me to evolve from a professional, academic, but also from a personal point of view. Benoît, you always considered my opinion. Compared to other students, you gave me a huge freedom, which I tried to use, and you allowed me to discover the world, literally, but also the hidden realities in the world of science.

Further, I am glad to count Prof. **Patrick Pale** among my PhD-supervisors, you helped me as well with your wise advice in times of scientific and personal stagnation. Patrick, I will profoundly miss our late-night discussions, you pushed my craziest ideas always to a next level. I hope that I will always keep on dreaming like a child, you showed me that this can work.

Then, I am profoundly honoured dear members of the jury, I am thanking you for having accepted to evaluate this work:

- Prof. **Johannes Lercher**: I attended your presentations at the NSC2014 and Pacifichem2015 conferences. In addition to my highest respect for your scientific work, I learnt to admire your presentation abilities. Thank you for your advice and constructive critique.

- Dr. **Svetlana Mintova**: I had the pleasure to meet you at ISAMMM6 and again at the Pacifichem2015, you know that I admire your work, your efficiency and your kindness. Your input as a *rapporteur* during the defense has helped this manuscript and myself to mature.

- Dr. **Pierre Braunstein**: During my M.Sc. studies I heard your name quite a few times, then as a young PhD your way to ask questions at conferences was inspiring. Unfortunately, I truly met you only at the very day of my defense. You did not only impress my whole family with your presidency of this jury. You are an inspiration in terms of scientific knowledge and eloquence. "You developed your own style to write, I would qualify it as Romanesque..." *Merci*!

- Dr. **Céline Chizallet**: We first met at the GéCat in Cluny, again at the GéCat in Obernai, while I had the pleasure to co-chair a session at your FCCat1 conference. "I am not a specialist in this field, but...?" Your curiosity makes you interested and ask the hardest questions that are not related to your field of specialty. This constitutes an example I will try to follow in the future.

- Dr. **Eric Hübsch**: Thank you for having accepted to judge this work, your presence and your comments added a flavour of real-world chemistry to this thesis. You certainly are an idol proving how it can be possible to combine ambitions in triathlon with a professional career in chemistry. I will always remember you attributing me a "Green Soul".

- Prof. **Lioubov Kiwi-Minsker**: Your wise advice was very welcome during this defense. It was a great pleasure to hear that you appreciated the way the manuscript was written. It has been risky to give this work a personal note. I am proud to be your scientific grandson.

During the last three years I have found numerous friends and made unforgettable experiences, which helped me to discover myself; in the laboratory, during teaching activities, at conferences, in sports or in family altogether.

In the laboratory I found a new family: **Valérie** remember "Green Chemistry is sexy", **Aurélien**, I will miss our discussions on cycling, doping and your kindness, **Victor** thank you for integrating me in your running team, **Jean-Marc** you pushed me to new levels of mechanistic thinking during our group meetings, I will miss your questions as much as our non-sensical discussions, you have all evolved to aunts and uncles, next to my two doctor-fathers.

Nico K. you have been an inspiration for how to love chemistry ever since I started my first year M.Sc. in Strasbourg. **Maryline**, *maman*, I hope you are proud of me, I am now able to buy my own flight tickets and I actually love to plan to attend conferences, while thinking of how you taught me all of this and much more. **Marie**, my Marie for whom I became a poet once, I miss you, thank you for so much, Joshua Kedison in his song gets "picture postcards from LA", you gave me real-life LA. **Anne-Sophie** (and **Armen** my big brother) it was a great pleasure to meet you, to learn from you and to work with you, I still remember our late-night working sessions very well. **Damien (DrHüber)** we were having a lot of fun together, it is sad that we could never finish our promising collaborative curiosity in chemistry. **Claire**, we suffered and partied together, you have such a huge heart stay who you are and be happy as much as you can, you are beautiful when you are happy. **Julie,** over time you really grew important to me, it was not a love at the first sight thing, but I already miss you and your patience to laugh at my jokes. **Ani** when we drank together, we were having those evenings, I wanted to say *unforgettable*, but sometimes this vicious ethanol was doing its job too well. **Joy**, *oh jolie Joy*, I will and do already miss you, we were surfing so many times the same wave of craziness. We were autocatalytically converting our energy into the best jokes, fun, songs, etc. all these sceptists just did not know how to appreciate our art. **Eric** you never really wanted to become my brother from another mother, but our collaborations, sports and parties were bringing us quite close, maybe you would agree to be distant cousins. **Solène**... this is yours too, I agree. We were this big crazy family, which shrunk until you arrived **Fatih** my new Turkish neighbour, we discussed and liked each other very quickly, stay who you are. **Olesia** from St. Peterburg, what a shame that I met you so late, we had a lot of fun in Strasbourg and I loved how you showed me your city, *C∏ACNbA*. Then, the newborn **Romain**, we could have become neighbours-friends, but you took the place, office of

someone who meant a lot to me and seriously you, your long legs and your *"cul sur la chaise*" will have room enough for your promising future without me.

Marcelo, **Elisa, Tiago** *e* **Alessandra** *do Brasil, agredeço a sua bondade*.

I do not forget the people I did not deeply relate with either because of our short common stay in LASYROC or your short stays, Postdoctoral fellows or M.Sc. internships, we all had fun together: **Catarina**, **Manel**, **Nico C**. and **Sophie**, good luck in your careers, **Roland** my Congolese brother thank you for my South-African experience, **Boris (Bobby)** we did not continue to swim a lot together, but man I loved it. **José** your Spanish temper is amazing. **Eric T., Fabien, Fabian** and **Gaëtan** interns in zeolite chemistry it was a pleasure to work with all of you. **Gaëtan** remember the *"defaitisme réaliste"*? **Marc** *"tu n'as pas fait le café*?" *Merci pour toutes les fois que tu l'as fait.*

Bruno and the NMR Team, **Lionel** and **Maurice** thank you for always welcoming me for crazy NMR discussions and having accepted to perform quite unusual and successful measurements, after all.

Before this work, the university of Strasbourg welcomed me in M.Sc. Green Chemistry studies: **Alex(is)** my adoptive, substituting brother. **Louis** de la Réunion, **Margaux** and **Carole** *les belles*, **Morgane**, now with your Lou, **Cynthia** and **Cécile A.** now working in Luxembourg, we were a team *Chimie Verte*.

Cécile V.C. now we are both on the verge of finding something new, I hope that you will find what really makes you happy and it would be perfect if our paths crossed again in the future. Me too, I loved discussing *"tout et n'importe quoi*" with you.

Niklas we met a bit late, but the last year of cycling while discussing science and everything else was absolutely amazing. I hope our friendship will live on.

Markus *"Ech schloen dech freckt*", no I would never hurt you, you are a too good friend to me, let's hope that we will see each other a bit more often in the next five years. **Laura**, I am so glad that we could manage to keep our cross-border friendship alive over the last years. I am looking forward to the holidays with you. In Freiburg during my B.Sc., I also wanted to thank a group of people who allowed me to engage on the path of insecure jobs and fun in science: **Gil**, **Liyu**, **BurkHardy**, **Julian**, **Thomas**, **Stefan** and **Oli**.

Friends! **Mark K.** it is sad that we could not continue our Latin discussions and sports sessions after our Masters. **Pit S.**, Pit^2 is only possible with you. **Pol K.**, glad to meet you again in the world of Chemistry after the world of cycling. **Eric Wirtz**, I am there for you and you were always there for me, friends for life may really exist. **Alain T.** in triathlon and **Michel Z.** in cycling: trainers, friends thank you for being my guides during part of my life. 46 days prior to

this defense, I realised a lifelong dream thanks to you, I became an Ironman, survived the hardest triathlon in the world, the Embrunman.

Rachel, my first true love, if I had to thank one single person, essential to the successful accomplishment of this work, it were you. A PhD lasts eight years, you stood by me, in every circumstances for seven and a half. After 94% of the task, we had to split our paths. Nonetheless, please be proud and thank your family (**Sonja**, **Aloyse**, **Steve**, **Eric** and **Rigoberto**) for having accepted me as one of yours.

Family! Thank you, cousins, aunts, uncles and especially my grand-parents **Pierre** R.I.P., **Nicole**, **Henri** and **Marie-Therèse** never stopped supporting me. My parents, **Simone** and **Claude** for giving birth to me, for pushing me through the hard times, during childhood and adolescence, you really made me understand and I finally accepted that it is ok to see the world with my eyes. You made a quartett, and we grew strong as a team. **Tom**, I am inspired and impressed by your sense for beauty and design, you participated to the esthetics of this work (SCAR and cover picture). **Max** you are overwhelmingly talented in so many things you will become a supreme teacher. **Lex** a car needs four wheels to be complete, so did we need you, I loved to suffer with you in triathlon, I am proud of you as a future air and space engineer.

As A. Dumas put it in 1844 and the Swiss turned it into their national motto: *Unus pro omnibus, omnes pro uno*. Family, friends and colleagues I am part of you and you are part of me.

II) Preface

"Live as if you were to die tomorrow. Learn as if you were to live forever."
M. Gandhi.

Adaptability is triumph! If there is one true theory, to quote B. Bryson "the single best idea that anyone has ever had" then it is evolution through adaptation,[1] or *Descendants with Modification* as it was originally called by its father, Charles R. Darwin. Evolutionary pressures are key to success, exponentially emerging diversity in any areas is controlled. In other terms, the evolutionary success of a lucky few is guided by the higher order evolutionary pressures. This theory has proven true for the evolution of life on earth, is applicable in economics and as well in science. Serendipitous discoveries are often hailed as revolutionary leaps. However, if one considers genetics in the evolution of life, the smallest "serendipitous" or rather accidental modifications can lead to dramatic changes in the final living being. Genetically encoded characteristics such as blindness, tall or small sizes prove only in combination with the respective environment as beneficial or deleterious. A (r)evolutionary modification needs to ease the adaptability to the environment. The exponential emergence of scientific work today is enlarging the pool of possibilities to adapt to future needs, they might not be of immediate revolutionary impact but part of the ever larger pool of possibilities. Bearing this in my mind, I feasted all of my little and large failures and discoveries. Indeed, I like to think that ones successes and the impact of ones successes is in direct relation to the total number and the number of the failed trials. "Enjoy the NO's, every NO is a step towards the next YES."

The following numbers will guide you through this work: **1** (one PhD done by one person who felt one suffering and one ultimate joy) **3** (during three years two supervisors and one student formed a *triumvirat*, where during the complicated moments my three brothers helped to see light in the dark) **5** (Born in the *primavera* the fifth month of the year, I feel attracted to green the colour of hope and sometimes find myself contemplating the quintessence of our being) **7** (Born the seventh day of may, working on the seventh floor, I will be defending my work in September the seventh month in the ancient roman calendar) **8** (I am grateful to the eight persons who will be evaluating this work).

[1] Bryson, B. *A Short History of Nearly Everything*, **2005**, Doubleday, NYC.

III) Table of Contents

IV) Symbols and abbreviations

The following abbreviations and symbols are listed herein in order to ease the reading of the core part of the work:

(ATR/CO)-FTIR	Fourier Transformed Infrared Spectroscopy
*BEA	IZA three letter code for the beta zeolite
*BEA-MC	Zeolite Beta-micron sized crystals
*BEA-NC	Zeolite Beta-nanocrystals
*BEA-NS	Zeolite Beta-nanosheets
1,2-DCE	Dichloroethane
a	acceleration
A	Area or surface [m^2]
AFP	Antifreeze protein
Ar	Argon gas
Ar-	Aromatic substituent on an organic molecule
ArI	Iodinated aromatic
BSST	Biosourced secondary template
CNSL	Cashew nutshell liquid
Đ	Dispersity
D_{eff}	Effective diffusivities
dppf	Bis(diphenylphosphino)ferrocene
dppm	Bis(diphenylphosphino)methane
dppp	Bis(diphenylphosphino)propane
EFAl	Extra-Framework-Aluminum
EMC	Energetically modified cement
F	Force [N]
FA	Fly Ash from South-Africa
FAU	IZA three letter code for the faujasite zeolite
GSK	GlaxoSmithKline
H-Nu	Nucleophile
HCP	Hydrocarbon Pool
HDA	1,6-hexanediamine
HPLC	High performance liquid chromatography
HRTEM-EDX	High Resolution Transmission Electron Microscopy - Energy Dispersive X-ray spectroscopy
IBM	Ice binding motif
IUPAC	International Union of Pure and Applied Chemistry
IZA	International Zeolite Association
K	Equilibrium constant
k	Boltzmann constant
MAS-NMR	Magic Angle Spinning Nuclear Magnetic Resonance Spectroscopy
MFC	Mass Flow Controller
MFI	Mordenite Framework Inverted (IZA three letter code for this zeolite morphology)
$Mt.year^{-1}$	Megaton per year [10^9 $kg.year^{-1}$]
MTO	Methanol-To-Olefins process
MTP	Methanol-To-Propylene process
√(CO)	Wavenumber [cm^{-1}]
NEt_3	Triethylamine
NNN	Next nearest neighbour
$ø_{molecule}(T)$	Temperature dependant molecular diameter
$ø_{pore}(T)$	Temperature dependant porous diameter
p_0	pressure in free space
PA	1-propylamine
$p_{conf.}$	pressure in confined space
pH	Indication for acidity: $-\log_{10}[H^+]$
Ph-	Phenyl substituent
$p_i(C_{x=})$	Partial pressure of a given olefin
pK_a	Acid dissociation constant
PMMA	Poly(methyl-methacrylate)
ppm	parts per million

PSS	Product Shape Selectivity
PTE	Positive Thermal Expansion
R	Ideal gas constant [8.314 J.(mol.K)$^{-1}$]
$R_{meth.}(C_{x=})$	Methylation reaction rate of a given olefin
RSS	Reactant Shape Selectivity
RT	Room Temperature
SAC	South African Coal
SAR	Silicon to Aluminum ratio
SASOL	Suid-Afrikaanse Steenkool-, Olie- en Gasmaatskappy
S_{BET}	Surface area calculated by the Brunauer Emmett Teller method
SBU	Secondary building unit
SCB	Sugar cane bagasse
SCBBH	Sugar cane bagasse basic hydrolysate
SDA	Structure directing agent
SEM	Scanning Electron Microscopy
T(Hal)CA	Tri(halogeno)isocyaniuric acid
TCCA	Trichloroisocyanuric acid
TEOS	Tetraethylorthosilicate
TFAOH	Trifluoroacetic acid
TIGAS	Topsoe integrated gasoline synthesis
TOF	Turnover frequency [mol(converted).(mol(catalytic active sites).h)$^{-1}$]
$TPA^{+}(OH/Br)^{-}$	Tetrapropylammonium hydroxide or bromide
TSS	Transition State Shape Selectivity
u.c.	unit cell
UAE	United Arab Emirates
USY	Ultra Stable Y zeolite
WHSV	Weight Hourly Space Velocity in [h^{-1}]
x	An additional exponential factor for γ, with $x \geq 1$, it traduces the quality of the selective fit between molecule and porous network
Xantphos	IUPAC name: 4,5-Bis(diphenylphosphino)-9,9-dimethylxanthene
XRD	X-ray diffraction
ZSM-5	Zeolite Socony Mobil-5
γ	Confinement factor traducing the fit between any considered molecule and the microporous network
ΔG_{act}	Gibbs activation enthalpy [kJ.mol^{-1}]
ΔH_{act}	Activation enthalpy [kJ.mol^{-1}]
ΔS_{act}	Activation entropy [J.K^{-1}]

V) Résumé (en français)

V.i. Introduction générale

Pendant les trois dernières années, j'ai pu travailler sur la conception sur mesure de catalyseurs hétérogènes pour l'application dans diverses réactions. J'ai pu, plus particulièrement, synthétiser des zéolithes, ces aluminosilicates cristallins et microporeux qui peuvent être utilisés comme catalyseur acide de Brønsted hétérogène avec la maille cristalline chargée négativement (**Figure 1**) et connus pour engendrer une sélectivité de forme. De plus au laboratoire nous avions la possibilité de les tester et d'observer ces dites propriétés dans plusieurs réactions, notamment la conversion du méthanol en oléfines légères (MTO).

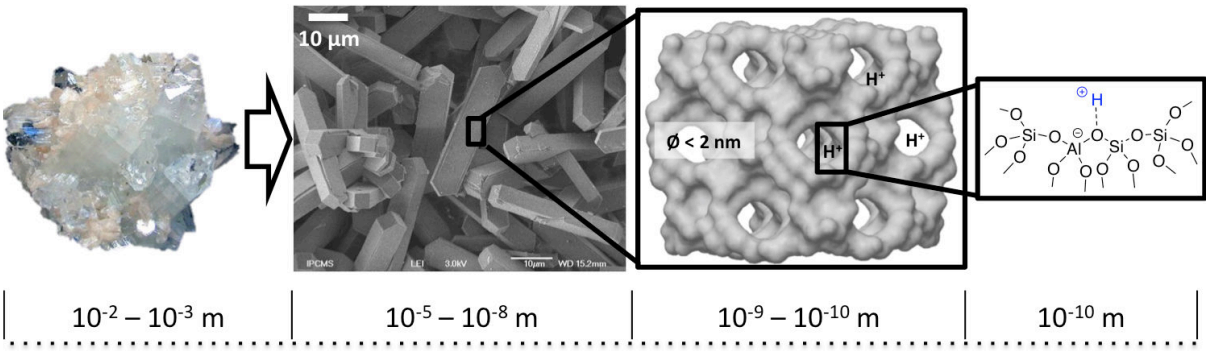

Figure 1. Les zéolithes: de leur découverte à leur conception sur mesure en tant que catalyseur hétérogène, acide de Brønsted.

La **Figure 1** présente les différentes propriétés des zéolithes. Ces "pierres bouillantes" d'après A.F. Crønsted qui les a découvertes, existent dans la nature sous forme de minéraux cristallins.[2] (p.ex. la stilbite, première zéolithe découverte, **Figure 1** gauche) Deux siècles plus tard, la communauté scientifique autour du pionnier R.M. Barrer réussit les premières synthèses artificielles au laboratoire. La **Figure 2** montre l'évolution des connaissances cumulées sur les zéolithes et les synthèses de zéolithe.[3] L'avantage de celles-ci, si l'on considère une éventuelle application en catalyse, est de pouvoir contrôler divers paramètres comme la taille des cristaux, la composition chimique et la densité de sites acides aussi bien que la structure même de la zéolithe. En effet, ce sont ces facteurs qui gouvernent considérablement leur activité, sélectivité et stabilité lors d'une application en catalyse.

[2] Cronsted, A.F. *Akad. Handl. Stockholm* **1756**, *18*, 120.
[3] a) Barrer, R.M. *J. Chem. Soc.* **1948**, 127. b) Barrer, R.M.; Hinds, L.; White, E.A. *J. Chem. Soc.* **1953**, 1466.

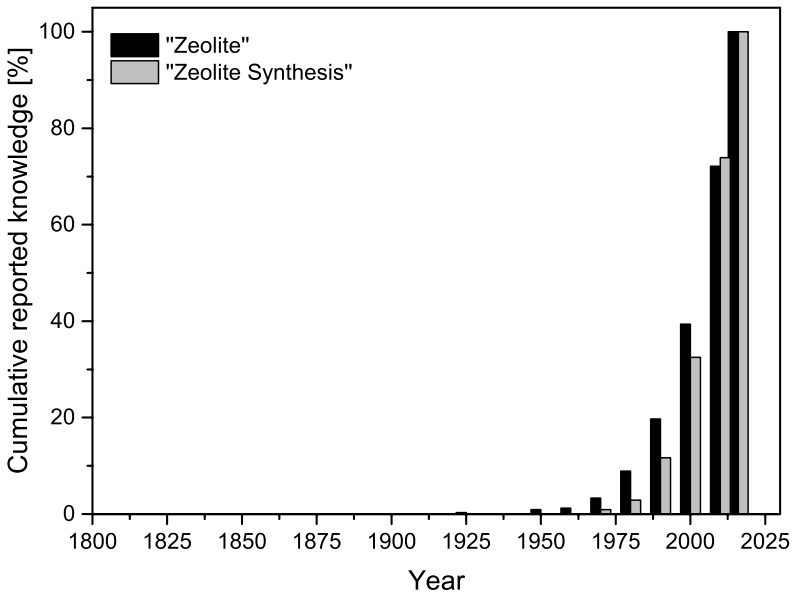

Figure 2. L'évolution des connaissances totales, cumulées et relatives concernant les zéolithes et la synthèse de zéolithes en fonction du temps. (Recherches faites sur Scifinder CAS en utilisant les termes indiqués entre ", et pendant les périodes indiquées en abscisse de ce graphique)

Bien que j'aie pu aborder un grand nombre de projets pendant cette thèse schématiquement illustrée dans la **Figure 3**, les résultats seront présentés dans mon manuscrit de la manière suivante: (une partie de ces sujets abordés et non présentés ont mené à des publications dans des journaux scientifiques)

1. Introduction générale qui rappellera tous les concepts nécessaires à la compréhension des différents chapitres.

2. Partie expérimentale qui présentera les matériels et méthodes utilisés pour réaliser le travail expérimental.

3. La réaction de conversion du méthanol en hydrocarbures (MTH) qui est la partie principale de mon travail.

4. L'économie circulaire du carbone et la chimie verte constituent le fil conducteur du quatrième chapitre qui liera les différentes thématiques abordées au cours de cette thèse.

5. Conclusion finale, qui permettra aussi d'ouvrir sur les suites potentielles à ce travail.

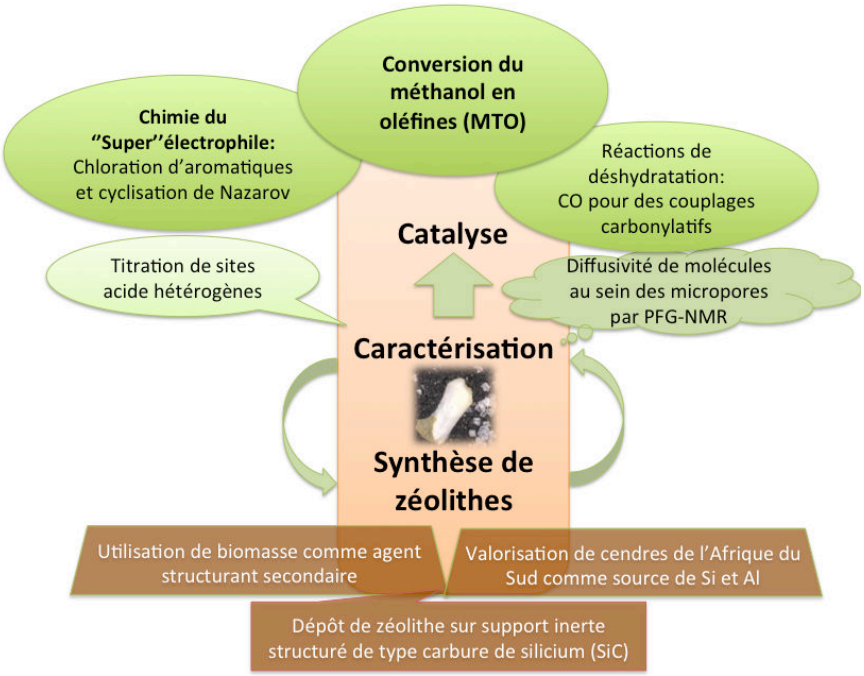

Figure 3. Représentation schématique des différents sujets abordés au cours de mes trois années de thèse.

Ce résumé rédigé en français ne touchera les sujets susmentionnés que de manière très superficielle, il est plutôt conçu comme une invitation à lire les travaux complets qui seront publiquement accessibles, en langue anglaise après ma soutenance.

V.ii. La réaction de conversion du méthanol en hydrocarbures (MTH)

Les problèmes sociétaux et environnementaux actuels nécessitent une remise dans le contexte d'origine de l'énergie utilisée et de la façon d'utiliser cette dernière. Le lauréat du prix Nobel, G. Olah a proposé une alternative très intéressante pour utiliser les ressources pétrolières et de gaz de manière plus efficace, pour libérer l'humanité de la dépendance des ressources fossiles au long terme. Cette approche est basée sur le méthanol, qui ainsi forme la base du concept de "l'économie du méthanol".[4] Selon ses travaux, le méthanol est l'hydrocarbure oxygéné le plus simple, sûr et le plus facile à stocker et à transporter. D'autre part, cette brique de base, elle-même facilement produite par le biais du gaz de synthèse (Syn-gas ou Met-gas dans ce cas concret),[5] peut-être aisément convertie, en une seule étape catalytique (**Figure 4**), en fraction essence (procédé MTG) ou en oléfines légères; l'éthylène et le propylène (procédé MTO). Les dernières

[4] Olah, G.A.; Goeppert, A.; Prakash, G.K.S. *Beyond Oil and Gas: The Methanol Economy*, Wiley VCH, Weinheim, Germany **2006**.

[5] Syngas: mélange gazeux de H_2-CO qui peut être obtenu de différentes manières par une oxidation partielle de toute source carbonée, p.ex. Charbon, gaz naturel, biomasse, etc. et peut être utilisé pour produire de manière contrôlée du méthanol. p.ex dans: a) Xu, K.; Cheng, Y.; Lin, J.; Wang, H.; Xie, S.; Pei, Y.; Yan, S. *J. Catal.* **2016**, *339*, 102. b) Cai, M.; Palčić, A.; Subramanian, V.; Moldovan, S.; Ersen, O.; Valtchev, V.; Ordomsky, V. V.; Khodakov, A. Y. *J. Catal.* **2016**, *338*, 227.

forment une partie majeure de la production d'hydrocarbures synthétiques[6] de grande valeur pour la chimie des polymères p.ex. polypropylène, polyméthylacrylate etc.[7] Ce procédé, découvert par la compagnie Mobil, est normalement conduit sur des zéolithes de taille de pores moyennes. Ainsi, la zéolithe ZSM-5 de morphologie MFI est parmi les candidats prometteurs. La structure MFI avec son architecture particulière, (**Figure 5**) mène à la fois à une haute sélectivité de forme et une haute conversion en méthanol.

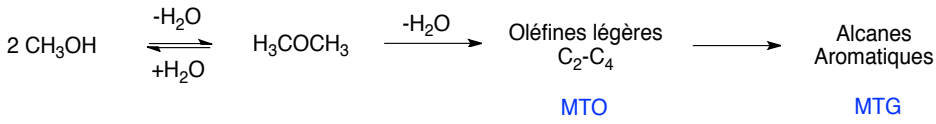

Figure 4. Schéma général de la conversion du méthanol en oléfines légères (Procédé MTO) et dans certains cas la production conséquente d'aromatiques et d'alcanes (Procédé MTG).

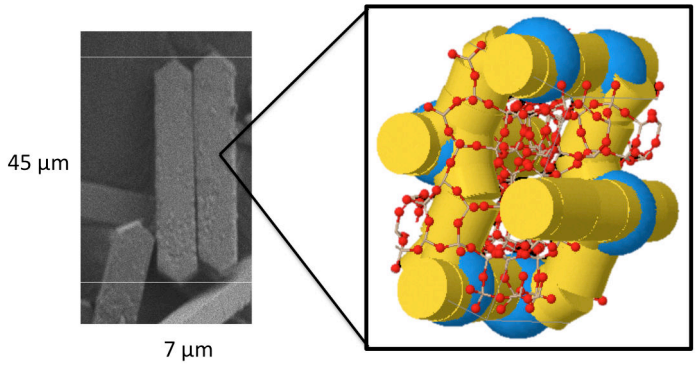

Figure 5. Architecture d'une maille élémentaire de zéolithe de type ZSM-5 avec sa porosité tridimensionnelle. Deux types de canaux (en jaune) sinusoïdaux (5.1 x 5.5 Å parallèle à l'axe cristallin a de la maille) et longitudinaux (5.3 x 5.6 Å le long de l'axe cristallin b de la maille) se croisent pour former des intersections (en bleu) d'un diamètre de 6 - 8 Å.

La synthèse d'oléfines légères a attiré l'intérêt de la communauté scientifique durant les dernières décennies afin de répondre à la demande mondiale, croissante en éthylène et en propylène.

La conception sur mesure des zéolithes est nécessaire pour garder une sélectivité élevée envers les oléfines légères. Les points majeurs pour le développement d'une génération de catalyseurs MTO améliorée, peuvent être classés en différentes catégories :

• Modification des propriétés intrinsèques d'une zéolithe avec pour but de réduire le nombre ou la force des sites acides, ou de varier les contraintes stériques pour améliorer davantage la sélectivité de forme.

• La voie fluorure pour la synthèse de zéolithes permet d'obtenir des zéolithes MFI avec une densité de sites acides réduite, une très haute qualité cristalline et des cristaux de taille élevée.

[6] Koempel, H.; Liebner, W.; Ag, L.; Main, D.-F. *Nat. Gas Convers.* **2007**, 261.
[7] a) Kissin, Y. V.; Zhou, Q.; Li, H.; Zhang, L. *J. Catal.* **2015**, *332*, 156. b) Ota, Y.; Ito, S.; Kobayashi, M.; Kitade, S.; Sakata, K.; Tayano, T.; Nozaki, K. *Angew. Chemie Int. Ed.* **2016**, DOI10.1002/anie.201600819

Tableau 1: Propriétés texturales pour une sélection de catalyseurs (Entrées 1-4; catalyseurs synthétisés selon notre stratégie, entrées 5 et 6; des zéolithes commerciales en comparaison)

Entrée	Zéolithe	Rapport Si/Al[a]	Densité de sites acides théorique (mmol $H^+/g_{zéolithe}$)[b]	Densité de sites acides (mmol $H^+/g_{zéolithe}$)		S_{BET}[e] (m^2/g)	S_{meso} (m^2/g)
				[c]	[d]		
1	H-ZSM-5FN	137	0.13	0.36	0.144	288	92
2	H-ZSM-5FS	139	0.13	0.21	0.127	425	55
3	H-ZSM-5FL	139	0.13	0.18	0.135	412	52
4	H-ZSM-5FLD	104	0.15	0.45	0.181	348	126
5	H-ZSM-5_{8020}	52	0.31	0.54		420	-
6[8]	H-ZSM-$5_{8020}P^3$	61	0.24	0.22		333	-

a: Analyse élémentaire par fluorescence aux rayons X (XRF),
b: La densité de sites acides théorique estimée avec le rapport Si/Al
c: Mesure d'échange isotopique H/D pour le nombre total de protons échangeables.
d: Désorption programmée thermale de propylamine (TPD) spécifique pour des sites acides de Brønsted forts.
e: Par mesures de N_2-adsorption désorption classiques.

En effet, la voie fluorure a plus particulièrement attiré notre attention parce qu'elle permet d'obtenir des matériaux hautement cristallins, sans défauts et à taille cristalline très modulable (voir **Tableau 1**). Étonnamment, ces matériaux se sont avérés très actifs, stables et sélectifs dans la réaction du MTO.[9] Par conséquent, mes travaux de thèse ont porté sur la préparation, la caractérisation approfondie de ces matériaux et leur application en MTO. Ultimement, l'idée était de pouvoir mettre en évidence les paramètres clés afin de s'orienter vers la conception sur mesure d'un catalyseur MTP (Sélectif envers le propylène) compétitif au niveau industriel.

Brièvement résumés, ces paramètres furent les suivants: une densité de sites acides très dispersée, une taille cristalline pouvant atteindre les 100 µm en longueur ainsi qu'une qualité cristalline la plus élevée possible. En d'autres termes, des cristaux parfaits, sans défauts avec une distribution de sites acides parfaitement homogène semblait être l'optimum à viser.

Après de nombreux efforts de synthèse, une sélection de catalyseurs sera présentée par soucis de clarté. Les résultats de caractérisation de ceux-ci sont présentés dans le **Tableau 1** ainsi que dans la **Figure 6**.

Pour résumer brièvement, ces résultats sont une forte indication pour le fait que notre meilleur catalyseur pour la réaction du MTO, synthétisé en suivant notre stratégie, consiste en effet en des cristaux de taille homogène (MEB), avec une dispersion de sites acides homogène (MET), de qualité cristalline très élevée (DRX) et sans défaut (^{27}Al-MAS-NMR et CO-FTIR).

[8] P^3 indique une triple passivation de la surface externe de la zéolithe commerciale en déposant de la silice amorphe en appliquant un traitement au tétraéthyleorthosilicate (TEOS), reporté dans p.ex.: Losch, P.; Boltz, M.; Bernardon, C.; Louis, B.; Palčić, A.; Valtchev, V. *Appl. Catal. A Gen.* **2016**, *509*, 30.
[9] Bleken, F. L.; Chavan, S.; Olsbye, U.; Boltz, M.; Ocampo, F.; Louis, B. *Appl. Catal. A Gen.* **2012**, *447-448*, 178.

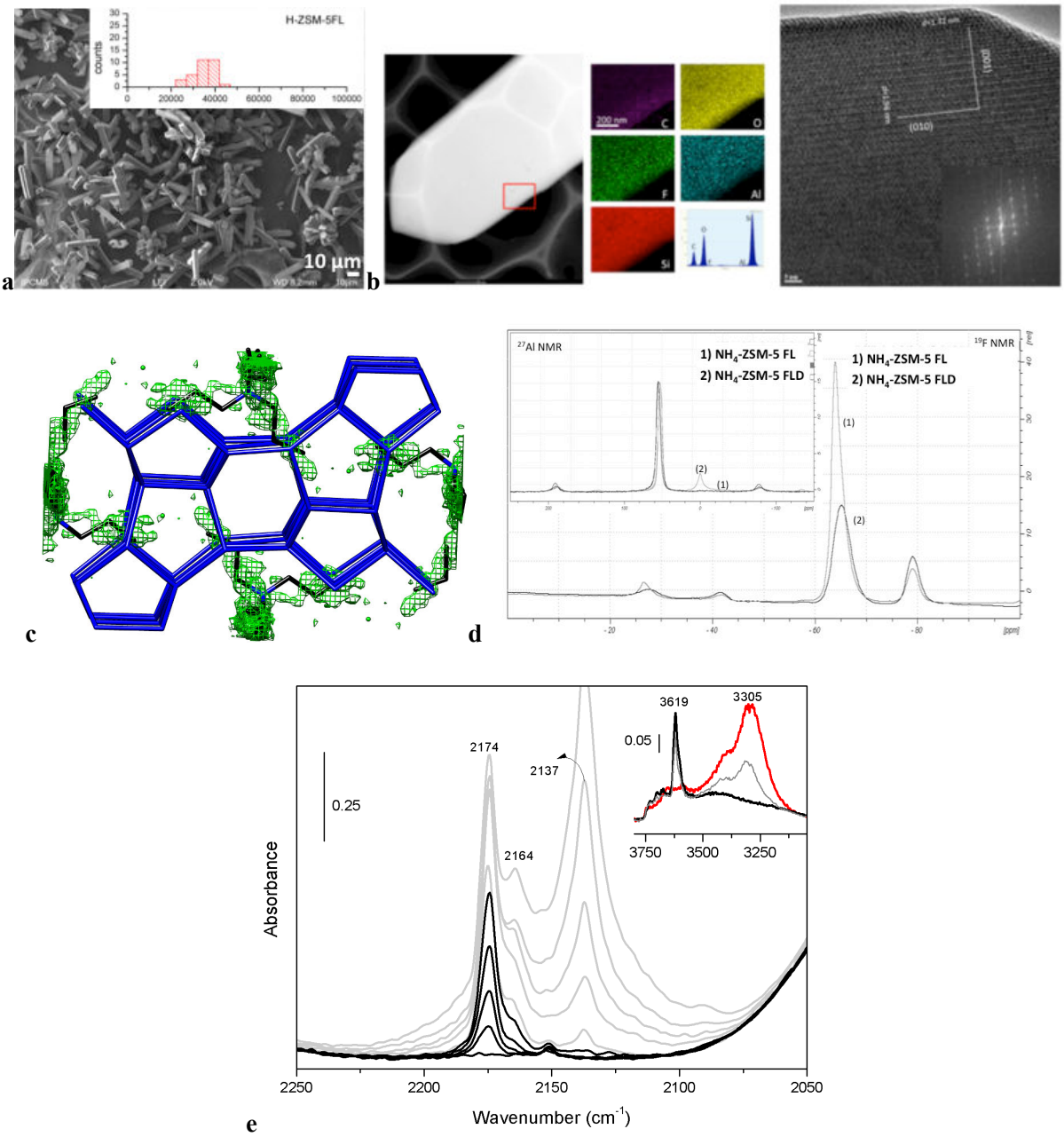

Figure 6. Caractérisation complète du meilleur catalyseur H-ZSM-5FL qui résulte de notre optimisation: a) Microscopie électronique à balayage (MEB), b) Microscopie électronique à transmission (MET) avec cartographie des éléments, c) Résolution structural via la diffraction aux rayons X du synchrotron, d) ^{27}Al-MAS-NMR de deux échantillons indiquant l'absence de défauts dans H-ZSM-5FL, e) idem pour les spectres infrarouge de H-ZSM-5FL avec adsorption-désorption de monoxyde de carbone à basse température (77 K).

Les résultats catalytiques pour une sélection de catalyseurs sont présentés dans le **Tableau 2** (conversion et sélectivités) et la **Figure 7** (la stabilité de trois différentes zéolithes). Il faut souligner la sélectivité élevée envers le propylène de H-ZSM-5FL. En effet, comparée aux autres zéolithes testées (commerciales et synthétiques), celle-ci ressort comme étant le catalyseur MTP le plus prometteur. De plus, en termes de stabilité, cette zéolithe est à nouveau la plus prometteuse.

Tableau 2. Résultats catalytiques (conversion et sélectivités envers les différents produits) pour la réaction du MTO d'une sélection de catalyseurs.

Entrée	Zéolithe	Conversion [%]	Sélectivités [%]					
			CH_4-C_4H_{10}	$C_{2=}$	$C_{3=}$	$C_{4=}$	$C_{5=}$	C_{6+} aromatiques
1	H-ZSM-5FN	99	4	16	39	15	16	10
2	H-ZSM-5FS	99	4	6	39	20	22	9
3	**H-ZSM-5FL**	**99**	**1**	**6**	**45**	**19**	**20**	**9**
4	H-ZSM-5FLD	99	7	20	35	13	14	11
5[a]	H-ZSM-5FLD	99	1	10	44	18	19	8
6	H-ZSM-5_{8020}	99	12	13	33	14	15	13
7	H-ZSM-$5_{8020}P^3$	99	13	24	30	10	11	12

Données catalytiques obtenues après 1h en ligne dans des conditions standardisées: 60 mg de catalyseur dans un réacteur tubulaire en quartz, 450°C, WHSV 1.2h^{-1}.
[a] Expérience faite avec le d_4-méthanol pour mettre en évidence un éventuel effet isotopique.

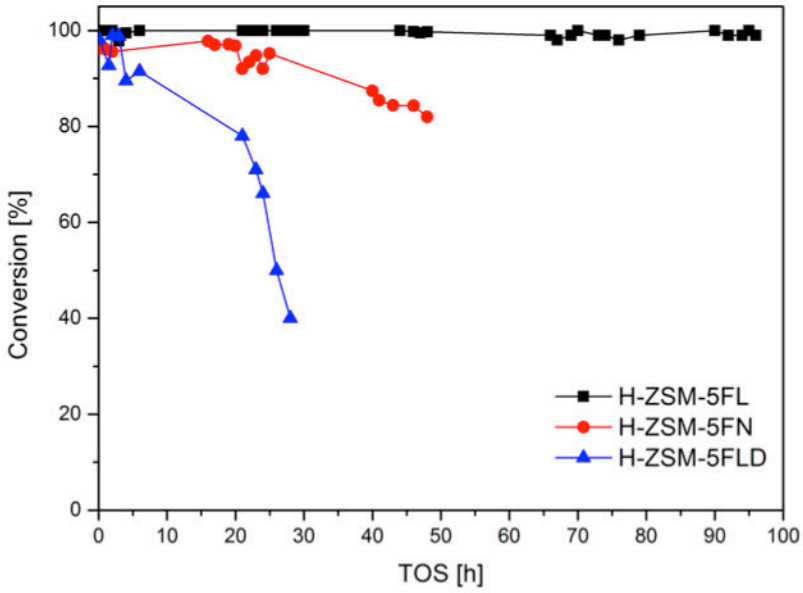

Figure 7. Conversion de méthanol en oléfines pour différentes zéolithes, en fonction du temps en ligne (time-on-stream TOS). Comparaison entre H-ZSM-5FL (les cristaux parfaits), H-ZSM-5FLD (des grands cristaux présentant des défauts au niveau de leur structure cristalline), H-ZSM-5FN (cristallites de taille nanométrique).

La rationalisation de ce résultat contre-intuitif constituera une grande partie de ma thèse. Contre-intuitif, parce qu'en catalyse hétérogène, il est admis que plus les particules du catalyseur sont grandes, plus une réaction donnée sera affectée ou limitée par la diffusion. Or, notre H-ZSM-5FL est composée de monocristaux de taille très élevée comparé aux catalyseurs industriels, et est tout de même très active, sélective et surtout stable.

De manière à fournir un travail complet, les catalyseurs ont été caractérisés après leur utilisation dans la réaction du MTO par spectrométrie infrarouge (**Figure 8**). Ces analyses montrent que la H-ZSM-5FL ne présente guère d'espèces de coke polyaromatique (bandes

d'absorption caractéristiques 1250 - 1750 cm^{-1}), en général une cause de désactivation, qui sont pourtant présentes de façon plus ou moins conséquente sur la zéolithe commerciale et la zéolithe triplement passivée.[8]

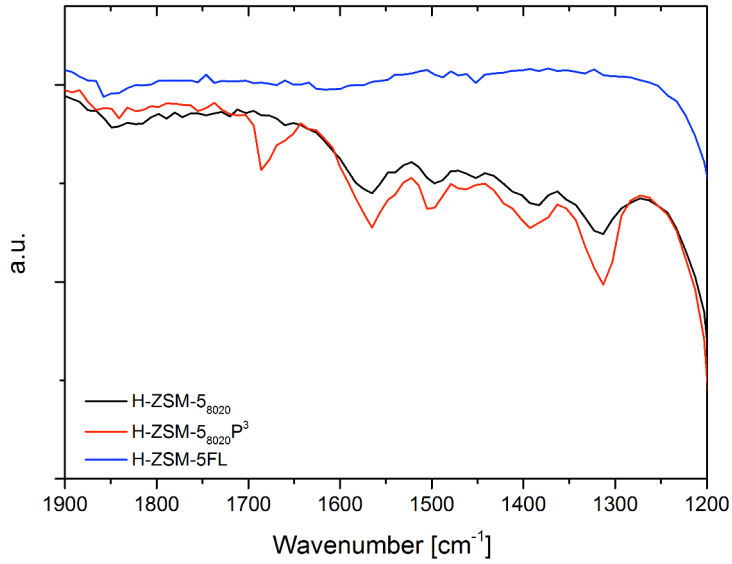

Figure 8. Analyse infrarouge de catalyseurs utilisés: H-ZSM-5FL toujours active au bout de 100 h en ligne, comparé à la zéolithe commerciale H-ZSM-5_{8020} et la zéolithe triplement passivée.[8]

Finalement, j'aimerais conclure cette partie en indiquant que cette mise au point de catalyseur était garantie en passant par un processus d'amélioration continue, Synthèse-Caractérisation-Application-Rationalisation, nous a permis d'obtenir un catalyseur MTP compétitif au niveau international. Ainsi ce projet a culminé par dépôt de projet de maturation industrielle en collaboration avec Conectus - La SATT Alsace et BASF. L'objectif étant de mettre à l'échelle cette synthèse de catalyseur développé au sein de notre groupe.

V.iii. L'économie circulaire du carbone et la chimie verte

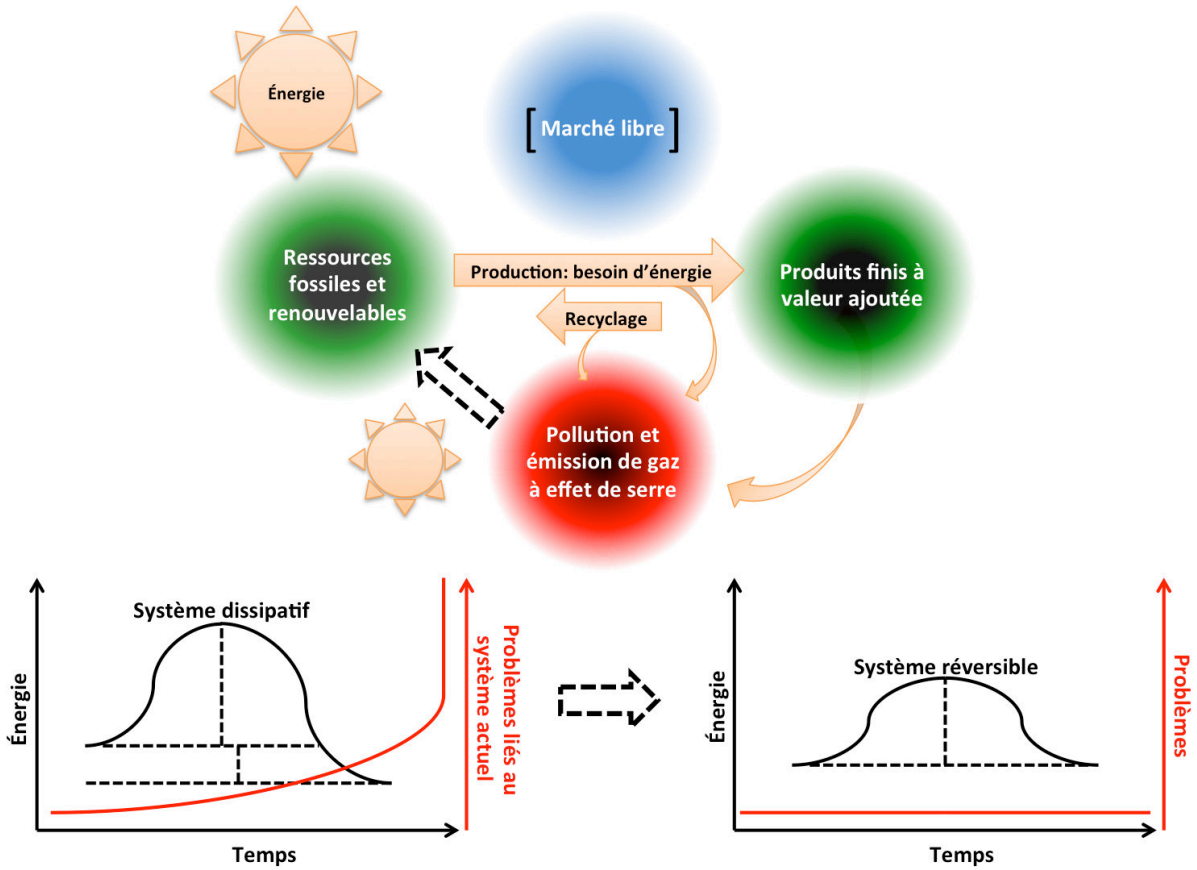

Figure 9. Représentation schématique du système économique actuellement prédominant, qui est de nature dissipative: ***Supra***: Les ressources fossiles majoritairement et renouvelables dans une moindre mesure sont transformées en des produits finis à valeur ajoutée tout en utilisant de l'énergie. Le "catalyseur" de cette transformation est le marché libre, qui génère des bénéfices en passant par la croissance. Bien qu'il y ait des tentatives de "recyclage" d'énergie et de produits à la fin de leur cycle de vie, le système actuel reste dissipatif. Toute pollution et plus particulièrement les gaz à effet de serre générés ne sont pas retransformés en ressources renouvelables. ***Infra sinister***: Le système économique actuel considéré par un chimiste consiste en des produits plus bas en énergie que les ressources et donc il n'est pas favorable de repasser par ceux-ci, ce qui sur le long terme génère une quantité importante de problèmes. ***Infra rectus***: Il serait bénéfique de tendre vers un système réversible dans lequel il serait facilement possible de passer des déchets aux ressources à nouveau.

Pendant la période de ma thèse j'ai eu la chance d'avoir eu à faire à des sujets très différents (**Figure 3**), qui avec un certain recul semblent pourtant tous être liés. Le fil conducteur était évidemment les zéolithes. Mais ma force motrice était et est toujours une volonté de changer quelque chose, même si cela est assimilable à une bataille contre des moulins à vent.

Nous vivons dans une période assez mouvementée en ce qui concerne l'environnement, notre environnement: sa protection fait face à son exploitation et pis encore sa détérioration. Pas plus tard qu'en décembre de l'année dernière (2015) nous avons finalement vu les chefs des états les plus émetteurs-pollueurs se mettre d'accord sur un but commun: limiter le réchauffement

climatique anthropogène à 1,5°C avec un maximum absolu à ne pas dépasser de 2°C d'ici 2100.[10] Pendant cette Conférence des Nations unies sur les changements climatiques (COP21) il y a donc finalement eu démonstration d'une volonté commune vers un changement. Afin d'atteindre ce but ambitieux des 1,5 ou 2°C, il faudra limiter dramatiquement les émissions de gaz à effet de serre et notamment du dioxyde de carbone (CO_2). D'autre part, il faudrait augmenter sa séquestration, et dans le meilleur des cas, son utilisation de façon exponentielle. Or, cette molécule est thermodynamiquement la plus stable en ce qui concerne le cycle du carbone. Donc, le résultat d'une analyse de vie banale d'un produit quelconque contenant du carbone montre que chaque atome de carbone finira un jour sous la forme de CO_2. Évidemment, le processus naturel de la photosynthèse permet une certaine séquestration et utilisation de cette molécule. Par contre, l'équilibre atmosphérique entre le diazote, le dioxygène et le CO_2 qui a permis un certain effet de serre (causant une température moyenne terrestre de 15°C[11]) et ainsi notre évolution, est d'ores et déjà perturbé. En effet, les bio-machineries dans les chloroplastes contenues dans toute plante n'arrivent plus suffisamment à séquestrer le CO_2 anthropogène.

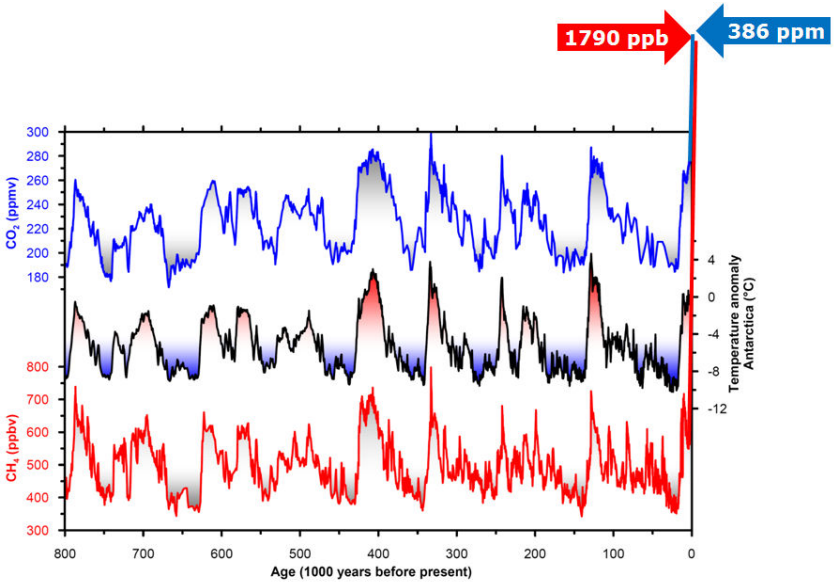

Figure 10. Analyse de l'évolution des gaz à effet de serre CO_2 et CH_4 dans l'atmosphère terrestre au cours des 800 mille dernières années. Ces données ont pu être obtenues dans le cadre du forage EPICA en Antarctique (analyse des carottes de glace).[12]

La **Figure 9** illustre schématiquement la problématique du système économique actuel qui pousse à la pollution en passant par le biais de la création de bénéfices. De plus, une potentielle remédiation à celle-ci est représentée. Il est évidemment nécessaire d'insister sur le fait que je ne

[10] L'Accord de Paris **2015** qui peut être retrouvé en ligne sous: http://unfccc.int/files/meetings/paris_nov_2015/application/pdf/paris_agreement_french_.pdf
[11] La température moyenne terrestre sans effet de serre naturel serait autour de - 18°C et n'aurait donc pas favorisée notre évolution: http://www.cnrs.fr/cw/dossiers/dosclim1/sysfacte/effetserre/index.htm#tempmoy
[12] Communiqué de presse du CNRS du 14 mai 2008: http://www2.cnrs.fr/presse/communique/1339.htm

vais pas "réinventer la roue", mais plutôt essayer de représenter les possibilités disponibles pour pallier à cette problématique. Il faut noter que l'idée d'un marché du CO_2 n'est pas nouvelle, par contre elle fut mal exécutée à l'époque du protocole de Kyoto en 1992 (carbon emission trading) et ne généra guère de changement. Au lieu de pénaliser les émetteurs il serait préférable de rajouter une valeur réelle au CO_2 pouvant générer des bénéfices supplémentaires à une entreprise émetteuse. Ainsi, comme suggéré sur la **Figure 9** en bas à droite, un système réversible ou circulaire est envisageable et pourrait permettre d'éviter des problèmes majeurs. Ces concepts sont présentés dans les travaux du Dr. J . Sherwood que j'ai pu rencontrer à Berlin,[13] lors de la conférence Green and Sustainable Chemistry.[14] Le mouvement de l'économie du méthanol mené par le prix Nobel G. Olah fait évidemment partie intégrante d'un tel concept et en constitue la partie la plus développée.[15]

Le but dans ce chapitre sera de revoir les possibilités disponibles à ce jour, leur applicabilité et rentabilité économique. "L'économie de l'acide formique", peu connue à l'heure actuelle présente toutefois de nombreux avantages. Cette molécule prometteuse comme molécule de stockage de dihydrogène pour l'économie du dihydrogène[16] peut aussi servir de source de monoxyde de carbone[17], via la réaction de déshydratation ou réaction de Morgan et ainsi être considérée comme une molécule ambivalente de stockage liquide du Syngas. Ce dernier peut être considéré comme une source de méthanol, mais aussi de divers hydrocarbures de manière directe par le procédé Fischer-Tropsch. Alors que la production de l'acide formique se fait actuellement en utilisant du méthanol, du monoxyde de carbone et de grandes quantités d'eau,[18] il a été rapporté que sa production peut se faire de manière contrôlée, sélective et rentable à partir du CO_2.[19]

Ce chapitre de thèse aura évidemment comme fin de montrer le lien entre mes autres sujets avec cette idéologie d'une chimie renouvelable, ou verte étant une partie *sine qua non* d'une économie circulaire / réversible / renouvelable. **Figure 11** montre, schématiquement les différentes étapes d'une addition séquentielle de valeur à chaque entité de carbone potentiellement issu de nos émissions de CO_2. Ainsi, même si la finalité du cycle de vie de chaque atome de carbone et d'aboutir en du dioxyde de carbone, de nombreuses alternatives sont déjà accessibles, ou en cours de développement.

[13] Clark, J. H.; Farmer, T. J.; Herrero-Davila, L.; Sherwood, J. *Green Chem.* **2016**. DOI10.1039/C6GC00501B
[14] http://www.greensuschemconf.com
[15] Olah, G. A.; Goeppert, A.; Prakash, G. K. S. *J. Org. Chem.* **2009**, *74*, 487.
[16] Mellmann, D.; Sponholz, P.; Junge, H.; Beller, M. *Chem. Soc. Rev.* **2016**. DOI: 10.1039/c5cs00618j
[17] Supronowicz, W.; Ignatyev, I. A.; Lolli, G.; Wolf, A.; Zhao, L.; Mleczko, L. *Green Chem.* **2015**, *17*, 2904.
[18] Reutermann, W.; Kieczka, H. *Formic acid,* in *Ullmann's Encyclopedia for Industrial Chemistry*, **2002**, Wiley-VCH, Weinheim, Germany.
[19] For pre industrial research: a) Chailand, N.; Sava, X.; Röper, M. *Method for producing formic acid*, WO 2008116799 A1, **2008**, BASF. b) Schaub, T.; Paciello, R. A. *Angew. Chem.* **2011**, *123*, 7416.
Some selected publications of current academic research: a) Chen, L.; Guo, Z.; Wei, X.-G.; Gallenkamp, C.; Bonin, J.; Anxolabéhère-Mallart, E.; Lau, K.-C.; Lau, T.-C.; Robert, M. *J. Am. Chem. Soc.* **2015**, *137*, 10918. b) Zhang, S.; Kang, P.; Ubnoske, S.; Brennaman, M. K.; Song, N.; House, R. L.; Glass, J. T.; Meyer, T. J. *J. Am. Chem. Soc.* **2014**.

Dans ce contexte ce travail exposera les résultats obtenus sur les sujets suivants: en un premier lieu la valorisation de cendres du charbon de l'Afrique du Sud pour la synthèse de zéolithes sera présentée. L'utilisation de biomasse comme agent dirigeant de structure secondaire peu cher lors de la synthèse de zéolithes avec une porosité complexe sera le sujet de la deuxième partie de ce chapitre. L'halogénation d'aromatiques en continu et catalysé par des zéolithes constituera la troisième partie. Finalement il sera montré que la carbonylation d'aromatiques avec du monoxyde de carbone issu de l'acide formique pourra produire des molécules organiques plus complexes.

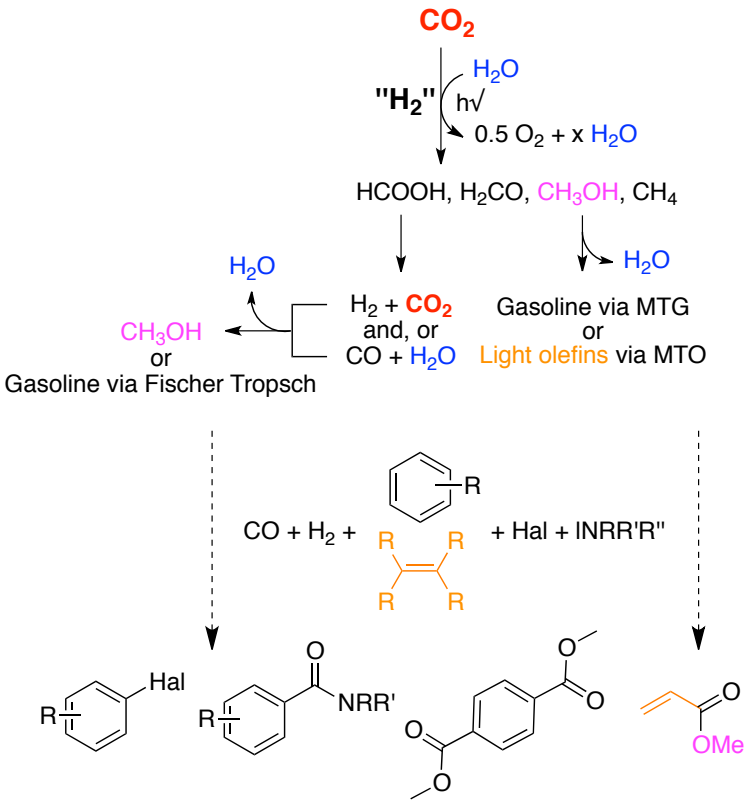

Figure 11. L'idée du "carbon upgrading", donc la valorisation, l'addition de valeur successive à un atome de carbone, initialement issu du CO_2. À chacune de ces étapes, les zéolithes acides ou dopées aux métaux sont des catalyseurs potentiellement applicables à grande échelle.

V.iv. Conclusion générale

Ce travail était basé sur deux grands piliers, la réaction du MTO avec des catalyseurs conçus sur mesure et d'un autre côté de multiples applications de zéolithes au concept général de la chimie verte ou renouvelable. Différentes conclusions restent donc à retenir:

Il a été possible de concevoir sur mesure un catalyseur compétitif pour convertir le méthanol sélectivement en propylène. Ce catalyseur a été d'une nature surprenante, à savoir des cristaux donc particules catalytiques de grande taille. Ceci nous a mené à investiguer son

comportement plus en détail, et par boucle itérative d'améliorer de façon continue ses performances.

D'un autre côté divers sujets qui passaient par la valorisation de cendres du charbon de l'Afrique du Sud pour la synthèse de zéolithes, à l'utilisation de biomasse comme agent dirigeant de structure secondaire peu cher, à l'halogénation d'aromatiques en continu et catalysé par des zéolithes, jusqu'à la carbonylation d'aromatiques pour produire des molécules organiques plus complexes ont été abordé au cours de cette thèse. Ces sujets plutôt divergents, convergent pourtant vers une idéologie commune, l'économie circulaire du carbone et la chimie verte.

General Introduction

1.1. Goals

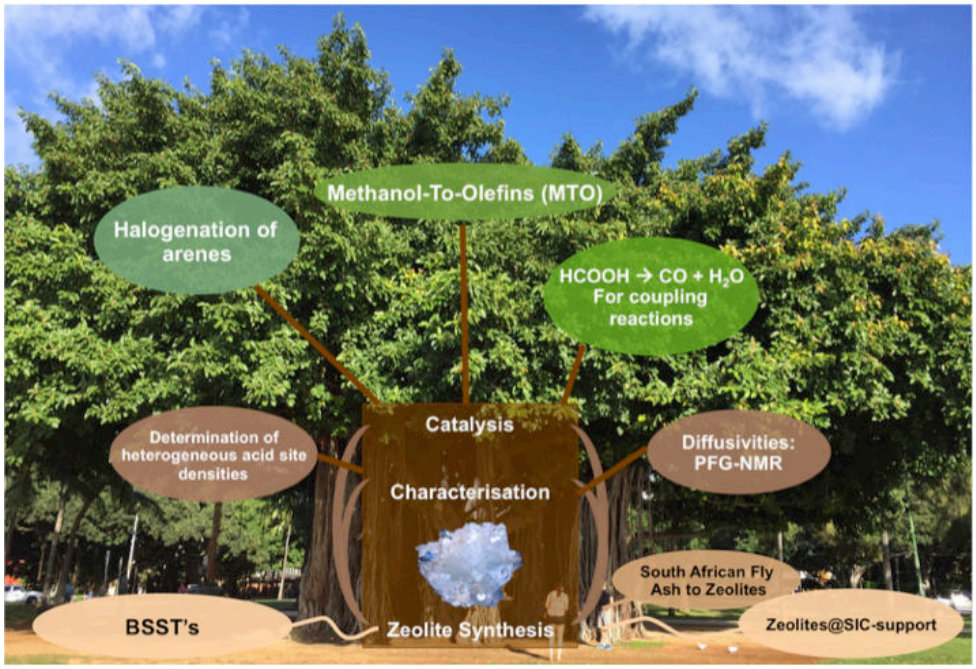

Figure 0-1. Schematic summary of my work.

The figure above is depicting a Banyan tree, whose offspring is born by the growth of roots down from the enlightened top, and superimposed the interconnectivity of my various subjects treated during the last three years. In analogy to this magnificent tree, the trunk of my work was the synthesis and characterisation of zeolites. These crystalline, microporous aluminosilicates can be used in Brønsted acid catalysis. During the last three years, I learned to cope with a lot of failures, but also succeeded in various studies and applications, depicted as roots and branches.

This thesis revolved around a holistic approach encompassing the synthesis of zeolites, their thorough state-of-the-art characterisation and their application in different industrially relevant Brønsted acid catalysed reactions. Lastly, being confronted with a global overview of my different projects, I enjoyed trying to find reasons for the different observed results.

Furthermore, this approach allowed a constant quest for an optimal catalyst for a given reaction. Indeed, the four parts: **S**ynthesis, **C**haracterisation, **A**pplication and **R**ationalisation are key to a continuous improvement approach from a catalyst, found as a "hit" in an initial screening test, towards the most competitive and applicable catalyst at the larger scale. This approach has

been profoundly inspired by William Edwards Deming's continuous improvement concept in economics.[20]

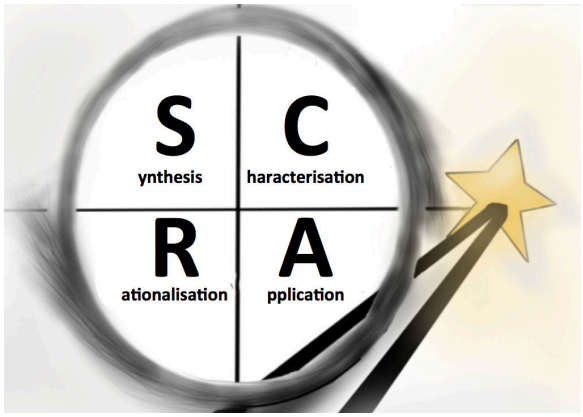

Figure 0-2. Continuous improvement approach based on the SCAR-method. (*Drawn by TL*)

1.2. Outline of the Work

This thesis is presented in four distinct chapters preceded by a summary in French and this general introduction. The first chapter consists of a literature review aiming to introduce the concepts necessary for a proper understanding of the later chapters. In a second step, the experimental part will expose the materials and methods used to accomplish this work. In the third chapter, the main project of this PhD-thesis will be detailed: work related to the application of rationally conceived H-ZSM-5 zeolites to the Methanol-To-Hydrocarbons (MTH) reaction. The fourth chapter is an attempt to take a few steps back and look critically at the work in a more global context. Herein the diverging contributions covering various secondary projects are shown to converge towards one ideology; a sustainable world. This manuscript will end with final concluding remarks and future perspectives.

[20]Deming, W.E. **1986**, *Out of the Crisis*. MIT Center for Advanced Engineering Study.

Chapter 1 Literature review

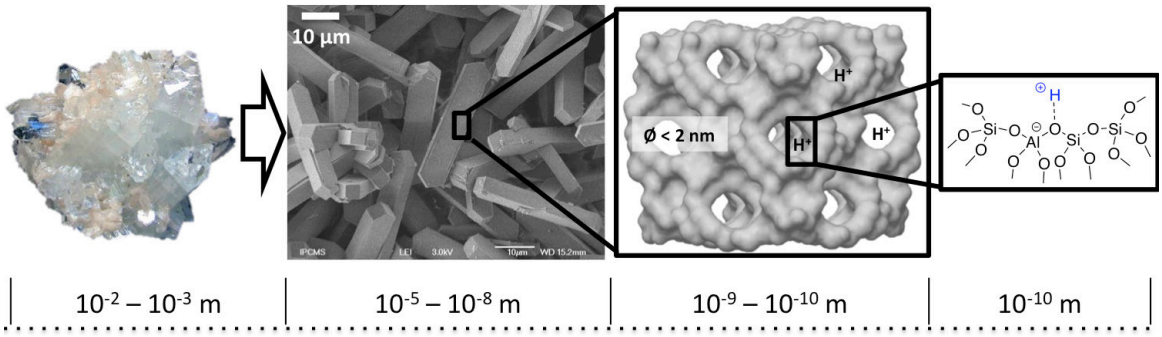

Figure 1-1. ***Sinister***: Zeolites occur in nature as crystalline minerals. ***Rectus***: Today they can be produced in a controlled manner. A peculiar attention has to be turned to the multiple scales that are controlled, from the smallest of atoms; a quasi naked proton up to a 3D periodically, highly structured porous crystal.

ABSTRACT: Herein the reader will be briefly familiarised with the general concepts, which are necessary for a proper understanding of the later presented work.

The section is divided in three main parts. Zeolites will be defined and their physico-chemically relevant parameters considering their application in catalysis discussed in further detail. In a second part their synthesis possibilities are presented and the state-of-the-art comprehension of zeolite crystal growth briefly introduced. Lastly, their application in industrially relevant catalysis are displayed.

This chapter is partially based on the following manuscript:

"A General Overview on the Methanol to Olefins Reaction: Recent Catalyst Developments" Boltz, M.; Losch, P.; Louis, B. *Adv. Chem. Lett.* **2013**, *1*, 247–256.

1.1. Zeolites

Zeolites are crystalline microporous aluminosilicates, which are defined and differ one from another through their three dimensional arrangement of tetrahedra. They exhibit the following chemical composition $M_{x/n}(AlO_2)_x(SiO_2)_y$. z H_2O where M is the cation compensating the negatively charged framework. Even though these tetrahedra are generally silicate SiO_4 and aluminate AlO_4, various other heteroatoms such as phosphate PO_4[21] stannate SnO_4[22] or germanate GeO_4[23] can also lead to zeotype structures.

The definition of zeolites, from their occurrence as natural mineral to their application as tailor-made heterogeneous, porous, Brønsted acidic catalysts is schematically represented at the different scales on **Figure 1-1**.

1.1.1. Definition - From their Discovery to Heterogeneous Catalysis

I remember myself gazing at a natural stilbite crystal on the eastern coast of Iceland, in September 2014. I felt amazed, recalling that Axel Fredrik Cronsted baptised this type of mineral "zeolite" 258 years earlier,[24] and thinking that this was part of the materials family I am working on today in order to apply them in catalysis. Today, 231 different zeolite structures are accepted and reported by the International Zeolite Association (IZA)[25], a number, which keeps on growing constantly. They are referenced by a three-letter code derived from their original name according to the rules set up by the IUPAC commission in 1979.[26] Millions of theoretical structures have been predicted,[27] indicating the unexplored potential of this cheap material but also, considering the slow growth, the huge challenges faced in conceiving such new structures.

The number of conceivable zeolites is limited by the stability of the frameworks formed from the secondary building units (23 possible SBU's), which are limited in turn by their possible connections between the primary entities, the T-atoms or T-sites. (Mainly SiO_4 and AlO_4 tetrahedra, also "members" in zeolite rings) The common representation of zeolite rings does not present atoms at the intersections but links between these "members". The Loewenstein rule,[28] indeed postulates that two AlO_4 members cannot be located in direct vicinity in a zeolitic structure, thus implying that zeolites must have a silicon to aluminium-ratio superior to one (SAR > 1).

[21] a) Choi, M.; Srivastava, R.; Ryoo, R. *Chem. Comm.* **2006**, 4380. b) Hereijgers, B. P. C.; Bleken, F.; Nilsen, M. H.; Svelle, S.; Lillerud, K.-P.; Bjørgen, M.; Weckhuysen, B. M.; Olsbye, U. *J. Catal.* **2009**, *264*, 77.
[22] Ouyang, X.; Hwang, S. J.; Xie, D.; Rea, T.; Zones, S. I.; Katz, A. *ACS Catal.* **2015**, *5*, 3108.
[23] a) Sun, J.; Bonneau, C.; Cantín, A.; Corma, A.; Díaz-Cabañas, M. J.; Moliner, M.; Zhang, D.; Li, M.; Zou, X. *Nature* **2009**, *458*, 1154. b) Paillaud, J. L.; Harbuzaru, B.; Patarin, J.; Bats, N. *Science* **2004**, *304*, 990.
[24] Cronstedt, A.F. *Akad. Handl. Stockholm*, **1756**, *18*, 120.
[25] Updated in July **2016**: http://izasc.biw.kuleuven.be/fmi/xsl/IZA-SC/ft.xsl
[26] IUPAC Physical Chemistry Division, *Pure Appl. Chem.* **1979**, *51*, 1091.
[27] Pophale, R.; Cheeseman, P.A.; Deem, M.W. *Phys. Chem. Chem. Phys.* **2011**, *13*, 12407.
[28] Loewenstein, W. *Am. Mineral.* **1954**, *39*, 92.

In general, zeolites are classified by their topologies defining the type and size of small (< 4.5 Å, 8-member rings (MR)), medium (< 6 Å, 10-MR), large (< 8 Å, 12-MR) and ultralarge micropores (> 8 Å, > 14-MR). The variability of these pore dimensions permits a selective accommodation of molecules inside this network. The connectivity between the pores, forming the latter network determines the diffusion of guest molecules in 1D, 2D or 3D channel systems.

Zeolites also served as inspiration. Since their discovery, the mastery of their synthesis and their high value in shape selective catalysis, chemists dream of others types of well-defined porous structures. This quest has led to a constant emergence of novel materials with potential catalytic applications. Indeed, several other fields of porous materials have recently evolved, such as mesoporous materials, hierarchical systems, metal-organic-frameworks (MOF's) and zeotype molecular sieves (for instance zeolite imidazolate frameworks ZIF's).[29]

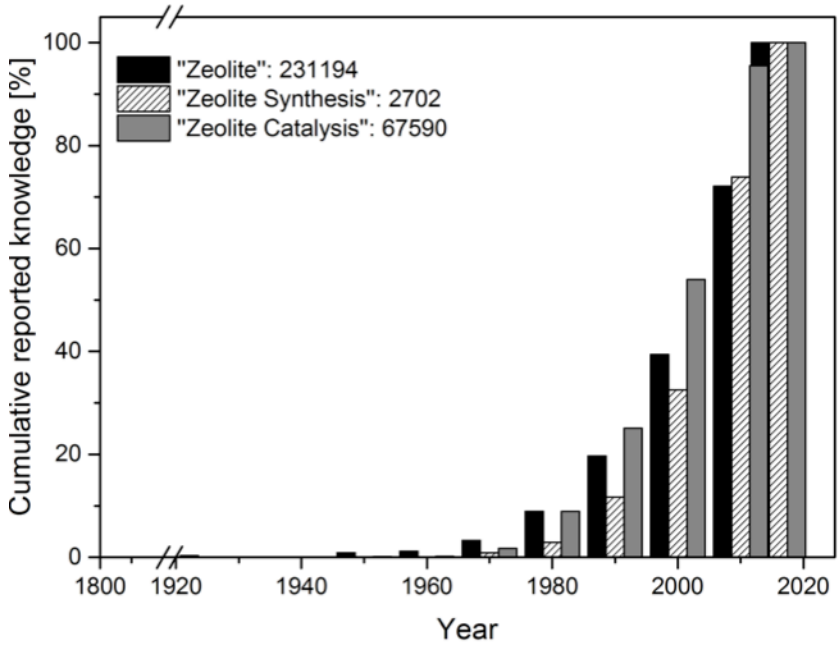

Figure 1-2 The evolution of the total, cumulative and relative knowledge concerning zeolites, their synthesis and their application in catalysis (the fastest growing domain) as a function of time. (Scifinder CAS using the terms in " ", numbers represent the total sum of the reports found for each topic)

Figure 1-2 shows the evolution of the total, cumulative and relative knowledge reported on zeolites, their synthesis and their application in catalysis, from their baptism by A.F. Cronsted in the 18th century (literally from Greek "*zein lithos*": boiling stone) via the expansion of their family with the first controlled synthetic zeolites by R.M. Barrer (1950's - 1970's),[30] the

[29] Cejka, J.; Corma, A.; Zones, S. Eds., *Zeolites and Catalysis: Synthesis, Reaction and Applications*, Wiley-VCH, Weinheim, **2010**.
[30] Barrer, R.M. *J. Chem. Soc.* **1948**, 127.

emergence of the (silico)aluminophosphates thanks to E.M. Flanigan in the eighties,[31] up to now where these materials are the most consumed heterogeneous catalysts worldwide in terms of tonnage and value.

1.1.2. Properties - Application - Adaptability

Zeolites detain a special place in the realm of inorganic solids: the above mentioned properties are supplemented by their high surface area (> 300 $m^2.g^{-1}$) and a high thermal stability, which render them attractive materials for a wide range of applications. Herein, we will consider their three main utilisations, namely as ion-exchangers, in adsorption processes and in heterogeneous catalysis.[32]

In terms of tonnage use these three major applications can be partitioned as follows: Detergents (73 %), adsorbents and desiccant (10 %) and catalysis (17 %). However, if we consider the economic value of the three domains, the part which this thesis will focus on, namely catalysis stands out with a value of 1.65 billions € per year, thus only 117000 t / year make up 55 % of the total economic value, being 3 G€ / year.[33]

1.1.2.1. Ion exchanger

Zeolites exhibit a negatively charged framework, these charges are compensated by electrostatically bound, and thus easily exchangeable cations. The exchange capacity of a zeolite is therefore related to the amount of cations present in the solid material and in turn directly linked to the amount of aluminium present in the framework (or the Silicon-to-Aluminium Ratio SAR).

In the use as *water softeners* zeolites have rapidly replaced eutrophication-inducing phosphates, such as sodium triphosphate as ion exchangers.[34]

They have been as well highly useful as capturing material for hazardous, radioactive isotopes, mainly $^{137}Cs^{+}$, released during the nuclear disasters of Fukushima in Japan five years ago, and Chernobyl in the Soviet Union in 1986.

Lastly, it is noteworthy that this ion exchanger ability and the related ion exchanged products do not necessary have to be a waste material. In fact, in the recent decades zeolites have been used to be loaded with catalytically active metal ions, which could then be used as

[31] Flanigan, E.M.; Lok, B.M.; Lyle Patton, S.T.; Wilson S.T. *Pure and Appl. Chem.* **1986**, *58*, 1351.
[32] Corma, A. *Chem. Rev.* **1995**, *95*, 559.
[33] Rhodes C. *Zeolites and World Markets, Energy Balance*, **2006**.
[34] Ghobarkar, H.; Schäf, O.; Guth, U. *Prog. Solid State Chem.* **1999**, *27*, 29.

heterogeneized catalysts in traditionally homogeneously catalysed reactions,[35] or as hybrid catalysts in the oil refining industry.[36]

1.1.2.2. Adsorption - Separation

Zeolites are widely applied at large scale in adsorption and separation processes. In the late 1950's they have been reported to dry gases through adsorption of water.[37] For the same reason, they are used to dry organic media and solvents. In a related approach, zeolites are currently investigated for their CO_2-removal potential.[38]

These typical adsorption and separation properties are governed by the zeolite's hydrophobicity, the nature of the charge compensating cation (M^{n+}) and the size and shape of the pores. The latter properties led to useful applications, such as the separation of xylene isomers and of linear / branched alkene mixtures, O_2 / N_2-separation by distillation from air, etc.

These amazing properties clearly justify the term *molecular sieves* as they are often commonly called.

Depending on the target adsorption or separation process, zeolites can be tuned in order to better match the given process. The presence and nature of the cations in the porous network can be modulated; the size and shape of pores and apertures depend on different zeolite topologies and can be chosen. When it comes to hydrophobicity the tuning becomes more challenging, even though a rule of thumb is generally accepted: *the higher the SAR, the less aluminium and in turn the less charges are present in the porous network and therefore the higher the hydrophobicity*. In reality, the hydrophobicity is also linked to the presence and amount of structural defects (Si-OH species) in the zeolite and the nature of the metal cation present in the zeolite.

1.1.2.3. Heterogeneous Catalysts - Zeolites in industry

In the case of a proton compensating the negative charge in the framework, a zeolite can be considered as a heterogeneous Brønsted acid. This acidity is comparable in strength to commonly applied mineral acids.[39] However, under certain conditions especially under high

[35] a) De Vos, D. E.; Dams, M.; Sels, B. F.; Jacobs, P. A. *Chem. Rev.* **2002**, *102*, 3615. b) Olmos, A.; Louis, B.; Pale, P. *Chem. A Eur. J.* **2012**, *18*, 4894. c) Olmos, A.; Rigolet, S.; Louis, B.; Pale, P. *J. Phys. Chem. C* **2012**, *116*, 13661. d) Chassaing, S.; Bénéteau, V.; Pale, P. *Catal. Sci. Tech.* **2016**, *6*, 923. e) Chassaing, S.; Bénéteau, V.; Louis, B.; Pale, P. *Curr. Org. Chem.* **2016**, *20*, 1.
[36] Primo, A.; Garcia, H. *Chem. Soc. Rev.* **2014**, *43*, 7548.
[37] McKetta, J.J. *Petroleum Processing Handbook*, Marcel Dekker, Inc. New York, **1992**.
[38] Lin, L.-C. C.; Berger, A. H.; Martin, R. L.; Kim, J.; Swisher, J. A.; Jariwala, K.; Rycroft, C. H.; Bhown, A. S.; Deem, M. W.; Haranczyk, M.; Smit, B. *Nat. Mater.* **2012**, *11*, 633.
[39] Auroux, A. *Top. Catal.* **2002**, *19*, 205.

temperatures, these acid sites combined with their non-flat environment can catalyse reactions only possible in a *superacidic* medium.[40]

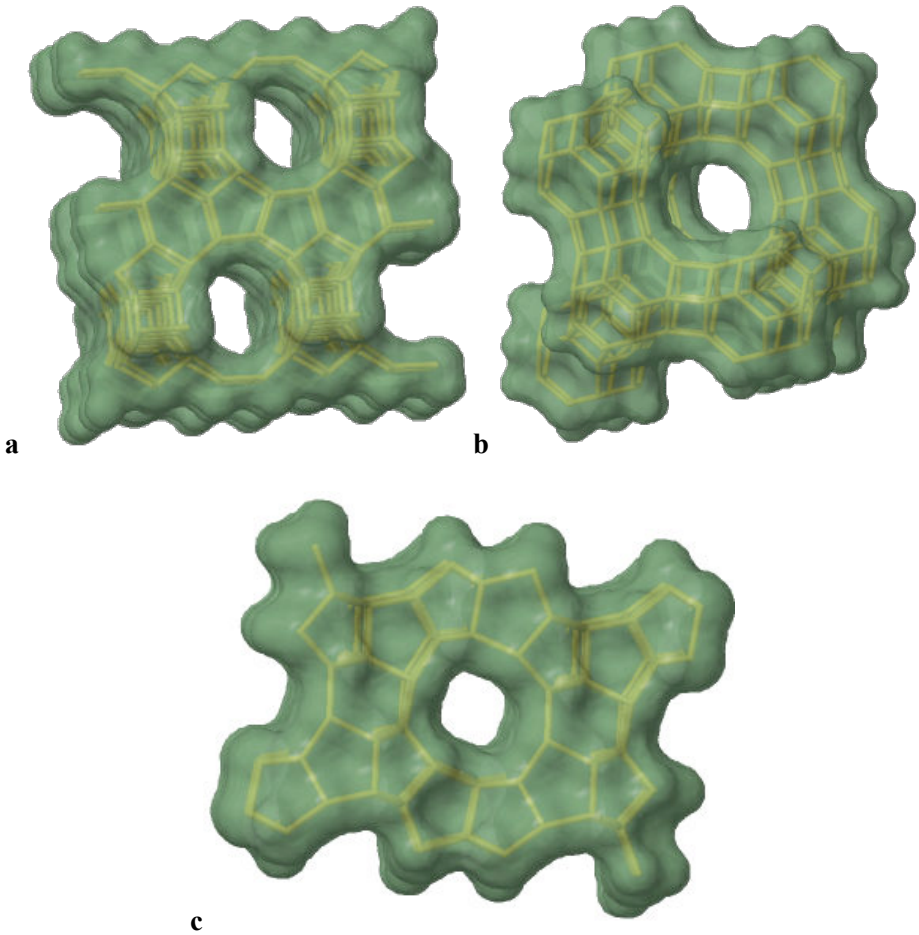

Figure 1-3. Three of the "Big Five" with which we work in the group: a) *BEA: a 3D-porous 12-MR zeolite with a pore diameter of 6.68 Å, b) FAU: a 3D-porous 12-MR zeolite containing supercages with typical diameters of 7.35 Å for the channels and 11.24 Å concerning the supercage, c) MFI: a 3D-porous 10-MR zeolite with a pore diameter of 4.70 Å.[41]

Among the 231 existing zeolite structures the most studied are the "Big Five": Mordenite (MOR), Y (FAU), beta (*BEA), Ferrierite (FER) and ZSM-5 (MFI). However 17 zeolites are currently used in industry as shape selective and Brønsted acidic mineral and all of them are synthetically prepared: AEL, AFI, BEA, CHA, EDI, FAU, FER, GIS, LTA, LTL, MER, MFI, MOR, MTT, MWW, TON, RHO.[42] It has been estimated that zeolites are produced and used at a 5 Mt/year scale.[43] However, synthetic zeolites amount only up to 36% of this total consumption.

[40] "Superacid" is a term coined J.B. Conant in **1927** to describe acids stronger than classical mineral acids. Gllespie introduced the term "magic acid" to describe HSO_3F/H_2SO_4-mixtures while Olah's work with $FSO_3H.SbF_5$-magic acid which protonated hydrocarbons in the 1960's would eventually lead to his Nobel prize. Tanabe, K.; Hattori, H. *Solid superacids*, Ertl, G.; Krözinger, H.; Weitkamp, J. Eds., in *Preparation of Solid Catalysts*, Wiley-VCH Verlag, **1999**.
[41] These data can be found on the official site of the Internation Zeolite Association (IZA) the zeolite database: http://izasc.ethz.ch/fmi/xsl/IZA-SC/ft.xsl
[42] McCusker L.B. *Introduction to Zeolite molecular sieves* **2007**, 13.
[43] Yilmaz, B. *Chines J. Catal*. **2012**, *33*, 3.

The areas of application are vast with more than 70 industrial processes, ranging from oil refining to fine chemistry.[44] Interestingly, the sole Fluid Catalytic Cracking (FCC) process accounts for more than 95 % of synthetic zeolite consumption.

In the future, mixed or renewable feedstock will be a new challenge and opportunity for potential large-scale applications of zeolites in petrochemistry.

a. Brønsted Acids

As mentioned earlier, zeolites are acidic minerals, it is however important to distinguish between the chemical nature of an acid site; Brønsted vs. Lewis, the density of these sites, their strength and their location in the solid acid.[45]

Thus far, we have seen that zeolites can be heterogeneous Brønsted acids (cf. **Figure 1-1**), and that their acid strength may vary as a function of the (reaction)-temperature. Obviously, the acid site density is directly related to the framework aluminium content. The silicon/aluminium-ratio contains therefore important information considering the acid site density of the bulk material. However, the acid site strength of these bridging hydroxyl groups Si-(OH)-Al is intrinsically adjustable. The Si-O-Al bond angle differing from one zeolite topology to another, impacts the partial charge and the acid strength, hence the lability of the H-Zeolite bond.[46], this important parameter is governed by the distribution of aluminum atoms in the zeolite framework, or in other terms, the chemical composition in the close vicinity. This effect is related to the global electronegativity of the framework (with EN(Si) > EN(Al)), which has been first defined by Sanderson.[46] It can be therefore stated that the lower the Al-content in a zeolite is, the higher the resulting acid strength will be. Additionally, the next nearest neighbour (NNN) concept is based on this phenomenon, taking into account the T-atoms in the coordination sphere of one Al-atom. To clarify, one Al T-atom is necessarily (see Loewenstein's rule) coordinated by four Si T-atoms, but in the next coordination sphere (9 T-atoms in the case of a FAU-zeolite for instance), the next nearest neighbours NNN's can vary in nature.[23a] The more Al-atoms are present in this NNN-positions the lower the resulting acid strength will be.[47]

In analogy to weakly coordinating anions (WCA's),[48] the above described effect is complemented by the charge delocalisation, which is improved in the case of more disperse acid sites. Hence, this concept indicates as well an increase in acid strength with a decrease in Al-

[44] Hölderich, W.F. *Appl. Catal. A Gen.* **1999**, *181*, 399.
[45] Chizallet, C.; Raybaud, P. *Angew. Chem., Int. Ed.* **2009**, *48*, 2891.
[46] Hunger, M. in *Zeolites and Catalysis: Synthesis, Reactions and Applications*, Cejka, J.; Corma, A.; Zones, S. Eds., Wiley-VCH, Weinheim, Germany, **2010**, 493.
[47] Pine, L.A. Maher, P.J.; Wachter, W.A. *J. Catal.* **1984**, *85*, 466.
[48] Krossing, I.; Raabe, I. *Angew. Chem., Int. Ed.* **2004**, *43*, 2066.

content. Lastly, the spatial non-flat environment around aluminosilicate typical Brønsted acid sites can have an exaltation effect of the considered acid strength.[49]

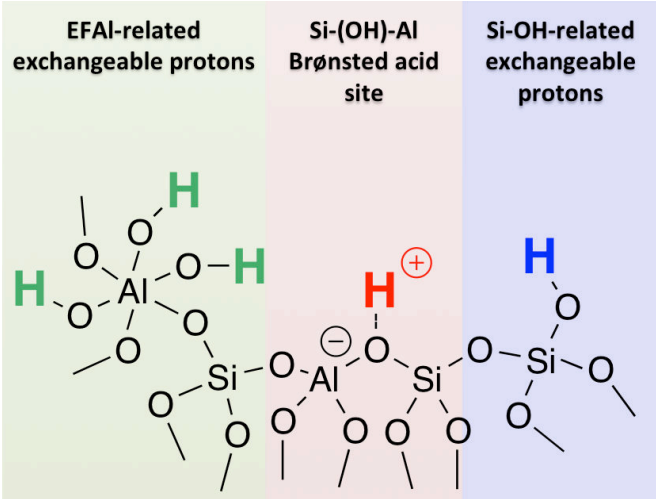

Figure 1-4. Schematic representation of the different Brønsted acidities encountered in zeolitic solid acids, from the left to the right: Octahedrally coordinated extraframework aluminum species (EFAl) can act as weak Brønsted acids upon hydration (green), the zeolite typical bridging hydroxyl groups Si-(OH)-Al act as rather strong up to very strong Brønsted acids (red), structural defects, or terminal Si-OH exhibit a weak acid strength, comparable to conventional silica (blue).

Figure 1-4 presents the different Brønsted acidities, which can be found in zeolites, from the weakly acidic terminal silanols, to hydrated EFAl-related exchangeable protons up to the strongly acidic Si-(OH)-Al bridging hydroxyl groups.

b. Shape Selective Microporous Solids

Shape selectivity, in general, was the property of zeolites, which made me get addicted to the quest of trying to understand why, where and most of all how does this work. Furthermore, the question is intriguing whether we might potentially benefit and control this property, while designing a catalyst.

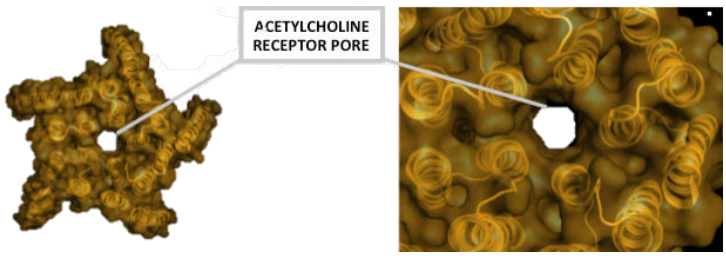

Figure 1-5. Acetylcholine receptor pore as an example for Reactant shape selectivity in nature.

Having a certain biochemistry background, I feel attracted to the analogy to the utmost highly selective behaviour encountered in nature, and more specifically in enzymes. The regular and well-defined pores of molecular dimension are able to discriminate reactants and products by size and shape, since they may present significant

[49] Leydier, F.; Chizallet, C.; Costa, D.; Raybaud, P. *J. Catal.* **2015**, *325*, 35.

differences in diffusivity through a given porous network.[50] Indeed, the product distribution of a number of chemical reactions seems to shift away from the thermodynamical one, if the formation and diffusion of molecules is inhibited by the constraints imposed by the pore walls. Three generally accepted shape selectivities are complemented by five shape selectivity-related concepts, which are still under debate. Very interesting and complete reviews are covering this topic.[51] While explaining the different types of shape selectivities, I will try to allude the respectively described phenomena to a counterpart found in nature.

Reactant Shape Selectivity (RSS): This type of selectivity has an impact on mixtures of reactants. Bulky and small molecules will not be transformed in the same way into the desired products, depending on their size with respect to the limiting pore diameter of the zeolite.

Molecules different in size and shape may thus have different accessibilities to the active sites present in the porous network. Key governing parameters of this type of selectivity are the geometry of the pore-entrance and the intra-pore diffusional properties of the reacting molecules. Interesting examples are the selective cracking of n-alkanes and n-alkenes with respect to their branched isomers in small pore zeolites.[52]

A counterpart in nature for this behaviour can be found in the Acetylcholineesterase (AChE), a membrane protein, which lets selectively diffuse acetylcholine into its receptor pore to hydrolyse it, thereby ensuring a neurotransmitter function (**Figure 1-5**).[53]

Product Shape Selectivity (PSS): A reaction forming differently sized and shaped products inside the microporous space may underly this type of selectivity. In brief, the products whose spatial dimensions best fit, or at least do not exceed the pore dimensions will diffuse more readily out of a zeolite crystal and thus impact the final product distribution. As an example of zeolite chemistry the selective disproportionation of toluene to *para*-xylenes is noteworthy,[54] while in the realm of nature one might see a similar behaviour in *Moorella theroacetica*'s Carbon monoxide dehydrogenase / Acetyl-CoA synthase, where only CO diffuses through the hydrophobic channel while the second product, water is immediately released.[55]

Transition State Shape Selectivity (TSS): A catalytic reaction occurring inside the confining zeolitic micropores may be controlled by the steric constraints of the channel- or cage-dimensions on the considered transition state. Hence, the formation of bulky transition states and intermediates may be forbidden depending on this relationship. The beneficial use of this property

[50] Weitkamp, J. *Solid State Ionics* **2000**, *131*, 175.
[51] a) Degnan, T.F. *J. Catal.* **2003**, *216*, 32. b) Marcilly, C. *Top. Catal.* **2000**, *13*, 357.
[52] Corma, A. *J. Catal.* **2003**, *216*, 298.
[53] Miyazawa, A.; Fujiyoshi, Y.; Unwin, N. *Nature* **2003**, *423*, 949.
[54] Fechete, I.; Wang, Y.; Védrine, J.C. *Catal. Today* **2012**, *189*, 2.
[55] Ragsdale, S. W.; Kumar, M. *Chem. Rev.* **1996**, *96*, 2515.

is widely exemplified in the use of the MFI-zeolite in several reactions from MTO,[56] to the cracking of paraffins.[57] In these reactions *TSS* inhibits the formation of large, carbonaceaous, in some cases deactivating coke species. Lipase enzymes and in general the very selective hydrolysis catalysing enzymes can be assimilated as nature's masterpiece for *TSS*. Inside their reactive pockets the catalytic triade is selectively producing the later used products, exhibiting unachievable selectivities with classical chemistry.[58]

The three above mentioned shape selectivities are graphically depicted in **Figure 1-6**. The complete picture however, is somewhat more complex as these three above presented shape selectivities, since 5 other shape selectivity concepts have been reported and are debated (Inverse Shape Selectivity ISS, Molecular Traffic Control MTC, pore mouth and key-lock shape selectivity, the "Window Effect" and the "Nest Effect").[51] Furthermore, *RSS*, *PSS* and *TSS* may co-impact the product distribution during one single catalytic reaction. Hence, the reality of the observed facts may lie in the grey zones of these concepts.

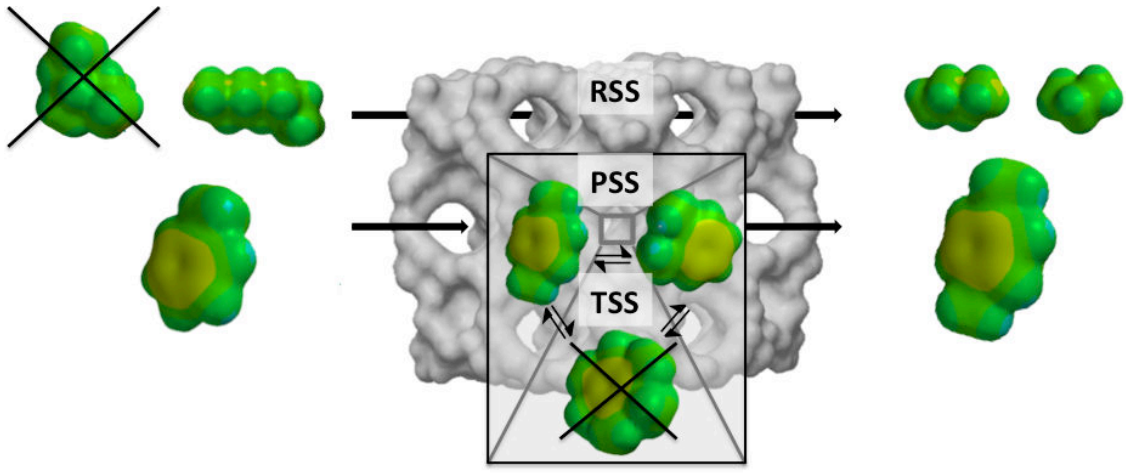

Figure 1-6. Schematic representation of the different shape selectivities for two typically shape selective reactions: ***supra***: paraffins cracking, ***infra***: toluene methylation to *para*-xylene.

The sheer existence of these effects is very important to be acknowledged. Considering this grey zone behaviour, interesting advances have been made towards more reliable predictions, taking into account thermodynamic effects by simulations.[59]

Besides the molecular shape selectivities, the ***confinement effect*** originates from the interplay between longer range attractive and short-range repulsive interactions. Barthomeuf first introduced this solid solvent concept in 1979.[60] After these first indications on the importance of the electric field gradient, a consequence of Al- and cation-distributions, Derouane introduced the

[56] Xue, Z.; Zhang, T.; Ma, J.; Miao, H.; Fan, W.; Zhang, Y.; Li, R. *Microporous Mesoporous Mater.* **2012**, *151*, 271.
[57] Liers, J.; Meusinger, J.; Reschetilowski, W. **1993**, *16*, 422.
[58] Kung, H. H.; Kung, M. C. *Catal. Letters* **2014**, *144*, 1643.
[59] Smit, B.; Maesen, T.L.M. *Nature*, **2008**, *451*, 671.
[60] Barthomeuf, D. *J. Phys. Chem.* **1979**, *83*, 249.

new concept of confinement effect in the late eighties.[61] This effect is based on non-covalent interactions between the framework and molecules located in the zeolite pores. Two different forces are responsible for this effect: the repulsive Pauli interaction is acting in the short range (< 2 Å), while the attractive van der Waals force rather acts in the long range (3 - 5 Å). Hence, the origin of this remarkable effect lies in the surface curvature of the internal surface of zeolite channels, cages and external "pockets".[62] These effects are indeed responsible for the above described shape selectivity, selective adsorption and enhanced diffusivity, which is the reason why Derouane assimilated microporous materials such as zeolites to solid solvents.[62c]

Derouane described in his work three concepts forming the so called confinement: - *nest effect* - he describes minimum energy points on the sorbate-zeolite van der Waals potential surface, - *floating molecule* - van der Waals and Pauli forces cancel each other out and lead to enhanced diffusivities, or levitating molecules, - *creep motion* - when a significant number of atoms (molecules), or more generally electron density presents a minimal energy toward the pore area, they will have a collective jump. This ***confinement*** is a topology related phenomenon and can act synergistically to the zeolites' acidity. Thus, interpretation of experimental results can be tricky. Experiments show that the true impact of confinement is only detectable in a 2 - 15 Å range sized pores.[63]

c. Hierarchical Porosity

Hierarchical porosity is a recently evolved term describing complementary porous networks of different porous diameters. Generally accepted are the zeolite typical microporosity (ø < 20 Å), the mesoporosity (20 < ø < 500 Å) and the macroporosity (500 Å < ø),[64] which may ease the access to the shape selective active sites. (cf. **Figure 1-7**) It is important to note that the molecule-surface interactions in the larger pores are not impacted by any kind of confinement since this surface curvature becomes approximately flat. The obvious advantage of such a complementary porosity is the eased access and exit to and from the shape selective active sites and the reduction of the residence time for reactants and products, hence limiting deleterious consecutive reactions.[65]

---

[61] Derouane, E. G.; Andre, J.; Lucas, A. A. *Chem. Phys. Lett.* **1987**, *137*.
[62] a) Derouane, E. G. *Chem. Phys. Lett.* **1987**, *142*, 200. b) Derouane, E. G.; Andre, J.-M.; Lucas, A. A. *J. Catal.* **1988**, *73*, 58–73. c) Derouane, E. G. *J. Mol. Catal. A* **1998**, *134*, 29.
[63] a) Bhan, A.; Iglesia, E. *Acc. Chem. Res.* **2008**, *41*, 559. b) Gounder, R.; Iglesia, E. *Chem. Commun.* **2013**, *49*, 3491. c) Gounder, R.; Iglesia, E. *J. Am. Chem. Soc.* **2009**, *131*, 1958. d) Gounder, R.; Jones, A. J.; Carr, R. T.; Iglesia, E. *J. Catal.* **2012**, *286*, 214.
[64] IUPAC. *Compendium of Chemical Terminology, (the "Gold Book")* A. D. McNaught, A. Wilkinson. Blackwell Scientific Publications, Oxford **1997**.
[65] a) Lopez-Orozco, S.; Inayat, A.; Schwab, A.; Selvam, T.; Schwieger, W. *Adv. Mater.* **2011**, *23*, 2602. b) Schwieger, W.; Machoke, A. G.; Weissenberger, T.; Inayat, A.; Selvam, T.; Klumpp, M.; Inayat, A. *Chem. Soc. Rev.* **2015**. c) Schwieger, W.; Machoke, A. G.; Weissenberger, T.; Inayat, A.; Selvam, T.; Klumpp, M.; Inayat, A. *Chem. Soc. Rev.* **2016**, *45*, 3305.

It is important as well to highlight the drawbacks frequently encountered with hierarchically porous materials. For instance, the quality of secondary, or a potential tertiary porosity may be deleterious to the targeted selectivity, since less shape selective active sites are present, more defects may be exhibited by such a material, and an increased parallel presence of non-shape selective active sites.[66] These problems render the advantage of the use of hierarchically porous materials sometimes insignificant. It is important to target a high quality interconnectivity between the different porosities, when dealing with hierarchical porosities and aiming an improved mass transport behaviour with a conserved high shape selectivity.[67]

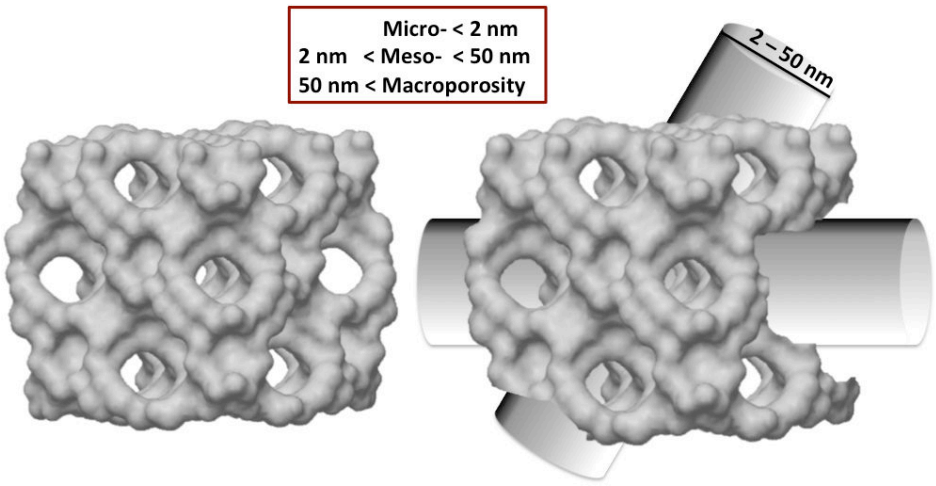

Figure 1-7. Schematic representation of an example of a complementary secondary porosity, here; channel-like mesopores.

1.1.3. Challenges - Benefits and Drawbacks

So far we have seen what zeolites are, for what they are mainly used. We also have had some insight on the way zeolite's physicochemical properties can be applied, sometimes even controlled, to conceive catalysts. The latter case is frequently referred to as rational design.[68] Nevertheless, and as mentioned in the very beginning of this thesis theoretical zeolite structure predictions indicate a possible 2.6 million stable zeolite structures.[27] The reality, the huge discrepancy between these two realms is strongly anticlimactic.

In practical terms, one might have to consider this problematic from another viewpoint: Do we need so many more zeolite structures? Are those we know not *ADAPTABLE* enough in order to answer a great deal of our needs?

Indeed as compared to for instance, metal organic frameworks (MOF's) the discovery of new zeolitic structures is incommensurably slow. The contrasting rapidly growing domain

[66] Milina, M.; Mitchell, S.; Crivelli, P.; Cooke, D.; Pérez-Ramírez, J. *Nat. Commun.* **2014**, 1.
[67] a) Verboekend, D.; Pérez-Ramírez, J. *Catal. Sci. Technol.* **2011**, *1*, 879. b) Friedrich, H.; Jongh, P. E. De; Bulut, M.; Donk, S. Van; Kenmogne, R.; Finiels, A.; Hulea, V.; Fajula, F. *Angew. Chem., Int. Ed* **2010**, *49*, 10074.
[68] Moliner, M.; Rey, F.; Corma, A. *Angew. Chem., Int. Ed.* **2013**, *52*, 13880.

accounts already to 7 % of the total Cambridge Structure Database (CSD), with 54,341 records on their last update in May 2015.[69] One has to note that the zeolite structure discovery is limited by its tetrahedral primary building blocks, which can form only a limited number of secondary building blocks (SBU's). In contrast, MOF's are much more flexible in this aspect since they can arise from a complex interplay of a myriad of organic linkers and octahedrally vs. tetrahedrally vs. linearly coordinating metal ions, or even metal clusters.[70]

However, at the industrial level zeolites have proven to be thermally stable up to temperatures relevant for large scale applications, they are mechanically resistant, and even though there are not as many new structures discovered, the mere possibility of varying some key parameters attributes them a high degree of adaptability to various processes. Indeed, the sole MFI structure, which will be discussed in further detail in this work, can be applied in processes where high acidity is needed,[71] and the contrary is also true.[72] Considering its shape selective microporosity, it can be complemented by meso- or macroporosities limiting mass transfer related problems during a reaction.[73] Last but foremost, zeolites are cheap and easily produced at large scale. How they are synthesised, why they are so adaptable and so cost-efficient will be the topic of the next section.

1.2. Synthesis of Zeolites

Zeolites are commonly synthesised under hydrothermal conditions. From a Sol-Gel composed of a silica source, an alumina source (Tetrahedra-"T"-source), a mineralizing agent (either OH^- or F^-), a structure directing agent (SDA) and a solvent, under autogeneous pressure and temperatures ranging from room temperature[74] to 300 °C zeolites are formed. Thus, many parameters need to be controlled, which renders the understanding of the zeolite growth mechanisms relatively challenging.[75]

In general the crystallization of zeolites happens from an inhomogeneous hydrogel, formed by the T-sources, the mineralizing agent and the SDA's via a supersaturated solution, which favours the nucleation of initial nuclei that then grow to form larger crystallites.[76] Once, the concentration shifts below the supersaturation limit, no new nuclei are formed and the present

[69] https://www.ccdc.cam.ac.uk/support-and-resources/support/case/?caseid=9833bd2c-27f9-4ff7-8186-71a9b415f012 last checked: July **2016**.
[70] Zhou, H.-C. Long, J.R.; Yaghi, O.M. *Chem. Rev.* **2012**, *112*, 673.
[71] Bij, H. E. Van Der; Meirer, F.; Kalirai, S.; Wang, J.; Weckhuysen, B. M. *Chem. Eur. J.* **2014**, *20*, 16922.
[72] Wang, C.; Xu, J.; Qi, G.; Gong, Y.; Wang, W.; Gao, P.; Wang, Q.; Feng, N.; Liu, X.; Deng, F. *J. Catal.* **2015**, *332*, 127.
[73] Tarach, K. A.; Tekla, J.; Makowski, W.; Filek, U.; Mlekodaj, K.; Girman, V.; Choi, M.; Góra-Marek, K. *Catal. Sci. Technol.* **2016**, DOI: 10.1039/c5cy01866h.
[74] Mintova, S.; Olson, N. H.; Valtchev, V.; Bein, T. *Science* **1999**, *283*, 958.
[75] Grand, J.; Awala, H.; Mintova, S. *CrystEngComm* **2016**, *18*, 650.
[76] Kirschhock, C.E.A.; Feijen, E.J.P.; Jacobs, P.A.; Martens, J.A. in *Handbook of Heterogeneous Catalysis, Volume 1*, Ertl, G.; Knozinger, H; Schüth, F.; Weitkamp, J. Eds. **2008**, pp. 160-178.

crystallites continue to grow as long as T-sources are available. It is important to note that there are complex dissolution-recrystallization processes occurring parallel to the actual crystal growth.[77]

If we consider zeolite syntheses more into details, it is noteworthy that the above statements are no law of nature, but rather a rule with many exceptions. It has indeed been reported that zeolites can be obtained without the use of a template,[78] or that zeolites can be produced without a solvent (water-free zeolitization of starting materials).[79] Hence, I will now expose the roles played by the different components during a classical zeolite synthesis.

T-sources: Different types of silica sources can be used in a zeolite synthesis, ranging from liquid silicate-esters,[80] to alkaline siliceous solutions[81] up to solid silica containing materials.[82] The interesting point using the latter strategy is to play with the above mentioned complex dissolution-recrystallization processes and thus the possibility to obtain hybrid, deposited materials on prestructured surfaces.[83] The silicon-source is considered to be more a governing factor than the aluminum source, since silica sources of different degrees of polymerization can be applied, while aluminum-sources usually readily dissolve. As aluminum-sources soluble aluminum salts are most frequently employed, but dissolved-recrystallized aluminum from an alumina support can lead as well to supported zeolites.[84]

Mineralizing agent: The mineralizing agent plays the role of the crystallization catalyst, dissolving the T-monomers from their respective sources and then decoordinating, while condensating to form nuclei and ultimately crystallites. The hydroxide anion (OH^-) or the fluoride anion (F^-) are mainly responsible for dissolving T-sources during zeolite syntheses. Hence pH plays a huge role during the hydrothermal synthesis.[85] In case of a synthesis in fluoride medium one needs to adapt properly the pH to neutrality to avoid competition between the two mineralizing agents.[86] The following bond energies indicate a stark discrepancy between the fluoride and hydroxide affinity towards the T-sources: Si-F: 565 $kJ.mol^{-1}$, Si-O: 452 $kJ.mol^{-1}$, (Si-F's bond is almost 2 % shorter than the Si-O bond: 1.63 Å) Al-O: 502 $kJ.mol^{-1}$ and Al-F: 675

[77] Maldonado, M.; Oleksiak, M. D.; Chinta, S. *J. Am. Chem. Soc.* **2013**, *135*, 2641.
[78] a) Ng, E.-P.; Chateigner, D.; Bein, T.; Valtchev, V.; Mintova, S. *Science* **2012**, *335*, 70. b) Awala, H.; Gilson, J.-P.; Retoux, R.; Boullay, P.; Goupil, J.-M.; Valtchev, V.; Mintova, S. *Nat Mater* **2015**, *14*, 447.
[79] Wu, Q.; Wang, X.; Qi, G.; Guo, Q.; Pan, S.; Meng, X.; Xu, J.; Deng, F.; Fan, F.; Feng, Z.; Li, C.; Maurer, S.; Müller, U.; Xiao, F.-S. *J. Am. Chem. Soc.* **2014**, *136*, 4019.
[80] Ivanova, S.; Lebrun, C.; Vanhaecke, E.; Pham-Huu, C.; Louis, B. *J. Catal.* **2009**, *265*, 1.
[81] Meng, X.; Xiao, F. *Chem. Rev.* **2014**, *114*, 1521.
[82] Kooyman, P. J.; Van der Waal, P.; van Bekkum, H. *Zeolites* **1997**, *2449*, 50.
[83] a) Ivanova, S.; Vanhaecke, E.; Dreibine, L.; Louis, B.; Pham, C.; Pham-Huu, C. *Appl. Catal. A Gen.* **2009**, *359*, 151. b) Ivanova, S.; Louis, B.; Ledoux, M.-J.; Pham-Huu, C. *J. Am. Chem. Soc.* **2007**, *129*, 3383. c) Jiao, Y.; Jiang, C.; Yang, Z.; Zhang, J. *Microporous Mesoporous Mater.* **2012**, *162*, 152. d) Jiao, Y.; Yang, X.; Jiang, C.; Tian, C.; Yang, Z.; Zhang, J. *J. Catal.* **2015**, *332*, 70. e) Ocampo, F.; Yun, H. S.; Pereira, M. M.; Tessonnier, J. P.; Louis, B. *Cryst. Growth Des.* **2009**, *9*, 3721.
[84] Lai, R.; Yan, Y.; Gavalas, G. R. *Microporous Mesoporous Mater.* **2000**, *37*, 9.
[85] Yang, S.; Navrotsky, A. *Chem. Mater.* **2002**, *14*, 2803.
[86] Serrano, D. P.; Grieken, R. Van *Microporous Mesoporous Mater.* **2001**, *46*, 35.

kJ.mol^{-1}.[87] Indeed, the T-F bond is stronger, which means that intermediate T-F monomeric species present and necessary during zeolites crystallization, are more stable than T-OH monomers in alkaline medium. Thus, the considered F-medium crystallization needs a higher lattice energy release, the main reason for the high quality crystals obtained, which are generally larger in size. According to Pokrovski *et al.* the formation of the T-O-T bond (Si-O-Al) becomes thermodynamically favoured at temperatures between 90 - 150°C. They performed an in depth study on the Si-O-Al dimer formation (lattice energies are not considered) in neutral to slightly acidic medium and evidenced the following free enthalpies of association: $\Delta G(25°C) = 14$ kJ.mol^{-1}, $\Delta G(90°C) = 2$ kJ.mol^{-1} and $\Delta G(150°C) = -9$ kJ.mol^{-1}.

Structure directing agent (SDA): The SDA's act as *templates*, classically possessing a positive charge they are thus interacting by electrostatic forces with the negatively charged T monomers. The latter self-assemble around the SDA's and condensate to nuclei and then crystallites under the impact of high temperature and pressure, autogeneous conditions during the hydrothermal synthesis. Various types of cations can be used on this purpose, from cheap and naturally occurring (alkali-) metal cations, up to designed organic cations. The latter are reported to be potentially designed in order to obtain new zeolite structures.[68]

It is important to summarise, in order to refer to what was stated in the section above, that none of the ingredients to synthesise a zeolite is expensive, relative to MOF's or other currently developed materials, and thus the resulting synthesis can be considered as cheap.

1.2.1. Natural Zeolite

Natural zeolites are occurring in volcanic regions on earth. Basically what is needed is naturally highly alkaline brines, able to dissolve silica species and high temperatures and pressures. Around forty naturally occurring zeolite structures have been uncovered.[41]

Figure 1-8. Natural Stilbite-zeolite, I saw in September 2014 in Austurland in eastern Iceland.

The harsh environment around volcanic hotspots amazingly not only hosts the *Thermus aquaticus* bacteria discovered in 1969, whose thermostable polymerase enzyme literally mutated the molecular biology sciences and allowed the evolution of bioengineering. [88] Indeed, the polymerase

[87] a) Benson, S.W. *J. Chem. Educ.* **1965**, *42*, 502. b) Luo, Y.R. *Bond Dissociation Energies* **2009**. presenting compiled data from NIST, NASA, CoDATA and IUPAC at 298.15 K (room temerature conditions). b) Luo, Y. R. *Comprehensive Handbook of Chemical Bond Energie*s, **2007** CRC Press, Boca Raton, FL.
[88] Brock, T.D.; Freeze, H. *J. Bact.* **1969**, *98*, 289.

chain reaction (PCR) of utmost importance in today's biosciences shares the same environment of evolution than today's highly engineered zeolite catalysts.

The natural zeolites are not really useful in catalysis applications due to their large number of defects and rather large crystallite sizes. They can be employed in large-scale ion exchange applications. For instance after the Fukushima nuclear disaster, local and natural clinoptilolite zeolite was used for $^{137}Cs^{+}$- capture.[89]

1.2.2. Different Synthesis Routes

As shown above we can distinguish between two different mineralizing agents, which are generally employed: the hydroxide anion is used in the so-called *alkaline route* and the fluoride anion dubs the *fluoride route*.

1.2.2.1. Alkaline Route

The alkaline-route is basically the reproduction in the laboratory under controlled conditions of what has happened in nature near the volcanic areas. This route is the most applied to produce zeolites at large and commercially relevant scales.

1.2.2.2. Fluoride Route

The fluoride route is the strategy employed to obtain highly crystalline materials exempted from defects.[90] As already indicated T-F bonds are stronger than T-O bonds and thus the main reason for the resulting high quality zeolites. The crystal growth of larger crystallites in fluoride medium is particularly subjected to Ostwald ripening phenomenon.[91] This effect, relies on the Gibbs-Thomson-effect described in the original words of the Nobel laureate of 1909 Wilhelm Ostwald *"da nach bekannten Prinzipien ein feines Pulver löslicher sein muß als ein grobes, ebenso wie kleine Tröpfchen einen größeren Dampfdruck haben als große.*" Freely translated: Based on well-known principles larger particles must be less soluble than smaller particles. Local concentration gradients favour the production of larger crystallites.

In addition to the fact that larger crystals may induce mass transfer limitations during catalytic applications, the fluoride route's main downside is the high toxicity and corrosion of fluoride, which renders it not easily applicable at large scale.[92]

[89] Ames, L.L. *The American Mineralogist*, **1960**, *45*, 689.
[90] a) Louis, B.; Kiwi-Minsker, L. *Microporous Mesoporous Mater.* **2004**, *74*, 171. b) Arichi, J.; Louis, B. *Cryst. Growth Des.* **2008**, *8*, 3999.
[91] a) Jorge, M.; Auerbach, S.M.; Monson, P.A. *J. Am. Chem. Soc.* **2005**, *127*, 14388. b) Chen, X.; Qiao, M.; Xie, S.; Fan, K.; Zhou, W.; He, H. *J. Am. Chem. Soc.* **2007**, *129*, 13305.
[92] Mitsui, G.; Dote, T.; Adachi, K.; Dote, E.; Fujimoto, K.; Shimbo, Y.; Fujihara, M.; Shimizu, H.; Usuda, K.; Kono, K. *Toxicol. Ind. Health* **2007**, *23*, 5.

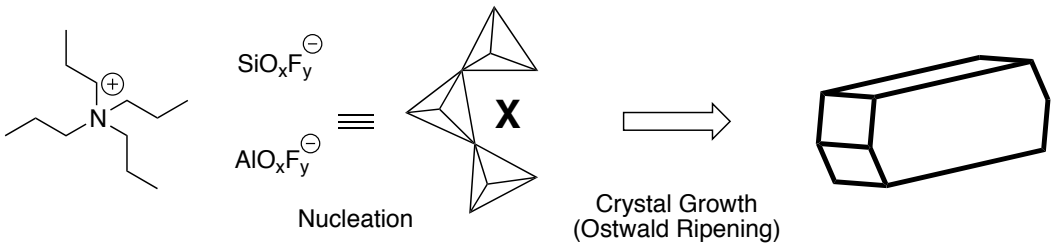

Figure 1-9. Simplified schematic representation of the fluoride assisted zeolite crystal growth.

1.2.3. Hierarchy

We have defined above the term hierarchical zeolites. It is important to note that different methods exist to introduce these so-called secondary or tertiary porosities. In general we classify them in two families: the constructive introduction of mesoporosity is called *bottom up* strategy, while destructive ones are baptized *top down* methods.

1.2.3.1. Bottom-up

The use of secondary, soft and hard templates, such as carbon nanotubes (CNT's), biomass, amines and surfactants,[93] has been reported multiple times, and associated to the creation, the "growth" of controlled mesoporosity.[94]

In addition to this, the use of macroporous supports (SiC, alumina, glass, Fe_xO_y, etc.) with a controlled growth of micro- (and meso-) pores containing zeolites on their surface can be considered as part of the bottom up strategy.[95]

1.2.3.2. Top-down

This method is in contrast to the aforementioned, a destructive and generally cheaper alternative where a synthesised microporous material is partly destroyed, chemically or physically, in order to create an adjacent mesoporosity. [96]

Such chemical or physical treatments are dubbed *post-treatments* and encompass the vastly used alkaline desilication, steam assisted dealumination,[97] to the more carefully applied

[93] A review: Chal, R.; Gérardin, C.; Bulut, M.; van Donk, S. *ChemCatChem* **2011**, *3*, 67. and a selection of articles covering this topic: a) Li, K.; Valla, J.; Garcia-Martinez, J. *ChemCatChem* **2014**, *6*, 46. b) Choi, M.; Cho, H. S.; Srivastava, R.; Venkatesan, C.; Choi, D.-H.; Ryoo, R. *Nat. Mater.* **2006**, *5*, 718. c) Kim, J.; Park, W.; Ryoo, R. *ACS Catal.* **2011**, *1*, 337.
[94] a) Pérez-Ramírez, J.; Christensen, C. H.; Egeblad, K.; Christensen, C. H.; Groen, J. C. *Chem. Soc. Rev.* **2008**, *37*, 2530. b) Zhao, X. S.; Su, F.; Yan, Q.; Guo, W.; Bao, X. Y.; Lv, L.; Zhou, Z. *J. Mater. Chem.* **2006**, *16*, 637.
[95] a) Jiao, Y.; Jiang, C.; Yang, Z.; Liu, J.; Zhang, J. *Microporous Mesoporous Mater.* **2013**, *181*, 201. b) Louis, B.; Reuse, P.; Kiwi-Minsker, L.; Renken, A. *Appl. Catal. A Gen.* **2001**, *210*, 103.
[96] Silaghi, M.; Chizallet, C.; Raybaud, P. *Microporous Mesoporous Mater.* **2014**, *191*, 82.
[97] Valtchev, V.; Majano, G.; Mintova, S.; Pérez-Ramírez, J. *Chem. Soc. Rev.* **2013**, *42*, 263.

fluoride etching,[98] but they reach also up to very sophisticated methods such as heavy ion bombardment for the creation of macropores.[99]

1.2.4. The ZSM-5 Zeolite

During this PhD-thesis, the synthesis, characterisation and application of ZSM-5 zeolite with the MFI-topology will stand out, thus I will introduce its peculiarities more into detail in this section. The framework structure of the ZSM-5 zeolite, the three dimensional network of channels is formed by 10 membered-rings. Commonly, we consider straight and sinusoidal pores. (**Figure 1-10**) The respective pore diameters are suitable for the accommodation of a variety of small organic molecules. Then, the Brønsted acid sites in ZSM-5 are reportedly stronger than for many other zeolites.[100] This particular combination of acidic properties and pore architecture enabled their use as solid acid catalyst in the oligomerization of light olefins,[101] the isomerization of aromatics[102] and the Methanol-To-Hydrocarbons (MTH) reaction,[103] to name just a few.

Many synthetic procedures reported the syntheses of highly crystalline zeolite ZSM-5 crystals.[104] For a better understanding of the chemistry of zeolite ZSM-5, large coffin shaped zeolite ZSM-5 crystals have been extensively studied as a model system.[105] Their interesting morphology and complex intergrown structure determine the accessibility of the crystalline interior and ability of reactants / products to reach / leave the active sites. In the recent years, one of the intriguing discussions is related to the exact three-dimensional structure of the zeolite intergrowth,[106] consisting of at least six individual subunits, and its impact on the diffusion and reaction of a large variety of probe molecules and catalytic reactions. Indeed, the examples comprise methanol-to-olefins (MTO),[107] and straining oligomerization reactions with furfuryl alcohol[108] and styrene derivatives.[109]

[98] Qin, Z.; Lakiss, L.; Gilson, J.; Thomas, K.; Goupil, J.; Fernandez, C.; Valtchev, V. *Chem. Mater.* **2013**, *25*, 2759.
[99] Valtchev, V.; Balanzat, E.; Mavrodinova, V.; Diaz, I.; Fallah, E. *J. Am. Chem. Soc.* **2011**, *133*, 18950.
[100] Xu, B.; Sievers, C.; Hong, B.; Prins, R.; van Bokhoven, J.A. *J. Catal.* **2006**, *244*, 163.
[101] Stöcker, M. *Microporous Mesoporous Mater.* **2005**, *82*, 257.
[102] a) Ahn, J. H.; Kolvenbach, R.; Neudeck, C.; Al-Khattaf, S. S.; Jentys, A.; Lercher, J. A. *J. Catal.* **2014**, *311*, 271. b) Ahn, J. H.; Kolvenbach, R.; Al-Khattaf, S. S.; Jentys, A.; Lercher, J. A. *Chem. Comm.* **2013**, *49*, 10584.
[103] Ilias, S.; Bhan, A. *J. Catal.* **2014**, *311*, 6.
[104] Jablonski, G.A.; Sans, L.B.; Gard, J.A. *Zeolites*, **1986**, *6*, 396.
[105] Nordvang, E. C.; Borodina, E.; Ruiz-Martínez, J.; Fehrmann, R.; Weckhuysen, B. M. *Chem. Eur. J.* **2015**, *21*, 1.
[106] a) Karwacki, L.; Kox, M. H. F.; de Winter, D. A. M.; Drury, M. R.; Meeldijk, J. D.; Stavitski, E.; Schmidt, W.; Mertens, M.; Cubillas, P.; John, N.; Chan, A.; Kahn, N.; Bare, S. R.; Anderson, M.; Kornatowski, J.; Weckhuysen, B. M. *Nat. Mater.* **2009**, *8*, 959. b) Hofmann, J. P.; Richard, M.; Jiang, T.; Chahine, G. A.; Schülli, T. U.; Meirer, F.; Weckhuysen, B. M. *Angew. Chem., Int. Ed.* **2016**, *55*, 7496. c) Ristanović, Z.; Hofmann, J. P.; Deka, U.; Schülli, T. U.; Rohnke, M.; Beale, A. M.; Weckhuysen, B. M. *Angew. Chem. Int. Ed.* **2013**, *52*, 13382.
[107] Mores, D.; Kornatowski, J.; Olsbye, U.; Weckhuysen, B. M. *Chem. Eur. J.* **2011**, *17*, 2874.
[108] Ristanović, Z.; Hofmann, J. P.; De Cremer, G.; Kubarev, A. V.; Rohnke, M.; Meirer, F.; Hofkens, J.; Roeffaers, M. B. J.; Weckhuysen, B. M. *J. Am. Chem. Soc.* **2015**, *137*, 6559.
[109] Ristanović, Z.; Hofmann, J. P.; Richard, M.-I.; Jiang, T.; Chahine, G. A.; Schülli, T. U.; Meirer, F.; Weckhuysen, B. M. *Angew. Chemie Int. Ed.* **2016**, *55*, 1.

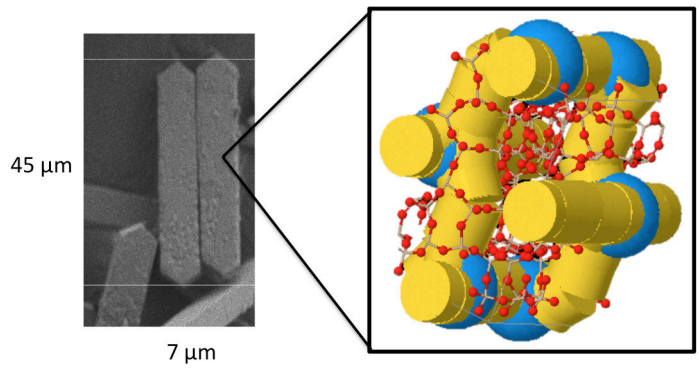

Figure 1-10: ***Sinister***: A home made H-ZSM-5 single crystal under scanning electron microscope (SEM). ***Rectus***: A ZSM-5 (MFI) crystallographic unit cell, presenting a three dimensional porosity. Two distinct pore types (yellow) sinusoidal ones (5.1 x 5.5 Å parallel to the crystalline a-axis) and straight ones (5.3 x 5.6 Å in the crystalline b-direction) from larger intersections (in blue: 6 - 8 Å).

Due to their crystallite size (100 x 20 x 20 μm^3) these large crystals have been optimal model catalysts for a variety of microscopy techniques. This topic has been extensively investigated by Weckhuysen's group in Utrecht and covered in numerous publications and the recent PhD-thesis of Z. Ristanovic.[110]

In the third chapter of this work, the production of large highly crystalline ZSM-5 material of an unprecedented quality, active in catalysis will be described. Hence, this material may be an interesting new model catalyst to investigate.

1.2.5. Characterisation Techniques: No ONE mighty Technique!

In the application of zeolites in catalysis the following is frequently seen: a new catalytic reaction is generally tested with a series of different commercially available zeolites, in order to have an idea which type of parameters are crucial for the given reaction. This general screening is then followed by a thorough determination and eventual adaptation, or adjustment of these parameters in order to obtain a desired catalyst. The only way to be able to procede such a feedback-looped approach is to get as many information by characterisation on the tested materials as possible. Unfortunately, there is no one mighty technique, which may give all the sought information, but a combination of various X-ray diffraction, spectroscopic, microscopic, gas-sorption and titration techniques lead to a somewhat complete picture of a considered catalyst. The characterisation techniques used in the frame of this work are described in detail in Chapter 2. In order to understand what the catalyst is doing during a reaction numerous *in situ* and *ad operando* experiments are currently developed.[111]

[110] Ristanovic, Z. Zeolite Chemistry Studied at the Level of Single Particles, Molecules and Atoms, **2016**.
[111] a) Mores, D.; Kornatowski, J.; Olsbye, U.; Weckhuysen, B. M. *Chem. Eur. J.* **2011**, *17*, 2874. b) Kerssens, M. M.; Sprung, C.; Whiting, G. T.; Weckhuysen, B. M. *Microporous Mesoporous Mater.* **2014**, *189*, 136. c) Ristanović, Z.; Hofmann, J. P.; De Cremer, G.; Kubarev, A. V.; Rohnke, M.; Meirer, F.; Hofkens, J.; Roeffaers, M. B. J.; Weckhuysen, B. M. *J. Am. Chem. Soc.* **2015**, 150413104838006.

Now considering ZSM-5 zeolites, which will be deeply studied in this PhD-thesis: the ability to synthesise well defined zeolite-crystals and to tune their distinct properties such as their Si/Al-ratio, the architecture of their microporous voids, according to the application is without parallel in heterogeneous catalysis.[112] I believe that the benefits of using well-defined single crystalline zeolite samples are mostly related to the fundamental understanding of catalytic processes occurring in zeolites. However, we will see in Chapter 3 that single crystalline zeolites can also be of true catalytic value. In space- and time-averaged experiments, for instance carried out in a catalytic bed, many details on diffusion, sorption and catalysis are either lost or very difficult to obtain. In many cases it is important to determine whether the catalysis is taking place in the microporous network or only close to the external surface. In the case of complementary porosities present in one catalyst it is also important to distinguish in which channels / cages the reaction is occurring. Lastly, the role of defects during catalysis is important to be investigated; it shall never be underestimated, especially when dealing with large crystals.[113]

1.3. Catalytic Reactions of Potential Industrial Relevance

In our group, we try to focus on the development and improvement of reactions, which are of industrial relevance. Thus, we try to design catalysts on multiple scales: from the active site, *i.e.* a naked proton, via the crystal its shape and its porosity, up to the design of the reactor with the coating of catalytically active materials on structured, reactor-compatible and inert supports.

The main project during the last three years was the deeper understanding of the complex, but very relevant Methanol-To-Olefins reaction catalysed by tailor made H-ZSM-5 zeolites. My PhD-thesis will be organized in two main chapters, with first the MTO-part and then a summary of the rather successfully treated side-projects. The latter are related to each other in terms of a continuous improvement approach and in more general terms, my motivation in treating them was *carbon upgrading*, the idea to add efficiently value to carbon using zeolites as catalysts, in order to infinitesimally help in the creation of a sustainable carbon cycle. The interested reader may have a glance at Sels *et al.*'s recent and exhaustive review of recent developments in the use of zeolites and zeolite-like materials in catalysis and other areas.[114]

1.3.1. Methanol-To-Olefins (MTO)

In the last decades, a great deal of interest has been devoted to the replacement of fossil fuels, due to their supposed impoverishment, or at least the increasingly difficult access to their fossil resources. In this perspective and with the development of the new concept of “methanol economy” introduced by G. Olah, methanol has become a very interesting alternative to fossil

[112] Boudart, M. *Chem. Rev.* **1995**, *95*, 661.
[113] Schoonheydt, R. A. *Angew. Chem., Int. Ed.* **2008**, *47*, 9188.
[114] Sels, B.; Kustov, L. *Zeolites and Zeolites-like Materials*, **2016**, Elsevier.

energies. Indeed, this molecule is largely investigated as hydrogen storage molecule, CO_2-reduction product,[115] is currently easily synthesised from syn-gas and what is interesting for us it can be converted into hydrocarbons when in contact with zeolites at high temperatures as it is depicted on **Figure 1-11**. Hence, the methanol to hydrocarbons (MTH) reaction and in particular the methanol to olefins (MTO) process are new key steps for the production of light olefins for the polymer industry but also for bulk chemistry applications and gasoline as a side product.[116]

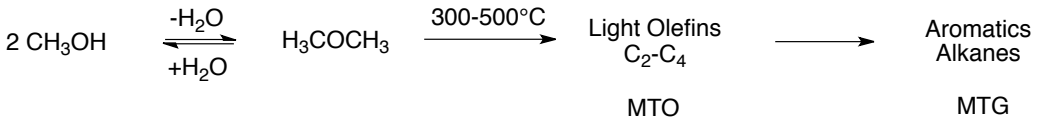

Figure 1-11. General reaction scheme for the Methanol-To-Hydrocarbons reaction.

In the later chapter three the MTO-process will be introduced in further detail. Thus, this introduction summarises different strategies for the development of an efficient MTO catalyst, the "evolution" of the MTO mechanisms, and also the recent studies in the design of a ZSM-5 catalyst.

First of all, it is important to note that the MTO-mechanism is utterly complex and a great deal of interest and a long time of academic research has been spent in order to increase our understanding of the elementary reactions occurring during this process. Indeed, as I mentioned the SCAR-strategy earlier, this continuous improvement approach strongly relies on understanding elementary steps and the ability to discriminate a non-relevant from a key intermediate step. Thus, the increase of the deep knowledge on a process results in the long run in an optimised catalyst and ultimately a better process.

I quote from a recent summarizing review by Bhan *et al.*[117], there are "six major chemistries involved in the hydrocarbon pool mechanism for MTH - olefin methylation, olefin cracking, hydrogen transfer, cyclization, aromatic methylation, and aromatic dealkylation."

The MTH reaction was discovered by accident in the Mobil Central Research Laboratories in the early 70's, while they tried to react methanol and isobutane to produce MTBE (methyl-*tert*-butylether) over acidic zeolites, as their newly discovered ZSM-5 zeolite.[118] Later the Methanol-To-Gasoline (MTG) process knew a certain success and was commercialized in New-Zealand. The MTG-reaction ran there from 1986 onwards producing 600 kt of gasoline per year, a third of

[115] Walspurger, S.; Haije, W. G.; Louis, B. *Isr. J. Chem.* **2014**, *54*, 1432.
[116] Wei, Y.; Yuan, C.; Li, J.; Xu, S.; Zhou, Y.; Chen, J.; Wang, Q.; Xu, L.; Qi, Y.; Zhang, Q.; Liu, Z. *ChemSusChem* **2012**, *5*, 906.
[117] Ilias, S.; Bhan, A. *ACS Catal.* **2013**, *3*, 18.
[118] a) Chang, C.D.; Lang; W.H.; Silvestri, A.J. *Manufacture of light olefins*, US4062905, **1977**. b) Chang, C.D.; Silvestri, A.D. *ChemTech*, **1987**, 624-631. c) Chang, C.D. *Catal. Rev. Sci. Eng.* **1983**, *25*, 1. d) Hutchings G.J.; Hunter, R. *Catal.Today* **1990**, *6*, 279. e) Chang C.D. *Catal. Rev. Sci. Eng.* **1984**, *113*, 102. f) Chang. C.D.; Chu, C.T.W.; Socha, R.F. *J. Catal.* **1984**, *86*, 289.

the nations demand. [119]. In the long term however, oil prices on the stock market dropped again and rendered this technology unprofitable, so that only the methanol-producing unit was kept in service.

The academic interest in this reaction however, never faded and nowadays the MTO-technology has become profitable. Herein I would like to focus on the evolution of the mechanistic understanding of this complex reaction.

The long debate on the formation of the first carbon-carbon bond during this reaction was led a long time by Haw and co-workers, [120] resulted in the emergence of more than 20 different possible pathways for the formation of the initial C-C bond.[121] It is the very recent contribution of Lercher's group that casted even more light on this shady domain.[122] They discovered indeed, that "infinitesimal" small quantities (below the detection limits of certain instruments) of carbon monoxide may act as the nucleophilic species needed in this first elementary step (cf. **Figure 1-12** in red).

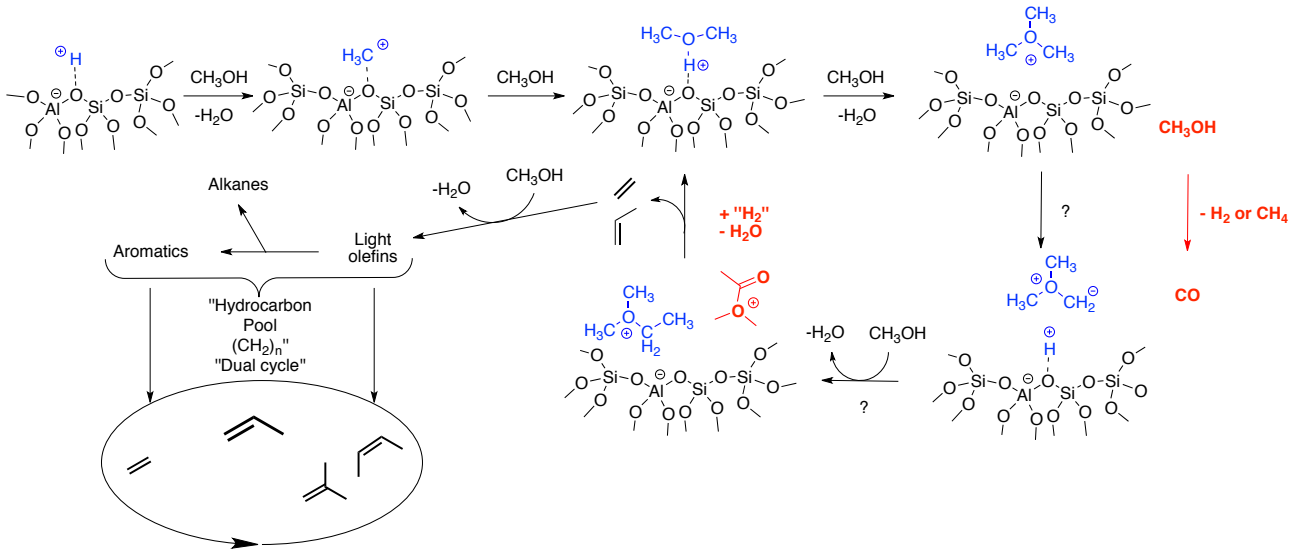

Figure 1-12. The long debate on the formation of the first carbon-carbon bond: more than 20 different possible mechanisms have been proposed, in blue is represented the "ylide route" and in red the very recently reported "carbon monoxide route".

[119] Spivey, J.; Dooley, K.M.; Han, Y.-F. *Catalysis*, Vol. 26, **2014**, RSC-Publishing.
[120] a) Haw, J. F. *Phys. Chem. Chem. Phys.* **2002**, *4*, 5431. b) White, J. L.; Beck, L. W.; Haw, J. F. *J. Am. Chem. Soc.* **1992**, *114*, 6182.
[121] a) Stöcker, M. *Micropor. Mesopor. Mater.* **1999** *29*, 3. b) Štich, I.; Gale, J. D.; Terakura, K.; Payne, M. C. *J. Am. Chem. Soc.* **1999**, *121*, 3292.
[122] Liu, Y.; Müller, S.; Berger, D.; Jelic, J.; Reuter, K.; Tonigold, M.; Sanchez-Sanchez, M.; Lercher, J. A. *Angew. Chemie Int. Ed.* **2016**, *55*, 1.

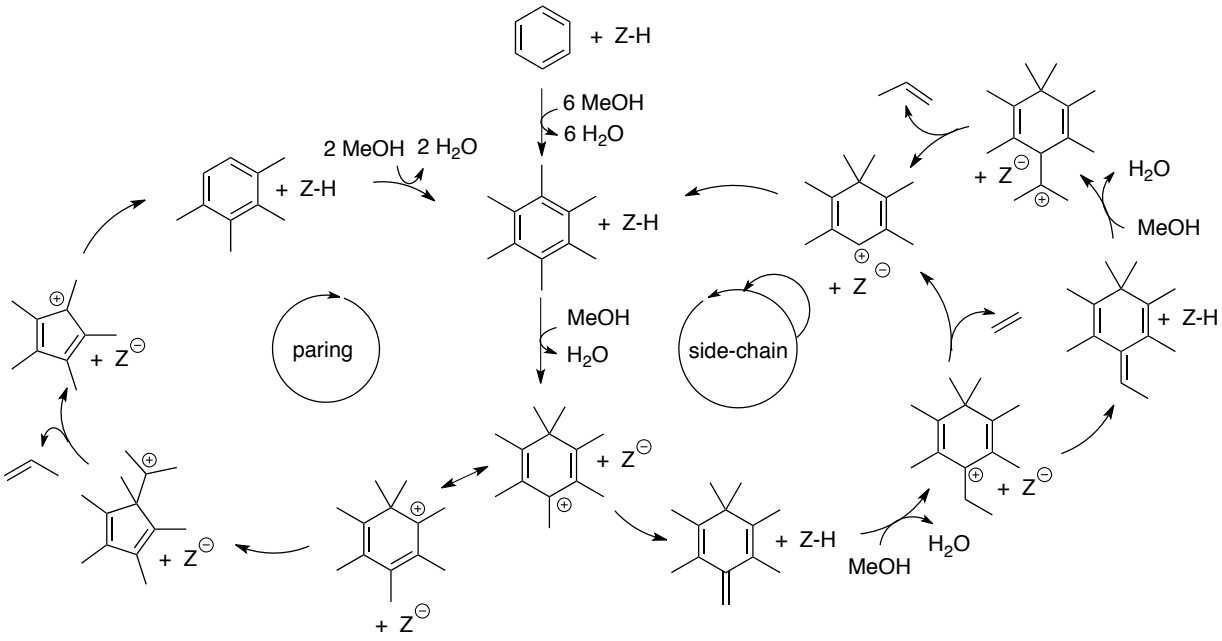

Figure 1-13. The aromatics based hydrocarbon pool (HCP) autocatalytic cycle, which favours the production of light olefins, combined from the mechanistic insights of Mole,[123] Langner,[124] Kolboe,[125] and Sullivan,[126] described in Haw's review[127] and redrawn from Lesthaeghe *et al.*[128]

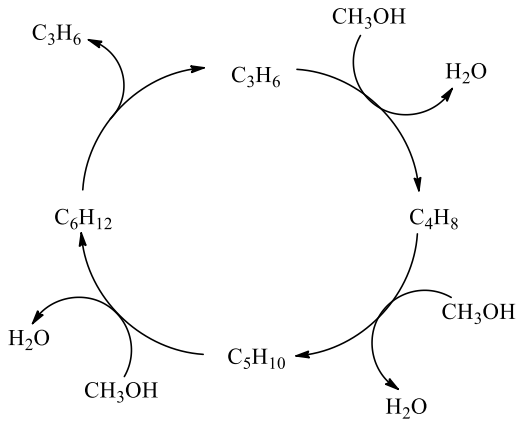

Figure 1-14. Olefins inter-conversion redrawn from M. Bjørgen *et al.*

Subsequently to this first C-C bond formation, or the induction period, an autocatalytic regime takes over,[129] during which shape selectivity, respectively the nature of the used zeolite plays a key role. As represented in the **Figure 1-13** an aromatic based hydrocarbon pool (HCP) has been initially proposed by Mole *et al.*, and then further developed to its current understanding by the groups of Langner, Kolboe and Sullivan. In brief, the aromatics HCP based mechanism proposes different ways of hybrid organic-inorganic catalysts (Zeolite-O^-(aromatics-H)$^+$ complexes) generating olefins in a continuous manner. Indeed, two main routes have been reported, the *side chain* growth and

[123] Mole, T.; Bett, G.; Seddon, D. *J. Catal* . **1983**, *84* , 435.
[124] Langner, B. E. *Appl. Catal.* **1982**, *2* , 289.
[125] a) Kolboe, S. *Appl. Catal.* **1986**, *40* , 711. b) Dahl, I. M.; Kolboe, S. *Catal. Lett.* **1993**, *20*, 329. c) Dahl, I. M.; Kolboe, S. *J. Catal.* **1994**, *149* , 458-464. d) Dahl, I. M.; Kolboe, S. *J. Catal.* **1996**, *161*, 304. e) Mikkelsen, O.; Ronning, P. O.; Kolboe, S. *Microporous Mesoporous Mater.* **2000,** *40*, 95. f) Arstad, B.; Kolboe, S. *Catal. Lett.* **2001**, *71*, 209.
[126] Sullivan, R. F.; Egan, C. J.; Langlois, G. E.; Sieg, R. P. A *J. Am. Chem. Soc.* **2001**, *123*, 8137.
[127] Haw, J. F.; Song, W.; Marcus, D. M.; Nicholas, J. B. *Acc. Chem. Res.* **2003**, *36*, 317.
[128] Lesthaeghe, D.; Horré, A.; Waroquier, M.; Marin, G. B.; Van Speybroeck, V. *Chem. Eur. J.* **2009** *15,* 10803.
[129] Patcas, F. *J. Catal.* **2005**, *231*, 194.

cracking cycle occurs in large pore zeolites, while the aromatics *paring* route is supposed to occur rather in space limited medium pore zeolites.

Later Bjørgen *et al.* found that as represented first in **Figure 1-14** olefins can interconvert over acidic zeolites. As depicted in **Figure 1-15**, they showed that depending on the zeolite structure used, the above mentioned aromatics based HCP mechanism running in large pore, for instance SAPO-34 zeotype catalyst, can be in competition with an olefins based catalytic cycle, which is mainly occurring in small pore zeolites such as ZSM-22.[130]

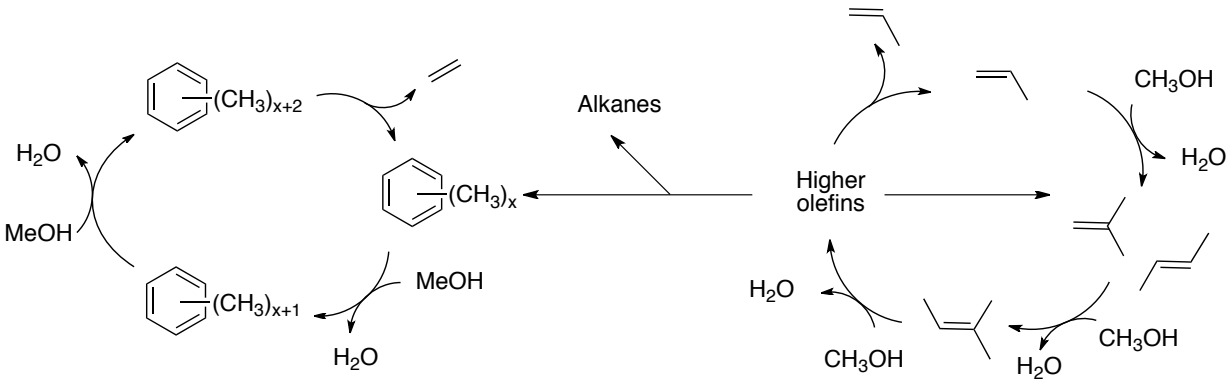

Figure 1-15. Dual cycle concept as it was proposed by M. Bjørgen *et al.*[130]

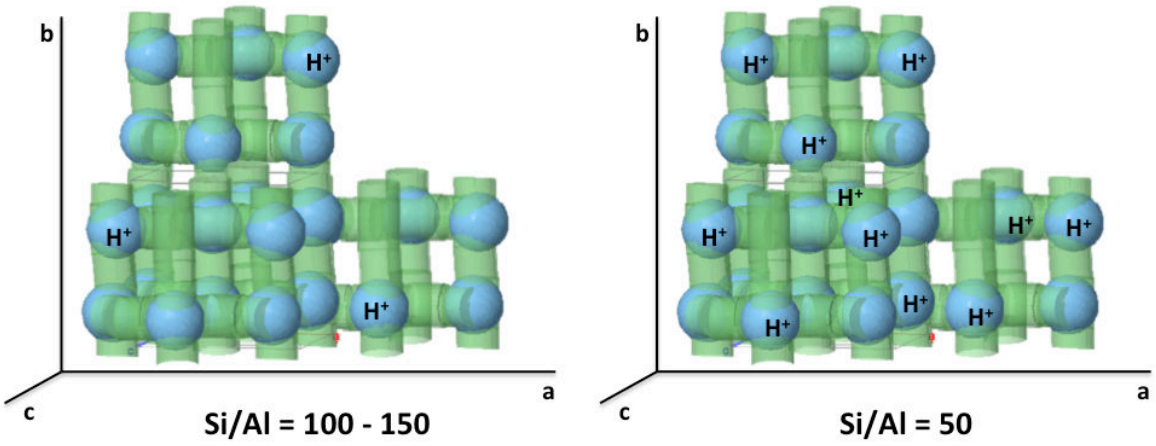

Figure 1-16. Different acid site dispersities modelled for a 4 unit-cell MFI-type zeolite. ***Sinister*** Acid sites are far one from another for SAR = 100 - 150 typically leading to an olefins cracking catalytic cycle. ***Rectus*** Acid sites in close vicinity for a SAR = 50 favouring the aromatics based HCP mechanism.

The particular porous topology of ZSM-5 zeolites; medium pore sized channels and larger intersections are expected to lead to a strong competition between both cycles.

Indeed, this particular and vastly used zeolite can be designed in order to favor the aromatics based or the olefin cracking based cycle. For instance, a high acid site density leading

[130] Bjørgen, M.; Svelle, S.; Joensen, F.; Nerlov, J.; Kolboe, S.; Bonino, F.; Palumbo, L.; Bordiga, S.; Olsbye, U. *J. Catal.* **2007**, *249*, 193.

to in turn close acid sites and frequently a high content of structural defects is favouring the aromatics based cycle. Thus the inversely conceived zeolites exhibiting a low acid site density combined to a high crystalline quality is improving the occurrence of the olefins based cycle.

These two types of zeolites and two types of mechanisms lead to different product distributions; the aromatics based HCP leads to high concentrations of ethylene and aromatics in the product stream, while among the products of the olefin based cycle mainly light olefins and to a major part propylene are detected.

Finally, I would like to redirect the reader at this point to Chapter 3 dealing with the herein obtained results on this topic; the synthesis and characterisation of large, perfect and single-crystalline H-ZSM-5 zeolites, which have proven to be very competitive Methanol-To-Propylene (MTP)-catalysts. The counterintuitive behaviour of these large crystals in terms of the absence of mass transfer limitations has led to several attempts of rationalising the observed phenomena.

1.3.2. Carbon Upgrading and Green Chemistry

In the same ideological concept than the methanol economy, and in parallel to the very current interest in the limitation in carbon dioxide emissions, I imagined linking my other treated subjects in the larger frame of a *carbon upgrading* concept.

According to, for instance Styring *et al.* we do already have the technological potential of leading totally carbon neutral lives and to install a zero-carbon economy, or better a cyclic carbon economy.[131] However, due to political pressures, lobbying and the resulting cheap prices of fossil resources, we are still running the race of "burning" these resources in an accelerating manner. Indeed burning, since in the long run every carbon atom, even though recycled once or twice, ends up as the thermodynamically most stable CO_2, and in an accelerating manner since our global economy is currently based on a growth dependency.

It has been proven however, that it is possible to tackle this economic and political inertia by proposing cost efficient alternatives, avoiding the necessity of subsidies.[132] As a general alternative concept one may think about efficient *carbon upgrading*. In such a general concept, green chemistry,[133] would largely exceed the current target of a sustainable chemistry. In fact in such a scenario green chemistry would play a key role in the development of a sustainable or cyclic economy based on efficient *carbon upgrading*.

In the close future, it will be possible to produce dihydrogen in a sustainable manner by photocatalytic water splitting reactions. Then it is possible to directly convert, captured CO_2 to its hydrogenated C_1-counterparts; formic acid (HCOOH), formaldehyde (H_2CO), methanol (CH_3OH)

[131] Styring, P.; Quadrelli, E.A.; Armstrong, K. *Carbon Dioxide Utilisation, Closing the Carbon Cycle*, **2014**, Elsevier.
[132] Jacobson, M. Z.; Delucchi, M. A. *Energy Policy* **2011**, *39*, 1154.
[133] Sheldon, R. A. *Green Chem.* **2014**, *16*, 950.

and methane (CH_4).[115] The methanol economy is based on a selective and cheap production of methanol, which is currently not easily achieved if starting from CO_2, proven by the rather humble success of G. Olah's inspiring demonstration plant in Iceland; Carbon Recycling International.[134] Currently, it is efficiently produced from syn-gas or met-gas (CO and 2 equivalents of H_2). Hence at the moment, the methanol economy is presenting a gap to become part of a more general *carbon upgrading*. Processes such as MTP are commercialized and competitive in the production of propylene from methanol,[135] as compared to the classic production by cracking the naphta fraction of fossil oil.[136] Nonetheless, as long as the used methanol is produced by the gasification of Chinese coal to met-gas,[137] such processes are not part of *carbon upgrading*.

Currently, CO_2 in its oxidation state of C^{+IV} can be used in polyurethane industry, whilst the potential use in terms of tonnage is far off the true CO_2-emissions.[138] Formic acid (C^{+II}) can be easily, selectively and competitively obtained from CO_2 and is used in bulk chemistry or as H_2-carrier.[139] In my opinion the potential of this molecule is currently underestimated, since it is only produced at a yearly < 1 Mt-scale. it is widely studied as H_2-storage and carrier molecule, however it can also be used as a "liquid hydrated carbon monoxide"-source.[140] Therefore, this easily accessible molecule may act as a hybrid syn-gas (CO, H_2) liquid phase storage and carrier platform in the near future. Formaldehyde (C^0) is generally avoided as a product at considerable large scale due to its high toxicity. Highly reduced methanol (C^{-II}) is indeed the key molecule for the methanol economy and remains obviously a target molecule of choice in terms of its further use in MTH-processes, but as well as H_2-storage and carrier in fuel cells. It is already produced, albeit mainly from natural gas and coal, at a yearly > 50 Mt-scale with a forecasted annual growth of 4 %.[141] Methane, the totally reduced (C^{-IV}) product from CO_2 is still considered as a potent molecule in a Power-to-Gas concept,[142] in which superfluously produced energy by nuclear sources or irregularly produced Wind, Water and Solar (WWS) electricity may be converted and stored in the chemical bonds of the methane molecule. The advantage of this concept is that methane can be fed in the already available natural gas-infrastructure.[115]

---

[134] Progress of this inspiring project can be followed on www.carbonrecycling.is, last checked in July **2016**.
[135] Koempel, H.; Liebner, W.; Ag, L.; Main, D.-F. *Nat. Gas Convers.* **2007**, 261.
[136] Vogt, E. T. C.; Weckhuysen, B. M. *Chem. Soc. Rev.* **2015**.
[137] van Dyk, J. C.; Keyser, M. J.; Coertzen, M. *Int. J. Coal Geol.* **2006**, *65*, 243.
[138] Maciel, M.; Louis, B. *Catal. Remediat. Environ. Concerns* **2013**, 533.
[139] a) Schuchmann, K.; Müller, V. *Science* **2013**, *342*, 1382. b) Chapovetsky, A.; Do, T. H.; Haiges, R.; Takase, M. K.; Marinescu, S. C. *J. Am. Chem. Soc.* **2016**, jacs.6b01980.
[140] Supronowicz, W.; Ignatyev, I.; Lolli, G.; Wolf, A.; Zhao, L.; Mleczko, L. *Green Chem.* **2015**.
[141] Aasberg-Petersen, K.; Stub Nielsen, C.; Dybkjaer, I.; Perregaard, J. *Large Scale Methanol Production from Natural Gas, Haldor-Topsøe*. and The annual report of the Methanex company, **2014**: https://www.methanex.com/sites/default/files/investor/annual-reports/Methanex-Annual-Report-2014.pdf
[142] Götz, M.; Lefebvre, J.; Friedemann, M.; Manuel, G.; Graf, F.; Bajohr, S.; Reimert, R.; Kolb, T. *Renew. Energy* **2016**, *85*, 1371.

Interestingly, as shown in the **Figure 1-17** zeolites Brønsted acidic or doped with metals are playing a key role in each step of the *carbon upgrading* ideology. **Figure 1-18** shows the economic potential of such an ideology, and the room for improvement becomes visible if we consider the different scales: even though the production of methanol and formic acid is rapidly growing it is not yet facing the extent of the current CO_2 emissions estimated at yearly Gt-scales. I calculated the value addition per carbon atom at the different steps in chemistry. Interestingly the value of carbon dioxide sourced carbon is potentially increased by multiple orders of magnitude, and this already at the first steps of this sequential approach. Today's limitation is depicted in red, the price for hydrogen, which can however be considered to decrease substantially in the near future.[143] Indeed, analogously to the Power to Gas idea with methane, *Air Liquide* is leading the industrial development of a Power to Hydrogen concept. Moreover, important scientific advances in photochemical water splitting (photocatalytic H_2-production) are regularly reported. M. Graetzel, for instance, is expecting a true competition between these technologies.[144]

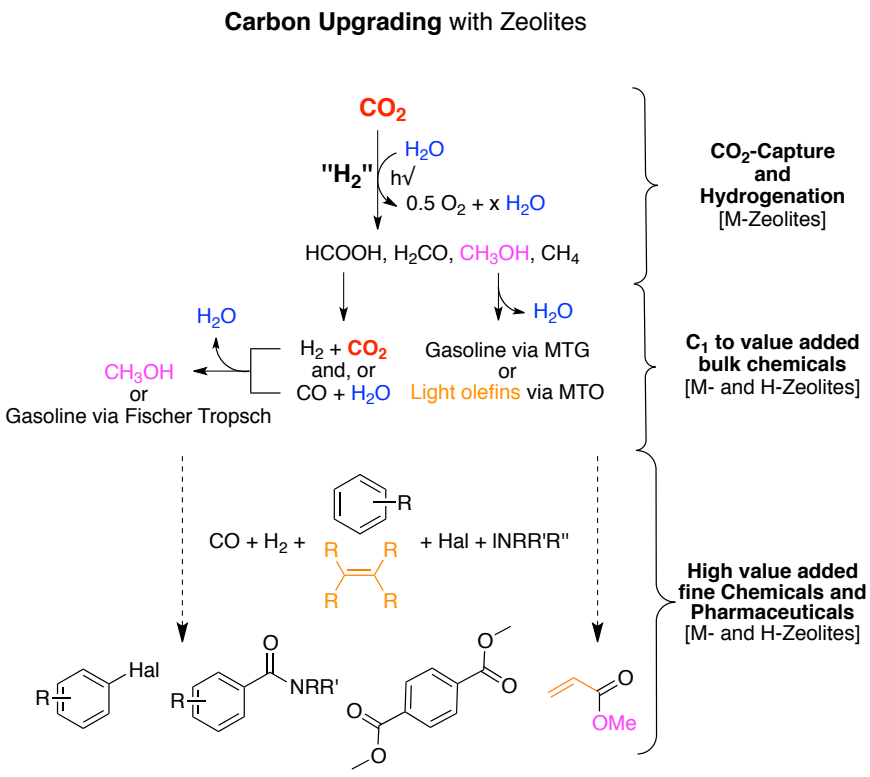

Figure 1-17. Schematic representation of *Carbon Upgrading*: from CO_2 to fine chemicals and pharmaceuticals, and the potential use of zeolites (metal-doped M-Zeolite or Brønsted acidic H-Zeolite) in the intermediate steps.

[143] Large companies such as Air Liquide are "quietly" paving the way for a cost-efficient H_2-economy https://www.airliquide.com/connected-innovation/hydrogen-quiet-revolution

[144] Jingshan, L.; Jeong-Hyeok, I.; Mayer, M. T.; Schreier, M.; Nazeeruddfn, M. K.; Nam-Gyu, P.; Tilley, S. D.; Hong Jin, F.; Gratzel, M. *Science* **2014**, *345*, 1593.

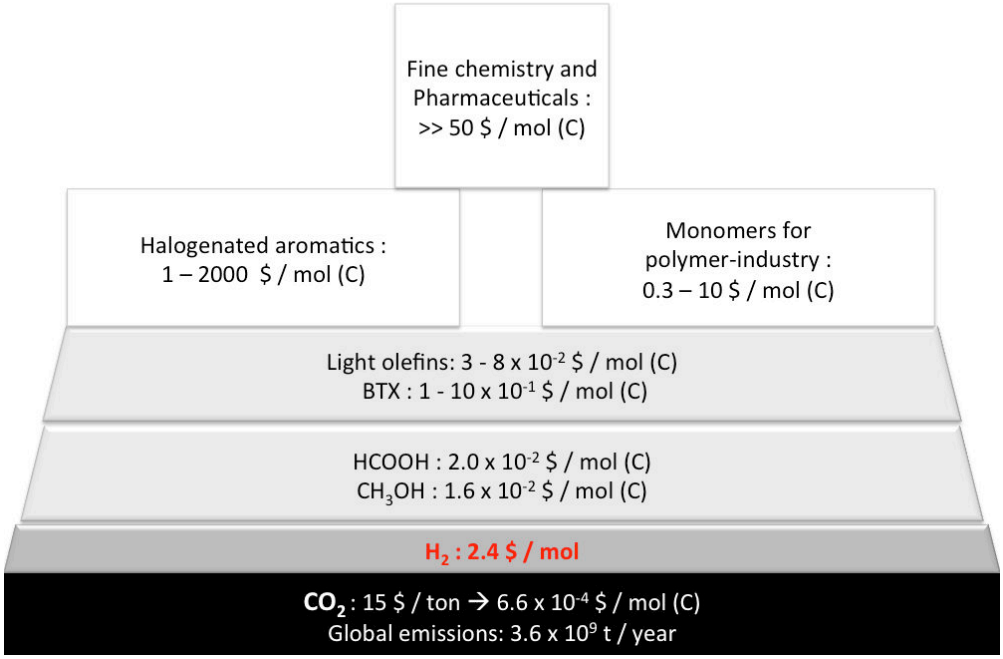

Figure 1-18. Pyramidal representation of the potential economic impact of *carbon upgrading,* the value per carbon atom with today's chemistry can be multiplied by up to 6 orders of magnitude. Prices were estimated using the CO_2-price forecast data,[145] and large-scale chemistry manufacturer data.[146]

Ultimately, the fourth chapter of this thesis gives more insight into the subjects concerning this big picture of sequentially and efficiently adding value to prime carbon building blocks.

[145] Luckow, P.; Stanton, E. A.; Fields, S.; Biewald, B.; Jackson, S.; Fisher, J.; Wilson, R. *2015 Carbon Dioxide Price Forecast*, **2015**, Synapse Energy Economics Inc. Cambridge, Massachusetts.

[146] The price evolution of large scale produced chemicals is constantly updated and can be checked on the following websites: https://www.alibaba.com/products/benzene.html a) Benzene: Yonghua Chemical Technology (Jiangsu) Co., Ltd.; b) Methanol: Shijiazhuang Xinlongwei Chemical Co., Ltd. c) Formic acid: Zibo Pulisi Chemical Co., Ltd.

Chapter 2 Experimental Part

ABSTRACT This chapter will expose the materials and methods used to accomplish the present work, from the zeolite syntheses to their thorough characterisation, their use in different catalytic reactions up to some attempts of modelling and simulation in order to better understand the observed results.

2.1. Zeolite Syntheses

2.1.1. Alkaline Biomass

Prior to the zeolite synthesis 300 mg of sugar cane bagasse are treated with an alkaline solution (150 mL, NaOH, 0.1 M, $pH_{0,\ measured}$ = 11) for 24 h at r.t. and under vigorous stirring 770 rpm. After the reaction the pH value of the solution dropped to $pH_{1\ measured}$ = 8 - 9 and the final mass of dry fibers decreased to 160 mg. Thus 140 mg of organic molecules have been hydrolized and solubilized in the alkaline solution.

The addition of this solution, which contained extracted organic compounds from the bagasse was performed during the ageing step.

2.1.1.1. Biomass templated Zeolite Syntheses

The synthesis exhibited the typical following molar composition: Al_2O_3: SiO_2: TPA: H_2O = 1; 53.6; 16; 6666 ($NaAlO_2$: TEOS: TPAOH: NaCl: H_2O 1; 26.8; 8; 13; 3333). The gel was aged during 1h at room temperature under stirring (700 rpm). Afterwards, the solution was poured in a Teflon-lined stainless steel autoclave (60 mL effective volume) and heated at 443 K during 66 h. After this hydrothermal treatment, the solution was filtered and washed with distilled water several times. The solid was dried overnight at 388 K. The solid, obtained in its sodium form, was ion-exchanged three times in a 1M NH_4NO_3 aqueous solution at 353 K under stirring for 1h (per exchange step). After, filtration and drying, the ammonium-form was calcined at 823 K for 15 h to produce acidic H-MFI zeolite.

Table 2-1. Synthesis conditions of the various tested conditions.

Entry	Zeolite	Si/Al Gel	Ageing [h]	Syn Time [h]	Syn. Temp. [°C]	Si-source	Primary template	Secondary template
1	H-ZSM-5_{72}	26.8	1	65	170	Aerodisp w7520n	TPAOH	Sugar cane bagasse basic hydrolysate (SCBBH)
2	H-ZSM-5_{18}	13.4	1	65	170	Aerodisp w7520n	TPAOH	SCBBH
3	H-ZSM-$5_{8\ Fail}$	6.7	1	65	170	Aerodisp w7520n	TPAOH	SCBBH
4	H-ZSM-5_{13}	8.9	1	65	170	Aerodisp w7520n	TPAOH	SCBBH
5	H-ZSM-5_{8}	6.7	1	144	170	Aerodisp w7520n	TPAOH	SCBBH

2.1.1.2. Investigating the Supramolecular Impact of Biomass on the Self Assembly during Crystallization[147]

Water crystallization with biomass related inhibition / structuration: Four different samples (5 mL each) were prepared in sealed 10 mL vials; first a reference solution consisted in a diluted NaOH aqueous solution at pH 10-12, then a sugarcane bagasse hydrolysate at pH 14 was prepared as described above (as used in LTA, LTL and GIS, FAU syntheses). The third and fourth sample were bagasse and lignin hydrolysates at pH 10-12, as used in MFI syntheses, and whose preparation occurred as described above. Freeze experiments were carried out as follows: Samples were cooled down to 279 K during two hours in order to start the freezing at isothermal conditions. Then, the samples were put into a deep freeze chamber at 255 K. Crystallization was observed / filmed in the deepfreeze chamber with a Nikon Coolpix AW130, which allowed the time-lapsing of the freeze experiment enabling the estimation of the respective crystallization durations.

[147] Louis, B.; Gomes, E. S.; Coelho, T.; Lutzweiler, G.; Losch, P.; Silva, A. V; Faro, A. C.; Romero, T.; Osman, M. Ben; Balanqueux, A.; Bernardon, C.; Pereira, M. M. *Nanosci. Nanotechnol. Lett.* **2016**, *8*, 1–7.

2.1.2. Fly Ash[148]

Acid leaching of fly ash and extraction of iron: The acid leaching method used in this study was adapted from the one proposed by Liu *et al*. [7] Fly ash (FA) (30 g) was mixed with 60 mL of sulphuric acid (95-99 %) in a 100 mL Parr bomb digestion vessel, which was placed in a pre-heated oven at 250 °C for 4 h. Thereafter, the digestion vessel was removed from the oven and allowed to cool before handling. The slurry was mixed with 180 mL of de-ionized water in a 500 mL beaker. The mixture was heated at 85 °C while stirring for 30 min, filtered while hot and the FA residue was washed three times with 100 mL of boiling de-ionized water. The filtrate was retained to recover Al. Iron particles accumulated onto the magnetic bar during stirring were extracted and dried overnight in an oven at 60 °C. The FA residue, called PL, was dried at 80 °C overnight in an oven and used in the synthesis of ZSM-5 zeolite.

Extraction of aluminium: All the filtrates obtained during the washing of PL were transferred to a volumetric flask and adjusted to 500 mL by adding de-ionized water. The solution was transferred to a beaker and heated without stirring at 115 °C. It was then removed from its heating source and allowed to naturally cool to room temperature, during which a precipitate (precipitate 1) was formed, filtered, air dried overnight and then calcined at 850 °C for 2 h. The remaining filtrate was allowed to stand for 2 days. Upon which, a white precipitate (precipitate 2) was formed, filtered, air dried overnight and then calcined at 850 °C for 2 h.

Synthesis of ZSM-5 from fly ash: PL (0.75 g) was mixed with 1 g of TPABr, 0.75 g of fumed silica, 0.25 g of NaOH in 20 mL of de-ionized water. The obtained gel, with a molar ratio of Al_2O_3: SiO_2: TPA: H_2O = 1; 11.6; 1.8; 613.8 was stirred in a closed Teflon liner at 25 °C for 2 h. The Teflon liner was then placed in its digestion vessel and was put in a pre-heated oven at 160 °C for 72 h. Thereafter, the digestion vessel was removed from the oven and allowed to cool down. The solid product was filtered, washed with de-ionized water and dried in an oven at 70 °C. The dried solid was put in a porcelain crucible and calcined in a furnace under the atmospheric pressure at a heating rate of 15 °C/min and held at 550 °C for 3 h. The solid was taken out of the furnace and was allowed to cool down. Then, it was mixed with de-ionized water and stirred for 5 min in order to remove the calcined TPABr. It was then filtered, washed with de-ionized water and dried in an oven at 70 °C. Na-ZSM-5 zeolite was ion-exchanged with 0.5 M NH_4NO_3 solution at a zeolite/NH_4NO_3 ratio of 1:10 at 80 °C for 1 h and this was repeated 4 times with a fresh NH_4NO_3, dried overnight at 100 °C and calcined at 550 °C for 3 h with a ramping temperature of 15 °C/min.

2.1.3. Supported Zeolite@SiC[149]

Prepation of α-SiC ceramic foam: 20%-PMMA α-SiC-foams were prepared at the Engineering Ceramics Group, Korea Institute of Materials Science[150]. α-SiC was added as inert filler and Al_2O_3 and Y_2O_3 were added as sintering additives. Two kinds of pore formers: expandable microspheres (461DU40, Expancel, Sundsvall, Sweden) and poly(methyl methacrylate) (PMMA) spheres (particle size 8 μm, Sunjin, Korea), were used to generate duplex pore structure.

Zeolite syntheses: Prior to the zeolite syntheses, α-SiC silicon carbide monolith pieces (0.2 g – 0.5 g) have been calcined in static air at 550 °C during 18h.

ZSM-5 coatings on silicon carbide via alkaline route: The synthesis gel was prepared by adding H_2O, $NaAlO_2$, tetraethyl orthosilicate (TEOS), NaCl, tetrapropylammonium hydroxide (TPAOH) = 1000; 0.18; 0.0049; 2.31; 1.44, respectively in molar ratio along with previously treated α-SiC monolith. The gel was then vigorously stirred and aged for 1h at room temperature. The mixture was transferred to a Teflon-lined stainless steel autoclave (75ml) and heated at 170 °C under autogenous pressure for the respective synthesis duration. The resulting solid was filtered on a nylon membrane and dried in an oven at 115 °C overnight.

[148] Messingue, R.N.M.; Losch, P.; Sedres, G.; Musyoka, N.M.; Fatoba, O.O.; Louis, B.; Pale, P.; Petrik, L.F. *CR Chimie* **2016** accepted.
[149] Losch, P.; Boltz, M.; Soukup, K.; Song, I.-H.; Yun, H. S.; Louis, B. *Microporous Mesoporous Mater.* **2014**, *188*, 99–107.
[150] Song, I.-H.; Kwon, I.-M.; Kim, H.-D.; Kim, Y.-W. *J. Eur. Ceram. Soc*. **2010**, *30*, 2671-2676.

ZSM-5 coatings on silicon carbide via fluoride route: The synthesis gel was prepared by adding H_2O, $NaAlO_2$, TEOS, TPABr, NH_4F = 1000; 0.15; 25.5; 0.91; 28.1 to the treated SiC support. The gel was then vigorously stirred and aged for 1h at room temperature. Likewise to the alkaline procedure, the mixture was then transferred to an autoclave (75 mL) and heated at 170 °C under autogenous pressure. Finally, the solid was filtered on a nylon membrane and dried in an oven at 115 °C overnight.

Analcime-crystals grown on silicon carbide via alkaline route: The synthesis gel was prepared by adding H_2O, $NaAlO_2$, NaCl, TPAOH = 1000; 0.18; 2.31; 1.44 to the previously treated SiC. The gel was vigorously stirred and aged for 1h at room temperature. The mixture was then transferred to an autoclave (75 mL) and heated at 170 °C under autogenous pressure for several days (from 1 – 30 days). Again, the solid formed was filtered on a nylon membrane and dried in an oven at 115 °C overnight.

2.1.4. Fluoride

Table 2-2. Synthesis of ZSM-5 zeolites in fluoride medium, molar ratios of the gel composition.

Entry	**1**	**2**	**3**	**4**
Zeolite	**ZSM-5FN**	**ZSM-5FLD**	**ZSM-5FS**	**ZSM-5FL**
Synthesis volume [mL]	133	85	70	50
H_2O	10400	10400	10400	10400
TPABr	7	7	3.5	7
NH_4F	112	112	112	112
SiO_2	100	100	100	100
Al_2O_3 ($NaAlO_2$)	0.5	0.5	0.5	0.5
Acid	5 drops HF	5 drops HCl	5 drops HF	5 drops HF
pH	6.9	6.9	6.9	6.9
Aging [h]	2	2	2	2
Synthesis [h]	48	48	144	144
Crystalline yield [%]	66	79	85	92

ZSM-5 zeolites were synthesised in fluoride medium and the following parameters have been investigated: density of Brønsted acid sites, crystal size, chemical composition and crystalline quality. The so-called MFI-F catalyst was prepared via fluoride-mediated route adapted from our previous studies.[151] The samples were named ZSM-5F respectively. All ZSM-5 samples obtained in NH_4-form were calcined in static air during at least 6 h at 823 K to obtain their corresponding H-form. A typical procedure for synthesizing a ZSM-5-F was as follows (for instance Entry 2, Table S1): 70 mL of distilled water were poured in a 150 mL-Erlenmeyer flask. Under vigorous stirring, $NaAlO_2$ (0.120 g), TPABr (0.907 g) and NH_4F (2.020 g) were consecutively added. Finally, 2.925 g of silica (Aeroperl 300/30, Evonik) were slowly added during 5 min. The pH of the gel was adapted to 7 by adding a few drops of a given acid. As-produced synthesis gel was aged under vigorous stirring (700 rpm) for 2 h. Meanwhile, the pH and fluoride anions concentration were monitored during ageing and after hydrothermal synthesis by means of Horiba LAQUAact pH/ORP/ION METER D-73. The gel was then autoclaved at 443 K for 48 or 144 hours.

[151] a) Bleken, F. L.; Chavan, S.; Olsbye, U.; Boltz, M.; Ocampo, F.; Louis, B. *Appl. Catal. A Gen.* **2012**, *447-448*, 178–185. b) Losch, P.; Laugel, G.; Martinez-Espin, J. S.; Chavan, S.; Olsbye, U.; Louis, B. *Top. Catal.* **2015**. c) Losch, P.; Boltz, M.; Louis, B.; Chavan, S.; Olsbye, U. *CR Chimie* **2015**, *18*, 330–335.

2.2. Characterisation Techniques

2.2.1. Microscopy Techniques

2.2.1.1. Optical Microscopy

Some samples with large enough crystallite sizes (20 - 100 µm) could be analyzed by optical microscopy using a TRAVELER USB microscope allowing 10x 60x and 200xfold magnification.

2.2.1.2. Scanning Electron Microscopy (SEM)

Scanning Electron Microscopy (SEM) micrographs were acquired on a JEOL FEG 6700F microscope working at 9 kV accelerating voltage. The Si / Al ratios of the materials were determined by EDX analysis coupled with the SEM chamber.

The crystal size distribution was estimated by measuring 30 random c-axis lengths per zeolite using Image J software and previously obtained SEM-micrographs. These 30 measurements resulted in different gaussian distributions representing the homogeneity of the crystal size distribution. Additionally, SEM micrographs were used to calculate crystal size distributions and respective Dispersities (Đ) using reported equations, M being replaced by the crystal sizes.[152]

$$Đ = M_w/M_n \quad (2.1)$$

$$Đ = (\text{c-axis length})_w/(\text{c-axis length})_n \quad (2.2)$$

2.2.1.3. Transmission Electron Microscopy (TEM)

HR-TEM images have been recorded using an image Cs corrected FEI TITAN transmission electron microscope that was operated at 300kV. The sample for transmission electron microscopy was prepared by dipping a copper TEM grid with a holey carbon support film into the powder sample.

2.2.2. X-Ray Diffraction (XRD)

2.2.2.1. Powder XRD

X-ray diffraction (XRD) patterns were recorded on a Bruker D8 Advance diffractometer, with a Ni detector side filtered Cu K_α radiation (1.5406 Å) over a 2θ range of 5° to 60°.

2.2.2.2. Rietveld Refinement

Synchrotron powder diffraction data were collected on the Materials Science Beamline at the Swiss Light Source (SLS) in Villigen, Switzerland[153] . The indexing of the XPD patterns was performed using Topas,[154] which was also used for the Rietveld refinement.[155] The structure drawings were produced using CrystalMaker[156] and the profile plots with the program ppp14.[157]

[152] Dispersity: http://www.iupac.org/publications/pac/81/2/0351/
[153] P. R. Willmott, P. R. *et al. Synchrotron Radiat*. **2013**, *20*, 667.
[154] Coelho, A. A., Indexing of powder diffraction patterns by iterative use of singular value decomposition, *J. Appl. Crystallogr.,* **2003**, *36*, 86-95.
[155] Coelho, A. A. TOPAS-ACADEMIC v5.0. **2012**.
[156] CrystalMaker Software Ltd., O., UK, http://www.crystalmaker.com.
[157] Graesslin, J. Ph.D. Thesis, ETH Zurich, **2013**.

Table 2-3. Synchrotron powder diffraction data collection parameters for the samples ZSM5-F.

Synchrotron facility	SLS
Beamline	Material Science
Diffraction geometry	Debye-Scherrer
Detector	MYTHEN II
Monochromator	Si 111
Wavelength	0.7086 Å
Sample	rotating 0.3 mm capillary
Nominal step size	0.004 °2θ
Detector positions	4
Exposure time	4 x 80 s
2θ range	3.2−29.9 °2θ

Table 2-4. Crystallographic data from the Rietveld refinement of ZSM5-F.[a]

Chemical composition	$\|(C_{12}H_{28}N)_2F_{1.4}\|[Si_{96}O_{192}]$	
Unit cell		
a	20.07309(6) Å	
b	19.95733(6) Å	
c	13.40854(5) Å	
Space Group	*Pnma*	
Data points	10240	
Contributing reflections	750	
Geometric restraints	218	
T-O	1.61(1) Å	48
O-T-O	109.5(20)Å	72
T-O-T	145(8)°	26
C-N	1.51(1) Å	4
C-C	1.55(1) Å	8
C-N-C	109.8(20)°	6
C-C-C	111.0(20)°	4
C-C-N	116(20)°	4
Parameters		
structural	151	
profile	8	
R_F	0.071 Rbragg	
R_{wp}	0.116	
R_{exp}	0.016	

[a] The numbers given in parentheses are the esd's in the units of the least significant digit given. Each restraint was given a weight equivalent to the reciprocal of its esd.

2.2.3. Dynamic Light Scattering (DLS)

DLS experiments were performed with zeolite synthesis gels sampled prior and during the synthesis, as well as with the final zeolite crystalline products. Samples were prepared by suspending less than 1 mg in 1 mL dist. H_2O, this suspension was then treated 5 min in an ultrasonic bath in order to homogenize the sample. The measurement was then carried out in a Delsa™ Nano C Particle Analyzer from Beckman Coultier.

2.2.4. Porosity Characterisation

2.2.4.1. Classic Textural Characterisation

The textural properties involving the BET surface area (S_{BET}) were evaluated from classical nitrogen physical adsorption–desorption isotherms measured at 77 K by means of ASAP2020M equipment (Micromeritics). In addition, t-plot measurements were used to differentiate external surface area and microporous area. Prior to analysis, the samples were outgassed at 373 K for 1h and 573 K for 15 h.

2.2.4.2. Gas Transport Characterisation

Thorough gas transport analysis was performed: Gas-transport parameters were determined according to the mean transport-pore model (MTPM),[158] while performing counter-current gas diffusion measurements in Graham's diffusion cell (Detailed results for the later presented H-ZSM-5FLD and H-ZSM-5FL samples are presented in **Table 2-5** and **Figure 2-1**).[159]

Table 2-5. Thorough textural analysis of ZSM-5FLD and ZSM-5FL samples by Ar-adsorption desorption experiments.

Entry	Zeolite	S_{BET} [m^2/g]	S_m [m^2/g]	V_m [mm^3_{liq}/g]	V_{intr} [cm^3/g]	r_{He} [g/cm^3]	r_{Hg} [g/cm^3]	e [g/cm^3]
1	H-ZSM-5FLD	335	314	69.8	1.51	2.18	0.54	0.75
2	H-ZSM-5FL	368	305	134	1.05	2.37	0.58	0.76

S_{BET} BET surface area
S_m Mesopore surface area
V_μ Micropore volume
V_{intr} Total intrusion volume determined by high-pressure mercury porosimetry
ρ_{He} Skeletal density
ρ_{Hg} Bulk density Porosity

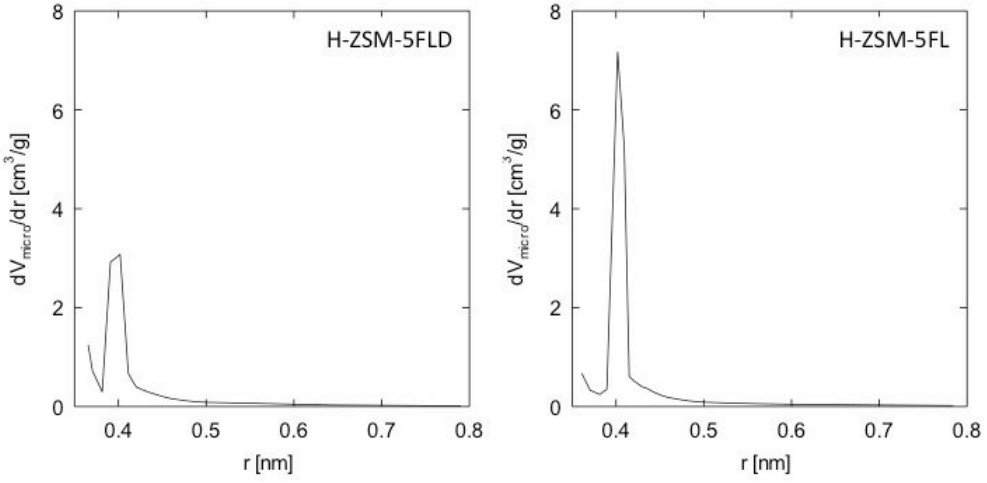

Figure 2-1. Micropore-size distribution for H-ZSM-5FLD (left) and H-ZSM-5FL (right).

MTPM assumes that the decisive part of the gas transport takes place in transport-pores that are visualized as cylindrical capillaries with radii distributed around the mean value <r> (first model

[158] Schneider P. Multicomponent isothermal diffusion and forced flow of gases in capillaries. *Chem. Eng. Sci. 33* **1978**, 1311–1319.
[159] Valuš J., Schneider P. A novel cell for gas counter-diffusion measurements in porous pellets. *Appl. Catal. 1* **1981**, 355–366.

parameter). The width of this distribution is characterised by the mean value of the squared transport-pore radii, $\langle r^2 \rangle$ (the second model parameter). The third model parameter is the ratio of porosity, ε_t, to tortuosity of transport-pores, q_t, $\psi = \varepsilon_t/q_t$. Parameters $\langle r \rangle$ and ψ; $\langle r^2 \rangle$ and ψ, appear always as their products, hence they will be presented in that forms, i.e. $\langle r \rangle\psi$ and $\langle r^2 \rangle\psi$. (Note that $\langle r \rangle^2 = \langle r^2 \rangle$ only when the distribution of transport-pores is symmetrical.) The model parameters (transport parameters) are material constants of the porous solids and thus, they are independent of temperature, pressure, kind as well as concentration of the gases used.

Binary and ternary gas diffusion measurements were performed in the Graham's diffusion cell described elsewhere.[160] Measurements of the counter-current diffusion were made with simple, non-adsorbable gases (i.e. hydrogen, helium, nitrogen and argon). This should guarantee the absence of the surface diffusion of adsorbable gases. One cell compartment was flushed with one gas (A), the other compartment either with another single gas (B) or with a mixture of two gases (B+C). This arrangement is denoted e.g. as A/B+C. The following five pairs of the binary gas mixtures were used for diffusion measurements: N_2/H_2, N_2/He, Ar/N_2, Ar/He and Ar/H_2. In order to extend an accuracy of the optimised transport parameters combination of the six different ternary gas mixtures were employed too, as follows: (He + N_2)/H_2, (Ar + He)/H_2, (Ar + N_2)/He, (Ar + H_2)/He, Ar/(N_2 + H_2) and finally, Ar/(N_2+ He). The use of all gases combinations (18 experimental points, every experimental point was three times repeated) is suggested as means of increasing the confidence of the evaluated transport parameters.

The net volumetric diffusion flux density, V, was determined by using digital bubble flowmeter connected directly to the cell compartment, which was closed after the steady-state was attained (in the configuration used it was always lower compartment). The net molar diffusion flux density, N^d, was then obtained from the following equation:

$$N^d = Vp/\left(R_g TS\right) \tag{2.3}$$

where p is the atmospheric pressure, T the laboratory temperature, R_g the universal gas constant and S the total cross-section of pellets in the impermeable holder. Diffusion flux densities of individual gases, N_i (i = A, B, C), were determined from the Graham's law according to:

$$\sum_{j=A,B,C} N_i^d \sqrt{M_i} = 0 \tag{2.4}$$

with gas molecular weights M_i (i = A, B, C). Evaluation of transport parameters ψ and $\langle r \rangle\psi$ requires solution of $(n-1)$ modified Maxwell-Stefan diffusion ODE's (where n is the number of gases in the diffusion run) with splitted boundary conditions:

$$-c_T \frac{dy_i}{dx} = \frac{N_i^d}{D_i^k} + \sum_{\substack{j=A,B,C \\ j\neq i}} \frac{y_j N_i^d - y_i N_j^d}{D_{ij}^m} \qquad i=A,B,C \tag{2.5}$$

The diffusion driving force is the gradient of mole fraction of component i, y_i, along the distance coordinate x. D_{ij}^m is the effective diffusion coefficient of the pair i–j in the bulk (molecular) diffusion region:

$$D_{ij}^m = \psi \mathcal{D}_{ij}^m \tag{2.6}$$

with binary bulk diffusion coefficient $\mathcal{D}_{ij}^m$. D_i^k is the effective Knudsen diffusion coefficient of component i:

$$D_i^k = \psi \langle r \rangle K_i \tag{2.7}$$

with the Knudsen coefficient, K_i:

$$K_i = \frac{2}{3}\sqrt{\frac{8R_g T}{\pi M_i}} \tag{2.8}$$

[160] Soukup K., Schneider P., Šolcová O. Comparison of Wicke-Kallenbach and Graham's diffusion cells for obtaining transport characteristics of porous solids. *Chem. Eng. Sci. 63,* **2008**, 1003–1011.

The sum of squared differences between experimental and calculated net molar diffusion flux densities was used as the objective function for the parameter search.

Before diffusion measurements, powder samples were poured into one hole with dimensions of 8.5 mm x 14 mm (diameter x length) inside of an impermeable disk with one end coated with a fine metallic mesh under reproducible tapping to achieve closer powder-particles arrangement. Thereafter, impermeable disk filled with the samples was fastened and sealed into the diffusion cell. It must be noted that during measurements the gas diffusion transport takes place predominantly through voids between individual particles of the sample. For that reason, internal structure of zeolites reveal rather weak influence on optimised transport parameters.

Figure 2-2 assesses the agreement between all experimental and calculated net diffusion molar flux densities based on optimised transport parameters.

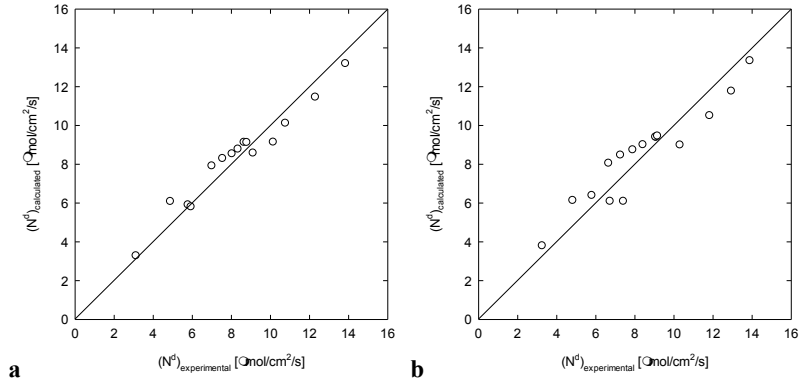

Figure 2-2. Comparison of experimental and calculated the net diffusion molar flux densities a) for H-ZSM-5FLD and b) for H-ZSM-5FL.

The statistical reliability of the obtained transport parameters can be assessed by means of their confidence regions evaluated at a significance level of 5%. Corresponding 95% confidence regions for selected relative critical sum of the squared deviations for all samples are depicted in **Figure 2-3** where the optimum parameter sets are highlighted as the full circles.

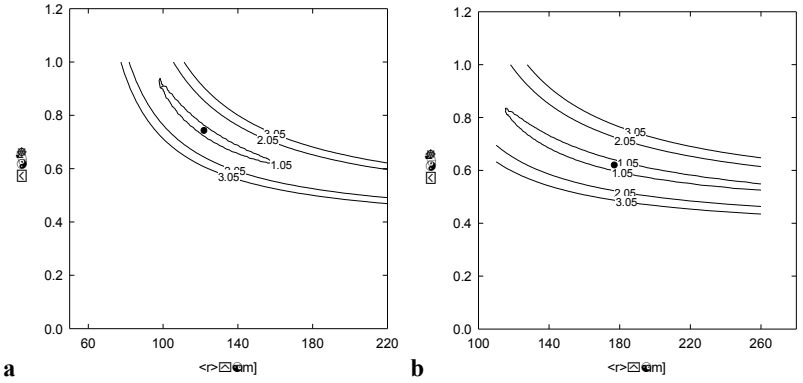

Figure 2-3. 95% confidence region of optimised transport parameters (full circle) for selected relative SSD a) for H-ZSM-5FLD and b) for H-ZSM-5FL..

2.2.5. Spectroscopy Techniques

2.2.5.1. ATR-FTIR

Infrared spectra of used or deactivated catalysts were acquired on an ALPHA spectrometer from Bruker equipped with OPUS software. Data were subsequently plotted on Origin software in order to superimpose and compare the coke specific absorption region (1200-1900 cm^{-1}).

2.2.5.2. (CO-)FTIR

Infrared spectroscopy (FTIR) spectra were recorded in controlled atmosphere at 2 cm^{-1} resolution on a Bruker Vertex 80 FTIR spectrophotometer, equipped with a MCT detector and using a homemade IR cell. FTIR spectra were collected in transmission mode on a thin film prepared by deposition of zeolite water suspension on a silicon wafer. The difference in the Brønsted acid strength of these samples was derived from CO adsorption. In order to compare the IR band intensities, spectra were normalized to the overtone mode at 2005 cm^{-1}.

2.2.5.3. Magic Angle Spinning (MAS)-NMR

^{19}F NMR were recorded on a on a Bruker MSL 300 spectrometer operating at 282.4 MHz using a 4-mm Doty probe and single-pulse excitation. A pulse length of 4 μs (π/2) with a recycle delay of 6 or 10 s and a spinning rate of 7-8 kHz were used. ^{19}F MAS NMR spectra were collected at both 13 and 15 kHz to assign spinning side bands. ^{27}Al (I = 5/2) MAS NMR was carried out with a Bruker Avance II 400 spectrometer operating at B_0 = 9.4 T (Larmor frequency ν_0 = 104.2 MHz) equipped with a Bruker 2.5 mm double channel probe. Samples were spun at 25 kHz, and free induction decays (FID) were collected with a π/12 rf pulse (0.5μs) and a recycle delay of 1s. Measurements were carried out with $[Al(H_2O)_6]^{3+}$ as external standard reference.

2.2.5.4. Pulsed Field Gradient (PFG)-NMR

Samples were prepared by following this typical procedure: 300 mg of an activated H-ZSM-5 zeolite were premixed with the considered liquid probe molecule (toluene, benzene or neopentane). It has been taken care that a loading of two molecules per unit cell was achieved, which is the most commonly applied loading for diffusion measurements at equilibrium conditions. Interestingly, we have to state that the loading and premixing for the neopentane samples had to be carried out in a 0°C cool-chamber in order to have "liquid" neopentane. After 1h agitation, solid premixed samples were transferred to an NMR-tube, to which a d_4-MeOD containing capped capillary was added (Calibration and Shim). As prepared tubes were capped and sealed with tape, in order to avoid any probe molecule evacuation.

Measurement of toluene and benzene self-diffusion coefficients were performed on a Bruker 600 MHz spectrometer - Avance III, equipped with a high strength z gradient probe DOTY Scientific, developing a pulse field gradient of 50 G/cm/A. The gradient coil was cooled by air flow and the sample was thermostated at 298 K. The gradient strength varied linearly between 16 and 302 G/cm in 40 experiments. Measurement of neopentane self-diffusion coefficients were performed with a BBI or a BBFO probe developing pulse field gradients of 5 G/cm/A. The gradient strength varied linearly between a minimum of 2 and a maximum comprised between 11 and 31 G/cm in 30 to 40 experiments.

Diffusion NMR data were acquired using a Stimulated Echo pulse sequence with bipolar z gradients. The diffusion time and the duration of the sinusoidal gradients were optimised for each sample. Typically the diffusion time was set between 2 and 10 ms (100 ms for the confined diffusion test) and the half-gradient delay between 400 and 700 μs. The gradient recovery delay was set to 200 μs. A recycling delay of at least 3.5 s was respected between scans. DOSY spectra are generated by the DOSY module of the software NMR Notebook, using Inverse Laplace Transform (ILT) driven by maximum entropy, to build the diffusion dimension.

2.2.6. Acid Site Characterisation

2.2.6.1. Elemental Analysis

X-ray fluorescence using a SPECTRO XEPOS spectrometer equipped with a 50-Watt end-window X-ray tube to excite the samples. The target changer, with up to 8 polarization and secondary targets, offers many different excitation conditions ensuring optimum determination of all elements from Na to U. The detection system consists of a 10 mm^2 Si-Drift Detector (SDD) with Peltier cooling and a spectral resolution of less than 155 eV at Mn Kα is achieved. Measurements were conducted in a He gas atmosphere..

2.2.6.2. H/D-Isotope Exchange

Acid site densities were evaluated by two complementary techniques; a homemade H/D-isotope exchange method, which quantifies the totality of exchangeable protons. This technique has been reported elsewhere and can briefly be described as follows:[161] An activated H-zeolite is subjected to a saturated D_2O-flow at 473 K, which leads to the exchange of zeolitic protons by deuterium cations. Then a liquid-nitrogen-cooled trap is connected to the all-glass setup in order to collect an H_xD_yO-fraction during thesamples subjection to H_2O-flow at 473 K. This H_xD_yO-fraction contains the quantitative information on the total exchangeable hydrons in the analysed sample.

It is used to hydrolyse trifluoroacetic anhydride consequently forming x CF_3COOH and y CF_3COOD, which can be quantified by NMR with an internal $CHCl_3/CDCl_3$-standard.

2.2.6.3. Propylamine TPD

Temperature programmed desorption of n-propylamine according to the method described by Gorte *et al.* which quantifies solely Brønsted acids characteristic for Si-(OH)-Al bridging sites. Detailed operating of these two methods is reported elsewhere.[162]

2.2.6.4. Development of an Aqueous Phase Amine Adsorption

During this work an aqueous phase titration method based on pH-variation upon adsorption of amine solutions has been developed. In order to carry out these expiments pH wa monitored during the adsorption process by means of Horiba LAQUAact pH/ORP/ION METER D-73. The following equations were adopted to extract an acid site density from the measured pH-difference.

$$pH_{(weak\ base)} = 7 + 1/2\ pK_a + 1/2\ \log(c_{amine}) \quad (2.9)$$

$$pH_{final} = 7 + 1/2\ pK_a + 1/2\ \log(c_{amine} - x) \quad (2.10)$$

$$\Delta pH = 1/2\ \log(C_{amine}(C_{amine} - x)^{-1}) \quad (2.11)$$

$$x = C_{amine} - C_{amine}\ 10^{(2\Delta pH)} \quad (2.12)$$

An aqueous solution of an amine, the probe molecule (propylamine or triethylamine) 100 mL at 0.1 M. This solution is then diluted by a factor of 100 in order to obtain 100 mL of 0.0001 M solution.The $pH_{(weak\ base)}$ of the latter is measured. The zeolite or alumina is weighed and dried for 30 min in an oven at 383 K, before addition to the solution. (10 - 20 mg for highly acidic H-Y and H-USY zeolites; 30 - 50 mg for medium acidic H-MOR and H-ZSM-5 zeolites; 600 - 800 mg for weakly acidic alumina) After 5 min at 500 rpm stirring at r.t. pH_{final} could be measured.

[161] Louis, B.; Walspurger, S.; Sommer, J. *Catal. Lett.* **2004**, *93*, 81–84.

[162] a) Louis, B. *et al. J Phys Chem C,* **2011**, *115*, 18603. b) Gorte R. J. *Catal. Lett.* **1999**, *62*, 1. c) Pereira, C.; Gorte, R. J. *Appl. Catal. A,* **1992**, *90*, 145.

2.3. Application

2.3.1.1. Set-up

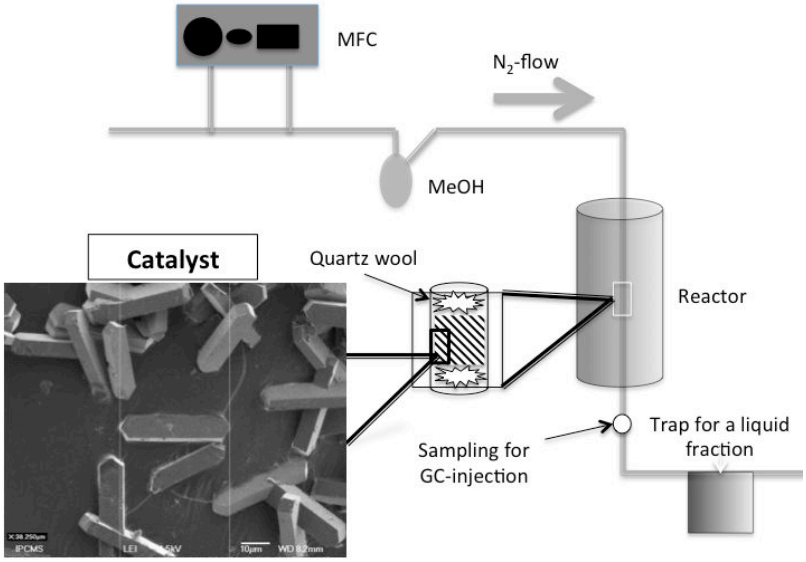

Figure 2-4. MTO-Setup used in our laboratory.

2.3.1. Methanol-To-Hydrocarbons Process

Prior to use, catalysts were calcined at 823 K with a gradient of 15 K/min in static air. H-zeolites were sieved and particles < 250 µm were used in the catalytic tests. 60 mg of zeolite was introduced in a tubular quartz reactor, packed between quartz wool plugs. A methanol-saturated nitrogen-flow was fed to the reactor at 673 K (WHSV = 1.2 $g_{MeOH.}(g_{cat.}h)^{-1}$). Samples, withdrawn at the reactor outlet were analyzed by GC (HP5890 Series II, Pona column, 50 m).

In order to investigate molecular positive thermal expansion MTO experiments were carried out under steady state conditions using per-deuterated d_4-MeOD since ∂(d(C-d)) < ∂(d(C-H)) at high temperatures due to the isotopic effects.

2.3.1.1. Variation of Parameters

A propylene-nitrogen gas mixture (1 / 20 ml/min) was fed to a zeolite containing reactor (60 mg), under MTO conditions. Reaction conditions were chosen in order to correspond to a theoretical 100 % yield in propylene under the above mentioned MTO conditions GHSV = 31.3 mmol(C)*(g(catalyst)*h)$^{-1}$ (even though in this case no water was present under these reaction conditions).

2.3.2. *n*-hexane Cracking

These experiments were performed in Brasil at the Federal University of Rio de Janeiro (UFRJ) thanks to collaboration: The n-hexane cracking has been chosen as a model reaction. The reactions were either carried out at 773 K or 873 K, during 2 h under nitrogen, using 0.03 g of catalyst. The paraffin was kept at room temperature in a saturator and then directed to the reactor using pure nitrogen as carrier gas. The reaction products were analyzed on-line by gas chromatography (Shimadzu GC-2010, Chrompack KCl/Al2O3 column, FID detector) after different times on stream.

2.3.3. Halogenation Reaction

2.3.3.1. Batch Reaction

Classic batch conditions: Catalytic reactions were initially carried out in 5 mL dichloroethane, to which iodobenzene (1 mmol, 0.112 mL, 1 equiv.), TCCA (0.34 mmol, 0.079 g, 0.34 equiv.) and the respective heterogeneous catalyst (100 mg) were added (isomass conditions were chosen). The solution was stirred at 80°C and 500 rpm velocity (a yellow colouration was observed). The samples withdrawn for GC analysis were treated to neutralise residual TCCA, Cl^0 - or Cl^{+X} species. Namely, 0.1 mL of the reaction mixture was filtered over a celite filled cartridge with 2 mL CH_2Cl_2 and vigorously stirred with 3 mL of a 10 wt-% $Na_2S_2O_3$ solution. From the resulting biphasic solution, the organic layer was separated and dried over Na_2SO_4 and finally injected in the gas chromatograph (GC II 5890 Hewlett Packard) equipped with a capillary column (PONA, 50 m) and a flame ionisation detector (FID). A typical chromatogram and integration results are given in S.I. (Figures S1 and S2).

In principle, the chlorination of iodobenzene leads to mono-, di- or tri-substituted aromatics. *Para*- and *ortho*-substituted aromatics are favoured. The degree of conversion and the selectivity toward the different products were calculated by taking into account the response factors from the reagent iodobenzene and those from the products (mono-, di- and tri-chlorinated aromatics) through the use of an external standard (n-heptane). For the different reaction conditions, different substrates and solvents were needed for the interpretation of GC results in order to determine conversions and selectivities. They were realizedd by adding the substrate (1 mmol), dichloroethane (0.08 mL, as internal standard) to 5 mL of solvent. 0.1 mL were extracted and mixed with 2 mL of EtOAc. The solution was injected three times in the gas chromatograph.

Then, blank experiments were carried out without catalyst and with two homogeneous catalysts : sulphuric acid and aluminum trichloride, tested under iso-site conditions with respect to 100 mg H-ZSM-5 zeolyst CBV2314, ergo 0.148 mmol H^+ or Al which corresponded to; 8 µL H_2SO_4 and 20 mg $AlCl_3$. Besides, different solvents (5 mL) were tested in the benchmark reaction with iodobenzene (1 mmol, 0.112 mL, 1 eq.), TCCA (0.34 mmol, 0.079 g, 0.34 equiv) and commercial *BEA zeolite (100 mg).

After replacing hazardous solvents (Table 4), the scope of *BEA-catalysed halogenation reactions was evaluated by testing different halogenating agents: N-chlorosuccinimide (NCS, Aldrich, 99%), N-bromosuccinimide (NBS, Aldrich, 99%) and N-iodosuccinimide (NIS, Alfa Aesar, 99%).

Batch conditions (optimised): Reactions were carried out in 5 mL acetic acid, aromatic substrate (1 mmol, 1 eq.), TCCA (0.34 mmol, 0.079 g, 0.34 equiv), dichloroethane (1 mmol, 0.08 mL) as an internal standard for GC analysis and *BEA (100 mg) were added (isomass conditions). The solution was stirred at 80°C and 500 rpm velocity (a pale yellow colouration was observed). The samples withdrawn for GC analysis were treated to neutralise residual TCCA, acetic acid, Cl^0 - or Cl^{+X} - species. Namely, 0.1 mL of the reaction mixture was filtered over celite filled cartridge with 2 mL EtOAc and vigorously stirred with 3 mL of a 10 %wt. K_2CO_3 solution. From the resulting biphasic solution, the organic layer was separated and dried over Na_2SO_4 and finally injected in the gas chromatograph (GC II 5890 Hewlett Packard) equipped with a flame ionisation detector (FID).

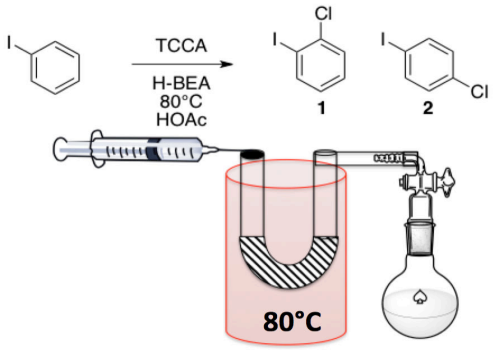

Figure 2-5. Continuous-flow synthesis of chloroarenes.

2.3.3.1. Continuous Flow Process

A glass U-shaped tubular reactor (Figure 2) was used in a continuous flow chlorination operation. The reactants TCCA (316 mg, 1.36 mmol), iodobenzene (0.448 mL, 4 mmol) and dichloroethane as an internal standard (0.32 mL, 4 mmol) were previously solubilised in acetic acid and charged into a 20 mL syringe. The U-shaped glass reactor was packed with 33 mg of respective *BEA zeolite. Those loadings were chosen to set the same contact time corresponding to 12 consecutive runs under batch conditions.

Recycling was tested; solid catalysts were re-engaged up to ten times after centrifugation and washing three times with 5 mL H_2O/EtOH (50/50). No re-activation was needed between consecutive runs.

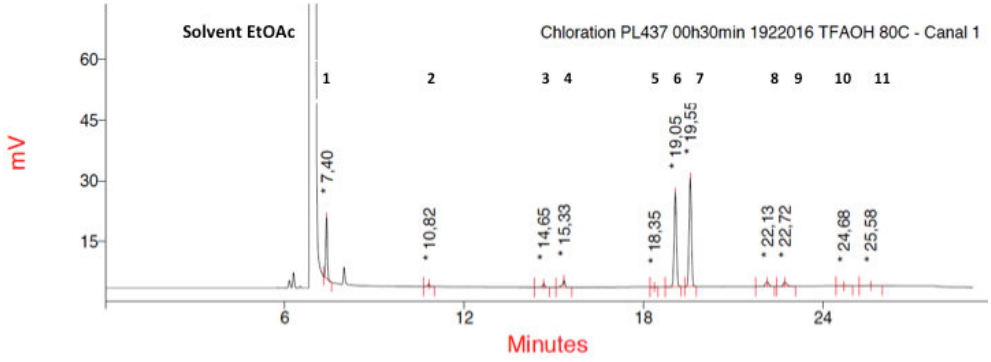

Figure 2-6. Typical chromatogram corresponding to entry 13 in **Table 4-12**.

Prog : 110°C 7 min 15°C/min 270°C x 10 min
Flux : He 17 PSI
Inj : 300°C
Det : 270°C

Résultats d'intégration

#	Nom du pic	Tr.	Aire	% Aire
1	Internal Standard DCE	7.40	55,61	**15,07**
2	Chlorobenzene	10.82	2,74	**0,74**
3	Impurity	14.65	3,96	**1,07**
4	Iodobenzene	15.33	9,88	**2,68**
5	*m*-chloroiodobenzene	18.35	0,13	**0,04**
6	*p*-chloroiodobenzene	19.05	127,39	**34,53**
7	*o*-chloroiodobenzene	19.55	149,96	**40,65**
8	dichloroiodobenzene	22.13	9,66	**2,62**
9	dichloroiodobenzene	22.72	8,65	**2,34**
10	trichloroiodobenzene	24.68	0,15	**0,04**
11	trichloroiodobenzene	25.58	0,77	**0,21**
SOMME			368,90	100,00

Figure 2-7. Analysis of the typical chromatogram corresponding to entry 13, **Table 4-12**. Integration areas of these chromatogram-peaks are used to calculate the reactions conversion and respective selectivities.

2.3.4. Zeolite-catalysed HCOOH Dehydration and Pd-catalysed Carbonylation

2.3.4.1. General Procedure for the Formation of CO

Solid acid (300 mg) (see Table 1) were packed between two quartz wool plugs into a U-shaped glass tube, with at one end, a rubber septum to allow the addition of formic acid and at the other end, either a glass flask filled with brine to measure the volume of CO produced or a trap and a tube filled with $MgSO_4$ and connected to a flask containing the Pd catalyst and the required reagent (see below). Then the CO-reactor was heated to 150°C and HCOOH (10 mmol, 0.38 mL) was slowly injected over a period of 15 minutes. During this injection of formic acid, CO gas was produced.

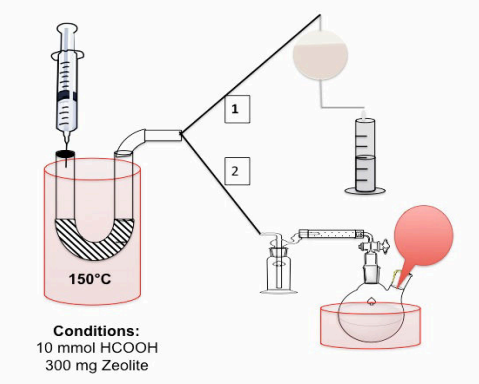

Figure 2-8. Scheme of the reactor set up to study the formation of CO from HCOOH mediated by solid acids (line 1) and its connection to classical reactor for carbonylation reactions (line 2).

2.3.4.2. General Procedure for the Carbonylation Reaction

Using the above-mentioned system, iodoarene (1 mmol), the appropriate amine (2 mmol), $PdCl_2$ (1.77 mg, 0.01 mmol), Xantphos (5.78 mg, 0.01mmol), triethylamine (270 µL, 2 mmol) and THF (3 mL) were added in an oven-dried 25 mL two-necked flask under argon. The flask was connected to the zeolite-catalysed CO producing system (see above) and flushed with CO (0.2 mL of HCOOH). The mixture was stirred at 60 or 80 °C under 1 atm of CO (balloon pressure, 0.38 mL of HCOOH) until completion of the reaction (monitored by TLC, typically 1-16 h; see Tables 3-4). Upon completion, the reaction was quenched with 1 N HCl_{aq} (5 mL) and the product was extracted with EtOAc (3x10 mL). The organic extracts were combined and washed with sat. $NaHCO_3$, brine and dried over $MgSO_4$. Evaporation of the solvent gave a brownish oil, which was purified by flash chromatography on silica gel.

The formed amides, esters and lactone are known compounds and exhibit spectroscopic data identical to those reported in the literature.

2.4. Modelling-Microkinetics

Simulations of inter active site diffusion lengths were carried out on a 4 unit cell model crystal which extends in the three space directions (a, b and c). Molecular kinetic diameters were estimated with Spartan software, while their *positive thermal expansion* (PTE) was estimated considering each covalent bond as Newtonian behaving oscillator contributing to

γ, a confinement factor has been introduced which basically traduces the fit between any considered molecule, its temperature impacted diameter ($ø_{molecule}(T)$) due to PTE, and the microporous network with its temperature impacted diameter ($ø_{pore}(T)$) due to NTE:

$$\gamma = \left(e^{-\left(1-\frac{ø_{pore}(T)}{ø_{molecule}(T)}\right)^2}\right)^x \qquad (2.13)$$

γ's function was chosen to be a bell shaped curve describing an optimal fit, with its maximum at 1 and minimum at 0. The power **x** ≥ 1 has been added to this function to be able to attenuate the

functions impact on the resulting diffusional velocity due to more or less selective fits. This consequently leads to a possible change, due to confinement effects, in the speed distribution ($f_{3D}(\mu)$) and the most likely diffusional velocity (μ_p).

$$f_{3D}(\mu) = \sqrt{(\frac{p^{\gamma}*A}{2\pi kTa})^3} 4\pi\mu^2 e^{-\frac{p^{\gamma}*A*\mu^2}{2kTa}} \quad (2.14)$$

$$\mu_p = \sqrt{\frac{2\pi kTa}{p^{\gamma}*A}} \quad (2.15)$$

Interestingly, simple calculations show that 60 mg of ZSM-5FL zeolite correspond to 0.19 cm^3 However, the effective accessible volume is of 0.012 cm^3 (microporous volume), hence the reactive volume is truly confined by a factor (at least) 10. Hence, a certain impact of confinement in the MTO reaction appears plausible.

Shape selectivity should be observed leading to high amounts of butenes and probably some branched pentenes. However, the major product remains propylene on ZSM-5 zeolites. It is therefore of fundamental importance to analyze and understand the influence of temperature rise on molecular diameters (PTE) and (even) on the zeolite framework (NTE).

Temperature related variations of zeolites porous diameters were estimated using the data from Cha *et al.* in their work on negative thermal expansion in high SAR ZSM-5 zeolites.[163]

We conversely used both, experimental D_{eff} data and the above described D_{eff} predictability for different molecules in different nanoporous solids to estimate unit-less microkinetics parameters.[164] Our main interest lay in the determination of the Thiele modulus (ϕ), which can be considered as the square root of the Damköhler number of the second order Da_{II}. The second parameter we estimated using our data was the Thiele-Weisz-Wagner-Wheeler degree of utilization (ψ) of a porous catalyst.

$$\Phi = L\sqrt{\frac{kc_s^{n-1}}{D_{eff}}} \quad (2.16)$$

$$\Psi = \Phi^2\eta = \frac{l^2}{D_{eff}\, c_A} r_{eff} \quad (2.17)$$

In these equations; L is the diffusion length here pore-length [m], k the reaction rate constant [$mol.h^{-1}.m^3$], c_S the surface concentration [$mol.m^3$], n the reaction order of the considered reacting molecule, D_{eff} the effective diffusities measured by DOSY experiments and temperature-corrected using the above mentioned Maxwell-Boltzmann equations [$m^2.h^{-1}$], l is the pore length [m], c_A the concentration of the considered substrate [$mol.m^{-3}$] and r_{eff} its related reaction rate [$mol.h^{-1}.m^3$].

[163] Cha, W.; Jeong, N. C.; Song, S.; Park, H.; Cao, T.; Pham, T.; Harder, R.; Lim, B.; Xiong, G.; Ahn, D.; Mcnulty, I.; Kim, J.; Yoon, K. B.; Robinson, I. K.; Kim, H. *Nat. Mater.* **2013**, *12*, 729.

[164] a) Chemical Reactor Analysis and Design (2nd Edition), Gilbert F. Froment, Kenneth B. Bischoff, **1990**, John Wiley & Sons b) Fundamentals of Chemical Reaction Engineering (1st Edition), Mark E. Davis, Robert J. Davis, **2003**, The McGraw-Hill Companies, Inc.

Chapter 3 Perfect H-ZSM-5 Crystals: Stone of Wisdom for MTO-Catalysis?

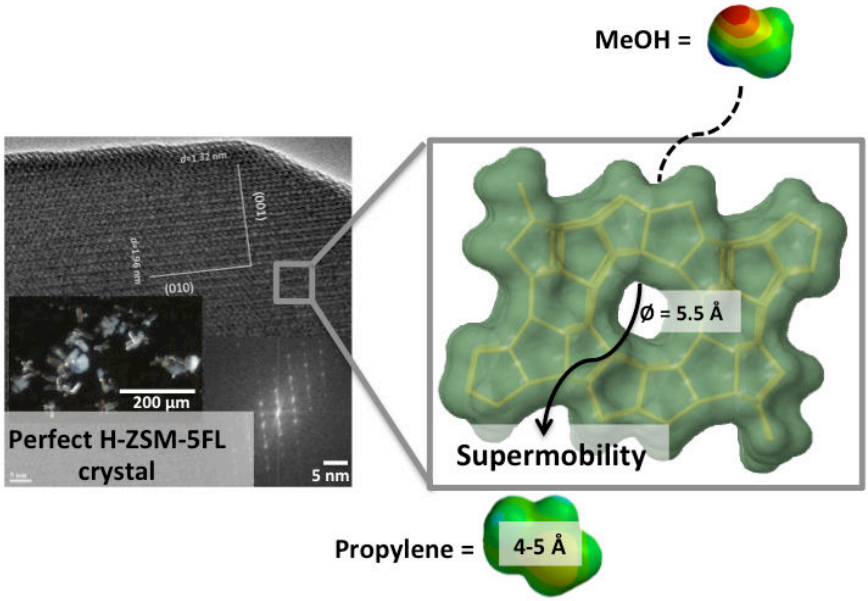

ABSTRACT: Large ZSM-5 zeolite crystals synthesised in fluoride medium show an astonishing activity, stability as well as selectivity towards light olefins in the Methanol-To-Olefins (MTO) reaction. By properly controlling the synthesis parameters, ZSM-5 single crystals of unprecedented high quality are produced. The synthesis of those nearly perfect crystals exempted from surface defects and exhibiting a perfectly homogeneous acid site distribution that permits to eliminate ubiquitous, usually uncontrollable variables such as structural defects, external non selective surface acid sites and extra-framework aluminum (EFAl) species. The present study highlights the synthesis, characterisation, application and subsequent rationalisation, using Maxwell-Boltzmann based diffusion models of this outstanding MTP (Methanol-To-Propylene) catalyst, appearing as a potential model-catalyst to build structure / activity relationships. Its thorough characterisation was performed by SEM, HRTEM, CO-FTIR, ^{27}Al and ^{19}F MAS-NMR, Rietveld structure refinement, BET and PFG-NMR techniques.

This chapter is presenting the main part of my PhD-work and is partly based on the following peer-reviewed manuscripts:

"Binderless Zeolite Coatings on Macroporous α-SiC Foams" Losch, P.; Boltz, M.; Soukup, K.; Song, I.-H.; Yun, H. S.; Louis, B. *Microporous Mesoporous Mater.* **2014**, *188*, 99–107.

"Catalyst optimisation for enhanced propylene formation in the methanol-to-olefins reaction" Losch, P.; Boltz, M.; Louis, B.; Chavan, S.; Olsbye, U. *CR Chimie* **2015**, *18*, 330–335.

"Phosphorous Modified ZSM-5 Zeolites: Impact on Methanol Conversion into Olefins" Losch, P.; Laugel, G.; Martinez-Espin, J. S.; Chavan, S.; Olsbye, U.; Louis, B. *Top. Catal.* **2015**, *58*, 826–832.

"Impact of external surface passivation of nano-ZSM-5 zeolites in the methanol-to-olefins reaction" Losch, P.; Boltz, M.; Bernardon, C.; Louis, B.; Palčić, A.; Valtchev, V. *Appl. Catal. A Gen.* **2016**, *509*, 30–37.

"Perfect ZSM-5 Crystal: Structure-Diffusion-Activity Relationship in MTO-Catalysis?" Losch, P.; Pinar, A.B.; Soukup, K.; Willinger, M.; Chavan, S.; Vincent, B.; Pale P.; Louis, B. *J. Catal.* **2016**, *accepted*.

"Mesoporous ZSM-5 Zeolites in Catalysis." Losch, P.; Hoff, T.; Bernardon, C.; Kolb, J.; Tessonnier, J.-P.; Louis, B. **2016**, *in preparation*.

3.1. Introduction to Large ZSM-5 Crystals in MTO-Catalysis

Heterogeneous catalysis is of tremendous importance in today's chemistry but also in everyday life. Indeed, the most important chemical processes producing for instance ammonia via the Haber-Bosch process, sulphuric acid via the contact process, or gasoline through Fluid Catalytic Cracking (FCC) are heterogeneously catalysed chemical transformations.[165] Precious insights have been gained in the understanding of heterogeneous surface catalysis, while studying *perfect* model catalysts culminating with the Nobel Prize award to G. Ertl in 2007.[166] Even though it is often stated that defects may act as active sites in heterogeneous catalysts,[167] the latter approach led to an utmost high degree of understanding. In spite of performing catalysis over a model catalyst, it is still possible to characterise surface defects and evaluate their impact in a reaction.[168]

Zeolites are crystalline, three-dimensional microporous aluminosilicates. The presence of defects as external silanols, Si-OH nests, intergrowths[169] and extra-framework Al species renders complicate a detailed surface understanding in a catalytic reaction. However, the synthesis of "perfect" zeolite crystals is all but trivial. With respect to aforementioned metal model catalysts, it remains nonetheless, wishful to reach a similar degree of understanding on the diffusion and reaction phenomena of molecules within zeolite pores.[170]

Among today's 231 existing zeolites, ZSM-5 possessing an MFI-type structure remains one of the most studied and useful in industry. Thanks to its particular three dimensional channel topology, a high selectivity towards light olefins, valuable building blocks in polymer chemistry or initial backbones for the synthesis of organic bulk chemicals such as amino acids,[171] is achieved via FCC and the Methanol-To-Olefins (MTO) processes. Interestingly, propylene with 14.3 Mt per year is the second topmost produced chemical in the U.S. today (80 Mt worldwide), right after sulphuric acid and ranked before sodium hydroxide or ammonia. The catalytic cracking

[165] a) Fechete, I.; Wang, Y.; Védrine, J. C. *Catal. Today* **2012**, *189*, 2. b) *Zeolites and Catalysis, Synthesis, Reactions and Applications,* Cejka, J.; Corma, A.; Zones, S. Wiley-VCH, Weinheim; **201**0.

[166] *Reactions at surfaces: From atoms to complexity,* Ertl, G.; Nobel Lecture, December 8, **2007.**

[167] a) Somorjai G. A.; Bratlie K. M.; Montano M. O.; Park J. Y.; *J. Phys. Chem. B.* **2006**, *110*, 20014. b) Behrens, M.; Studt, F.; Kasatkin, L.; Kühl, S.; Hävecker, M.; Abild-Pedersen, F.; Zander, S.; Girgsdies, F.; Kurr, P.; Kniep, B.-L.; Tovar, M.; Fischer, R. W.; Nørskov, J. K.; Schlögl, R. *Science* **201**2, *336*, 893.

[168] a) Murzin, D. Y. in Engineering Catalysis, de Gruyter, Berlin, **2013**. b) Nørskov, J. K.; Bligaard, T.; Rossmeisl, J.; Christensen, C. H.; *Nature Chem.* **2009**, *1*, 37. c) Tao, F.; Dag, S.; Wang, L.-W.; Liu, Z.; Butcher, D. R.; Salmeron, M.; Somorjai G. A. *Nano Lett.* **2009**, *9*, 2167.

[169] Karwacki, L.; Kox, M. H. F.; de Winter, D. A. M.; Drury, M. R.; Meeldijk, J. D.; Stavitski, E.; Schmidt, W.; Mertens, M.; Cubillas, P.; John, N.; Chan, A.; Kahn, N.; Bare, S. R.; Anderson, M.; Kornatowski, J.; Weckhuysen, B. M. *Nat. Mater.* **2009**, *8*, 959.

[170] a) Ristanović, Z.; Hofmann, J. P.; De Cremer, G.; Kubarev, A. V.; Rohnke, M.; Meirer, F.; Hofkens, J.; Roeffaers, M. B. J.; Weckhuysen, B. M. *J. Am. Chem. Soc.* **2015**, *137*, 6559. b) Jacobsen, C. J. H.; Madsen, C.; Houzvicka, J.; Schmidt, I.; Carlsson, A. *J. Am. Chem. Soc.* **2000**, *122*, 7116.

[171] a) *Chemical and Petroleum Manufacturers of India*, Data for **2012**. b) *American Chemical Council 2013 Statistics*. Data for **2012**. c) *APPE (Association of Petroleum Producers in Europe).* Data for **2012**, d) *Data from IHS* **2011**.

of hydrocarbons (FCC) and MTO processes are focussing on light olefins production. However, the targeted high selectivity can be altered by the presence of high amounts of non-selective external acid sites. Coke formation and subsequent catalyst deactivation can also be strongly influenced by those external non-shape selective sites.[172]

Consequently, the rational design of ZSM-5 zeolites to achieve high catalytic performances has become a frequent objective in acid catalysis. Manifold proof has been reporting; the smaller catalyst particles are, the faster a reaction will proceed and overcome diffusional limitations.[173] However, the rise of nanometric catalysts is frequently accompanied with an increase in external and/or internal structural defects in addition to the presence of numerous non-selective external sites.[174] In this context we will present herein the counter-intuitive utility of large and nearly perfect *model* ZSM-5 crystals.

Wragg *et al.* conducted an interesting study related to the MTO reaction over SAPO-34 materials, where an *ad operando* study involving sophisticated diffraction and microscopic techniques led to significant mechanistic understanding.[175] Recent progress in understanding complex surface chemistry mechanisms occurring during MTO using ZSM-5 catalysts is rather based on a combination of several spectroscopic methods (*ad operando* FTIR, UV-vis micro-spectrometry, etc.) as well as computational modelling.[176] The prime C-C bond formation, which initiates an autocatalytic cycle, was under a severe debate until recently.[177,178] The dual cycle concept has been introduced by Bjørgen *et al.* leading to new insights and several interesting reviews are covering this topic (**Figure 3-1**).[179] The essentials in brief, methanol is auto-catalytically reacting over ZSM-5 zeolites to form a hydrocarbon pool (HCP), which acts as a hybrid catalyst. This hydrocarbon pool is either working in an olefin-methylating-cracking or in

[172] a) Smit, B.; Maesen, T. L. M. *Nature* **2008**, *451*, 671. b) Kunkeler, J. P.; Moeskops, D.; van Bekkum, H. *Microporous Mesoporous Mater.* **1997,** *97,* 6513.
[173] a) Choi, M.; Na, K.; Kim, J.; Sakamoto, Y.; Terasaki, O.; Ryoo, R. *Nature* **2009**, *461*, 246. b) Awala, H.; Gilson, J. P.; Retoux, R.; Boullay, P.; Goupil, J.; Valtchev, V.; Mintova, S. *Nat. Mater.* **2015**, *14*, 447. c) Ng, E.-P.; Chateigner, D.; Bein, T.; Valtchev, V.; Mintova, S. *Science* **2012**, *335*, 70. d) Hibbe, F.; Chmelik, C.; Heinke, L.; Pramanik, S.; Li, J.; Ruthven, D. M.; Tzoulaki, D.; Kärger, J. *J. Am. Chem. Soc.* **2011**, *133*, 2804.
[174] Mintova, S.; Gilson, J.-P.; Valtchev, V. *Nanoscale* **2013**, *5*, 6693.
[175] Wragg, D. S.; Brien, M. G. O.; Bleken, F. L.; Michiel, M. D.; Olsbye, U. *Angew. Chem., Int. Ed.* **2012**, *51*, 7956.
[176] a) Sun, X.; Mueller, S.; Liu, Y.; Shi, H.; Haller, G. L.; Sanchez-Sanchez, M.; van Veen, A. C.; Lercher, J. A. *J. Catal.* **2014**, *317*, 185. b) Hemelsoet, K.; Qian, Q.; De Meyer, T.; De Wispelaere, K.; De Sterck, B.; Weckhuysen, B. M.; Waroquier, M.; Van Speybroeck, V. *Chemistry Eur. J.* **2013**, *19*, 16595. c) Van Speybroeck, V.; De Wispelaere, K.; Van Der Mynsbrugge, J.; Vandichel, M.; Hemelsoet, K.; Waroquier, M. *Chem. Soc. Rev.* **2014**, *43*, 7326. d) Lesthaeghe, D.; Van Speybroeck, V.; Marin, G. B.; Waroquier, M. *Angew. Chem., Int. Ed.* **2006**, *45*, 1714.
[177] a) Haw, J. F.; Song, W.; Marcus, D. M.; Nicholas, J. B. *Acc. Chem. Res.* **2003**, *36*, 317–326. b) Wang, W.; Buchholz, A.; Seiler, M.; Hunger, M. *J. Am. Chem. Soc.* **2003**, *125*, 15260–15267. c) Abubakar, S. M.; Marcus, D. M.; Lee, J. C.; Ehresmann, J. O.; Chen, C.-Y.; Kletnieks, P. W.; Guenther, D. R.; Hayman, M. J.; Pavlova, M.; Nicholas, J. B.; Haw, J. F. *Langmuir* **2006**, *22*, 4846.
[178] Liu, Y.; Müller, S.; Berger, D.; Jelic, J.; Reuter, K.; Tonigold, M.; Sanchez-Sanchez, M.; Lercher, J. A. *Angew. Chem., Int. Ed.* **2016**, *55*, 5723.
[179] a) Olsbye, U.; Svelle, S.; Bjørgen, M.; Beato, P.; Janssens, T. V. W.; Joensen, F.; Bordiga, S.; Lillerud, K. P. *Angew. Chem., Int. Ed.* **2012**, *51*, 5810. b) Bjørgen, M.; Svelle, S.; Joensen, F.; Nerlov, J.; Kolboe, S.; Bonino, F.; Palumbo, L.; Bordiga, S.; Olsbye, U. *J. Catal.* **2007**, *249*, 195.

an arene methylation and possibly side chain growth-cracking regime, or most likely a combination of both.

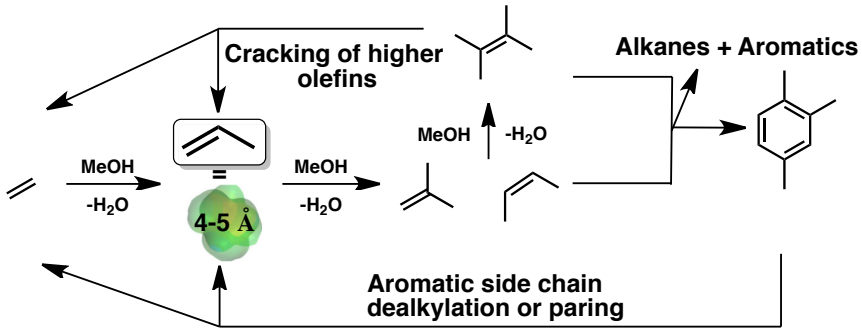

Figure 3-1. MTO on H-ZSM-5: Generally accepted reaction pathways at quasi steady state conditions producing high amounts of propylene.

Additionally, detailed kinetic studies under industrially relevant conditions were performed in Lercher's group, to study the behaviour of ZSM-5 zeolites in the MTO-reaction.[180] These seminal studies estimated reaction rates of intermediate steps, unexpectedly[181] indicating that hex-1-ene cracking may lead to a considerable formation of ethylene, whereas propylene is non-negligibly produced by the cracking of aromatic side-chains. Consequently, a "modified" dual cycle concept arose.

Herein, we present the synthesis, application and thorough characterisation of a ZSM-5 model catalyst. An initial aim was the synthesis of an outstanding MTP-catalyst guided by an earlier stated hypothesis by Armaroli *et al.*: "high quality and low acidic ZSM-5 crystals should be powerful MTO-catalysts".[182] We were able to prove this assumption and to decipher a link between the high quality of as-obtained crystals and their tremendous activity, stability and selectivity, using our data.

3.2. Large crystals vs. Nano and Hierarchy: The Surprise

This work did of course not start from scratch, but was based on a previous study in which it could be evidenced that neither hierarchical porosity nor nano-sized ZSM-5 crystallites are necessarily an advantage for the MTO reaction.[9] Surprisingly, it was found that a first generation of large ZSM-5 crystals synthesised in fluoride medium (ZSM-5F) were effectively converting methanol into olefins.

[180] a) Van Speybroeck, V.; Van der Mynsbrugge, J.; Vandichel, M.; Hermelsoet, K.; Lesthaeghe, D.; Ghysels, A.; Marin, G. B.; Waroquier, M. *J. Am. Chem. Soc.* **2011**, *56*, 47. b) Sun, X.; Mueller, S.; Liu, Y.; Shi, H.; Haller, G. L.; Sanchez-Sanchez, M.; van Veen, A. C.; Lercher, J. A. *J. Catal.* **2014**, *317*, 185. c) Sun, X.; Mueller, S.; Shi, H.; Haller, G. L.; Sanchez-Sanchez, M.; van Veen, A. C.; Lercher, J. A. *J. Catal.* **2014**, *314*, 21.

[181] Svelle, S.; Joensen, F.; Nerlov, J.; Olsbye, U.; Lillerud, K. P.; Kolboe, S.; Bjørgen, M. *J. Am. Chem. Soc.* **2006**, *128*, 14770.

[182] Armaroli, T.; Simon, L. J.; Digne, M.; Montanari, T.; Bevilacqua, M.; Valtchev, V.; Patarin, J.; Busca, G. *Appl. Catal. A Gen.* **2006**, *306*, 78.

Thus my focus was laid on a potential optimisation and the production of a second and third generation of such catalysts and more challengingly, we aimed to understand why these large crystals are producing such high amounts of propylene and over such a long time on stream.

3.3. Feedback looped optimisation of large ZSM-5 crystals

A feedback looped optimisation approach was chosen to design a second generation and a third generation of H-ZSM-5F catalysts. Indeed, strictly following the continuous, iterative improvement approach (cf. **SCAR**) several parameters were varied in order to identify the crucial ones. Hence, in the second generation H-ZSM-5F catalysts the following parameters were played with: the acid site density, while adjusting Si/Al-ratios in the syntheses gels, crystallite sizes by varying various parameters such as the crystallization time, and the crystalline quality by using fluoride medium in neutral or slightly alkaline conditions (HF, HCl, H_3PO_4 and $AlBr_3$ were used to adjust the pH).

3.4. Identification of Key Parameters

After these screening experiments, which will not be presented in much detail in this work we were able to identify the optimal parameters to seek, in order to conceive an optimal H-ZSM-5F zeolite for the MTO/P-reaction.

Namely, an optimal MTP-catalyst based on large H-ZSM-5F crystals (> 10 x 15 x 50 µm) seemed to need a Si/Al-ratio between 100 - 150, or very disperse acid sites as it was shown in **Figure 1-16** and will be further investigated in **Figure 3-20** during this chapter. The next crucial parameter to control was the crystalline quality, meaning that crystalline intergrowths, internal and external silanol defects as well as EFAl-species had to be avoided.

In other terms, the optimum MTP-catalyst seemed to be a perfect, only Brønsted acidity containing single crystalline ZSM-5 material, with large and homogeneously disperse crystal sizes.

3.4.1. Acidity

Figure 3-2 shows a compilation of the behaviour of catalysts developed in the last three years. It seems striking that a hyperbolic correlation could be evidenced indicating the drastic advantage of disperse acid site density if the production of light olefins is aimed. Indeed, the higher light olefins selectivity is obtained with a lower surface acid site density. This product distribution may originate in the phenomenon that the less acid sites are present and the larger the crystals are, the more shape selective microporous Brønsted acid sites will be responsible in the catalytic turnover of methanol to olefins passing by a dual cycle mechanism (cf. **Figure 1-15**). The latter in turn, may tend to run preferentially in the light olefins methylation-cracking regime

over the described catalysts. In order to generate the data for **Figure 3-2** an H/D isotope exchange technique (cf. Section **2.2.6.2.**) was used for the estimation of the total surface acidity since this technique has been reported to be able to titrate the totality of exchangeable hydrons (silanol groups and bridging Si-(OH)-Al),[183] and the total BET surface area was chosen to express the surface Brønsted acid site density in mol(H^+) per square meter. The later studied H-ZSM-5F zeolites, which will prove to be promising MTP-catalysts will exhibit a disperse acid site density (< 10^{-6} mol(H^+).m^2).

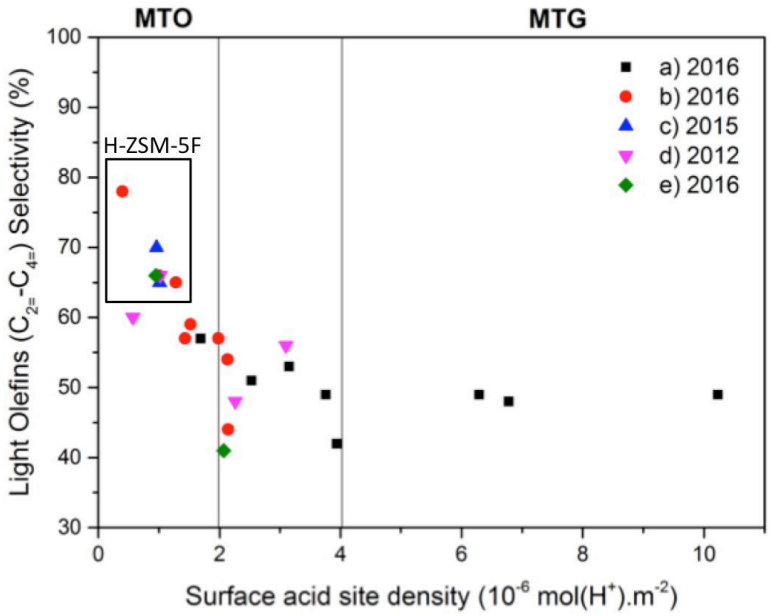

Figure 3-2. Hyperbolic correlation between light olefins ($C_{2=}$-$C_{4=}$) selectivity of various tested ZSM-5 zeolites and their respective calculated surface acid site densities (calculated using their titrated exchangeable hydrons, obtained with the previously described H/D-isotopic exchange technique, and the total BET surface area). Reported in: a) 2016[184], b) 2015[185], c) 2012[186] and d) 2016[187].

3.4.2. Crystal Morphology

It has been exposed in the Section **1.2.3.** that nanosized crystals and hierarchical porosity are highly sought characteristics in current zeolite catalyst development. It emerged, however from the present study, that small sized and mesoporous crystals exhibit a considerable amount of structural defects (internal and external Si-OH) as well as a non negligible quantity of non shape selective external Brønsted acid sites (Si-(OH)-Al). Since the MTO-reaction is selectively occurring in microporous space and should not be limited by mass transfer with the reactant (MeOH) and main products (light olefins $C_{2=}$, $C_{3=}$, $C_{4=}$), being smaller in size than the micropores

[183] Louis, B.; Vicente, A.; Fernandez, C.; Valtchev, V. *J. Phys. Chem. C* **2011**, *115*, 18603.
[184] Losch, P.; Boltz, M.; Bernardon, C.; Louis, B.; Palčić, A.; Valtchev, V. *Appl. Catal. A Gen.* **2016**, *509*, 30.
[185] Losch, P.; Laugel, G.; Martinez-Espin, J. S.; Chavan, S.; Olsbye, U.; Louis, B. *Top. Catal.* **2015**, *58*, 826.
[186] Bleken, F. L.; Chavan, S.; Olsbye, U.; Boltz, M.; Ocampo, F.; Louis, B. *Appl. Catal. A Gen.* **2012**, *447-448*, 178.
[187] Messingue, R.N.M.; Losch, P.; Sedres, G.; Musyoka, N.M.; Fatoba, O.O.; Louis, B.; Pale, P.; Petrik, L.F. *CR Chimie* **2016** *in press*.

of ZSM-5, it seems interesting to think of larger crystals with perfect microporous space and an infinitesimal amount of non shape selective external acid sites (**Figure 3-3**).

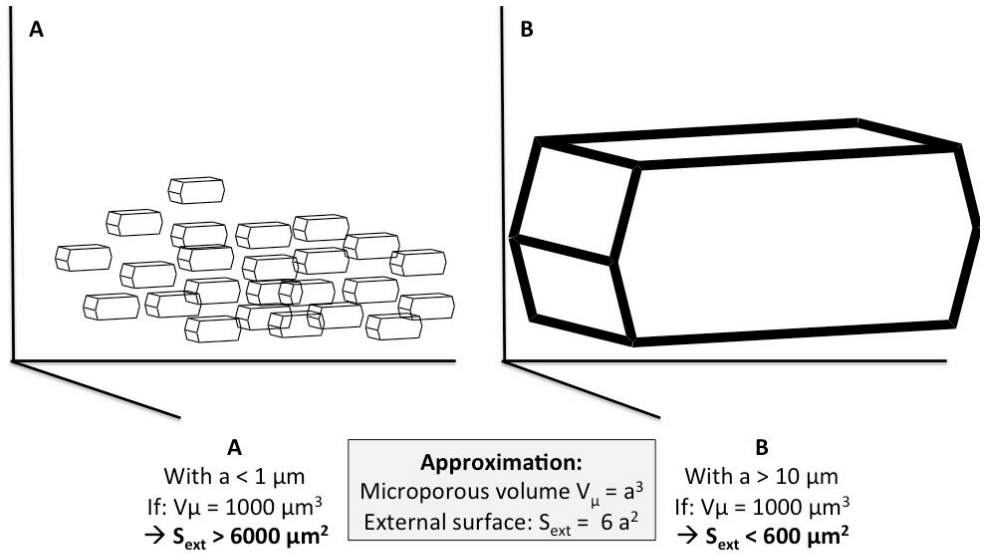

Figure 3-3. Small and large ZSM-5 crystals: albeit comparable in every other property than size (e.g. SAR, crystalline quality) the sheer exponential growth in external non shape selective surface with a shrinking in crystal size, renders it interesting to think of the application of large crystals in microporous catalysis.

3.4.3. Crystalline and Pore Quality

The present study evidenced during the initial screening of synthesis conditions that a high Si/Al-ratio combined with a neutral pH during the crystallization process guaranteed an extremely high crystalline quality. It is noteworthy that the pH control with HCl and phosphoric acid H_3PO_4 did not lead to the same high quality crystals than when the pH was adapted with a few drops of HF.

In a continuous aim of improving the large-scale applicability of our optimum catalyst, initial results indicate that the use toxic HF is no longer necessary and may be effectively replaced by other aluminum sources. Consequently, a scale-up project has already been set up, jointly with SATT Connectus and BASF.[188]

[188] The project's description can be found here: http://www.conectus.fr/fr/zeotail.

3.5. Towards the Optimum MTP-Catalyst Based on H-ZSM-5F

3.5.1. Detailed Synthesis of Selected Samples

The introduction of fluoride anions in zeolite synthesis[189] provided milder conditions, producing larger crystals with less defects and to more open structures with higher uptake of organocation and fluorine.[190] We thus prepared various ZSM-5 zeolites (named ZSM-5F) in fluoride aqueous solution at neutral pH, under conditions adapted from our previous studies.[191] Several factors, such as silicon source, fluoride concentration, volume, pH, chemical composition, were systematically evaluated (**Table 2-2**). To favor the formation of single, large and as perfect as possible crystals, highly diluted gels were used.

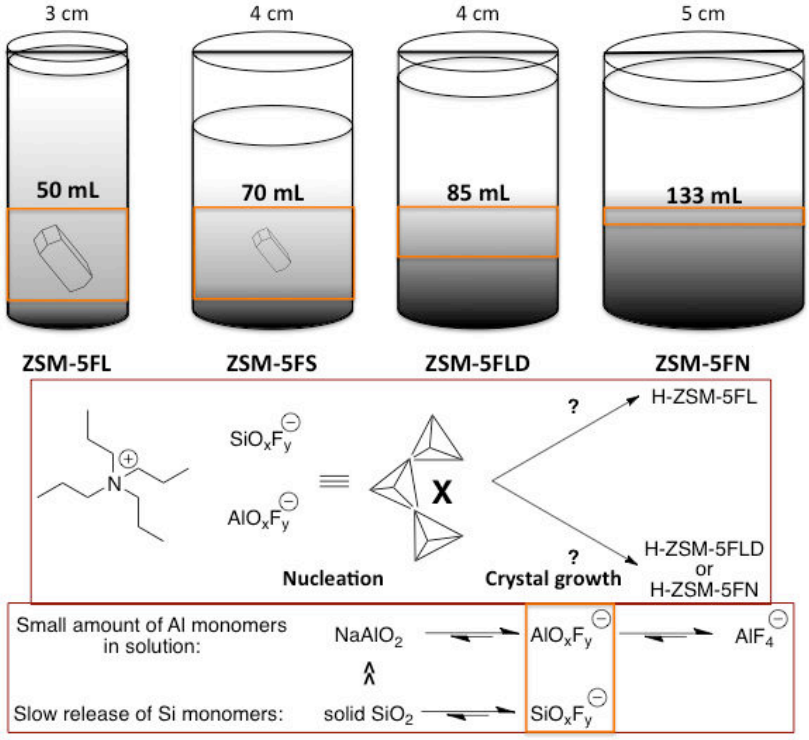

Figure 3-4. Varying concentration gradients during zeolite synthesis for the four studied zeolites, albeit initial gel concentrations are the same the lack of stirring leads to a slow sinking of intermediate crystallites (ZSM-5FN) or large formed single crystals (ZSM-5FL).

Solid silica proved to be the best Si source in the presence of ammonium fluoride, as expected from a slow release of $SiO_xF_y^-$ species under diluted conditions. Such species in the

[189] a) Camblor, M. A.; Villaescusa, L. A.; Diaz-Cabana, M. J. *Top. Catal.* **1999**, *9*, 59. b) Corma, A.; Puche, M.; Rey, F.; Sankar, G.; Teat, S. *Angew. Chem., Int. Ed.* **2003**, *42*, 1156. c) Flanigen, E.M.; Lok, B.M.; Patton, R.L.; Wilson, S.T.; Murakami, Y.; Ijima, A. (Eds.), *New Developments in Zeolite Science and Technology,* J.W. Ward, Kodansha Press, Tokyo, **1986**, p. 103.

[190] a) Xu, Y.; Maddox, P. J.; Couves, J. M. *J. Chem. Soc., Faraday Trans.* **1990**, *86*, 425. b) Kessler, H.; Patarin, J.; Schott-Darie, C. *Stud. Surf. Sci. & Catal.* **1994**, *85*, 75. c) Louis, B.; Kiwi-Minsker, L. *Microporous Mesoporous Mater.* **2004**, *74*, 171.

[191] a) Losch, P.; Laugel, G.; Martinez-Espin, J. S.; Chavan, S.; Olsbye, U.; Louis, B. *Top. Catal.* **2015,** *58*, 826. c) Losch, P.; Boltz, M.; Louis, B.; Chavan, S.; Olsbye, U. *CR Chimie* **2015**, *18*, 330.

presence of tetrapropylammonium bromide would lead to the formation of few nuclei, and thus to larger, high quality crystals (ZSM-5FL) (**Figure 3-4**). Monitoring the variation in fluoride concentration and the pH during ageing and zeolite formation confirmed these assumptions (**Figure 3-5**). Interestingly, the size of the autoclave reactor, which varied with increasing synthesis volumes strongly impacted the size and quality of so-formed MFI crystals: with larger autoclaves and synthesis volumes, smaller crystals (ZSM-5FS), or the presence of defects (ZSM-5FLD) or both (ZSM-5FN) were observed. This phenomenon could be tenatively linked to the concentration gradients that differ in different-sized cylinders at static conditions. In brief, one might expect a faster sinking rate of growing crystals in the large synthesis volumes resulting in smaller, or defects-containing crystals. However, all as-prepared ZSM-5 zeolites led to high crystalline yields (**Table 3-1**). Even though no optimal *defect-free* crystallization could be warranted for ZSM-5FN, the sole presence of the MFI-structure was ascertained by XRD (**Figure 3-6**)

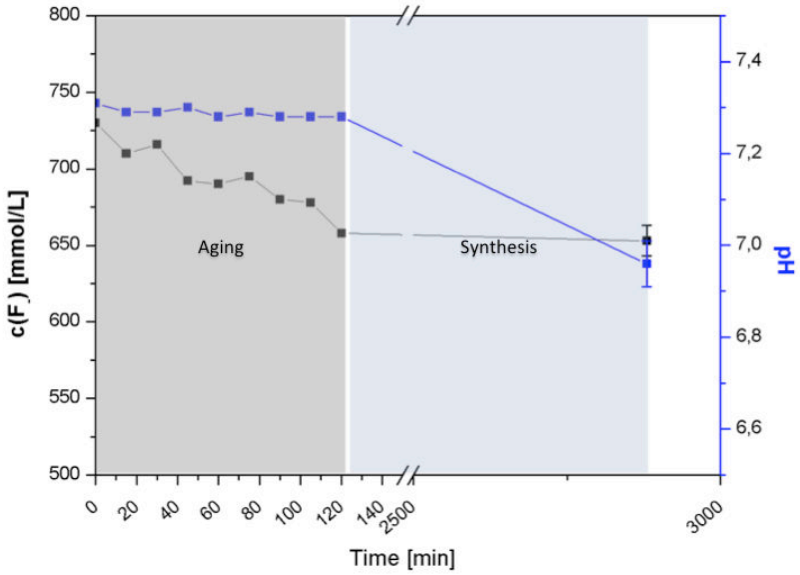

Figure 3-5. Fluoride ions concentration and pH variation during ageing and hydrothermal synthesis. The consumption of fluorides can be monitored during ageing; this consumption can be linked to the gradual dissolution of Aeroperl 300/30 silica, which acts as a SiO_xF_y monomer releasing reservoir.

3.5.2. Characterisation of this Selection

Besides, the quality of those crystals was evaluated by SEM observations (**Figure 3-7**) and their textural properties as well as Si/Al-ratios, theoretical and experimental Brønsted acid site (BAS) densities (strong BAS and total exchangeable protons) are reported in **Table 3-1**. These data indicate the absence of structural defects (Si-OH nests, EFAl-species etc.). in the H-ZSM-5FL and H-ZSM-5FS sample (entries 2 and 3), while the H-ZSM-5FN and H-ZSM-5FLD samples exhibit considerable amounts of non-BAS-linked exchangeable protons (entries 1 and 4), which could be titrated with an H/D-isotope exchange technique. The latter is a complementary

technique to the propylamine TPD that quantifies selectively the strong SI-(OH)-Al linked Brønsted acid sites.

Table 3-1. Textural properties of H-ZSM-5F zeolites.

Entry	Zeolite	Si/Al-ratio	Theoretical acid site density [mmol(H^+).$g_{zeolite}^{-1}$]	Acid site density [mmol(H^+).$g_{zeolite}^{-1}$]		S_{BET} [$m^2.g^{-1}$]	S_{meso} [$m^2.g^{-1}$]
				a	b		
1	H-ZSM-5FN	137	0.13	0.36	0.144	288	92
2	H-ZSM-5FS	139	0.13	0.21	0.127	425	55
3	H-ZSM-5FL	139	0.13	0.18	0.135	412	52
4	H-ZSM-5FLD	104	0.15	0.45	0.181	348	126

a: Total amount of exchangeable H^+: titrated by isotopic H/D-exchange technique.
b: Si-(OH)-Al bridging sites related Brønsted acid sites (BAS) quantified by propylamine-TPD.

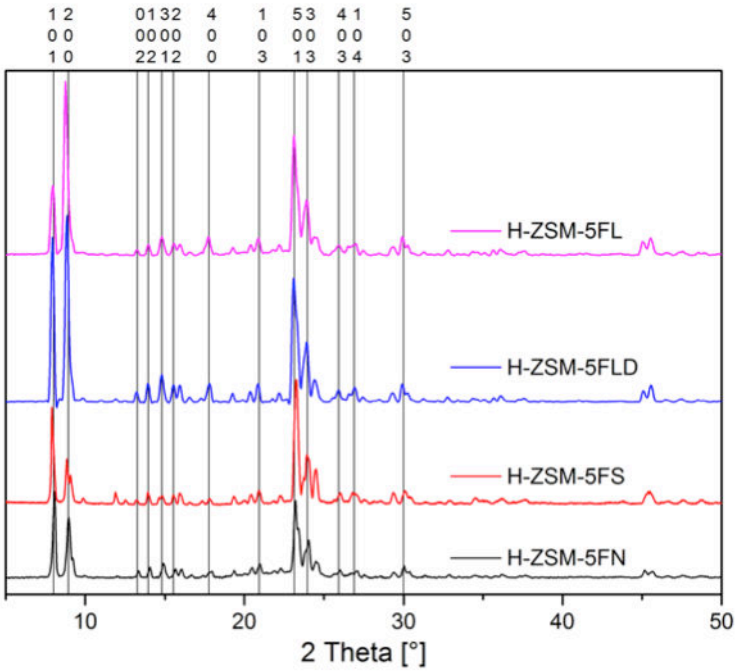

Figure 3-6. Powder XRD for the high quality H-ZSM-5FL and H-ZSM-5FN. Broader reflections peaks for H-ZSM-5FN are in line with the smaller size of these particles.

In addition to the S_{BET} and S_{meso} of the four samples, thorough gas transport measurements were performed and are presented in **Table 2-5**. We note the sole presence of micropores for H-ZSM-5FL and H-ZSM-5FS, whereas the microporous networks of H-ZSM-5N and H-ZSM-5FLD seem to be somehow obstructed, probably by various kinds of structural defects ZSM-5FS and ZSM-5FL exhibit a high crystalline quality as well as homogeneous size distributions (**Figure 3-7)**. Likewise, a dispersity index close to the unity was calculated for ZSM-5FS and ZSM-5FL samples. A deeper analysis of ZSM-5FL zeolite by HRTEM analysis (**Figure 3-8**) as well as

Rietveld refinement (**Figure 3-9**) allowed to prove an extremely high crystalline quality and excluding aluminum zoning and any subsequent formation of core-shell structure.

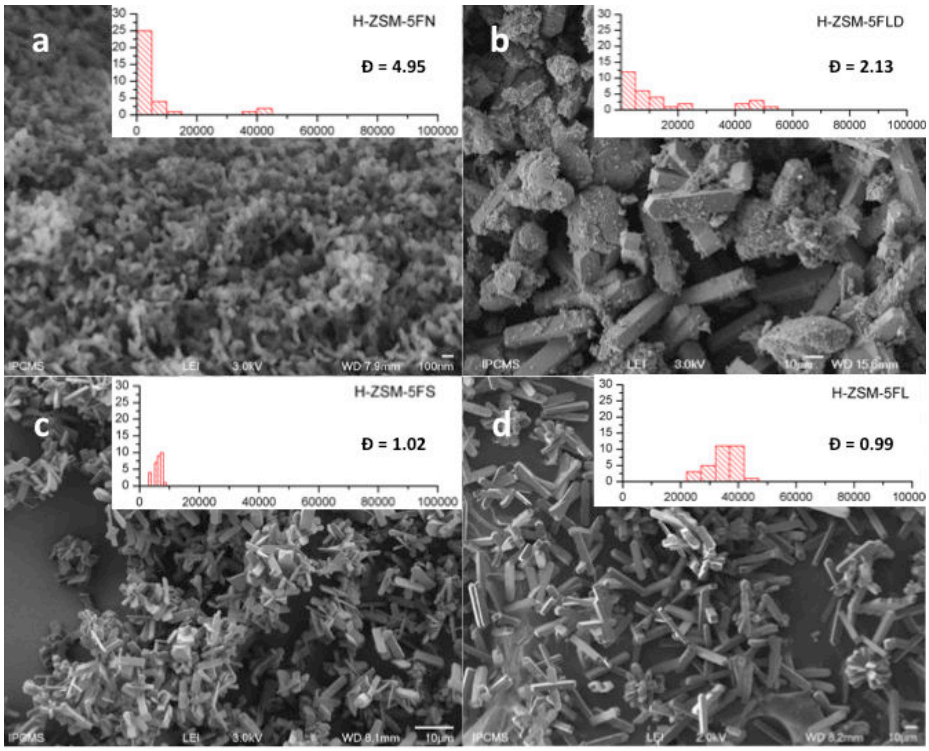

Figure 3-7. SEM images of as-synthesised zeolites: a) ZSM-5FN b) ZSM-5FLD c) ZSM-5FS and d) ZSM-5FL. Inserts show crystal size distributions (30 measurements: counts on the y axis and crystal sizes on the x-axis in nm) and calculated dispersities (Đ).

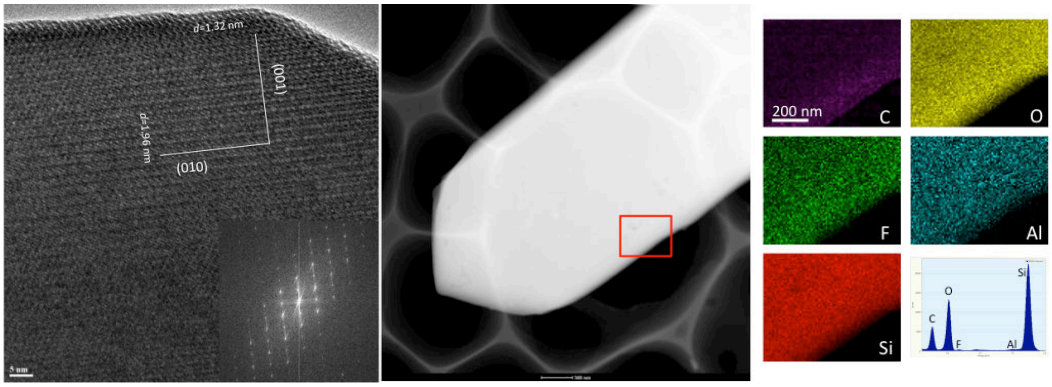

Figure 3-8. HRTEM and EDX analysis showing a perfectly homogeneous distribution of Al in as-synthesised ZSM-5FL crystal (cf. entry 3 in **Table 3-1**).

The diffraction pattern of the sample ZSM-5-FL was indexed in a primitive orthorhombic unit cell (a = 20.07309(6), b = 19.95733(6), c = 13.40854(5) Å), and the systematic absences were compatible with the space group *Pnma*, as previously reported.[192] An initial optimisation of the geometry, using the published atomic coordinates, was performed using a distance-least-squares

[192] Baerlocher, C.; McCusker, L. B.; Olson, D. H. *Atlas of Zeolite Framework Types*; Elsevier: Amsterdam, **2007** and Baerlocher, C.; McCusker, L. B. *Database of Zeolite Structures* http://www.iza-structure.org/databases/.

procedure.[193] A first difference electron density map showed a cross-shaped electron density cloud at the intersection of the two sets of 10-ring channels, so a TPA^+ cation was placed at that position with the N atom on the mirror plane perpendicular to the *b* axis. The C atoms of two of the propyl moieties were also placed on that mirror plane because they refined to positions that were very close to it. A subsequent differences map showed an electron density peak in the $[4^1 5^2 6^2]$ cage that was interpreted as a fluoride ion located on the mirror plane perpendicular to the *b* axis. The occupancy for this model refined to 0.35 for the F^- anions (1.4 F^-/u.c.) and 0.99 for TPA^+, so it was set to 1 (4 TPA^+/u.c). This is in agreement with literature data.[194]

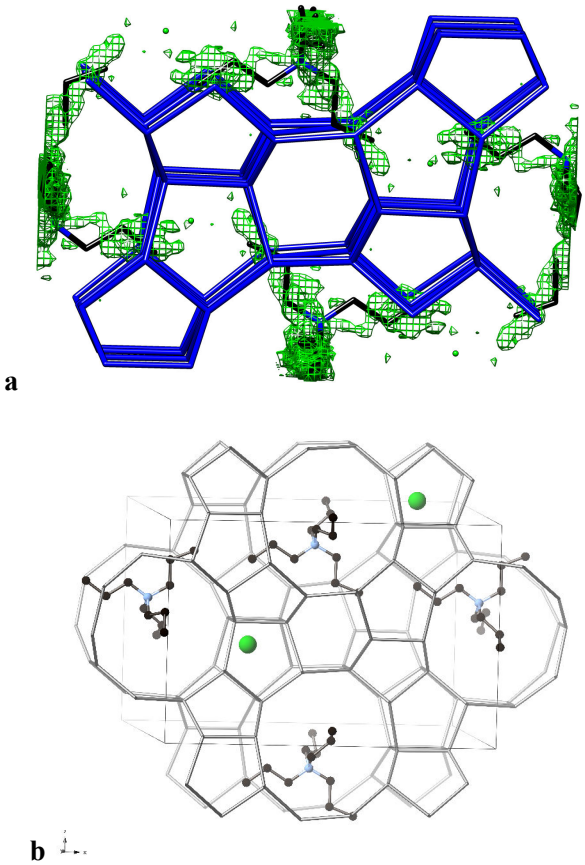

Figure 3-9. View of the MFI structure of sample ZSM5-FL down the b-axis, showing the 4 TPA^+ cations per unit cell. The green balls represent the location of fluoride anions. Framework oxygen atoms have been omitted for clarity.

[193] Baerlocher, C.; Hepp, A.; Meier, W.M.; *DLS-76, a FORTRAN program for the simulation of crystal structures by geometric refinemen*t, Institut für Kristallographie und Petrographie, ETH Zürich, Switzerland **1978**.
[194] a) Fyfe, C. A.; Brouwer, D. H.; Lewis, A. R.; Chezeau, J. M. *J. Am. Chem. Soc.* **2001**, *123*, 6882. b) George, A. R.; Catlow, C. R. A. *Chem. Phys. Lett.* **1995**, *247*, 408. c) Koller, H.; Wölker, A.; Eckert, H.; Panz, C.; Behrens, P. *Angew. Chem., Int. Ed.* **1997**, *36*, 2823. d) Burton, A.; Darton, R. J.; Davis, M. E.; Hwang, S. J.; Morris, R. E.; Ogino, I.; Zones, S. I. *J. Phys. Chem. B.* **2006**, *110*, 5273. e) Camblor, M.; Barrett, P.; Diaz-Cabanas, M.; Villaescusa, L.; Puche, M.; Boix, T.; Berez, E.; Koller, H. *Microporous Mesoporous Mater.* **2001**, *48*, 11. f) Camblor, M.; Corma, A.; Valencia, S. *Chem. Commun.* **1996**, *20*, 2365. g) Corma, A.; Puche, M.; Rey, F.; Sankar, G.; Teat, S. *Angew. Chem., Int. Ed.* **2003**, *42*, 1156. h) Villaescusa, L.; Wheatley, P.; Bull, I.; Lightfoot, P.; Morris, R. *J. Am. Chem. Soc.* **2001**, *123*, 8797.

Further refinement of this model with geometric restraints on bond lengths and angles for both the organic template and the framework yielded a reasonable geometry for the organic species as well as for the framework. The crystallographic data for this structure are given in **Table 2-3**. The arrangement of TPA^+ cations and fluoride anions within the MFI structure is shown in **Figure 3-9**. While two of the propyl arms lie on the mirror plane perpendicular to the *b* axis, and they point into the sinusoidal 10-ring channel, the other two propyl arms point into the straight channel and their C atoms are disordered over two positions with equal probability. This location is similar to the one found in two different structure analyses using laboratory single-crystal data.[195] This is also the location of other organic molecules such as *o*-xylene[196] and *m*-xylene[197] that are not used as SDAs but adsorbed on a calcined ZSM-5 sample. The occupancy factors refined to 4 SDAs per unit cell and the location of fluoride anions in $[4^15^26^2]$ cages, a similar position to that found in a single crystal refinement of pure silica ZSM-5.[195b] However, in that case fluoride anions interact with one of the Si framework atoms (Si−F = 1.91 Å), whereas in our case the shortest Si−F distance is 2.38 Å. Therefore, that Si does not show longer Si−O bond distances than the others, as usually found in case of Si−F interaction. Neither other extra-framework species were located, nor water molecules since only few molecules are expected to be present in such a hydrophobic zeolite (**Table 2-4**). **Figure 3-10** shows ^{19}F MAS NMR spectra for ZSM-5FLD and ZSM-5FL zeolites and ascertained the presence of two types of fluoride anions in as-synthesised samples. In contrast to ZSM-5FLD, highly crystalline ZSM-5FL zeolite exhibits a higher amount of fluoride species corresponding to the signal at - 63 ppm signal, whilst the signal at - 79 ppm was more pronounced in the zeolite containing defects. ^{19}F solid state NMR confirms therefore the presence of fluoride anions counterbalancing the positive charge of tetrapropylammonium cations (chemical shift at -64 ppm).[198] The signal with a chemical shift at -79 ppm is attributed to fluoride that is losely bound, or trapped into the micropores assuring the charge compensation and not detectable by Rietveld structure refinement due to its non-periodical arrangement.

[195] a) van Koningsveld, H.; Jansen, J. C.; van Bekkum, H. *Zeolites* **1987**, *7*, 564. b) Aubert, E.; Porcher, F.; Souhassou, M.; Petricek, V.; Lecomte, C. *J. Phys. Chem. B* **2002**, *106,* 1110.
[196] Nair, S.; Tsapatsis, M. *J. Phys. Chem.* **2000**, *104,* 8982.
[197] Fyfe, C. A.; Joseph Lee, J. S.; Cranswick, L. M. D.; Swainson, I. *Microporous Mesoporous Mater.* **2008**, *112*, 299.
[198] a) Guth, J. L.; Delmotte, L.; Soulard, M.; Brunard, N.; Joly, J. F.; Espinat, D. *Zeolites* **1992**, *12,* 929. b) Lombard, A.; Simon-Masseron, A.; Rouleau, L.; Cabiac, A.; Patarin, J. *Microporous Mesoporous Mater.* **2010**, *129,* 220.

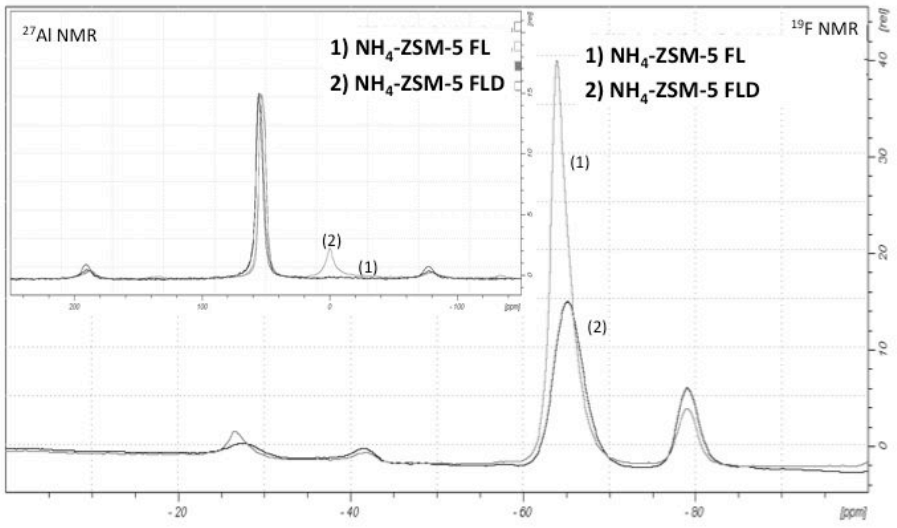

Figure 3-10. ^{19}F MAS NMR for as synthesised TPA^+ and NH_4^+ containing ZSM-5FL and ZSM-5FLD zeolites; inset: ^{27}Al MAS NMR for the two same samples.

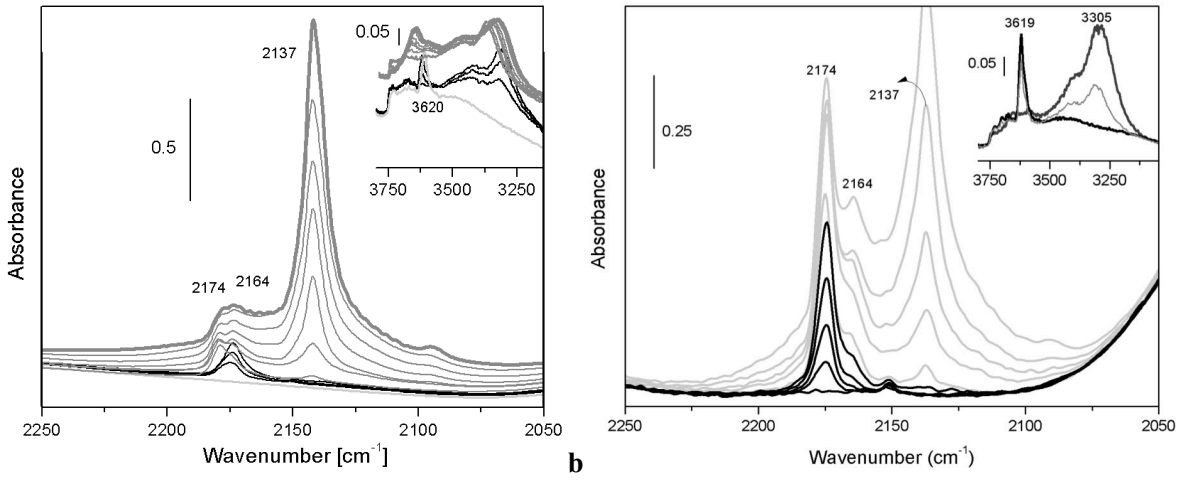

Figure 3-11. Low temperature CO adsorption FT-IR for a) H-ZSM-5FLD and b) H-ZSM-5FL. FT-IR spectra after pre-treatment at 873 K for 1 h, following CO adsorption at 77 K. **Insert:** the ν(OH) region; while the main graph presents the ν(CO) region. The CO coverage decreases successively from bold grey curve to light grey curve in the spectrum.

In the case of ZSM-5FL, the presence of octahedrally coordinated EFAl-species ($Al_{oct.}$) could be excluded by ^{27}Al MAS NMR (**Figure 3-10** insert), since no signal could be detected at 0 ppm. $Al_{oct.}$ species were, however, detected for H-ZSM-5FLD. Low temperature CO adsorption followed by FT-IR revealed the presence of a considerable amount of EFAl species, a clear peak at 2164 cm^{-1}, as well as some external and internal silanol defects (signal at 3700 cm^{-1}) in ZSM-5FLD zeolite (**Figure 3-11a**).[198a] In contrast, H-ZSM-5FL crystals did not exhibit any signal for silanol defects nor the presence of EFAl-species. Hence, solely bridging Si-OH-Al BAS are present within this zeolite: peak at 3619 cm^{-1} in the OH-stretching region and at 2174 cm^{-1} in the CO stretching region of the spectrum (**Figure 3-11b**).

3.5.3. MTO/P-reaction

Table 3-2. Catalytic activities and selectivities for the studied samples in the methanol-to-hydrocarbons reaction.

Entry	Zeolite	Conversion [%]	Selectivities [%]					
			CH_4-C_4H_{10}	$C_{2=}$	$C_{3=}$	$C_{4=}$	$C_{5=}$	$C_{6+\ aromatics}$
1	H-ZSM-5FN	99	4	16	39	15	16	10
2	H-ZSM-5FS	99	4	6	39	20	22	9
3	**H-ZSM-5FL**	**99**	**1**	**6**	**45**	**19**	**20**	**9**
4	H-ZSM-5FLD	99	7	20	35	13	14	11
5[a]	H-ZSM-5FLD	99	1	10	44	18	19	8
6	H-ZSM-5_{8020}	99	12	13	33	14	15	13
7	H-ZSM-5_{8020}P[3]	99	13	24	30	10	11	12

Catalytic data obtained after 1h on stream under standardized conditions; 60 mg catalyst in a fixed-bed quartz reactor, 450°C, WHSV 1.2h^{-1}; [a] Experiment carried out with d_4-methanol to evidence an isotope effect.
All of the homemade catalysts were compared to reportedly active MTO-catalysts, which are commercially available: entries 6 and 7.[184]

These different ZSM-5 zeolite catalysts were then tested in the transformation of methanol to olefins. **Table 3-2** presents the methanol (and dimethylether) conversion over calcined catalysts along with the selectivities towards the different hydrocarbons. H-ZSM-5FN led to a classical product distribution at full methanol conversion, producing a rather low quantity of light olefins (60 % cf. **Figure 3-2**).[199] Indeed, relatively high amounts of paraffins and aromatics were readily formed, suggesting the main occurrence of aromatics-based autocatalytic cycle for H-ZSM-5FN and H-ZSM-5FLD (entries 1 and 4), while the two H-ZSM-5FS and H-ZSM-5FL *perfect* samples (entries 2 and 3) exhibit a product distribution typical for an alkene-based autocatalytic cycle.

H-ZSM-5FS and H-ZSM-5FL (**Table 3-2**, Entry 3) led to the highest propylene selectivity; *i.e.* 45%. It needs to be mentioned at this point that no significant differences concerning either the characterisation (apart from the different crystallite sizes) or the catalytic behaviour could be noticed between these two *perfect* zeolites. Therefore the following part of the study will be focusing on the three catalysts; H-ZSM-5FN, H-ZSM-5FLD and H-ZSM-5FL. The latter MTP-catalyst exhibits exclusively microporosity and solely highly dispersed Brønsted acid sites, and in terms of stability out-competes the other two and two industrial commercially available samples (**Figure 3-12**). **Figure 3-13** depicts the linear relation between the MTO-productivity as a function of the methanol feed concentration, under MTO-relevant feed concentrations. Thus, we can expect a proper function of the catalytic bed under these conditions, even while using larger than usual ZSM-5FL crystals.

[199] Barger, P. *Methanol-to-olefins and beyond*, in *Zeolites for cleaner technology*, Eds. Guisnet, M.; Gilson, J.P. Vol 3, **2002**, Imperial College Press, London, England.

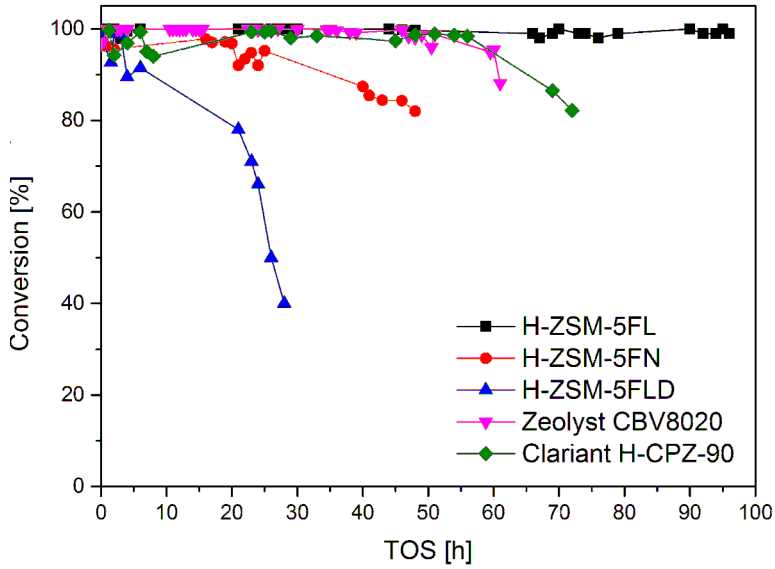

Figure 3-12. Methanol conversion as a function of the time on stream (TOS) for H-ZSM-5FL, H-ZSM-5FN and H-ZSM-5FLD. (Reaction conditions: 100% MeOH, WHSV = 1.2 h^{-1}, 450°C) **Zeolyst CBV8020** and **Clariant H-CPZ-90** are commercially available high-SAR ZSM-5 zeolites; 40 and 90 respectively.

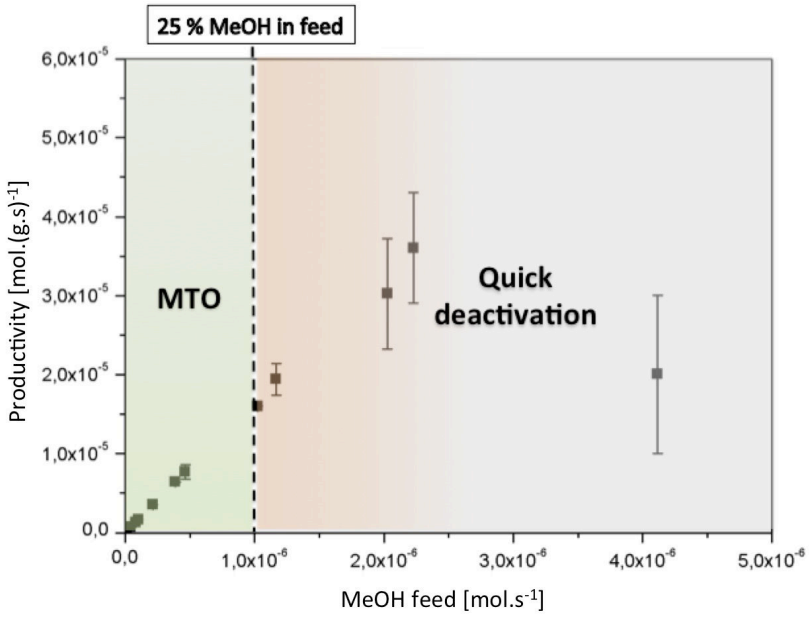

Figure 3-13. Light olefins productivity (total conversion of MeOH) as a function of the MeOH feed concentration for H-ZSM-5FL at the same reaction conditions as described above (450°C, 60 mg zeolite).

Interestingly, an experiment was performed flowing per-deuterated d_4-MeOD through H-ZSM-5FLD zeolite (**Table 3-2**, entry 5) and an isotopic effect could be evidenced (with respect to entry 4). **Figure 3-14** shows the distribution of products obtained at full d_4-MeOD- (a) or MeOH-conversion (b) over H-ZSM-5FLD zeolite at different temperatures. With stronger and shorter C-D bonds, d_4-MeOD led to a different product distribution compared to the one obtained for CH_3OH, especially in favour of propylene formation, achieving a $C_{3=}$-selectivity comparable to

H-ZSM-5FL (with CH_3OH). However, during this experiment still almost twice as much ethylene is detected over this catalyst than over H-ZSM-5FL. Several effects may be involved in this experiment's outcome; first the stronger C-D bond is limiting hydrogen-transfer (HT) reactions (in the given case deuterium-transfer (DT)). This is favouring the alkene-based autocatalytic cycle. Secondly, since this is not explaining *per se* the high propylene and still high ethylene selectivity, one may think of the shorter C-D bonds leading to smaller olefins. Therefore, in the defects containing ZSM-5FLD with non-perfect micropores, where (C-H)-MTP is not properly working, the combination of the two aforementioned effects may allow an optimal diffusion of smaller olefins and thus explaining the observation of a (C-D)-MTP.

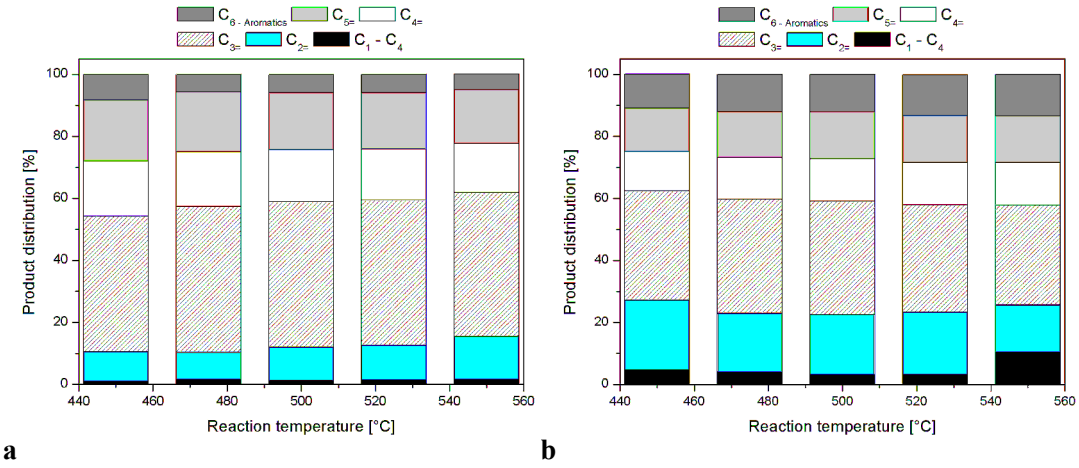

Figure 3-14. ZSM-5FLD catalyst selectivities at different reaction temperatures obtained at complete conversion of a) d_4-MeOD and b) MeOH.

Based on recent studies on Diels Alder reaction, where an optimal fit was found between the two protagonists, *methylacrylate and isoprene*, and the MFI zeolite framework (at low temperatures < 90°C), one may suggest a possible enhanced diffusivity of certain molecules in those large crystals. In our case, we chose to study propylene, *the target and major product formed over ZSM-5FL*, which has been used as a reactant to evaluate its conversion under MTO conditions (**Figure 3-15**). The fluoride-synthesised catalysts converted propylene above 300°C (other products than propylene appear in the product distribution). Interestingly, this is especially noticeable for the large H-ZSM-FL sample where logically molecules exhibit longer residence times during catalysis and thus are prone to undergo reactions. But, at temperatures above 400°C (MTO conditions), propylene is detected as major product again also for H-ZSM-5FL, indicating either a reaction producing selectively propylene or simply the fast diffusion of the latter through the completely microporous network. Under the studied conditions (Temperature!) the considered molecular diameter of propylene and ZSM-5's micropores may indeed perfectly fit, as we will see in a later section. A large and defect-free crystal with highly dispersed acid sites may warrant a

proper sorption of propylene within the pores, reducing the degrees of freedom of sorbates, manifested by a (limited) decrease in entropy.[200]

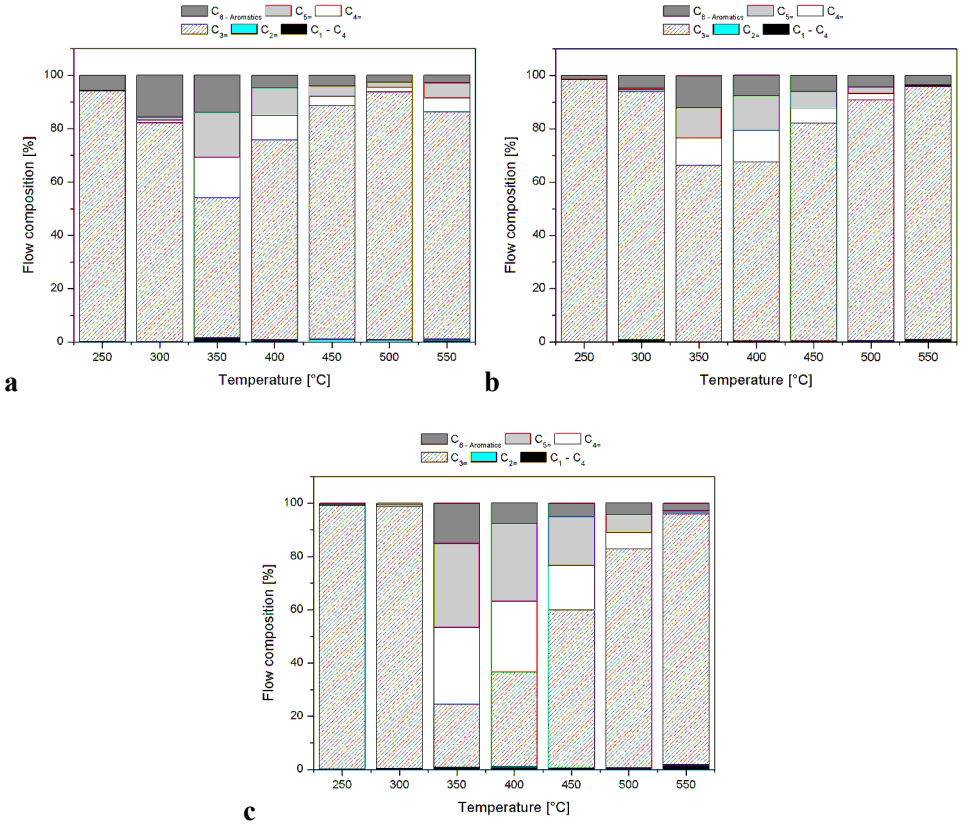

Figure 3-15. Distribution of products formed after propylene flown through the catalyst at different temperatures (250 - 550°C): a) H-ZSM-5FN b) H-ZSM-5FLD c) H-ZSM-5FL.

Post mortem analyses, after 100 hours time on stream were performed as well for H-ZSM-5FL and compared to previously reported active MTO-catalysts, namely H-ZSM-5_{8020} and H-ZSM-5_{8020}P[3] which are commercially available: entries 6 and 7 in **Table 3-2**.[184] As plotted in the **Figure 3-16** these analyses were carried out using FTIR and observing the coke-specific 1200-1900 cm^{-1} absorbance regions. Strikingly, after 100 hours on stream, while the H-ZSM-5_{8020}P[3] already deactivated,[184] hence a high amount of coke species could be expected and was detected, the H-ZSM-5_{8020} and our H-ZSM-5FL sample were still active, yet H-ZSM-5FL was the only seemingly totally exempt of coke species.

[200] Lercher, J. A.; Jentys, A. *Application of Microporous Solids as Catalysts, in Handbook of Porous Solids*, Eds. Schuth, F.; Sing, K.S.W.; Weitkamp, J. Vol 2, **2002**, WILEY-VCH Verlag GmbH, Weinheim, Germany.

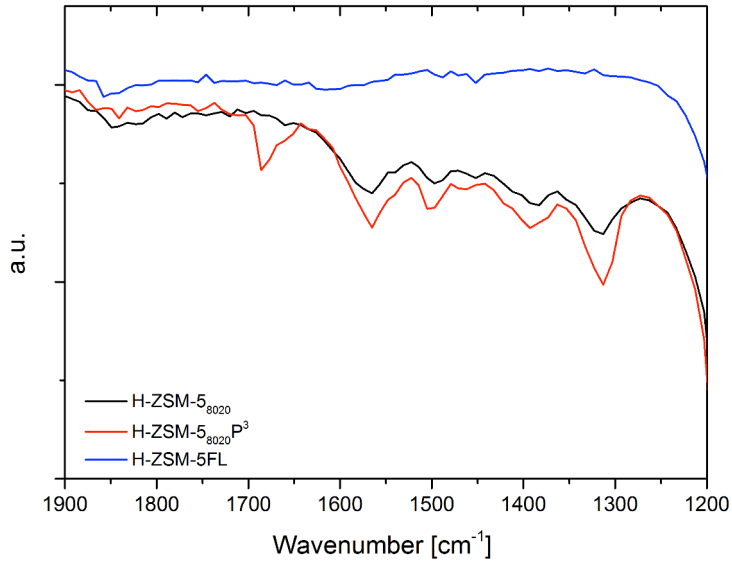

Figure 3-16. IR analysis of used H-ZSM-5FL after TOS = 100 h was compared to previously reported active MTO-catalysts H-ZSM-5$_{8020}$ and H-ZSM-5$_{8020}$P^3, which are commercially available: entries 6 and 7 in **Table 3-2**.[184] Coke specific absorbance region: 1200 - 1900 cm^{-1} with 1300 - 1600 cm^{-1} corresponding to aromatic C=C-stretching and 1600 - 1700 cm^{-1} to alkene C=C-stretching.

3.5.4. Why? Understanding these Paradoxically Behaving Catalysts

In order to underline our rising suspicion that our high quality H-ZSM-5FL zeolite seems to be a valuable candidate as a model and competitive MTP-catalyst, we performed Pulsed Field Gradient (PFG)-NMR spectroscopy with different model guest molecules (toluene, benzene and neopentane), selected for their various size and shape. PFG-NMR has been reported to be a powerful tool to measure molecular diffusivities in porous materials such as zeolites, and has allowed the discrimination between mesoporous and microporous diffusion.[201] **Figure 3-17** presents effective diffusivities of three different probe molecules, which were measured for the three studied zeolites.

The most commonly studied probe molecule toluene (**Figure 3-17a**) is showing two different diffusivities which can be attributed to be linked to intercrystalline mesoporous diffusion for the 10^{-8} m^2.s^{-1} part (for H-ZSM-5FN) and to intracrystalline microporous diffusion in the range of 10^{-9} m^2.s^{-1} (for all samples). The latter value is in agreement with what has been shown by adsorption-desorption measurements coupled with infrared spectroscopy.[202] Several spectra were recorded at different diffusion times for H-ZSM-5FL zeolites, exclusively containing micropores (**Figure 2-1**).

[201] a) Kortunov, P.; Vasenkov, S.; Kärger, J.; Valiullin, R.; Gottschalk, P.; Elia, M. F.; Perez, M.; Stöcker, M.; Drescher, B.; McElhiney, G.; Berger, C.; Gläser, R.; Weitkamp, J. *J. Am. Chem. Soc.* **2005**, *127*, 13055. b) Filippov, A.; Dvinskikh, S. V.; Khakimov, A.; Grahn, M.; Zhou, H.; Furo, I.; Antzutkin, O. N.; Hedlund, J. *Magn. Reson. Imaging* **2012**, *30*, 1022. c) Schneider, D.; Mehlhorn, D.; Zeigermann, P.; Kärger, J.; Valiullin, R. *Chem. Soc. Rev.* **2016** 10.1039/C5CS00715A.

[202] Mukti, R.R. *Sorption and transport of aromatic over MFI zeolites,* PhD-Thesis**, 2007**.

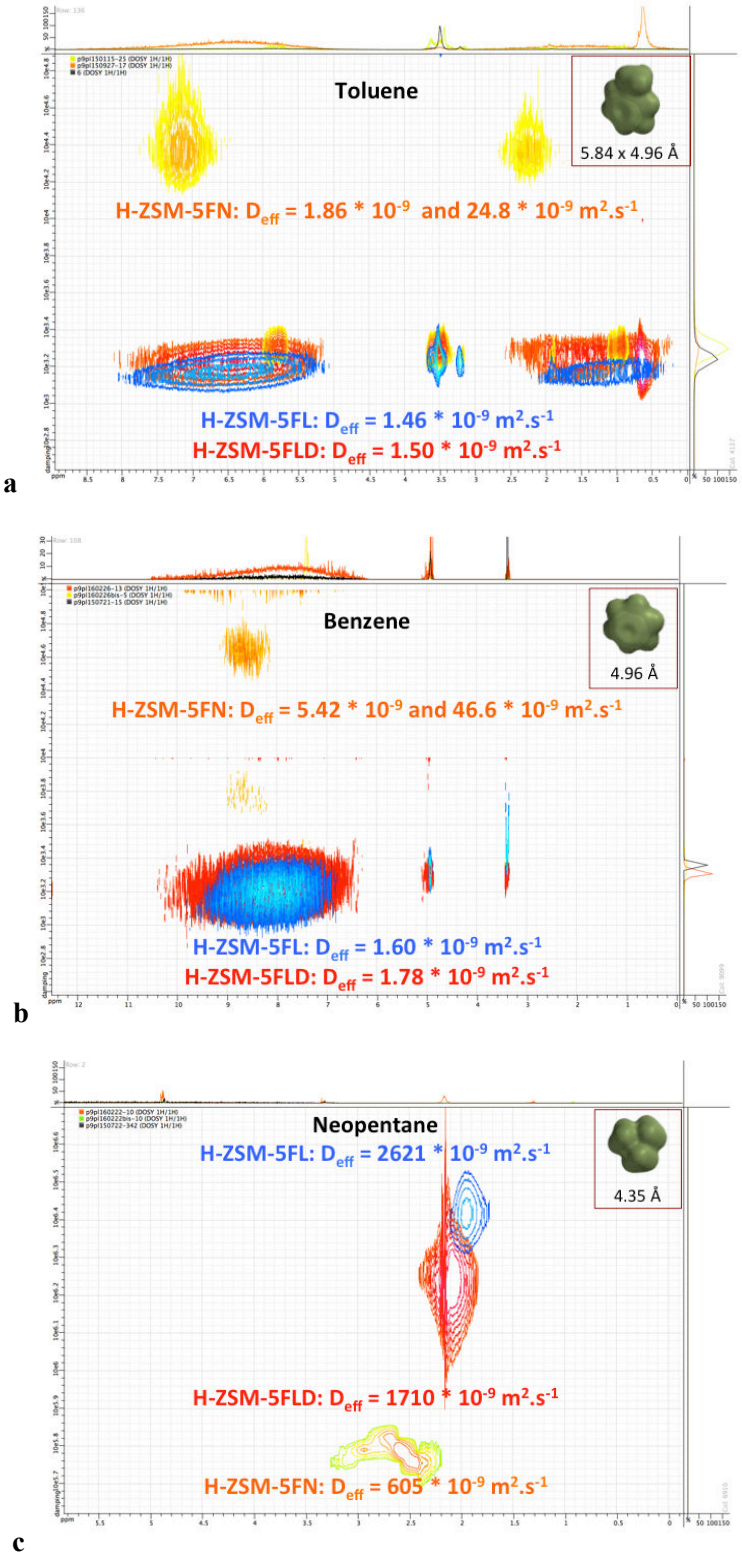

Figure 3-17. PFG NMR diffusion experiments over H-ZSM-5FN (yellow), H-ZSM-5FLD (red) and H-ZSM-5FL (blue) with three different probe molecules a) toluene, b) benzene and c) neopentane.

The linear fit between $D_{eff.}$ and diffusion times indicates a confined diffusion within the microporous network (**Figure 3-18**). It is important to note that, in a non-confined environment, measured diffusivities will not vary while varying diffusion times and that our large crystal sizes

combined with NMR time-measurement experiments are beneficial to monitor the intracrystalline diffusion. In **Figure 3-17b** the effective diffusivities of benzene behave the same way than those of toluene, with microporous diffusion (for the three samples) and supplementary mesoporous diffusion (for H-ZSM-5FN). Lastly, in **Figure 3-17c**, where neopentane's diffusivities are assessed, a surprising result was observed. In H-ZSM-5FN the quasi-spherical molecule, which perfectly fits ZSM-5's micropores (under room temperature conditions) is diffusing at $605*10^{-9}$ $m^2.s^{-1}$,[203] whereas for the larger high quality crystals it seems to diffuse roughly three-times faster with $1710*10^{-9}$ $m^2.s^{-1}$ in H-ZSM-5FLD and most impressively, four times faster with $2621*10^{-9}$ $m^2.s^{-1}$ in *perfect* H-ZSM-5FL. Thus the previously observed tendency D_{eff} (H-ZSM-5FLD) = D_{eff} (H-ZSM-5FLD) < D_{eff} (H-ZSM-5FN) seems to be inversed D_{eff} (H-ZSM-5FL) > D_{eff} (H-ZSM-5FLD) > D_{eff} (H-ZSM-5FN) leading to the same conclusion. It is necessary to note that for each probe molecule the diffusivity-distribution is larger over the defect-containing zeolite, as compared to the perfect ZSM-5FL sample. Thanks to these high quality crystals, it was possible to observe neopentane inside ZSM-5's micropores diffusing like a "floating molecule" or levitate as it has been predicted by Derouane *et al.*[204] and already attempted to be proven experimentally on NaX zeolite by Rajappa *et al*.[205]

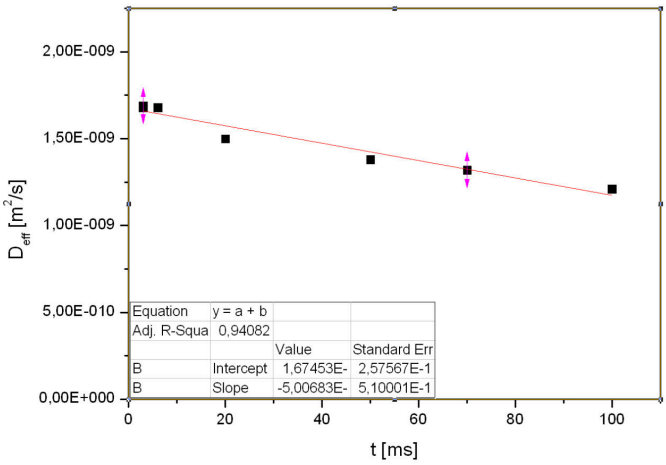

Figure 3-18. Linear fit of diffusivities in function of diffusion time indicating a confined diffusion for giant sized ZSM-5 zeolites.

[203] This order of magnitude 600 . 10^{-9} $m^2.s^{-1}$ is common for gas phase diffusion in ZSM-5 zeolites. For CH_4: D_{eff} = 900-1900 . 10^{-9} $m^2.s^{-1}$ Arzumanov, S. S.; Kolokolov, D. I.; Freude, D.; Stepanov, A. G. *J. Phys. Chem. C* **2015**, *119*, 18481.

[204] a) Derouane, E. G.; André, J.-M.; Lucas, A. A. *Chem. Phys. Lett.* **1987**, *137*, 336. b) Derouane, E. G.; André, J.-M.; Lucas, A. A. *J. Catal.* **1988**, *110*, 58. c) Lambin, P.; Lucas, A. A.; Derycke, I.; Vigneron, J. P.; Derouane, E. G. *J. Chem. Phys.* **1989**, *90*, 3814. d) Derycke I.; Vigneron, J. P.; Lambin, P.; Lucas A. A.; Derouane E. G. *J. Chem. Phys.* **1991**, *94*, 4620.

[205] Rajappa, C.; Krause, C.; Borah, B. J.; Adem, Z.; Galvosas, P.; Kärger, J.; Subramanian, Y. *Microporous Mesoporous Mater.* **2013**, *171*, 58.

3.6. Discussion and Proposed Rationalisation

Zeolite topologies are known to be a key factor regarding their activity and selectivity in catalysis.[179a] Comparing different pore architectures is a good starting point. Nevertheless, zeolites among one particular zeolite topology usually exhibit different crystal sizes, acid site densities and crystalline qualities. Additionally, it is well known that those key parameters may play important roles in activity and selectivity in acid-catalysed reactions.[180]

Herein, we focused on the synthesis and application of "perfect" crystals, which are active in the conversion of methanol into hydrocarbons and highly selective toward propylene. In sharp contrast to what was expected, we could establish, thanks to the thorough characterisation and catalytic data, that an almost *perfectly crystallized zeolite with a low Brønsted acid site density and a very large crystal size* is in fact an optimum to design a ZSM-5 zeolite for the MTP process. This paradigm change is fully counter-intuitive, since large crystals normally limit catalyst activity due to diffusional limitations of aromatics or relatively large olefins.

In the following part, we attempted to explain this interesting catalytic behaviour and its corresponding product distribution using our data and various reported tendencies concerning material physics and confinement linked shape selectivity.

Kemball has already evoked an interesting concept of diffusional supermobility in the 1950's.[206] This concept is based on the movements of a molecule exempted from any constraint. Depending on its length and diameter a molecule can move with respect to its rotational and vibrational degrees of freedom more or less rapidly in non-confined 3D space. However, a sorbed molecule in a porous host will suffer limitations in its movements and when its dynamical diameter (**Figure 3-21**) equals the porous diameter, then only two directions (forwards and backwards) are left to diffuse. Hence, its apparent diffusion may become "superfast", as illustrated in **Figure 3-21**. As seen in **Figure 3-17c** such an effect was observed for neopentane under ambient conditions, and this phenomenon may also play a role for propylene under MTP conditions.

Such effects are intrinsic to the confinement theory and should influence a product distribution during zeolite catalysis.[207] In contrast to Ryoo's work with 2-unit cell thick MFI crystals, where mass transfer limitations could be excluded,[208] regarding the above it becomes imaginable that our crystals with more than 5000 MFI unit cells in the crystalline a- and b-axes parallel to the crystals micropores might not be limited by mass transfer too.

[206] a) Kemball, C.; *Adv. Catal.*, **1950**, *2*, 233. b) Smit, B.; Maesen, T. L. M. *Nature* **2008**, *451*, 671.
[207] Derouane, E. G. *Chem. Phys. Lett.* **1987**, *142*, 200.
[208] Kim, J.; Choi, M.; Ryoo, R. *J. Catal.* **2010**, *269*, 219.

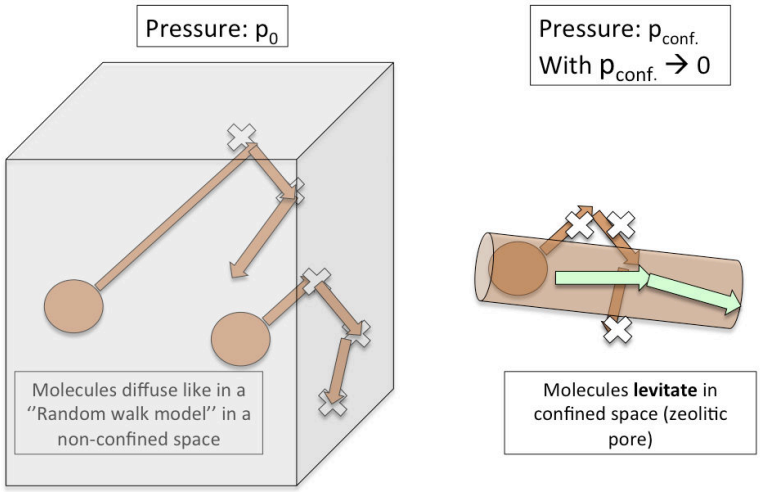

Figure 3-19. ***Sinister***: molecules can diffuse stochastically in a non-confined 3D space and exert a certain pressure on their recipient; ***Rectus***: in a confined "1D" space, "floating molecules" can get supermobile, they begin to levitate and no longer exert pressure on their recipient.

Indeed we observed in our MTO-studies that the quality of the crystals had an impact on the diffusion of molecules in the microporous network. In those experiments, the fewer defects were, the better catalytic performance was observed for as-made materials. Furthermore, a correlation could be established between the propylene selectivity and the (detrimental) presence of defects.

Therefore, it seems that free diffusion could be hindered by any kind of defects, such as the common presence of EFAl species or silanol defects. More surprisingly but interestingly, high acid site density may also be considered as a defect. Indeed, statistics based on our thorough characterisation of ZSM-5FLD and ZSM-5FL's porosities (**Figure 2-1** and **Table 2-5**) show that the mean diffusion path in ZSM-5 zeolites would be strongly influenced by different Si/Al-ratios (**Figure 3-20**). This model also shows that in ZSM-FL type materials, a molecule diffusing through the microporous network would diffuse through at least 5-6 channel intersections before encountering the next nearest acid site. This pathway would thus limit further reactions and therefore improve the selectivity.

The above-mentioned concept of diffusional supermobility is obviously also linked to the size and shape of the diffusing molecule. Interestingly, our MTO studies also suggest that molecular size plays a key role in this transformation. Indeed, the perdeuterated methanol experiment showed that under equilibrium conditions the molecular apparent sizes can lead to a change in the product distribution, shifted towards the production of diffusion-enhanced olefins.

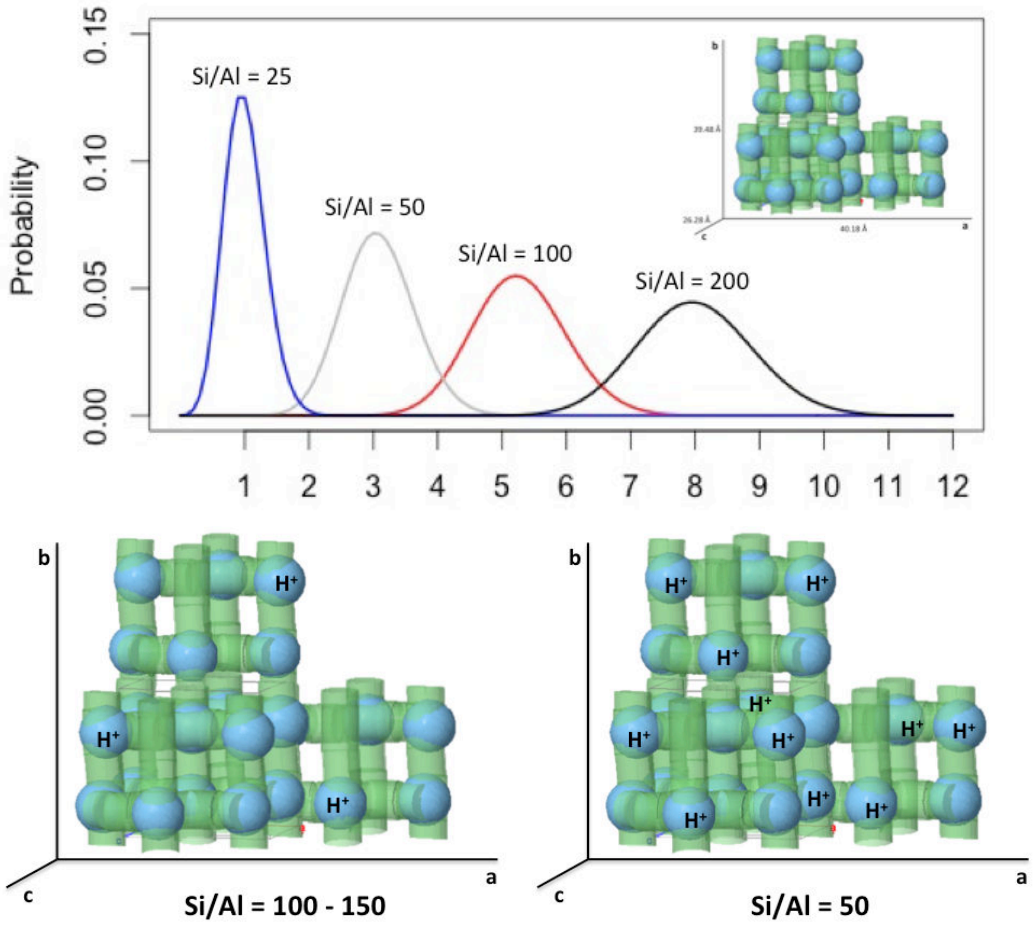

Figure 3-20. Probability of encountering a next active site (located in the blue spherical channel intersections) traced as a function of channel intersections to diffuse through. A 4-unit cell model for inter active site distance modelling: acid sites, preferably located at channel intersections (blue spheres) are more dispersed with increasing Si/Al-ratio: a molecule diffusing through the microporous network of H-ZSM-5FL, for instance, would diffuse through at least 5-6 other channel intersections before encountering a next acid site.

Moreover, the experiment with propylene fed at different temperatures shows as well that the production and diffusivity of propylene is enhanced at MTO/P relevant conditions, leading to the same conclusion.

The impact of diffusivities on the selectivity of a reaction, hence its final product distribution has already been evaluated with the Madon-Boudart and the Mears criteria for internal and external diffusion limitations.[209] However, such criteria allow evaluating whether a reaction is limited by diffusion or not and thus are not greatly important for the herein studied MTO-reaction, which is not limited by the diffusion of the reactant. **Figure 3-21a** explains why we may consider light olefins, the main products during the MTO-reaction as spheroidal molecules, enabling in turn the theoretical implementation of the levitation concepts. **Figure 3-21b** then, plots the theoretically predicted mean diffusional velocities using the later developed

[209] Madon, R. J.; Boudart, M. *Ind. Eng. Chem. Fundam.* **1982**, *21*, 438–447.

eq. 3.13 for the different light olefins once in free space and once in a *sphere-in-a-cylinder* confined space.

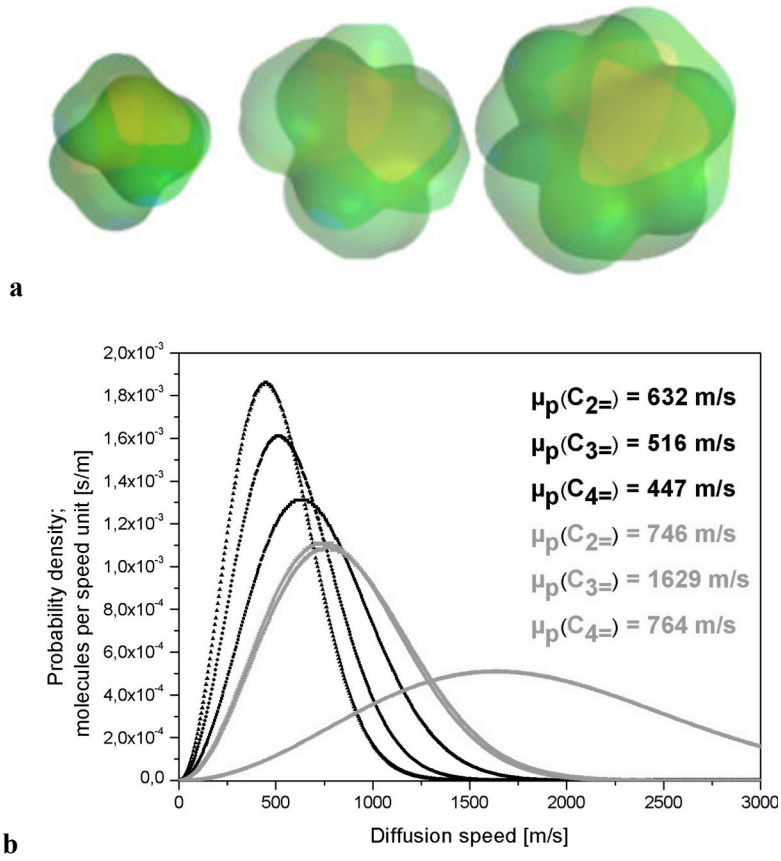

Figure 3-21. a) Dynamical molecular diameter at (r.t. - 523 - 773 K) of ethylene (3.5 - 4 - 4.5 Å), propylene (4.2 - 5 - 5.7 Å) and butylene (5.4 - 6.5 - 7.3 Å), respectively. They behave like oscillating expanding spheres at higher temperatures, such as the encountered process temperatures of 523 – 773 K. b) Calculated mean diffusional velocity for light olefins at MTO-operation temperatures (450°C) in free space (black curves) compared to when confined in a porous network (grey curves), using the equation 3.13.

The impact of higher apparent diffusivities is also true for the transition state level of adsorbed species. Recently, Lercher's group demonstrated that “adsorbed transition state species” on strong (as shown above, highly dispersed in ZSM-5FL) acid sites are all but static.[210] Especially at high temperatures, those "protons" in zeolites can be assimilated to superacids.[211] Krossing *et al*.[212] demonstrated the possible exalted mobility of cations on weakly coordinating anions. The ZSM-5FL framework possessing a high SAR without defects can be assimilated to a

[210] Zhi, Y.; Shi, H.; Mu, L.; Liu, Y.; Mei, D.; Camaioni, D. M.; Lercher, J. A. *J. Am. Chem. Soc.* **2015**, *137*, 15781.
[211] a) Haag, W.O.; Lago, R.M.; Weisz, P.B. *Nature* **1984**, *309*, 589. b) Mirodatos, C.; Barthomeuf, D. *J. Chem. Soc., Chem. Commun*. **1981**, 39. c) Louis, B.; Pereira, M. M.; Santos, F. M.; Esteves, P. M.; Sommer, J. *Chem. Eur. J.* **2010**, *16*, 573.
[212] a) Krossing, I.; Raabe, I. *Angew. Chem., Int. Ed.* **2004**, 43, 2066. b) Krossing, I. Eds. Reedijk, J.; Poeppelmeier, K. *Comprehensive Inorganic Chemistry II*, Vol 1. **2013**, Oxford: Elsevier 681-705. c) Rupp, A.; Roznyatovskaya, N.; Scherer, H.; Beichel, W.; Klose, P.; Sturm, C.; Hoffmann, A.; Tübke, J.; Koslowski, T.; Krossing, I. *Chem. Eur. J.* **2014,** *20*, 9794.

solid weakly coordinating anion, thus the main product propylene in its adsorbed state may diffuse rapidly (as well as its protonated form), whereas protonated butylenes and other olefins exhibit longer residence times within large crystals and can react further, forming even more propylene (**Figure 3-15**). Under those *quasi* steady-state conditions, it is therefore reasonable to expect a negligible contribution of adsorption / desorption processes with respect to diffusion of propylene within the crystal.

Despite its complexity,[213] the reaction kinetics of the MTO elementary reactions on ZSM-5 zeolites are well studied. Detailed reaction rates for methylation and cracking steps in the autocatalytic MTO reaction have been determined.[214,178] In terms of reactivity for methylation ($R_{meth.}$), the following tendency is observed: $R_{meth.}(C_{2=}) < R_{meth.}(C_{3=}) = R_{meth.}(C_{4=})$. In a very simplistic assumption, where MTP runs in an olefin based autocatalytic cycle, the reported catalytic results suggest, in order to compensate for the observed product distribution, and especially in our large crystals that effective diffusivities in ZSM-5 zeolite should be as follows: $D_{eff}(C_{3=}) >> D_{eff}(C_{2=}) = D_{eff}(C_{4=})$.

Additionally, under MTO conditions (> 400 °C), sufficient thermal energy is provided to methylate and crack any given olefin. However, the entropic part is highly impacted by the molecule-pore interactions and its impact on the Gibbs enthalpy of activation is directly linked to the reaction temperature.[215] The reaction is thus ruled by an optimum between Gibbs free energy barriers of diffusion and of previous, intermediate or subsequent reactions. Hence, in the case of H-ZSM-5FL (eq. 3.1):

$$\Delta(D_{eff}) >> \Delta(R_{meth./crack.})^{216} \qquad (3.1)$$

$$\Delta G_{act} = - R.T.\ln K = \Delta H_{act} - T.\Delta S_{act} \qquad (3.2)$$

The reaction can be described by the following equilibrium constant K (eq. 3.3) considering partial pressures of reactants and products with their respective coefficients (v - z):

$$K = \frac{p_i(C_{2=})^v p_i(C_{3=})^w p_i(C_{4=})^x p_i(C_{n=})^y p_i(H_2O)^z}{(p_i(MeOH)+p_i(DME))^z} \qquad (3.3)$$

We thought worthy to investigate the influence of positive thermal expansion (PTE) of molecules, negative thermal expansion (NTE) of porous materials, along with a Maxwell-Boltzmann distribution of diffusional velocities (μ) (eq. 3.5), to provide an empirical understanding of an optimal fit of a molecule within pores and its related enhancement in apparent effective diffusivities. Likewise, its impact on the above-mentioned equilibrium constant (eq. 3.3) has to be studied. As a general finding, a well-defined porous network may induce an apparent

[213] Park, T. Y.; Froment, G. F. *Ind. Eng. Chem. Res.* **2001**, *40*, 4187.
[214] a) Sun, X.; Mueller, S.; Liu, Y.; Shi, H.; Haller, G. L.; Sanchez-Sanchez, M.; van Veen, A. C.; Lercher, J. A. *J. Catal.* **2014**, *317*, 185.
[215] a) Gounder, R.; Iglesia, E. *Acc. Chem. Res.* **2012**, *45*, 229. b) Jones, A. J.; Carr, R. T.; Zones, S. I.; Iglesia, E. *J. Catal.* **2014**, *312*, 58.
[216] Derouane, E. G. *Microporous Mesoporous Mater.* **2007**, *104*, 46.

decrease in the partial pressure of a floating molecule (eq. 3.4), thus leading to a shift in the thermodynamic equilibrium towards the formation of this molecule (**Figure 3-21b**). The quasi-steady state at MTO reaction conditions is strongly shifted towards the production of light olefins; therefore Eq. 12 might better describe the inter-conversion (via the dual cycle) of light olefins. In addition, ZSM-5FL is rather hydrophobic and should favour (with respect to defective crystals) a continuous water release from the porous network and therefore shift the equilibrium toward products formation. Considering now, the product distribution, or in other words, the high propylene selectivity, a fluid supermobility concept can be applied to explain this unexpected behaviour.

As $p_{conf.} \rightarrow 0$ (3.4)

The general speed distribution will be impacted as following:

$$f_{3D}(\mu) = \sqrt{(\frac{m}{2\pi kT})^3} 4\pi\mu^2 e^{-\frac{m\mu^2}{2kT}} \quad (3.5)$$

with $p = \frac{F}{A} = \frac{ma}{A}$ (3.6)

Here, *F* is a force, *A* an area and *m* the considered molecule's mass, while *a* is an acceleration.

So $m = p * \frac{A}{a}$ (3.7)

Hence $f_{3D}(\mu) = \sqrt{(\frac{p*A}{2\pi kTa})^3} 4\pi\mu^2 e^{-\frac{p*A*\mu^2}{2kTa}}$ (3.8)

Now we are introducing γ (eq. 3.9 varying between 0 and 1 and impacting the partial pressuresunder equilibrium conditions in the MFI-framework), basically traducing the fit between any considered molecule, its temperature impacted diameter $ø_{molecule}(T)$, and the microporous network with its temperature impacted diameter $ø_{pore}(T)$:

$$\gamma = (e^{-(1-\frac{ø pore(T)}{ø molecule(T)})^2})^x \quad (3.9)$$

$$f_{3D}(\mu) = \sqrt{(\frac{p^\gamma.A}{2\pi kTa})^3} 4\pi\mu^2 e^{-\frac{p^\gamma.A.\mu^2}{2kTa}} \quad (3.10)$$

Leading to the most likely diffusional velocity:

$$\mu_p = \sqrt{\frac{2\pi kTa}{p^\gamma.A}} \quad (3.11)$$

Considering all the constants above, they arereplaced by *c* and *c′*, equations simplify in turn to the following:

$$f_{3D}(\mu) = \sqrt{(c.p^\gamma)^3} c'.\mu^2 e^{-p^\gamma.c.\mu^2} \quad (3.12)$$

$$\mu_p = \sqrt{\frac{1}{p^\gamma.c}} \quad (3.13)$$

By considering aforementioned confinement-linked pressure variation, it is possible to visualize its impact on effective diffusional speed by applying the Maxwell Boltzmann distribution and mapping it for the three $C_{2=}$, $C_{3=}$ and C_4 olefins either for the normal pressure or for a confinement-impacted apparent partial pressure.

As represented on **Figure 3-21a**, dynamic radii were estimated considering vibrational modes (stretching, bending etc.) at high temperatures, each C-C or C-H bond is considered to follow Newtonian mechanics. In free space the olefins behave like oscillating expanding spheres with an expansion being a function of temperature (between 293 K and 773 K) from 3.5 to 4.5 Å for ethylene, 4.2 to 5.7 Å for propylene and 5.4 to 7.3 Å for butylene. Besides this *positive thermal expansion* (PTE) phenomenon, the inverse one, *i.e; negative thermal expansion* (NTE) is frequently encountered for crystals. Once heated, porous crystals are known to contract, since the stretching vibrational mode has no impact in a crystal, the bending and twisting modes of Si-O-Si and Si-O-Al bonds lead to a net decrease in total crystal volume and in accessible volume. This has been elegantly studied and reported for ZSM-5 crystals exhibiting low acid site density by Cha *et al.*[217] As this volume variation is again due to vibrational modes, this phenomenon occurs in an oscillating manner. The MFI zeolite pore dimensions in crystalline a-*axis* may hence vary between; 5.500 - 5.473 - 5.445 Å for the respective temperatures 273, 523, 773 K.

Under MTO reaction conditions, a certain harmonization of these oscillations between the dynamic (propylene) molecular diameter and the accessible microporous diameter can be assumed. By considering methanol and MTO products as ideal gases, we can calculate the most probable speed for each molecule in a free space, using the Maxwell Boltzmann distribution (**Figure 3-21c**). As expected, by focusing on the three main olefins produced, ethylene smallest olefin is the fastest diffusive one.

On a non-shape selective catalytic surface, ethylene would preferentially escape if compared to larger olefins. Nonetheless, on such a surface, this can also be due to an enhanced production of polyaromatic species, which favour the production of ethylene by side-chain and paring mechanism (**Figure 3-1**).[218]

The impact that a pronounced degree of confinement has on diffusion speeds is higher for propylene than for ethylene and butylene (**Figure 3-21c**). The considered molecule may indeed diffuse faster than ethylene and $C_{3=}/C_{2=}$ ratios as experimentally observed can be modelled depending on the degree of confinement γ used.

[217] a) Cha, W.; Jeong, N. C.; Song, S.; Park, H.; Cao, T.; Pham, T.; Harder, R.; Lim, B.; Xiong, G.; Ahn, D.; Mcnulty, I.; Kim, J.; Yoon, K. B.; Robinson, I. K.; Kim, H. *Nat. Mater.* **2013**, *12*, 729. b) Bhange, D. S.; Ramaswamy, V. *Microporous Mesoporous Mater.* **2010**, *130*, 322.
[218] Ilias, S.; Bhan, A. *ACS Catal.* **2013**, *3*, 18.

Table 3-3. Thiele modulus (ϕ) for the series of H-ZSM-5F catalysts, estimated for four different molecules. (light grey background: Porous diffusion competes with the catalytic reaction, dark grey background: Porous diffusion inhibits the reaction)

	MeOH	Propylene	Toluene	Trimethylbenzene (TriMB)
H-ZSM-5FN	3×10^{-6}	5×10^{-5}	2×10^{-4}	2.3×10^{-3}
H-ZSM-5FLD	1×10^{-2}	3×10^{-2}	0.89	9
H-ZSM-5FL	4×10^{-3}	7×10^{-3}	0.28	3

Table 3-4. Thiele-Weisz-Wagner-Wheeler degree of utilization (ψ) for the series of H-ZSM-5F catalysts, estimated for four different molecules. (Light grey background: Porous diffusion competes with the catalytic reaction, dark grey background: Porous diffusion becomes rate-determining step)

	MeOH	Propylene	Toluene	Trimethylbenzene (TriMB)
H-ZSM-5FN	5×10^{-6}	1×10^{-9}	3×10^{-8}	5×10^{-6}
H-ZSM-5FLD	80	5×10^{-4}	4×10^{-1}	80
H-ZSM-5FL	8	5×10^{-6}	4×10^{-2}	8

Using our experimental data from the PFG-NMR study and the aforementioned considerations, we have estimated the Thiele modulus (ϕ) (**Table 3-3**) and Thiele-Weisz-Wagner-Wheeler degree of utilization (ψ) (**Table 3-4**) for our ZSM-5F catalyst series with the following probe molecules; methanol, propylene, toluene and trimethylbenzene. These estimations allowed us to conclude that our olefin producing large crystals are definitely not limited by intra-crystalline diffusion. Only medium to large aromatics over the defects containing large crystals lead to a pronounced inhibition by molecular diffusion. However, it has to be noted that these aromatics do not have to diffuse out of the pores in the MTO multi-step reaction, since they are produced and further react inside the microporous network.

In fine, we report a rationally conceived outstanding MTP catalyst, which happens to be more precious, it allowed us to investigate and present a global picture of well-studied elementary steps occurring during MTO on ZSM-5 catalysts. Under steady state conditions, considering all the data presented herein, our large ZSM-5FL model catalyst selectively producing propylene, led us to allude its behaviour in catalysis to an organ pipe which under certain conditions (temperature, diameter and length) produces selectively a certain note.[219]

Besides, the synthesis of such a highly ordered material opens another set of applications as, for example, a single crystalline model catalyst, with periodically arranged acid sites (if mass transfer limitations can be neglected). The latter could also demonstrate a huge potential for crystallographic studies, thanks to its high periodicity, especially by solving the structure of

[219] Pisani, U. *Acustica,* **1976**, *25,* 133.

trapped molecules.[220] Lastly, large defect-free zeolite crystals also work as excellent host-guest materials for performing supramolecular chemistry.[221]

3.7. Conclusion and Outlook

Large and defect-free ZSM-5 zeolite crystals were synthesised in fluoride medium. The latter catalysts demonstrated a high activity, stability as well as selectivity towards light olefins in the Methanol-To-Olefins (MTO) reaction. By properly controlling the synthesis parameters, ZSM-5 zeolite single crystals exempted from ubiquitous structural defects: external and internal silanols, extra-framework aluminium (EFAl) species, were obtained.

The present study highlights the synthesis, the thorough characterisation by SEM, HRTEM, CO-FTIR, ^{27}Al and ^{19}F MAS-NMR, Rietveld structure refinement, BET and PFG-NMR techniques, the application and subsequent rationalisation of these ZSM-5F zeolites as outstanding MTP (Methanol-To-Propylene) catalysts. Interestingly, the perfect large crystals (H-ZSM-5FL) behaved in a counter-intuitive manner in catalysis, being very selective towards propylene, very active and the most stable tested catalyst. Exempted from surface defects and exhibiting a perfectly homogeneous acid site distribution, ZSM-5FL catalyst can be used as a model catalyst. Indeed in the second part of this study, this defect-free zeolite allowed to decipher the importance of diffusion phenomena during MTP catalysis, governing the high propylene selectivity. Lastly a mathematical model using Maxwell-Boltzmann diffusion models was proposed to support experimental results.

The future prospect of this project is promising;[188] we currently try to adapt our optimal MTP-catalyst's synthesis to large scale, needing the substitution of HF during the synthesis. In terms of characterisation it will be interesting to perform two-dimensional ^{29}Si-CP-MAS-NMR to ascertain the absence of any kind of structural defects. Additionally, the large size of our conceived ZSM-5FL catalyst certainly renders them attractive model materials for *ad operando* measurments (introduced in section **1.2.5.**). Ultimately, even though statistical models were applied in this work, an interesting added value would have been periodic Density Functional Theory (DFT) or Molecular Dynamics (MD) modelling. The impact of different Si/Al-ratios and the amount of defects on force field and thereby on catalysis and diffusion might have given further insights.

[220] Inokuma, Y.; Kawano, M.; Fujita, M. *Nat Chem.* **2011**, *3*, 349. (b) Inokuma, Y.; Yoshioka, S.; Ariyoshi, J.; Arai, T.; Hitora, Y.; Takada, K.; Matsunaga, S.; Rissanen, K.; Fujita, M. *Nature* **2013**, *495*, 461.

[221] a) Brühwiler, D.; Calzaferri, G.; Torres, T.; Ramm, J. H.; Gartmann, N.; Dieu, L-Q.; Lopez-Duarte, I.; Martinez-Dıaz, M. V. *J. Mater. Chem.* **2009**, *19*, 8040. b) Szarpak-Jankowska, A.; Burgess, C.; De Cola, L.; Huskens, J. *Chem. Eur. J.* **2013**, *19*, 14925.

Lastly, the shaping of an MTP-catalyst supported on inert silicon carbide-SiC-supports is a topic I worked on earlier.[222] I choose to not present these results in detail in this chapter. Nonetheless, it is worthy to insist on its importance during the future scale-up process.

[222] Losch, P.; Boltz, M.; Soukup, K.; Song, I.-H.; Yun, H. S.; Louis, B. *Microporous Mesoporous Mater.* **2014**, *188*, 99–107.

Chapter 4 Carbon Upgrading and Green Chemistry

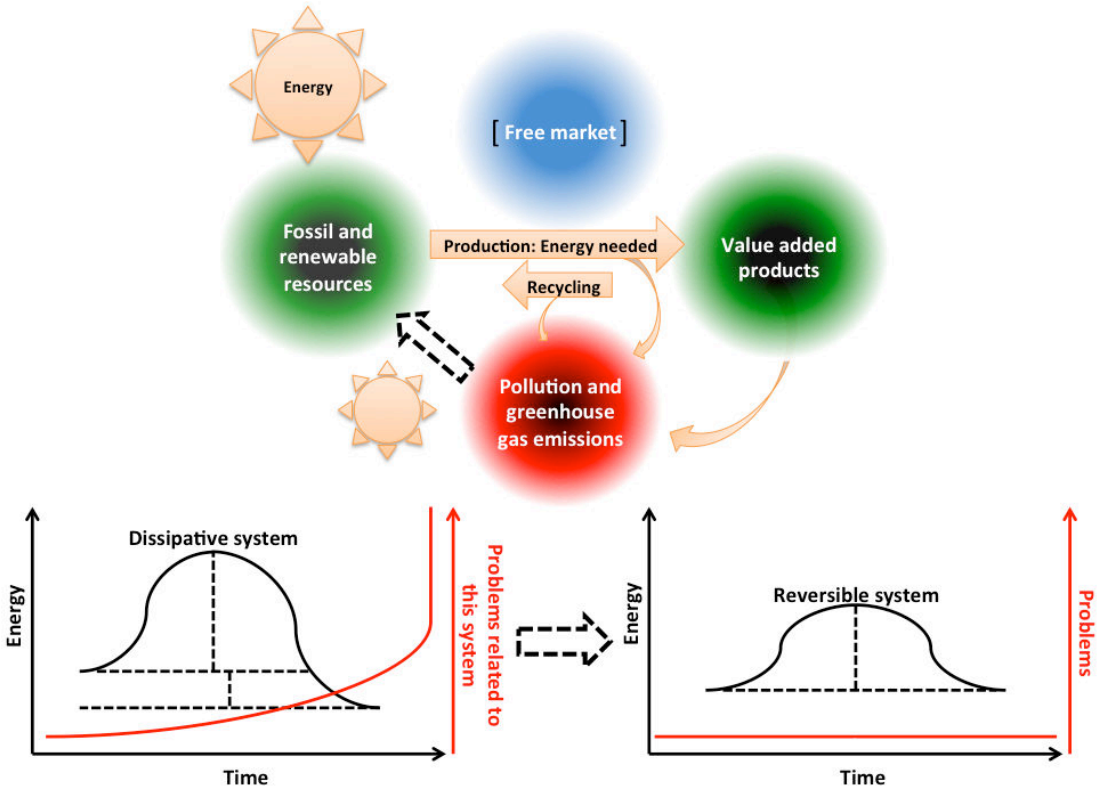

ABSTRACT: The scheme above presents today's predominant economic system, which is of dissipative nature. ***Supra***: Mainly fossil resources and renewables to a certain extent are transformed to finite value added products by the use of energy. The "catalyst" for this transformation is the free market aiming the generation of profit, via a seemingly necessary growth. Even though energy and products are attempted to be recycled today, at the end of their life cycle the current system remains dissipative. There is a lack in (re)-transforming pollution for instance emitted greenhouse gases into renewable resources. ***Infra sinister***: A chemist considering the current economic system: products are in general lower in energy than the resources, which they are made of, thus rendering it inefficient to come back to a renewable resource and thereby generating a considerable, accumulating amount of problems. ***Infra rectus***: It remains wishful to target a reversible system wherein waste products can be efficiently transformed into renewable resources.

This chapter will consist of a "few-steps-back" approach focussing on several projects. It will be structured as the following: at first a general view of a possible sustainable economy comprising a circular carbon economy, while in a second step the minor contributions that stem from this work, to this greater goal will be exposed. Some of these results led to peer reviewed publications:

"Ionic liquid immobilization on carbon nanofibers and zeolites: Catalyst design for the liquid-phase toluene chlorination" Losch, P.; Pascual, A. M.; Boltz, M.; Ivanova, S.; Louis, B.; Montilla, F.; Odriozola, J. A. *CR Chimie* **2015**, *18*, 324–329.

"Easy, Green and Safe Carbonylation Reactions through Zeolite-Catalysed Carbon Monoxide Production from Formic Acid" Losch, P.; Felten, A.-S.; Pale, P. *Adv. Synth. Catal.* **2015**, *357*, 2931–2938.

"Unraveling the Importance of Zeolite Crystal Morphology." Louis, B. Carvalho Rocha, C.; Balanqueux, B.; Boltz, M.; Losch, P.; Bernardon, C.; Bénéteau, V.; Pale, P.; Maciel Pereira, M. *L'Actualité Chimique*, **2015,** *393-394*, 2.

"Influence of Biomass Residues on the Metastability of Zeolite Structures" Louis, B.; Gomes, E. S.; Coelho, T.; Lutzweiler, G.; Losch, P.; Silva, A. V; Faro, A. C.; Romero, T.; Osman, M. Ben; Balanqueux, A.; Bernardon, C.; Pereira, M. M. *Nanosci. Nanotech. Letters* **2016**, *8*, 1–7.

"Eco-compatible zeolite-catalysed continuous halogenation of aromatics" Losch, P.; Kolb, J. F.; Astafan, A.; Daou, T. J.; Pinard, L.; Pale, P.; Louis, B. *Green Chem.* **2016**, *18*, 4714-4724.

"Transformation of South African coal fly ash into ZSM-5 zeolite and its application as an MTO catalyst." Messingue, R.N.M.; Losch, P.; Sedres, G.; Musyoka, N.M.; Fatoba, O.O.; Louis, B.; Pale, P.; Petrik, L.F. *CR Chimie* **2016**, *in press*.

4.1. Today's Challenges

In the introducing Chapter 1, it has been mentioned that my various other subjects will be linked within the frame of the *carbon upgrading* concept. The incremental addition of value to problematic carbon dioxyde and its subsequent products would render green chemistry not only a target for chemical industries to achieve an increasingly sustainable chemistry, but green chemistry would shift to a more central potition in a circular, or sustainable economy.

The necessity of CO_2-capture and sequestration, in the best scenario its valorisation becomes clear to everyone if one considers the undeniable anthropogenic climate change (**Figure 4-1**).[223, 115] Anthropogenic, since we release greenhouse gases in a accelerating fashion and this changes our environment in a drastic manner. We might soon be facing environmental pressures to which we will not be able to adapt anymore. Basic Darwinism tells us what happens to species, which cannot adapt to environmental pressures. Even though we, as a species have proven to be champions in adaptability, there are modifications of our environment, which we should avoid.

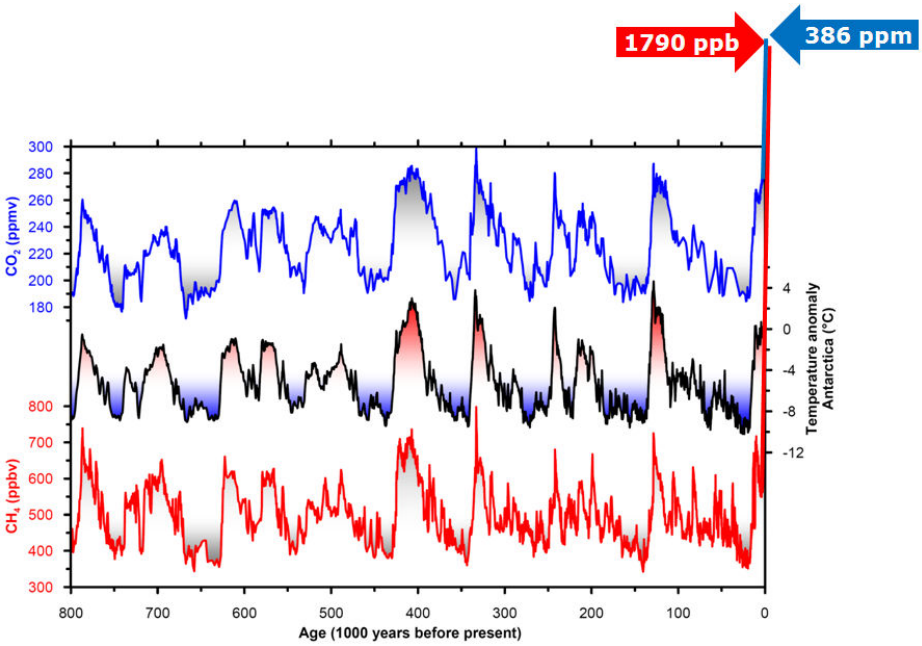

Figure 4-1. The evolution of the temperature and the greenhouse gases CO_2 and CH_4 in the terrestrian atmosphere during the last 800 thousand years. These data have been obtained in the EPICA-centre in Antarctica thanks to ice core drilling. The figure was taken from the original report.[223]

An increase of a few degrees in the global average temperature will further alter our environment. Predictions of the consequences incrementally depend (+ 1, 2, 3 or 4°C) on the

[223] a) Communiqué de presse du CNRS du 14 mai 2008: http://www2.cnrs.fr/presse/communique/1339.html b) Lüthi, D.; Le Floch, M.; Bereiter, B.; Blunier, T.; Barnola, J.-M.; Siegenthaler, U.; Raynaud, D.; Jouzel, J.; Fischer, H.; Kawamura, K.; Stocker, T. F. *Nature* **2008**, *453*, 379–382.

future global warming.[224] The best estimate prophesizes a 1.75°C global warming for 1000 Gt cumulatively anthopogenic CO_2 emitted. Currently we are at an estimated cumulative anthropogenic CO_2 emission of 500 Gt and the tendency is still growing. The foreseen consequences reach from merely more extreme weather conditions, up to more cataclismic views of a stopping Gulf stream, exponentially emitted greenhouse gases stored in the oceans and permafrost regions a decrease in crop yields, evermore dry summers, etc. Therefore, the *carbon upgrading* concept and a sustainable, circular carbon economies are utterly needed to be further developped.[225] These might render the emitted greenhouse gases a truly valuable starting material. Bearing the above stated in mind, the present Chapter will revolve around subjects related to this *carbon upgrading* concept. It will be composed of four distinct parts:

Carbon dioxide is vastly emitted by coal burning power plants. Such power plants yet face an additional problem. Indeed, they enormously contribute to the greenhouse gas emissions, but the less popularly known trouble is the gargantuan production of toxic fly ashes. Those nanoparticles are often deposited in open-air landfills and cause a lot of harm to groundwater, air and the health of the living beings that depend on this environment. The approach we tried to follow in this part in collaboration with our colleagues in South Africa (UWC) was to valorise this aluminosiliceous material in the synthesis of potentially catalytically active ZSM-5 type zeolites.

The second topic exposed will be the valorisation of sugar cane bagasse. This biomass source is produced at a huge scale and currently simply used as combustible. However, being composed of cellulose, hemicellulose and lignin it comprises a high degree of chemical complexity, which is lost when burned and turned into CO_2. The chemical separation and valorisation of more or less functionalised and depolymerised aromatics, mono- or disaccharides is quite challenging at the moment and not economically viable.[226] Thus, our strategy together with colleagues from the UFRJ in Brasil was to use bagasse, hydrolysed in some cases and benefit from its complex mixture of hydrophilic and hydrophobic zones, potential π-stacking areas and chelating properties. During the complex self-assembly mechanism of zeolite crystalline growth it has already been observed that the described material will interfere with growing aluminosilicate particles.[227,184] This work is hence in the continuity of earlier results of our group.[228]

---

[224] National Research Council report, *Climate Stabilization Targets: Emissions, Concentrations, and Impacts over Decades to Millennia*, **2011** Washington D.C., US.

[225] *Climate engineering*, *Geoengineering* or *climate intervention* (http://nas-sites.org/americasclimatechoices/public-release-event-climate-intervention-reports/) are not considered in the above mentioned predictions, however in my opinion proactivity and prevention should prevail over remediation.

[226] Batalha, N.; Silva, A.V.; Souza, M. O. De; Costa, M. C.; Gomes, E. S.; Silva, T. C.; Barros, T. G.; Gonåalves, M. L. A.; Caramo, E. B.; Santos, R. M.; Almeida, M. B. B.; Rodrigo, O. M. A. *ChemSusChem* **2014**, *7*, 1497–1506.

[227] Louis, B.; Gomes, E.S.; Coelho, T.; Lutzweiler, G.; Losch, P.; Silva, A.V; Faro, A.C.; Romero, T.; Osman, M. Ben; Balanqueux, A.; Bernardon, C.; Pereira, M.M. *Nanosci. Nanotechnol. Lett.* **2016**, *8*, 1–7.

[228] Bernardon, C. *"Les Zéolithes comme Catalyseurs «verts» pour la Synthèse Organique: de leur synthèse à façon à leurs applications en chimie organique."* PhD-Thesis **2016**.

The third part is as well a continuity of what has been obtained and observed by M. Boltz in our group.[229] The zeolite catalysed chlorination reaction of various aromatics hase been investigated. The next obvious step was then to try to render this reaction applicable at a larger scale and to widen its scope. It was possible to develop a continuous flow liquid-solid system where substituted aromatics could be iodinated, brominated and chlorinated in a selective manner. This work is therefore a discrete part of the *carbon upgrading* concept since in bulk and fine chemistry controlled halogenated aromatics exhibit a high added value. (**Table 4-14** and **Figure 1-18**)

The same remarks can be made for the potential formation of amides, esters or ketones from halogenated aromatics with CO and a palladium based catalyst. These Pd-catalysed coupling reactions generate in one step a huge added value. Their easy applicability, today at large scale led to the shared Nobel Prize for Heck, Negishi and Suzuki in 2010. Carbon monoxide, which can be added during these coupling reactions and lead to further complexity, on the other hand is frequently avoided in organic chemistry laboratories because of its toxicity. We wanted to propose herein an easy, cheap and safe alternative to the CO-bottle for the organic chemist. An *ex situ* CO-releasing zeolite catalysed formic acid dehydration could successfully be coupled to a Palladium catalysed carbonylation reaction.

[229] Boltz, M. *"Tailor-made Conception of Zeolites for Catalysis. From the Active Site to the Reactor."* PhD-Thesis **2014**.

4.2. Fly Ash for Zeolites

Figure 4-2. Turning a waste product from the coal burning industry into a valuable MTO-catalyst.

4.2.1. The Challenge

Nowadays coal is still widely used to generate electricity in coal power plants. In addition to the gargantuan emissions of carbon dioxide, which is a huge but solvable issue,[115] the inorganic ingredients of fossil coal reserves are forming nanoparticulate fly ash during the high temperature combustion process. Those nanoparticles are estimated to be produced at a scale of 25 Mt Fly ash (FA).year^{-1} in South Africa, where our collaboration started, and 800 Mt.year^{-1} worldwide[230] As it can be seen in the **Table 4-1** it mainly consists of SiO_2, Al_2O_3 and Fe_2O_3; it also contains potentially toxic elements that condense from the flue gas. The large-scale disposal and storage of fly ash is a source of air, soil and water pollution.[231] Several studies have been undertaken on the valorisation of fly ash, for instance to treat acid mine drainage,[232] to produce construction materials, to recover valuable metals,[233] and interestingly for us, to synthesise zeolites.[234]

[230] a) *Eskom Holdings' Integrated report*, **2014**. b) Kruger, R.A. *Coal Ash in South Africa: A valuable Resource* WOCA, **2015** Nashville.
[231] Ahmaruzzaman, M.A. *Process in Energy and Combustion Science* **2010**, *36*, 327-363.
[232] a) Petrik, L.F.; White, R.A.; Klink, M.J.; Somerset, V.S.; Burgers, C.L.; Fey, M.V. *International Ash Utilization Symposium*; Lexington: Kentucky, **2003**. b) Madzivire, G.; Gitari, W.M.; Vadapalli, V.R.K.; Ojumu, T.V.; Petrik, L.F. Minerals Engineering **2011,** *24*, 1467-1477.
[233] a) Hernandez-Exposito, A.; Chimenos, J.M.; Fernandez, A.I.; Font, O.; Querol, X.; Coca, P.; Pena, G. F. Chemical Engineering Journal. **2006**, *118*, 69–75. b) Liu, K.; Xue, J.; Zhu, J. *Light Metals* **2012**, 201-206.
[234] a) Musyoka, N.M.; Petrik, L.F.; Gitari, W.M.; Balfour, G.; Hums, E.. *Journal of Environmental Science and Health Part A*. **2012**, *47*, 337–350. b) Chareonpanich, M.; Namto, T.; Kongkachuichay, P.; Limtrakul, J. *Fuel Processing Technology* **2004**, *85*, 1623–1634.

Table 4-1. Elemental composition of South-African Coal Fly Ash.

Element oxides	Fly ash composition [%]
SiO_2	52
Al_2O_3	28
MO	7
Fe_2O_3	5
TiO_2	2
M_2O	1
(S, P, Mn, Sb, As, Ce, Th, U...)-oxides	5

After the oxidative high temperature combution process, toxic but also valuable metals can be found in the fly ash in their highly oxidised forms: MO are earthalkali metal oxides while M_2O are alkali metal oxides.

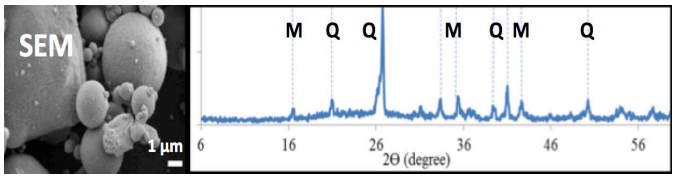

Figure 4-3. South-African Fly Ash: SEM and XRD.

It is important to note that these nanoparticles are a remarkable health and environmental issue, since usually stored in open air landfills they can get blown by the wind to local or close populated areas and cause severe lung diseases.[234a] On the other hand stored in constantly wetted ponds (consuming large quantities of water) their elemental composition causes strong alkalinity in the resulting brines, which regularly causes ground water pollution. The South-African Coal (SAC) is containing up to 25 % impurities with respect to its total mass.[235] Currently Fly Ash is not effectively valorised, even though the prevailing methods comprise acid mine water drainage,[236] or its use for the production of "Ultra"-resistant concrete *or* energetically modified cement (EMC).[237] In effect, the currently highest building on earth, the *Burj Khalifa* in Dubai (UAE) was built with EMC using FA from South Africa.

Economically the extraction of valuable metals is more promising: Grzymek (1976, 1978) and Bretsznajder (1974) in Poland developed two processes for the recovery of alumina from coal fly ash.[238] Nowadays, many processes for the recovery of alumina from fly ash such as sintering, acid leaching and HiChlor have been developed.[239] Magnetic extraction is used to recover oxides of iron from fly ash using de-ionized water, sulphuric acid or hydrochloric acid as mixing medium and a strong magnet to retain the extract in the mixing vessel.[240]

The transformation into zeolites constitutes an interesting complementary valorisation of FA as it is mainly composed of the T-units (Silica and alumina) building blocks for the synthesis

[235] Falcon, R.; Ham, A. J. *J. South African Inst. Min. Metall.* **1988**, *88*, 145–161.
[236] Gitari, W. M.; Somerset, V. S.; Petrik, L. F.; Key, D.; Iwuoha, E.; Okujeni, C. *World Coal Ash* **2005**.
[237] Sheath, J. *Civil Engineering / Siviele Ingenieurswese* **2010** *18*, 14.
[238] Hosterman, J.W.; Patterson, S.H.; Good, E.E. *World non bauxite aluminum resources excluding alunite;* U.S. Government Printing Office: Washington, **1990**; 51.
[239] Yao, Z.T.; Xia, M.S.; Sarker, P.K.; Chen, T. *Fuel* **2014**, *120*, 74-85.
[240] a) Paul, M.; Seferinoglub, M.; Ayçikc, G.A.; Sandströmd, A.; Paul, J. *Preprints of Papers-American Chemical Society, Division of Fuel Chemistry* **2004**, *49*, 978-982. b) Shoumkova, A.S. *Waste Management & Researc.* **2010**, *0*, 1–12.

of zeolites. Regarding the worldwide production of zeolites of about 5 Mt.year^{-1} with 3 Mt natural zeolite.year^{-1} (low value) and 1.7 Mt artificial zeolite.year^{-1} (high value),[241] and the previously stated amount of FA produced per year (800 Mt), it seems possible to satisfy the worldwide needs of raw materials for the synthesis of zeolites.

Fly ash has been used as a low cost source of SiO_2, Al_2O_3 in the synthesis of low value zeolites. Musyoka *et al.*[242] synthesised A, X, Na-P1 and cancrinite zeolites from South African fly ash. The alkaline hydrothermal process preceded by fusion or pectization (pretreatment) of the raw material has been applied to synthesise zeolites.[243] As aforementioned, the valuable extraction of alumina from fly ash increases the Si/Al ratio of the solid residue, which might turn it into a good starting material for the synthesis of high value ZSM-5 zeolite.

It may appear counterintuitive to aim for the production of highly siliceous catalysts, starting from low SAR fly ash. As in zeolite syntheses with FA a pretreatment is always necessary (very dense, hard and resistent Quartz and Mullite phases (**Figure 4-3**) need to be somewhat dissolved), this downside can be economically exploited if ZSM-5 materials with Si/Al-ratios around 100 are target for an eventual MTO-application. Then, 99 % of the alumina contained in fly ash can be extracted and sold as valuable starting material in the aluminum industry. Plus, SASOL South Africa's Oil-Company gaseifies its coal reserves and closely collaborates with Lurgi the largest MTO-industrial exploiter, especially turning Chinese coal into light olefins, or Methanol-To-Olefins (MTO). [244]

This study aims to use South African coal fly ash as cheap source for the extraction of metals and the synthesis of ZSM-5 zeolite, which is used as solid catalyst in the MTO reaction.

4.2.2. Zeolites from FA Potential Commercial Benefit

The ZSM-5 zeolite is conventionally synthesised using various types of organic structure-directing agents (templates).[245] Nevertheless, Narayanan *et al.* reported that ZSM-5 zeolite could be synthesised without a template. [246] Chareonpanich *et al.* synthesised ZSM-5 zeolite using lignite fly ash and rice husk ash as feedstock in order to adapt the SAR to the target value,[247] with

[241] Yilmaz, B.; Müller, U. *Top. Catal.* **2009**, *52*, 888–895.
[242] a) Musyoka, N.M.; Petrik, L.F.; Fatoba, O.O. Hums, E. *Minerals Engineering* **2013**, *53*, 9-15. b) Grela, A.; Hebda, M.; Lach, M.; Miku, J. *Microporous Mesoporous Mater.* **2016**, *220*, 155-162.
[243] a) Kuwahara, Y.; Ohmichi, T.; Kameqawa, T.; Mori, K.; Yamashita, H. *Journal of Materials Chemistry* **2010**, *20*, 5052-5062. b) van Der Gaag, F.J.; Jansen, J.C.; van Bekkum, H. *Template variation in the synthesis of zeolite ZSM-5*; Laboratory of Organic Chemistry; Delft University of Technology: Delft, **1985**.
[244] Cheng, K.; Gu, B.; Liu, X.; Kang, J.; Zhang, Q.; Wang, Y. *Angew. Chem., Int. Ed.* **2016**, *55*, 1–5.
[245] a) Tuan, H.T.; Bae, I.K.; Jang, Y.N.; Chae, S.C.; Chae, Y.B. Suhr, D.S. *Journal of Ceramic Processing Research.* **2010**, *11*, 204-208. b) Martinez, C.; Perez-Pariente, J. *Zeolites and ordered porous solids: Fundamentals and applications*; 3rd Feza School on zeolites & 5th International Feza Conference; Valencia, **2011**.
[246] Naraynan, S.; Sultana, A.; Krishna, K.; Meriaudeau, P.; Naccache, C. *Catal. Lett.* **1995**, *34*, 129-138.
[247] Chareonpanich, M.; Namto, T.; Kongkachuichay, P.; Limtrakul, J. *Fuel Processing Technology* **2004**, *85*, 1623.

tetrapropylammonium bromide (TPABr) as template. Kalyankar *et al.* synthesised ZSM-5 zeolite using fly ash obtained from a thermal power station in India. [248]

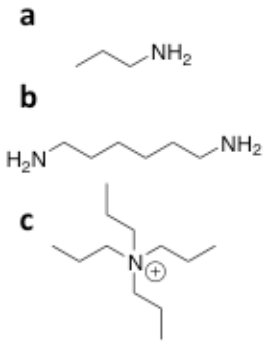

Figure 4-4. a) PA b) HDA c) TPA^+.

In this study, we decided to focus on three different SDA's in order to seek for the most cost efficient synthesis of an eventual catalyst. The most commonly used one for ZSM-5 synthesis is the tetrapropylammonium cation, which has been compared to 1,6-hexanediamine (HDA) and 1-propylamine (PA) in terms of their structure directing effect (**Figure 4-4**).

In an earlier study we had already found that acid lixiviates led to minor quality ZSM-5 crystals.[249] Yet several other attempts followed, using for instance the fluoride mediated route expecting a faster, better depolymerization of highly polymerized, dense quartz and mullite phases. As shown in **Figure 4-5** an intriguing result could be obtained following these trials, only fly ash and 5 wt-% of silicalite seeds resulted in a remarkable decrease in the quartz typical peak and highly crystallized ZSM-5 material were observed.

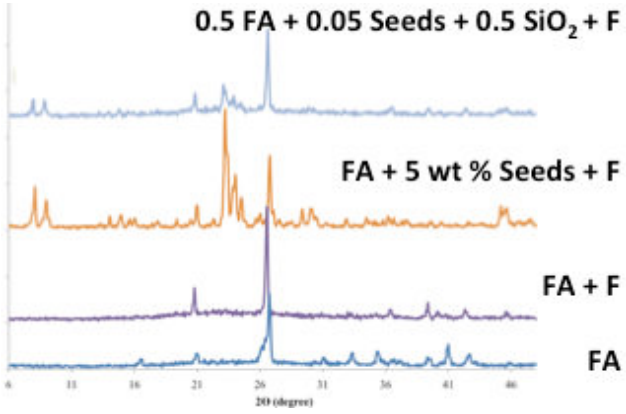

Figure 4-5. XRD-patterns of first generation ZSM-5 zeolites synthesised from FA, in fluoride medium.

Nonetheless, a future large-scale valorisation of fly ashes is not truly compatible with highly concentrated fluoride containing brines. Therefore we steered our course again towards alkaline brines.

Figure 4-6 shows the XRD-patterns of a second generation (left) and a third generation (right) of ZSM-5 zeolites from fly ash. Different harsh pretreatments were compared; the second generation was synthesised with fly ash residues previously treated by acid leaching. Those

[248] Kalyankar, A.N.; Choudhari, A.L.; Joshi, A.A. *International Journal of Basic and Applied Research*. **2011**, *1*, 59-63.
[249] Missengue, R.N.M.; Losch, P.; Sedres, G.; Musyoka, N.M.; Fatoba, O.O.; Louis, B.; Pale, P.; Petrik, L.F. *CR Chimie* **2016**, *in press*.

samples are therefore called AL and did not result in pure phase ZSM-5 zeolite, even with external silica addition. Consequently, this treatment can be considered to be not harsh enough to destroy the Quartz phases. In stark contrast to this, the fusion pretreatment allowed the production of pure phase ZSM-5 zeolites with all templates. These samples are called FFAE, for fusion fly ash extract.

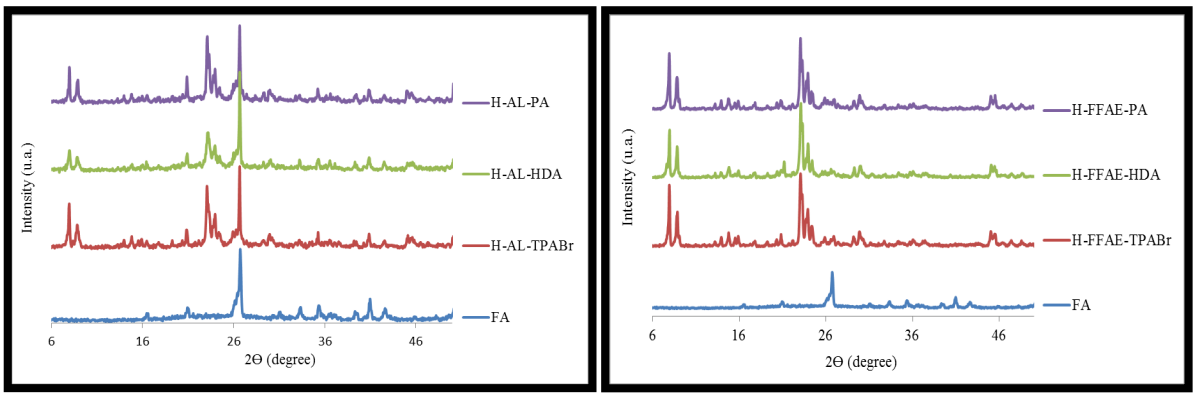

Figure 4-6. XRD-patterns of second and third generation ZSM-5 zeolites from FA: Acid leaching[250] was used as pretreatment for the zeolites synthesised on the left, while fusion treatment followed by oxalic acid washing[251] of FA allows the production of pure phase ZSM-5 (right).

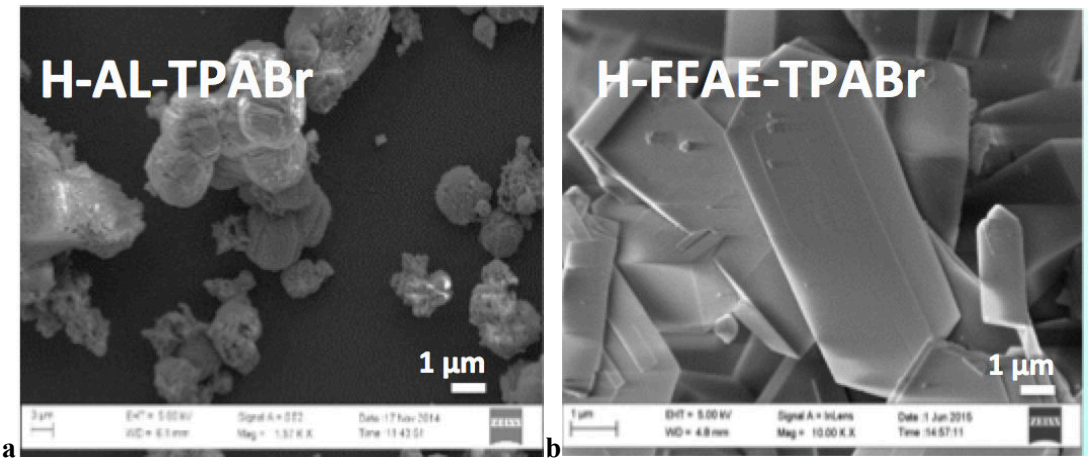

Figure 4-7. SEM micrographs of a) mixed phase zeolite obtained when acid leachate was used in the zeolite synthesis, b) pure phase third generation ZSM-5 zeolite could be observed after fusion treated starting material has been engaged in the zeolite synthesis.

Figure 4-7 depicts the SEM micrographs of AL-TPABr and FFAE-TPABr. It can be clearly seen that pure phase FFAE sample is composed of classical coffin shaped crystallites, while mixed phase AL sample does not exhibit a uniform crystalline morphology.

[250] Acid leaching procedure (AL): 100 g FA + 500 mL H_2SO_4, 200°C, 2h as it has been reported by Lai-shi *et al.* **2011**.
[251] Fusion procedure (FFAE): 50 g FA + 60 g NaOH, 550°C, 1.5 h as it has been reported by Musyoka *et al.* **2012** and Baldyga *et al.* **2012**. Herein an additional oxalic acid washing step was used to improve the quality of the engaged starting material.

Table 4-2. Textural properties of the different synthesised and later applied ZSM-5 zeolites.

Entry	Zeolite	Si/Al-ratio	S_{BET} [$m^2.g^{-1}$]
1	H-AL-TPABr	4	327
2	H-AL-HDA	5	353
3	H-AL-PA	5	39
4	H-FFAE-TPABr	36	459
5	H-FFAE-HDA	55	388
6	H-FFAE-PA	42	353

Table 4-2 presents the textural properties of the different synthesised and later applied ZSM-5 zeolites. The bulk Si/Al-ratio remains below 10 for the AL-samples, this indicates the presence of highly aluminum containing phases such as mullite. In sharp contrast, the FFAE-samples exhibit typical SAR for ZSM-5 samples. Moreover, an interesting trend can be observed. The coordination potential of the templates increases in line with the Si/Al-ratio, namely HDA > PA > TPA^+. This is an indication that some of the monomeric aluminum is complexated during the synthesis and no longer available for the crystallization of the final material.

4.2.3. MTO-Reaction

Table 4-3. Application of FA-sourced ZSM-5 in the MTO-reaction.

Entry	Zeolite	Conversion [%]	Selectivity $C_{2=}$ [%]	Selectivity $C_{3=}$ [%]	Selectivity $C_{4=}$ [%]
1	H-AL-TPABr	70	13	35	17
2	H-AL-HDA	73	9	34	15
3	H-AL-PA	48	18	32	12
4	H-FFAE-TPABr	99	12	29	11
5	H-FFAE-HDA	98	8	37	14
6	H-FFAE-PA	97	6	38	16

Catalytic data obtained after 1h on stream under standardized conditions; 60 mg catalyst in a fixed-bed quartz reactor, 450°C, WHSV 1.2h^{-1}.

The above described, synthesised and characterised zeolites have then been applied in the MTO-reaction under the same conditions reported in Chapter 3. Their catalytic activity and selectivity is exposed in **Table 4-3**. The mixed phase AL-samples convert methanol into light olefins, however they are rapidly dectivating (**Figure 4-8**). In contrast medium SAR FFAE-samples did quantitatively convert methanol into mainly light olefins. The high SAR H-FFAE-PA

and H-FFAE-HDA are the most promising in terms of light olefins selectivity. Additionally, the cheapest[252] template HDA led to the most stable catalyst.

Even though these selectivtiies and most of all stabilities are still far off industrially competitive MTO-catalysts, this strategy led to the synthesis of a promising and cheap MTO-catalyst from fly ash. Thus, this work may help to pave the way for a reasonable valorisation of fly ash.

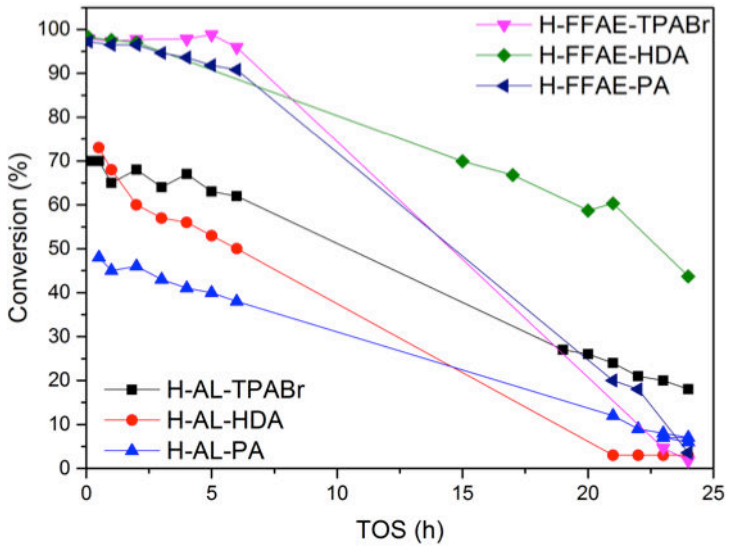

Figure 4-8. Long term stability in the MTO-reaction of different synthesised ZSM-5 zeolites.

4.2.4. Potential Impact and Outlook

The results presented in this study show an innovative route of synthesizing ZSM-5 from coal fly ash without any external silica source. The treatment of the fused coal fly ash with oxalic acid prior to the synthesis led to a pure ZSM-5 phase without adding an extra silica source; while the zeolite synthesised from the acid treated coal fly ash contained unreacted fly ash, despite the addition of a large amount of fumed silica to the hydrothermal synthesis. Moreover, the presence of unreacted coal fly ash phases (quartz and mullite) in the AL-products affected their catalytic efficiency compared to the FFAE-products. 1,6-hexanediamine led to the synthesis of the cheapest and most promising MTO catalyst in terms of selectivity towards light olefins and stability. It is tentatively proposed that HDA stabilises soluble aluminate species by its coordinating potential, whereby the Si/Al-ratio of the resulting material is increased, which is known to be beneficial for an MTO-catalyst.

[252] For HDA, TPABr and PA the available prices on the Aldrich-website were used with the respective consumption for the zeolite synthesis to estimate that the use of HDA as a template is 3 times cheaper than the classical TPA-route.

4.3. Biomass Templates in Zeolite Synthesis

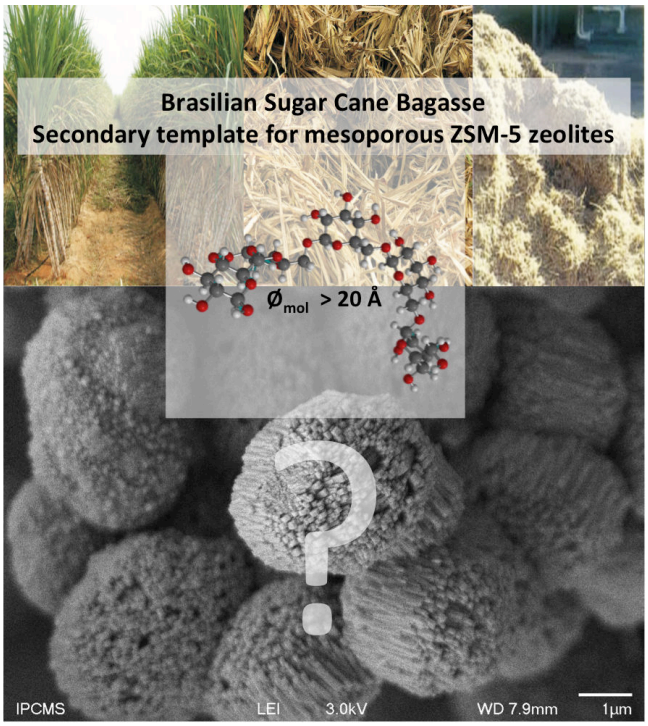

Figure 4-9. Sugar cane bagasse for the use as secondary template creating mesopores and governing the Silicon/Aluminum-ratio.

4.3.1. The Challenge

The challenge in this section is the valorisation of dry biomass such as sugar cane bagasse (SCB). In Brazil this waste material is currently produced at a yearly 250 Mt scale. Nowadays, its main valorisation is as combustible for the generation of electricity.

On the other hand, heterogeneous catalysis can indeed take benefit from the particular properties of self-assembled materials.[253] Hierarchically porous zeolites and more particularly the industrially relevant ZSM-5 zeolite need expensive secondary templates to introduce a regular secondary or tertiary porosity.[254] Large microcrystals (high residence time for the molecules within the crystal) favour shape-selective catalysis; on the other side nanocrystals (reduced diffusion path length) enhance the catalyst efficiency.[255]

Interestingly, different (cheap) treatments and hence different extracts of the above-described waste material can impact the ZSM-5 zeolite's crystal growth and rather excitingly

[253] a) Paramasivam, I.; Jha, H.; Liu, N.; Schmuki, P. *Small* **2012**, *8*, 3073. b) Pileni, M.P. *Acc. Chem. Res.* **2007**, *40*, 685–693. c) Loscertales, I.G.; Barrero, A.; Marquez, M.; Spretz, R.; Velarde-Ortiz, R.; Larsen, G. *J. Am. Chem. Soc.* **2004**, *126*, 5376–5377

[254] a) Do, M.H.; Wang, T.; Cheng, D.-G.; Chen, F.; Zhan, X.; Rioux, R.M.; Gong, J. *Small* **2014**, *10*, 4249. b) Andón, F. T.; Kapralov, A. a; Yanamala, N.; Feng, W.; Baygan, A.; Chambers, B.J.; Hultenby, K.; Ye, F.; Toprak, M.S.; Brandner, B.D.; Fornara, A.; Klein-Seetharaman, J.; Kotchey, G.P.; Star, A.; Shvedova, A.A.; Fadeel, B.; Kagan, V.E. *Small* **2013**, 1. c) Jo, C.; Cho, K.; Kim, J.; Ryoo, R. *Chem. Commun.* **2014**, *50*, 4175.

[255] Garcia, R.; Diaz, I.; Marquez-Alvarez, C.; Perez-Pariente, J. *Chem. Mater.* **2006**, *18*, 2283–2292.

introduce a regular mesoporosity.[256] Sugar cane bagasse has been reported to be composed of the following: 40% cellulose, 35% hemicellulose and 7% lignin.[257] Cellulose is a natural carbohydrate-based polymer and a polyfunctionalized alcohol, where the free hydroxyl groups in their monomeric units form hydrogen bonds with adjacent chains.[258] Hemi-cellulose consists of short, highly branched chains of sugars. In contrast to cellulose, which is a polymer of only glucose, hemicellulose is a polymer of five different sugars.[259]

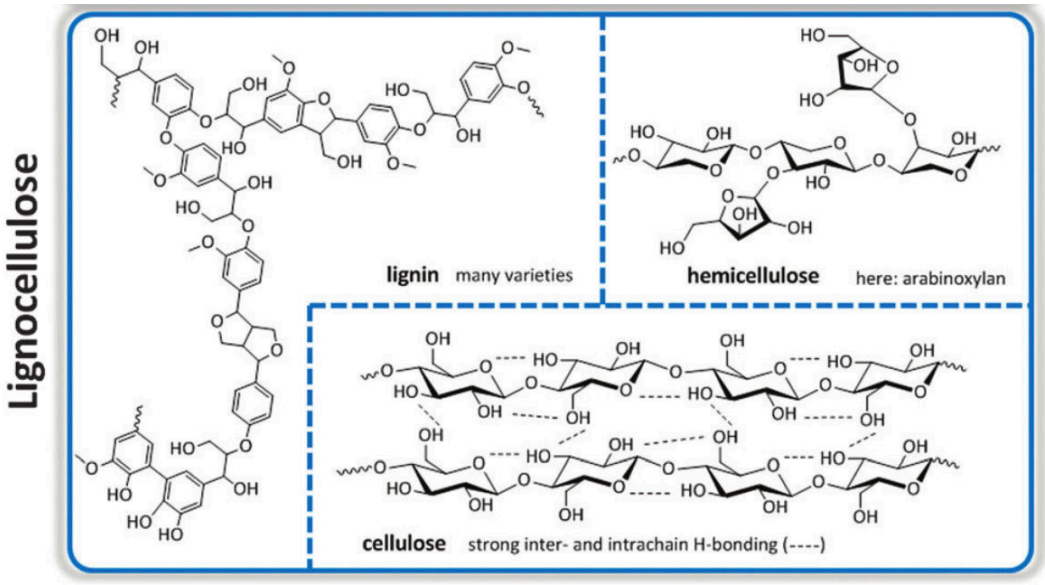

Figure 4-10. Structural representation of the three different SCB ingredients, lignin, hemicellulose and cellulose. This figure is taken from a recent review of Ennaert *et al*. on the potential and challenges of zeolite chemistry in the catalytic conversion of biomass.[260]

Several studies have already highlighted the influence of synthesis duration and temperature on the metastability of zeolites,[261] but also the addition of organic co-templates. One striking example remains the synthesis of mesoporous LTA zeolite by Ryoo *et al.*[262] with an addition of a surfactant to the synthesis gel. Valtchev *et al.*, have also obtained sophisticated morphologies,[263] while adding a leaf of *Equisetum arvense* to the gel, thereby enabling replication

[256] Ocampo, F.; Yun, H. S.; Pereira, M. M.; Tessonnier, J. P.; Louis, B. *Cryst. Growth Des.* **2009**, *9*, 3721–3729.
[257] Cunha, J.A.; Pereira, M.M.; Valente, L.M.M.; de la Piscina, P.R.; Homs, N.; Santos, M.R.L.; *Biomass & Bioenergy* **2011**, *35*, 2106-2116.
[258] a) Kondo, T.; Sawatari, C. *Polymer* **1994,** *35*, 4423–4428. b) Vu, D.; Marquez, M.; Larsen, G. *Microporous Mesoporous Mater*. **2002**, *55*, 93–101. c) Huber, G.W.; Iborra, S. Corma, A. *Chem. Rev.* **2006**, *106*, 4044–4098.
[259] Mäki-Arvela, P.; Holmbom, B.; Salmi, T.; Murzin, D.Y. *Catal. Rev. Sci. Eng*. **2007**, *49*, 197–340.
[260] Ennaert, T.; Van Aelst, J.; Dijkmans, J.; De Clercq, R.; Schutyser, W.; Dusselier, M.; Verboekend, D.; Sels, B. F. *Chem. Soc. Rev.* **2016**, 10.1039/C5CS00859J.
[261] a) Oleksiak, M. D.; Rimer, J. D. *Rev. Chem. Eng.* **2013**, *30*, 1. b) Navrotsky, A.; Trofymluk, O.; Levchenko, A. A. *Chem. Rev.* **2009**, *109*, 3885.
[262] Choi, M.; Cho, H. S.; Srivastava, R.; Venkatesan, C.; Choi, D.-H.; Ryoo, R. *Nat. Mater.* **2006**, *5*, 718.
[263] Valtchev, V.; Smaihi, M.; Faust, A.-C.; Vidal, L. *Angew. Chem. Int. Ed.* **2003**, 2782.

of the plant's surface morphology. Likewise, we have recently used sugar cane bagasse residues to produce MFI crystals having a nano-French fries morphology.[264,184]

Herein, we decided to study more deeply the metastability of MFI zeolites when sugar cane biomass residues are present in the gel. Furthermore, it has been possible to find a link between the presence of biomass residues in the synthesis gel and the final Si/Al-ratio of the resulting material, this in addition to the envisaged effect on the creation of a hierarchical porosity. This is advantageous compared to the recently demonstrated possibility that steam assisted crystallization (SAC) can lead to mesoporous MFI without a mesoporogen secondary template.[265] A last aim was a tentative rationalisation of the results using a thorough characterisation and comparing to reported data from the literature.

4.3.2. Zeolites Synthesised with Biomass Templating

As it has been stated in the experimental Section **2.1.1.1**: prior to the zeolite synthesis 300 mg of sugar cane bagasse were treated with an alkaline solution (150 mL, NaOH, 0.1 M, $pH_{0,\,measured}$ = 11) for 24 h at room temperature and under vigorous stirring. After the hydrolysis-reaction the pH dropped to $pH_{1\,measured}$ = 8 - 9 and the final mass of dry fibers decreased to 160 mg. The decrease in pH is an indication that hydroxides are consumed, which can be related to the basic hydrolysis of cellulosic, hemicellulosic and lignin compounds. Furthermore, mass balance reveals that 140 mg of organic molecules have been hydrolysed and solubilised in the alkaline solution, the so-called sugar cane basic hydrolysate (SCBH). This means, in a simplified manner we can estimate $C_6(H_2O)_6$ = 180 g.mol^{-1} as a probable mean molar mass, that about 0.78 mmol are solubilized in 150 mL of hydrolisate solution.

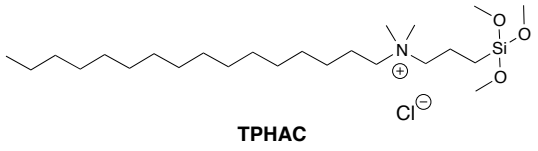

TPHAC

Figure 4-11. R. Ryoo's TPHAC.

The synthesis conditions and gel ratios of the herein investigated samples are exposed in Section **2.1.1.1.** in **Table 2-1**. Only 30 mL of the aforementioned SCBH are added to the respective synthesis gels, hence a probable mean 0.156 mmol of carbohydrate-like hydrolysed monomers will be interfering with the zeolite crystal growth under hydrothermal conditions. Compared to the 27 mmol of tetraethylorthosilicate (Si-source) and the 4 mmol of sodium aluminate (Al-source) in the gel, the biomass fraction seems infinitesimally small. A synthesis ratio considering the bio-sourced secondary template (BSST) can now be estimated: Si / Al / TPA / BSST = 27 / 4 / 8 / 0.156 (0.6 mol-% with respect to Si_{total}). This constitutes a striking

[264] Ocampo, F.; Cunha, J.A.; de Lima Santos, M.R.; Tessonnier, J.P.; Pereira, M.M.; Louis B. *Appl. Catal. A Gen.* **2010**, *390,* 102–109.
[265] Ge, T.; Hua, Z.; He, X.; Lv, J.; Chen, H.; Zhang, L. *Chem. Eur. J.* **2016**, *22*, 7895.

discrepancy compared to Ryoo's seminal work on secondary templates in the synthesis of MFI-zeolites,[262] wherein designed [3-(trimethoxysilyl)propyl]hexadecyldimethylammonium chloride ($[(CH_3O)_3\ SiC_3H_6N(CH_3)_2C_{16}H_{33}]Cl$, TPHAC) was used at a 4 mol-% scale with respect to Si_{total}. These molecules contain a surfactant-like long-chain alkylammonium moiety and a hydrolysable methoxysilyl group, linked together by a Si–C bond, which is chemically stable under various zeolite synthesis conditions (**Figure 4-11**).[266] In the following study we will see that BSST's are truly interfering with the MFI-crystal growth in a comparable, but somewhat different manner than reported by Ryoo's group with their rationally conceived secondary templates.

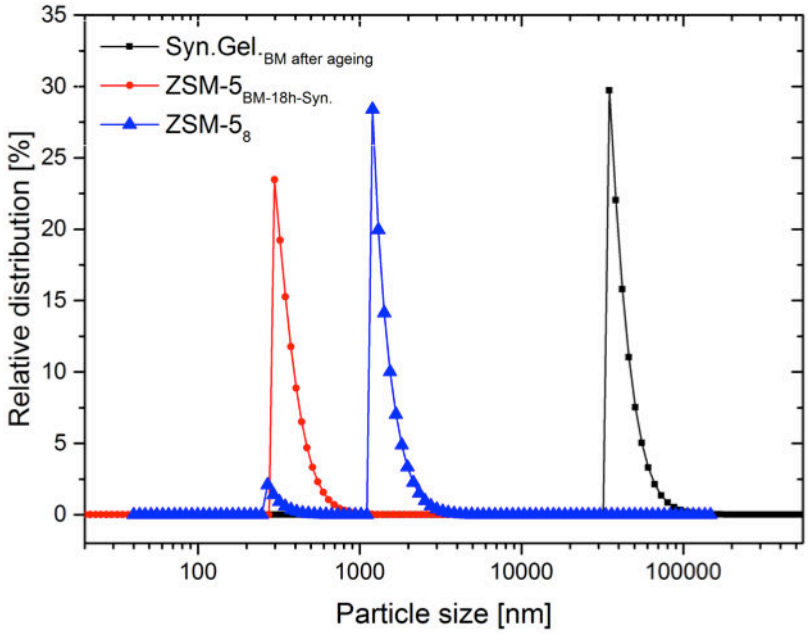

Figure 4-12. Dynamic light scattering (DLS) spectra, Number vs. Particle size of the synthesis gel containing BSST after the ageing (black), intermediate synthesis of 18h (red) and the ZSM-5_8 (blue).

Even though Dynamic Light Scattering (DLS) is a technique useful for characterising colloidal stable suspensions with particle sizes below one micrometer, we used this technique and the results are presented in **Figure 4-12**. Before synthesis a gel of "micelles" up to 100 µm can be observed, whereas after only 18h under synthesis conditions nanoparticles of 250 nm are formed very homogeneously and after a prolonged synthesis duration with the quantitative formation of ZSM-5_8, only a small amount of nanoparticles (about 250 nm) remain and most of the material (> 90 %) seems to be transformed to 1-3 µm sized aggregates. A partial validation of this technique considering zeolite crystal sizes is provided by SEM **Figure 4-15e**, whereas the strong tailing character of the curves above restricts elaborate conclusions from these DLS-results.

Superimposed XRD-patterns prove that pure MFI phases were obtained after all syntheses, short of ZSM-$5_{8\ Fail}$ (**Figure 4-13**).

[266] Jun, S.; Ryoo, R. *J. Catal.* **2000**, *195*, 237–243.

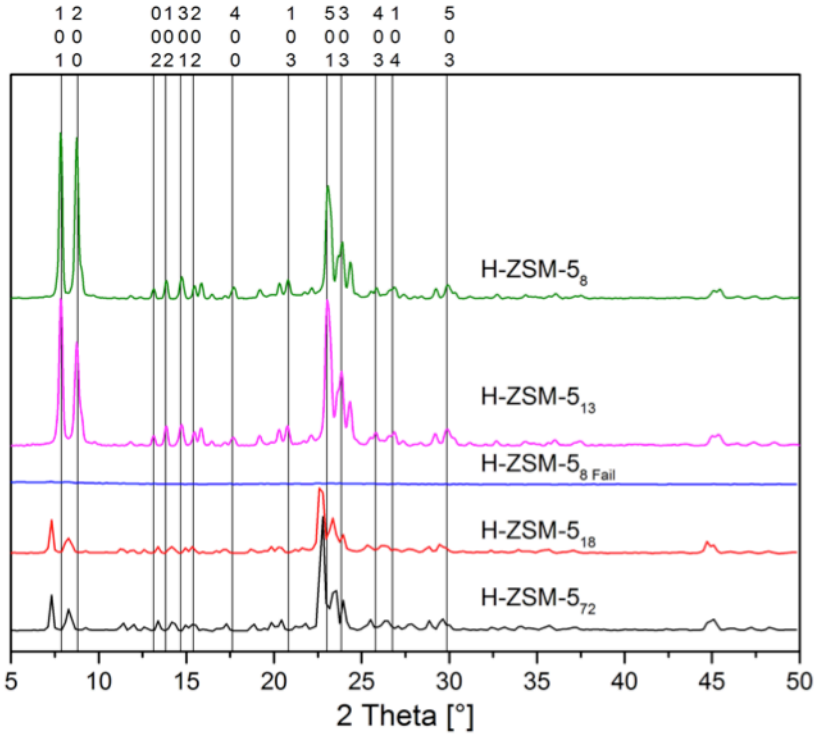

Figure 4-13. Powder XRD pattern for the 5 studied samples: Well crystallized MFI-phases except for the H-ZSM-$5_{8,\ Fail}$ sample. The 13 major characteristic MFI reflections are indexed.

Table 4-4. Textural properties, elemental composition, acid site density and crystallinity information of the different materials.

Zeolite	Si/Al-ratio[a]	$N_{theor.}(H^+)$ [mmol(H^+).g^{-1}][b]	$N_{exp.}(H^+)$ [mmol(H^+).g^{-1}][c]	S_{BET} [$m^2.g^{-1}$][d]	S_{Meso} [$m^2.g^{-1}$][d]	Crystalline yield [%][e]	Relative crystallinity [%][f]
H-ZSM-5_{72}	72	0.21	0.42	-	-	73	98
H-ZSM-5_{18}	18	0.82	0.56	-	-	72	86
H-ZSM-$5_{8\ Fail}$	9	1.60	0.25	7	5	63	< 30
H-ZSM-5_{13}	13	1.12	1.18	255	56	85	100
H-ZSM-5_8	8.3	1,71	1,53	392	100	89	91

a: XRF elemental bulk analysis.
b: Theoretical relation between Si/Al-ratio and Brønsted acid site (BAS) density can be calculated.
c: H/D-isotope exchange.
d: Specific surface area derived from N_2-adsorption desorption isotherms.
e: Crystalline yield considering the obtained solid mass with respect to the Si-source.
f: Relative crystallinity obtained by comparing integrated areas of the 13 major peaks observed in the XRD-pattern (**Figure 4-13**).

Table 4-4 gives the characterisation of herein compared ZSM-5 zeolites. Five different zeolites are compared which have been synthesised in very similar conditions (only varying Si/Al-ratio or synthesis time) and resulting in different materials. They have been characterised in terms of their elemental composition, acid site densities (theoretical based on Si/Al vs. H/D titrated, true Brønsted acid sites). Their total BET and mesoporous surface areas, their crystalline yield (resulting solid mass) and relative crystallinity (integration over the 13 major reflections cf. **Figure 4-13**) were determined as well. It is noteworthy that two samples were obtained with a Si/Al-ratio below 10, namely H-ZSM-$5_{8\ Fail}$ and H-ZSM-5_8. The two syntheses only differed in the

crystallization duration, H-ZSM-5_8's longer synthesis (144h vs. 65h for H-ZSM-$5_{8\ Fail}$ cf. **Table 2-1**) allowed the complete crystallization of H-ZSM-5 crystallites, in parallel with a excitingly high incorporation of aluminum in the crystalline framework. H-ZSM-5_{72}, H-ZSM-5_{18} and H-ZSM-5_{13} resulted as well quantitatively in MFI-zeolite. Importantly, the theoretically predicted and experimentally measured acid site densities closely match for H-ZSM-5_{13} and H-ZSM-5_8. Hence, it appears that every Al-site gave rise to an expected Brønsted acid site and further that these remain accessible to probe molecules. Thus a good quality of the porosity is needed, which is veritably reflected by the BET surface areas and the N_2-sorption measurements (**Figure 4-14**). Those nitrogen adsorption-desorption isotherms are of type I tending to IV (typical for micro-mesoporous materials) with an N_2-uptake starting at 0.4 p/p_0, while no actual porosity was detected for H-ZSM-$5_{8\ Fail}$. H-ZSM-5_{13} and H-ZSM-5_8 exhibits therefore a complex porosity, microporous and mesoporous in nature. Indeed, the hysteresis loop type IV[267] also indicates the presence of parallel meso- and microporosity. **Table 4-4** it is shown that more than a quarter of this samples total surface area can be linked to mesopores ($2 < ø < 50$ nm).

The latter consitutes sound evidence for the structure directing efficiency of the BSST, present only at very low concentrations during the zeolite synthesis. Since hardly any ZSM-5 zeolites with a SAR < 10 can be found in the literature, BSST's seem to favour the integration of aluminum in the zeolitic framework during the crystal growth. This is a finding, which deserves deeper studies in the near future.

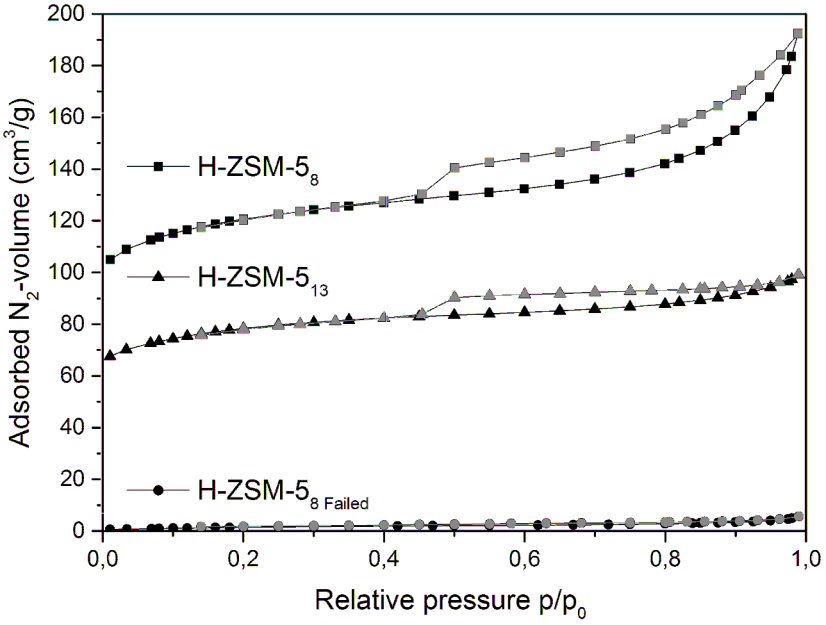

Figure 4-14. N_2-adsorption desorption isotherms of H-ZSM-$5_{8\ Fail}$, H-ZSM-5_{13} and H-ZSM-5_8.

[267] Thommes, M. *Chemie Ingenieur Technik* **2010**, *82*, 1059.

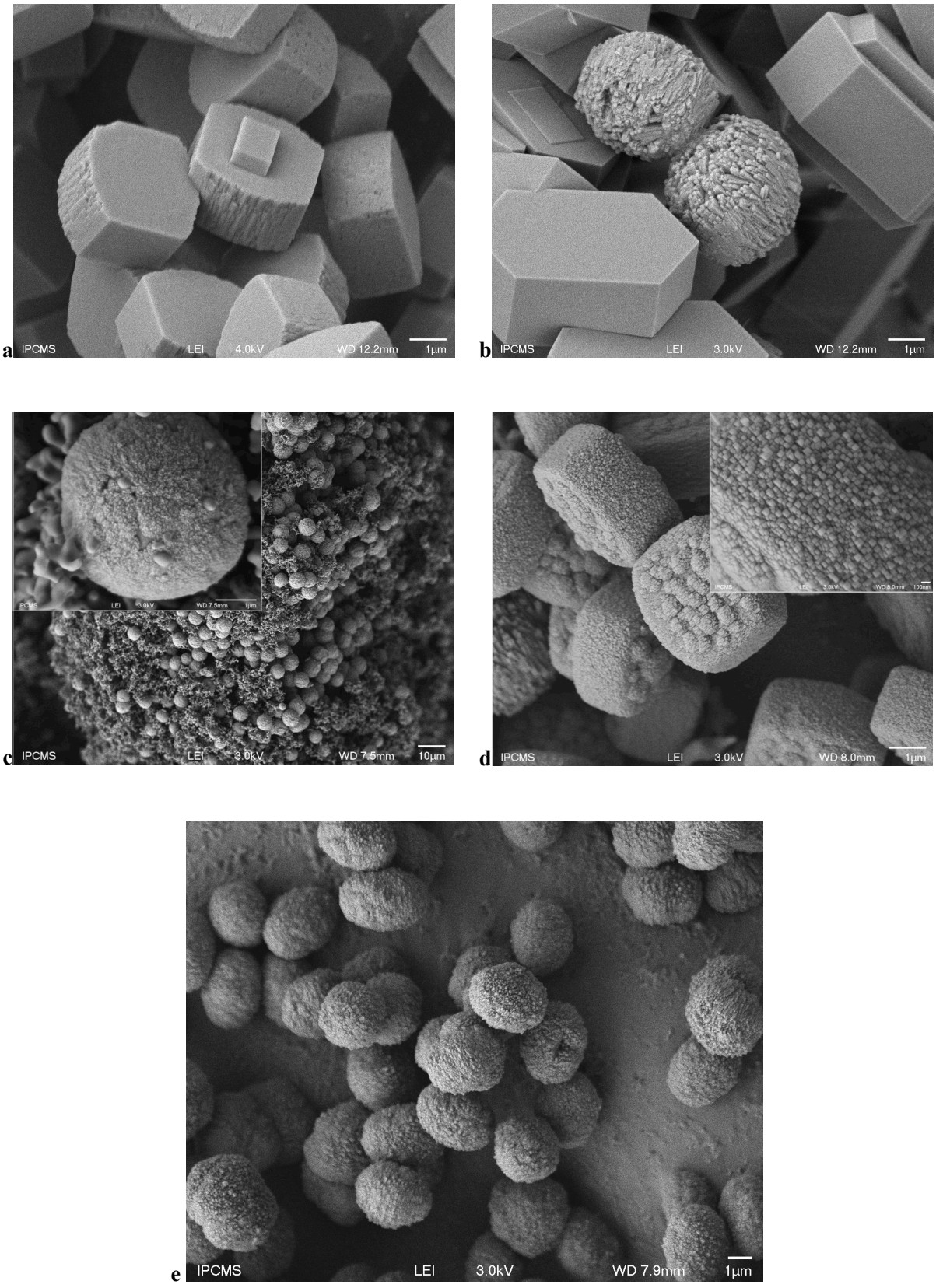

Figure 4-15. Scanning electron microscopy (SEM) micrographs of the 5 samples: a) H-ZSM-5_{72}, b) H-ZSM-5_{18}, c) H-ZSM-$5_{8\ Fail}$, (+ insert with higher magnification), d) H-ZSM-5_{13} (+ insert with higher magnification), and e) H-ZSM-5_{8}.

SEM micrographs in **Figure 4-15** display the different synthesised samples. Whilst in **Figure 4-15 a)** and **b)** coffin shaped crystals and a bimodal crystallization were observed and suggest a lesser effect of BSST, **Figure 4-15 c)** H-ZSM-$5_{8\ Fail}$, **d)** H-ZSM-5_{13} and **e)** H-ZSM-5_{8} are proof for the potential structure directing effect of BSST. Even though H-ZSM-$5_{8\ Fail}$ was not completely crystallized, some spherical mesoporous crystallites can already be observed (1-3 µm). Those identical synthesis conditions at a longer crystallization time eventually resulted in **Figure 4-15 e)** H-ZSM-5_{8}, the high Al-content mesoporous zeolite described above (1 - 3 µm aggregates of 50 - 100 nm crystallites) in line with DLS results. The same goes for H-ZSM-5_{13}, which shows a regular mesoporosity between aggregated 50 - 100 nm crystallites, in unison with **Table 4-4** and **Figure 4-14**.

SEM-EDX mapping of the elements (Si, O and Al) was performed for H-ZSM-5_{8} sample (**Figure 4-16**) and reveals that the aluminum is rather homogeneously dispersed throughout the crystal (no external or internal zoning, no egg-yolk, or core-shell structure). However, the crystal seems to have some local enrichments in aluminum in the vicinity of the crystals mesopores, while silicon is homogeneously dispersed.

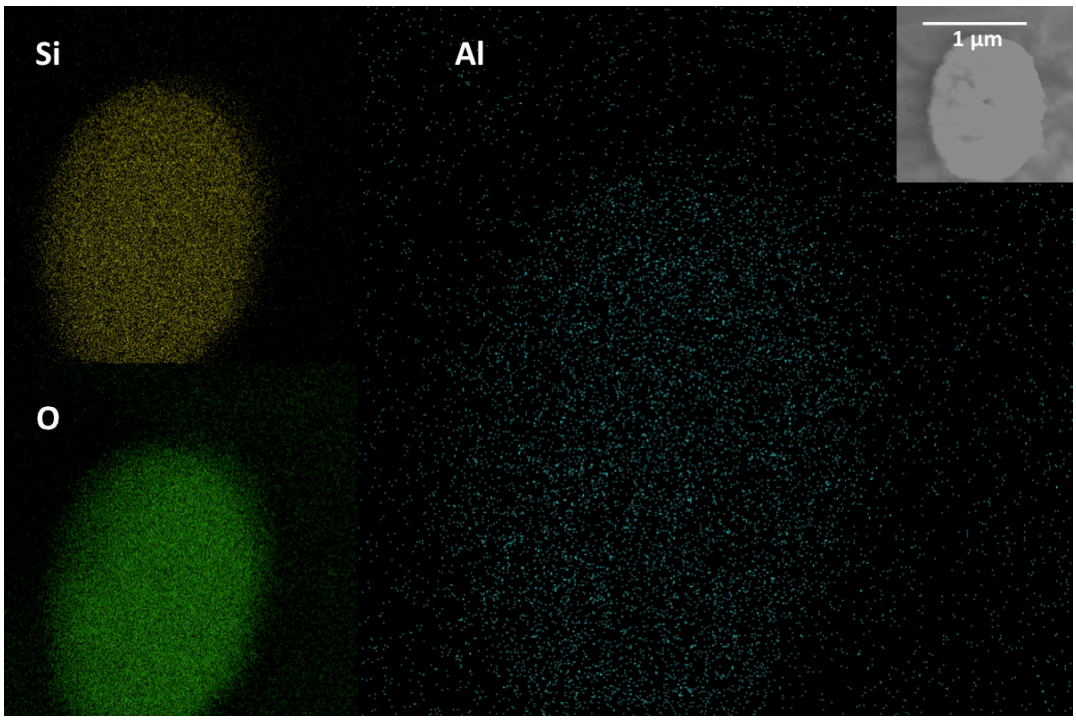

Figure 4-16. SEM-EDX elemental mapping of Si, Al and O on one crystallite of H-ZSM-5_{8}.

Then, **Figure 4-17** presents TEM pictures of this particular ZSM-5_{8} and proves the high quality of nanosized crystallites, which compose the micron sized aggregates (cf. **Figure 4-15)** The zeolites high quality micropores are visible and XRD reflections give evidence for the sole presence of the MFI-phase.

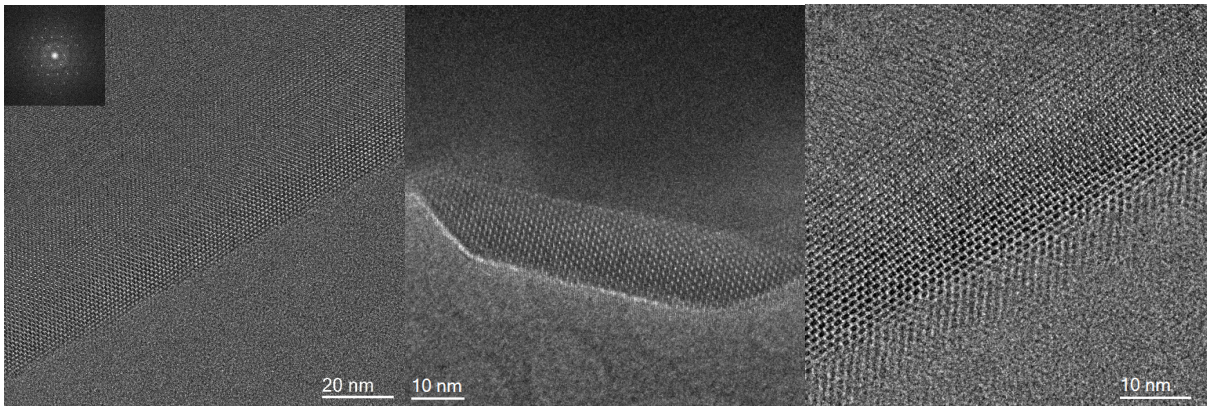

Figure 4-17. Cryo (transmission) electron microscopy (cryo-(T)EM) micrographs of H-ZSM-5[8].

4.3.3. Biomass-(BSST)-induced inhibition of water crystallization as a hint towards supramolecular self-assembly.

Self-assembly mechanisms where biomass derived secondary templates play a key role as structure directing agent and as well as metal-incorporation governing species are of crucial importance in biology. According to some researchers these complex interactions may even be at the very origin of life itself.[268] Indeed, silicates[269] and aluminates[270] are known to bind to carbohydrates in a way that diminishes their reactivity. Before getting to that, we tried to take a simplified approach to ease the understanding of the utterly complex phenomena occurring during BSST assisted crystallization. Therefore, we focussed on the crystallization of water in the presence of various BSST's.

Figure 4-18 and **Table 4-5** present the results obtained for four different aqueous solutions in a water crystallization experiment. Antifreeze proteins (AFP) inhibit the crystalline growth of ice by binding to ice nuclei with a planar site, a so-called ice-binding motif (IBM).[271] Analogously, one can assume that bagasse and lignin hydrolysates, amphiphilic in nature as well, may inhibit or direct the crystalline growth of ice in a certain way. Indeed, the herein presented data suggest that hydrolysates inhibit crystal growth; entries 3 and 4 show a freezing time increased by more than 30 % with respect to the reference in entry 1. For entry 2 this crystallization time even doubled with respect to the reference, this might however as well be linked to the higher pH in this sample. **Figure 4-18c** and **Figure 4-18d**, corresponding to entries 3 and 4 in **Table 4-5**, prove an additional structuring impact of bagasse and lignin hydrolysate solutions during ice crystallization. Indeed, similarly to concentrated antifreeze protein solutions,[271b] a crystalline growth in the form of needles is observed. Furthermore, in the case of

[268] a) Kostetsky, E. Y. *J. Biol. Phys.* **2005**, *31*, 607–38. b) Benner, S. A.; Kim, H.; Kim, M.; Ricardo, A. *Cold Spring Harb Perspect Biol.* **2010**, *2*, a003467.
[269] Lambert, J.B.; Lu, G.; Singer, S.R.; Kolb, V.M. *J. Am. Chem. Soc.* **2004**, *126*, 9611–9625
[270] Schilde, U.; Kraudelt, H.; Uhlemann, E. *Reactive Polymers* **1994**, *22*, 101–106.
[271] a) Sicherl, F.; Yang, D.S.C. *Natur,* **1995**, *375,* 427-431. b) Davies, P.L.; Hew, C.L. *FASEB Journal* **1990**, *4* 2460-2468.

lignin hydrolysate a concentration gradient is observed during the freezing process, the "coloured" part gradually concentrates in the centre of the vial, which froze last. Finally, it is important to mention that entry 3 in **Table 4-5** are the same conditions (BSST-hydrolysate) that have been used in the above described zeolite syntheses, and in particular for H-ZSM-5[8].

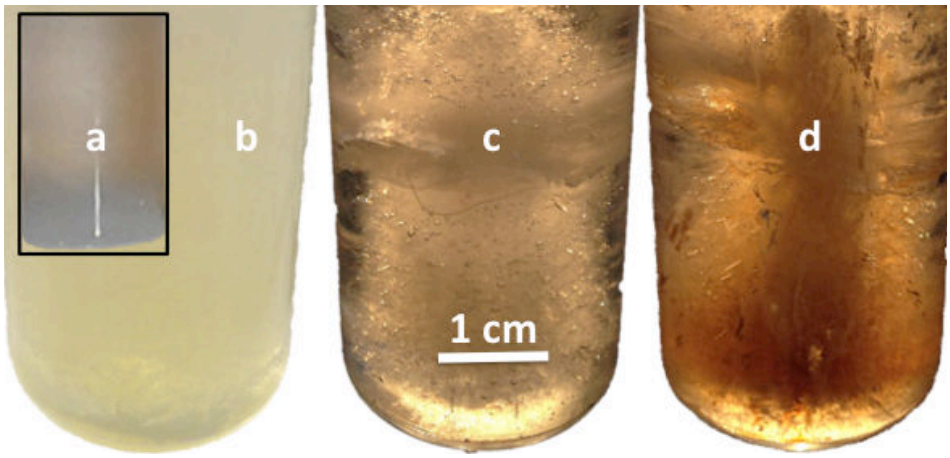

Figure 4-18. Four samples of water crystallization under biomass induced inhibition or structuration: a) Reference (entry 1, **Table 4-5**), b) Bagasse hydrolysate at pH 14 (entry 2, **Table 4-5**), c) Bagasse hydrolysate at pH 10-12 (entry 3, **Table 4-5**), d) Lignin solution at pH 10-12 (entry 4, **Table 4-5**).

Table 4-5. Four samples of water crystallization under biomass (BSST) induced inhibition and structuration.

Entry	Sample	pH	Freezing time [min][a]	Morphology
1	$H_2O_{dist.}$ + NaOH	10 - 12	30 - 90	-
2	Bagasse hydrolysate	14	> 180	-
3	Bagasse hydrolysate	10 - 12	40 - 120	Ice needles (**Figure 4-18c)**
4	Lignine solution	10 - 12	40 - 120	Ice needles + concentration gradient (**Figure 4-18d)**

a: Experiment carried out in a deep freeze chamber at 255 K and followed by a timelapse video analysis. The two different time values, e.g. 30 - 90 indicate the presence of the first ice crystallites and the full crystallization of the aqueous sample.

It is tempting to establish a parallel between the well-studied AFP crystal growth inhibiting and directing mechanisms and the biomass crystallization-retardation and structuration. It is interesting to further study and understand the impact of biomass residues during the self-assembly processes occurring during crystallization at different scales and dimensions (nano vs. macro, temperature vs. pressure vs. chemical composition). Nonetheless, this initial simplified study consists already of the necessary and sufficient hint for the supramolecular interference of BSST in crystallization processes.

4.3.4. Discussion

Consequently, and considering some facts of sugar-chemistry a global picture of the crystal growth mechanism will be evoked in this section.

According to Rendleman *et al.* sugars do readily degradate in the presence of $NaAlO_2$.[272] Alkaline degradation of sugars can already occur at 25°C and is hence a huge problem to cope with, in sugar separation chromatography. Additionally, degradation is likelier to occur on reducing sugars, aldoses such as glucose and galactose or ketoses like fructose. The latter first has to tautomerize to form the reducible aldehyde function. Non-reducing sugars for instance sucrose, the Glc(α1-2β)Fru disaccharide, or pyranosyl-glucose and furanosyl-fructose disaccharide does not act as a reducing agent under ambient conditions.[273] However, in our case its likely hydrolysis will release the reducing monosaccharides fructose and glucose. Sucrose, glucose, fructose and galactose are all sugars, which could be evidenced in sugar cane bagasse.[257, 228] Thus, during the hydrolytic alkaline treatment and the ageing step the sugar cane basic hydrolysate (SCBBH) will have evolved to partially oxidised, most probably conjugated, or even aromatised carbohydrates to form the actual BSST's.

Bearing the above discussed in mind, **Figure 4-19** proposes a schematic self-assembly mechanism for the crystal growth, which may result in the observed morphology, e.g. H-ZSM-5_8 (**Figure 4-15e)**.

The alkaline hydrolysis of sugar cane bagasse leads to the formation of soluble saccharidic and aromatic, negatively charged molecules (cf. experiments showed a decrease in pH and a loss in dry mass).[257] This hydrolysis of lignocellulosic biomass usually leads to degraded sugars and rather aromatic lignin-sourced products and has been reviewed multiple times.[274] We already estimated the presence of 0.156 mmol of hydrolysed organic molecules in our gel prior to synthesis in Section **4.3.2.** During the ageing process of the gel, those are changing in nature,[272] and form the actual BSST, which are interacting through electrostatic forces and their chelating potential with the T-monomers, whereby large micellar structures are formed (cf. DLS **Figure 4-12**).

A breakthrough study by Kästele *et al.* illuminated the chelation process of silicate species by saccharides.[275] With X-ray diffraction structure resolution experiments, they evidenced that saccharides and similar molecules are able to expand silicate's coordination sphere from the classically tetra-coordinated tetrahedron to penta-coordinated trigonal bipyramids and square pyramids, up to hexa-coordinated octahedra. Such a behaviour, the expansion of silicate's coordination sphere is commonly assumed and reported in fluoride mediated zeolite syntheses.[276]

[272] Rendleman, J.A.; Hodge J.E. *Carbohydrate Research,* **1975**, *44*, 155. Even though no in cipher value of a preferable aluminate coordination could be found, the chelation preference by saccharides for aluminate species is striking since alumina columns, not silica are used for the sacchide column chromatographies.
[273] Pratt, C.W.; Cornely, K. *Essential Biochemistry,* **2013**, Wiley, 626.
[274] a) Kumar, P.; Barret, D.M.; Delwiche, M.J.; Stroeve, P. *Ind. Eng. Chem. Res.* **2009**, *48*, 3713. b) Anwar, Z.; Gulfraz, M.; Irshad, M. *J. Rad. Res. Appl. Sci.* **2014**, *7*, 163.
[275] Kästele, X.; Klüfers, P.; Kopp, F.; Schuhmacher, J.; Vogt, M. *Chem. Eur. J.* **2005**, *11*, 6326–6346.
[276] Aubert, E.; Porcher, F.; Souhassou, M.; Lecomte, C.; Poincare, H. *J. Phys. Chem. B* **2002**, *106*, 1110–1117.

Thus the alcoolate, chelating coordinating groups seem to have an interjacent affinity towards the T-entities with respect to the weaker binding hydroxide anions and stronger binding fluoride anions. Intermediate T-BSST species may therefore induce a controlled crystallization, since they are more stabilised than T-OH species.

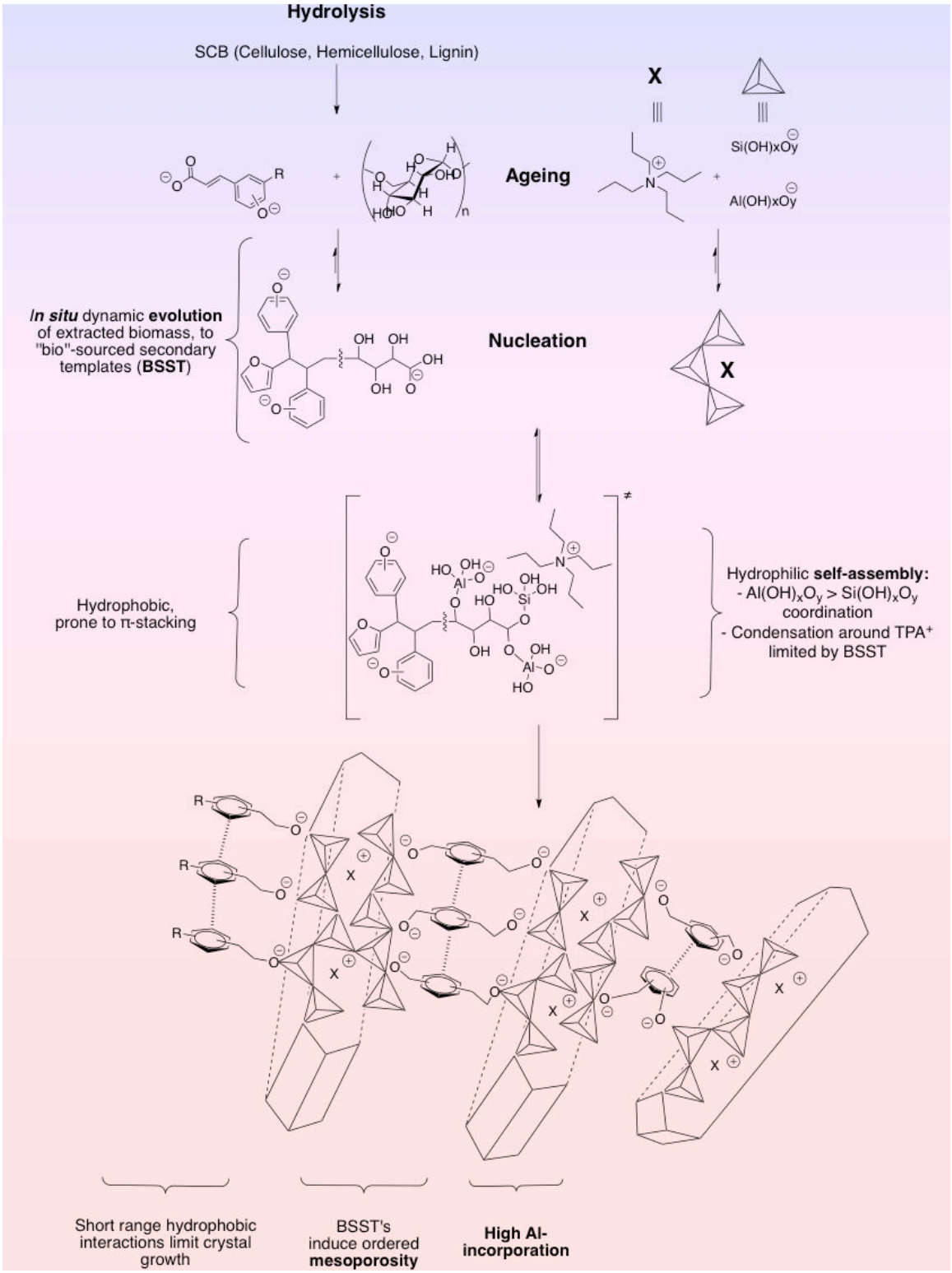

Figure 4-19. Proposed self-assembly mechanism taking into account all of the observed properties that have been previously described. From the top to the bottom: (Colourcode: the shift from blue to

red indicates the incremental increase of the reaction temperature from r.t. to 170°C) The alkaline hydrolysis of sugar cane bagasse leads to the formation of soluble saccaharidic and aromatic, negatively charged molecules.[257] These are interacting through electrostatic forces and their chelating potential with the T-monomers during ageing, where large micellar structures are formed (cf. DLS **Figure 4-12**). Upon heating during the synthesis, crystalline nuclei form and the biomass sourced organic molecules increasingly transform to thermodynamically favoured dehydrated, aromatic species,[277] consituting the actual BSST. These *in situ* evolving surfactant-like molecules interfere with the crystallization process: the chelation preference for aluminate species induces a higher Al-incorporation in the final crystal,[272, 275] while electrostatic forces keep the BSST's attached to the growing crystal, and the aromatic species may stabilise via π-stacking interactions the crystalline *a*- and *b*- axes, thereby preventing Ostwald ripening so that the crystalline growth remains limited to the crystalline *c*-axis. Consequently, the high complexity of the *in situ* evolved BSST's may as well be responsible for the controlled formation of homogeneous mesopores.

Upon heating during the synthesis, crystalline nuclei form and the biomass sourced organic molecules increasingly transform to thermodynamically favoured dehydrated, up to polyaromatic species.[272, 277] These surfactant-like molecules, the as-dubbed BSST's interfere with the crystallization process. The chelation preference for aluminate species may be responsible for higher Al-incorporation in the final crystal,[272, 275] while electrostatic forces keep the *surfactants* attached to the growing crystal. In the meantime, aromatic species via π-stacking interactions may stabilise the crystalline *a*- and *b*-axes of nano-sized highly energetic nuclei, thereby preventing Ostwald ripening so that the crystalline growth is limited to the crystalline monodirectional *c*-axis. Specifically for MFI-samples, the crystalline *c*-axis remains as the single possible direction of growth since the access to the crystals porosity is hindered (cf. MFI-unit cell representations in **Figure 1-10** or **Figure 1-16**). Less BSST-T-monomer interactions can consequently be expected in this direction. Ultimately, referring to the observed mesopore generation during these syntheses (cf. **Figure 4-14** and **Table 4-4**) the high complexity of the *in situ* evolved surfactant-like BSST's may as well be responsible for the controlled formation of homogeneous mesopores as depicted in the bottom part of **Figure 4-19**.

Figure 4-20 and **Figure 4-21** are a tentatively simplified version of the earlier detailed representation. Herein, the supramolecular interactions and processes are depicted in a more schematic overview, eventually leading to the observed crystal morphologies.

[277] The supernatant solution after the hydrothermal synthesis still contains part of the organic hydrolysate. In each synthesis it could be observed that this supernatant was considerably darker in colour than the initial solution. It is thus reasonable guessing to think of a partial "caramelisation" of engaged biomass. See Rendleman *et al.*[272]

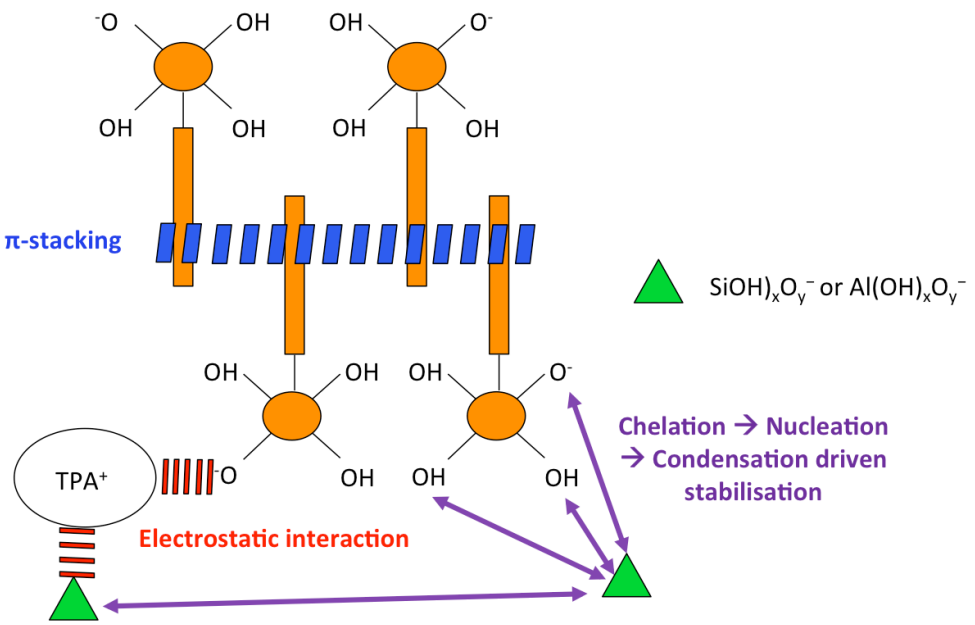

Figure 4-20. Schematic representation of the supramolecular interactions with interfering BSST during the self-assembly process of the zeolite crystal growth.

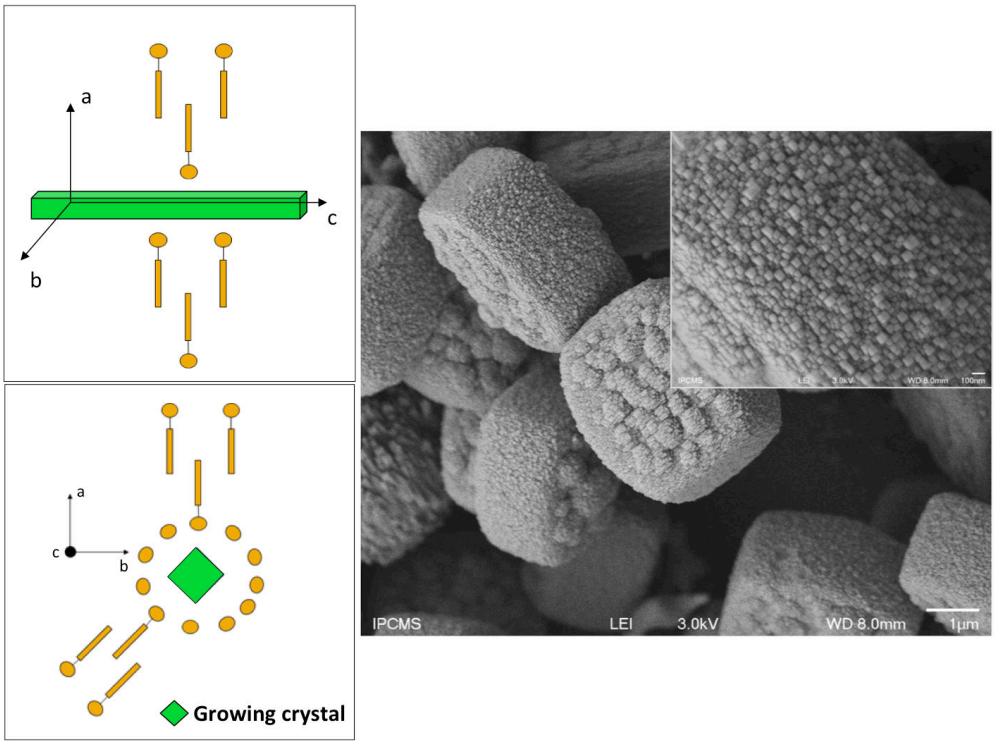

Figure 4-21. The possible link of the above discussed with the final obseved result in form of a mesoporous crystallite with high Al-incorporation, e.g. H-ZSM-5_{13} and H-ZSM-5_8.

4.3.5. Their Application in Catalysis

All of the five investigated catalysts were tested in two different catalytic reactions, the MTH-reaction and the n-hexane cracking reaction.

We did not expect to observe outstanding catalytic performances in this first application, especially considering our evidenced structure to activity relationships in Chapter 3. Exactly such a relationship between the different catalyst properties and their catalytic activity was sought for while performing these tests. **Table 4-6** presents the product distributions in the MTH reaction. It has to be noted that no long-term runs have been carried out with these catalysts. Only the high SAR H-ZSM-5_{72} sample led to a somewhat interesting production of $C_{2=}$-$C_{4=}$ light olefins 54 %, which is in line with **Figure 3-2** in the Section **3.4.1.** This is true as well for the other samples their rather high surface acid site density (> 4 x 10^{-6} mol(H^+).m^{-2}) resulted in a typical MTG-catalyst behaviour, bar entry 3 where no fully crystallized catalyst was engaged.

Table 4-6. Catalysts activities and selectivities in the Methanol-to-Hydrocarbons reaction.

Entry	Zeolite	Conversion [%]	Selectivities [%]					
			CH_4-C_4H_{10}	$C_{2=}$	$C_{3=}$	$C_{4=}$	$C_{5=}$	C_{6+} aromatics
1	H-ZSM-5_{72}	99	20	14	29	11	10	16
2	H-ZSM-5_{18}	99	18	15	23	12	8	24
3	H-ZSM-$5_{8\ Fail}$	0	0	0	0	0	0	0
4	H-ZSM-5_{13}	99	21	17	23	11	9	19
5	H-ZSM-5_{8}	99	18	17	25	14	8	18

Catalytic data obtained after 1h on stream under standardized conditions; 60 mg catalyst in a plug-flow quartz reactor, 450°C, WHSV 1.2h^{-1}; No long-term tests were undertaken, these samples are supposed to quickly deactivate.

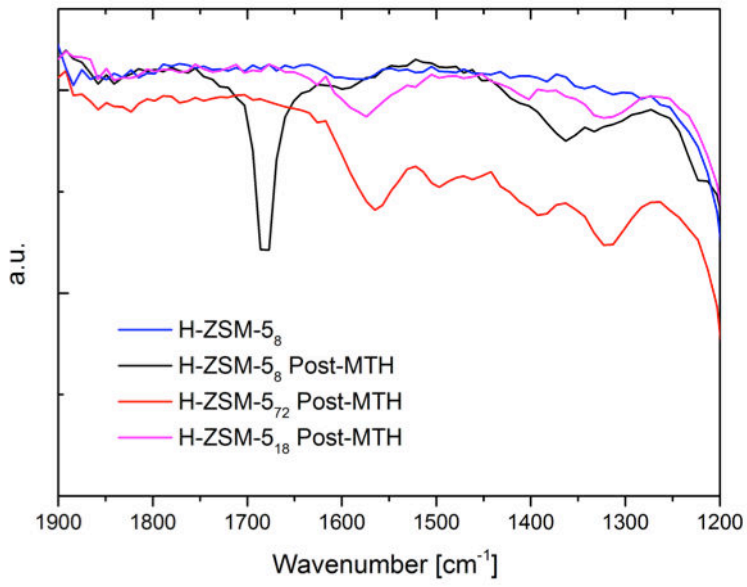

Figure 4-22. FTIR analysis of *"post mortem"* (after 2h on stream) catalysts after their application in the MTH reaction. Coke specific absorbance region: 1200 - 1900 cm^{-1} with 1300 - 1600 cm^{-1} corresponding to aromatic C=C-stretching and 1600 - 1700 cm^{-1} to alkene C=C-stretching.

"Post-mortem" analyses by FTIR are plotted in **Figure 4-22**: H-ZSM-5_{72} and H-ZSM-5_{18} exhibit a typical coke distribution on their surface ranging from 1300 - 1700 cm^{-1}, whereas H-

ZSM-5_8 presents a different kind and only one single type of coke (at 1650 - 1700 cm^{-1}) on its surface. The latter can be related to a strong alkene-C=C stretching vibration.[278]

The second application showed in contrast to the previous one interesting and competitive catalytic behaviours. Indeed, the reaction rate of the highly acidic H-ZSM-5_{13} and H-ZSM-5_8 were four and five times higher than the weaker acidic H-ZSM-5_{72} (entry 1, **Table 4-7**), even though the titrated number of exchangeable hydrons was only three to four times higher than in H-ZSM-5_{72} (cf. **Table 4-5**). In order to compare our results with literature data, we turned to reported data from Ocampo *et al.* who used the same reaction setup and conditions.[256] Their aim was to conceive a composite material starting with a designed porous glass monolith and growing catalytically active ZSM-5 zeolite on its surface. Their highly ordered composite mesoporous, material even with a lower number of Brønsted acid sites (entry 7, **Table 4-7**, Si/Al=20), was far more active than the compared highly acidic commercial catalyst (entry 6, **Table 4-7**, Si/Al=12). These results are in line with former studies reporting a higher activity of mesoporous zeolites in acid-catalysed transformations.[279]

In comparison however, the reaction rates of herein designed catalysts outperform the earlier ones by up to one order of magnitude (entry 7 vs entries 4 and 5). Even though Haag *et al.* reported a linear dependence between the number of Brönsted acid sites and n-hexane cracking activity,[280] the highly ordered mesoporosity and perhaps the controlled location of aluminum, thus the active sites play crucial roles as well in this acid catalysed reaction.

Table 4-7. Catalysis: n-hexane cracking, a model reaction for the FCC-process at 873 K.

Entry	Zeolite$_{(SAR)}$	Rate [mol.(g.s)$^{-1}$]	Alkene/Alkane-ratio	Propylene	Ethylene
1	H-ZSM-5_{72}	582	0.054	0.35	0.061
2	H-ZSM-5_{18}	-	-	-	
3	H-ZSM-$5_{8\ Fail}$	142	0.007	0.20	0.040
4	H-ZSM-5_{13}	2084	0.206	0.35	0.113
5	H-ZSM-5_8	2789	0.457	0.30	0.179
6[a]	Commercial H-ZSM-5[b]	32	0.95	0.26	0.14
7[a]	H-ZSM-5@glass composite[c]	210	1.14	0.35	0.13

a: These data are from an earlier study from our group reported by Ocampo *et al.* [256]
b: Commercial zeolite from Petrobras in Brasil with Si/Al = 12.
c: In their study Ocampo *et al.* conceived a ZSM-5@glass composite material exhibiting a well-defined structured hierarchical porosity and a Si/Al = 20.

Interestingly, the most acidic H-ZSM-5_8 (entry 5) proved to be the most selective towards alkenes amongst the herein prepared and studied samples. This particular selectivity is important since $C_{2=}$–$C_{4=}$ light olefins are valuable building blocks for the chemical industry, as monomers,

[278] Silverstein, R.M.; Bassler, G.C.; Morrill, T.C. *Spectrometric Identification of Organic Compounds.* 4th ed. New York: John Wiley and Sons, **1981**.
[279] Sun, Y.; Prins, R. *Appl. Catal. A* **2008**, *336*, 11–16.
[280] Haag, W.O.; Lago, R.M.; Weisz, P.B. *Nature* **1984**, *309*, 589–591.

or as starting compounds for the synthesis of fine chemicals. H-ZSM-5_{13} (entry 4) led to high propylene selectivity, with respect to ethylene. It did even exceed the previously reported composite catalyst (entry 7). The higher selectivity toward alkenes is generally explained by improved diffusion properties within hierarchical zeolite crystals.[281] Alkenes, being more reactive than alkanes, they are more readily transformed via acid-catalysed pathways when mass transfer constitutes a limiting factor. Hence, an increase in the contact time between the products and the Brønsted acid sites, as it is the case for the commercial sample (entry 6) and for H-ZSM-5_{72} (entry 1), will necessarily lead to a decrease in the alkene-to-alkane ratio.

4.3.6. Potential Impact and Outlook

Brasilian sugar cane bagasse being composed of cellulose, hemicellulose and lignin comprises a high degree of chemical complexity, which is lost when burned and turned into CO_2. The herein followed strategy was to use bagasse, hydrolysed in some cases and benefit from its complex mixture of hydrophilic and hydrophobic zones, potential π-stacking areas and chelating properties. During the self-assembly of zeolite crystal growth it could be evidenced that the described material and its extracted molecules could act as *in situ* evolved bio-sourced secondary templates (BSST) and interfere with growing aluminosilicates. In particular, this strategy led to the formation of highly acidic and mesoporous ZSM-5 particles.

Regarding the general frame of this Chapter 4 a critique might persist: Ultimately, BSST's are burned off as-formed crystals during the calcination step. Eventually, their carbon atoms end up, as CO_2 anyway so is this strategy really worth the effort?

Even though *in fine* BSST or SCB carbon atoms will lose their complexity, during the self-assembly process during the BSST guided zeolite synthesis they will imprint, or replicate their complexity in a certain way into the inorganic material. The latter highly complex zeolite is the actual added value in relation to the *carbon upgrading* concept, because it can be used multiple times in carbon valorising reactions such as MTG, the conversion of biomass to levulinic acid,[282] renewable feedstock based petrochemistry and many more.[260]

[281] Schmidt, I.; Krogh, A.; Wienberg, K.; Carlsson, A.; Brorsen, M.; Jacobsen, C.J.H. *Chem. Commun.* **2000**, *21*, 2157–2158.
[282] Van de Vyver, S.; Geboers, J.; Jacobs, P. A.; Sels, B. F. *ChemCatChem* **2011**, *3*, 82–94.

4.4. Zeolite Catalysed Continuous Flow Halogenation of Aromatics

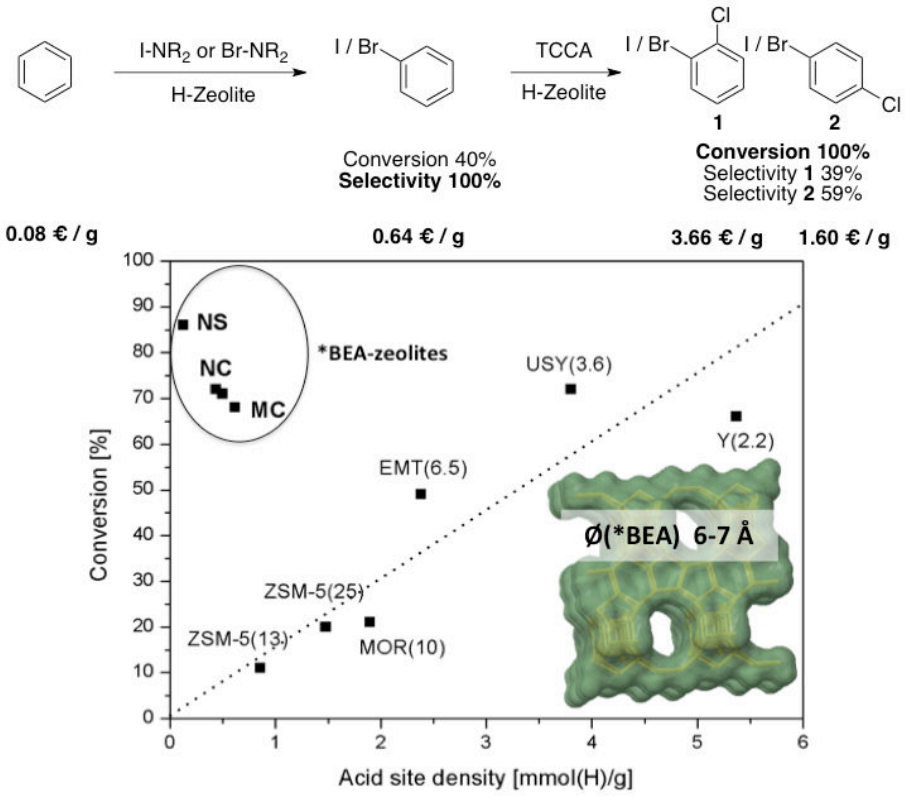

Figure 4-23. Eco-compatible halogenation reaction of aromatics using cheap halogenating agents and zeolite H-*BEA as a heterogeneous catalyst.

4.4.1. The Challenge

Halogenation of arenes leads to valuable starting molecules in fine chemistry as an entry towards the synthesis of dyes, bioactive compounds such as pesticides or pharmaceuticals.[283] This generally Lewis acid catalysed reaction is known since the 1950's and most commonly involves $FeCl_3$ as a catalyst.[284] Nowadays, it is implemented in industry at the megaton-scale and still facing an annual growth demand of roughly 5 %.[285] It is of paramount importance to underline the ongoing progress in sustainable arene production complementing the classic fossil resources. For

[283] a) Franck, H.-G.; Stadelhofer, J.W. *Industrial Aromatic Chemistry*, Springer-Verlag, Berlin, Heidelberg, **1988**, pp 224–226. b) Kroschwitz, J.I.; Howe-Grant, M.; Treacy, C.A.; Humphreys, L.J. *Encyclopedia of Chemical Technology*, vol. 6, Wiley, New York, **1993**, pp 109–113.
[284] Beck U.; Löser, E. *Chlorinated Benzenes and other Nucleus-Chlorinated Aromatic Hydrocarbons*, Ullmann's Encyclopedia of Industrial Chemistry, Wiley-VCH, Weinheim, **2012**.
[285] a) "Chlorobenzene: *Webster's Timeline History*, 1851 - 2007", **2010**, ICON Group International, Inc. b) http://www.icis.com/resources/news/2005/12/02/570444/chemical-profile-chlorobenzene/ ICIS Chemical Business (02 December **2015** 12:51) http://www.icis.com/resources/news/2005/12/02/570444/chemical-profile-chlorobenzene/

instance, biomass-derived dimethylfuran (DMF) and bioethanol are converted to renewable xylene.[286]

Unfortunately, industrial methods for the most commonly used aromatics halogenation reactions usually produce mixtures of regioisomers, difficult to separate, thus raising the production cost.[287] Notably, the Raschig-Hooker process has been industrially applied for a long time to produce chlorobenzene and phenol in a continuous flow process with hydrochloric acid and *in situ* generation of Cl_2 gas using a CuCl-$CuCl_2$ mixed catalyst.[288] Another drawback relies on the use of hazardous and corrosive acid 'catalysts' such as aluminum chloride, boron trifluoride, etc. which are required in over-stoichiometric amounts and cannot be recovered after the reaction course. Likewise, strong Brønsted acid catalysts such as sulphuric acid remain very corrosive and generate high amounts of salts as by-products.

Recently, the scientific community focused on developing more efficient and selective processes for the halogenation of arenes.[289] For instance, de Mattos *et al.* developed a methodology for the halogenation of deactivated arenes using trichloro- / trihaloisocyanuric acid (TC(Hal)CA) in a superelectrophilic medium (**Figure 4-24**).[290] TCCA is a stable and inexpensive solid, easily available in pool supplies, commonly used as swimming-pool disinfectant and bleaching agent. It is an efficient chlorine source due to its highly electrophilic chlorine content and has already been used in numerous chlorination reactions of diverse organic compounds as well as in oxidation reactions.[291,292]

These early studies have been carried out in homogeneous superacidic conditions, while the green chemistry principle of catalysis, encompassing both homogeneous and heterogeneous catalysis, is becoming increasingly ubiquitous in organic chemistry. Heterogeneous catalysts are easily adopted in gas-solid or liquid-solid flow processes; thereby they may allow to continuously

[286] a) Chang, C.-C.; Je Cho, H.; Yu, J.;. Gorte, R. J.; Gulbinski, J.; Dauenhauer P.; Fan, W. *Green Chem.* **2015**, *174*, 769. b) Chang, C.-C.; Green, S. K.; Williams, C. L.; Dauenhauer, P. J.; Fan, W. *Green Chem.* **2014**, *16*, 585. c) Zhang, X.; Wang, Z.; Xu, K.; Feng, Y.; Zhao, W.; Xu, X.; Yan, Y.; Yi, W. *Green Chem.* **2016**, DOI: 10.1039/x0xx00000x.
[287] Franck, H.-G.; Stadelhofer, J.W. *Industrial Aromatic Chemistry*, Springer-Verlag, Berlin, Heidelberg, **1988**, pp. 218–220.
[288] Ram, E. *Krishna's new concepts in organic chemistry*, Krishna Prakashan media, **2007**, pp 251.
[289] a) Smith, K.; Butters, M.; Paget, W.E.; Goubet, D.; Fromentin E.; Nay, B. *Green Chem.* **1999**, *1,* 83–90. b) Prakash, G.K.S.; Mathew, T.; Hoole, D.; Esteves, P.M.; Wang, Q.; Rasul, G.; Olah, G.A *J. Am. Chem. Soc.* **2004**, *126*, 15770–15776.
[290] a) Mendonça, G.F.; Sindra, H.C.; Almeida, L.S. De; Esteves, P.M.; De Mattos, M.C.S. *Tetrahedron Lett.* **2009**, *50*, 473–475. b) Mendonça, G.F.; Sindra, H.C.; Almeida, L.S. De; Esteves, P.M.; De Mattos, M.C.S. *Tetrahedron Lett.* **2009**, *50*, 473–475. c) Ribeiro, R. S.; Esteves, P. M.; De Mattos, M. C. S. *Tetrahedron Lett.* **2007**, *48*, 8747–8751. d) Sodré, L. R.; Esteves, P. M.; De Mattos, M. C. S. *J. Braz. Chem. Soc.* **2013**, *24*, 212–218.
[291] a) Mendonca, G.F.; Sanseverino A.M.; De Mattos, M.C.S. *Synthesis* **2003**, 45–48. b) Hiegel G.A.; Peyton, K.B. *Synth. Commun.* **1985**, *15,* 385–392; c) de Luca, L.; Giacomelli, G. *Synlett*. **2004**, 2180–2184;
[292] a) Tilstam, U.; Weinmann, H. *Org. Process Res. Dev*. **2002,** *6,* 384–393 b) Mishra, A.K.; Nagarajaiah, H.; Moorthy, J.N. *Eur. J. Org. Chem.* **2015,** 2733-2738.

producing high-value added chemicals.[293] In heterogeneously catalysed reactions, the key solid acid catalysts in petrochemistry, and increasingly in biomass reforming processes, remain zeolites.[294] In addition, to their three-dimensional crystalline microporous network, zeolites are characterised by a strong acidity. Those (often) synergetic properties led them to exhibit high conversions and excellent selectivities in many targeted reactions either in petrochemical processes but in more complex reactions as well, for instance biomass conversion.[295,296] Smith *et al.* highlighted the advantages and limitations of zeolites uses in electrophilic aromatic substitutions, leading, in general, to higher *para*-selectivities.[297]

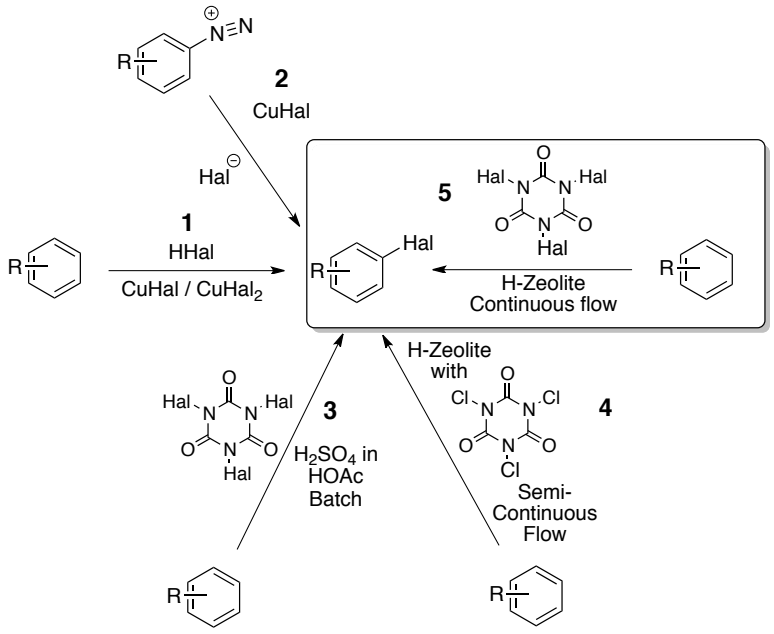

Figure 4-24. Different reaction pathways to produce halogenated aromatics 1) Raschig-Hooker process,[288] 2) Sandmeyer reaction, 3) T(Hal)CA in superelectrophilic medium,[289,290] 4) Semi-continuous chlorination reaction,[298] 5) Heterogeneous continuous flow process presented herein.

Our group recently transposed batch conditions for activated aromatics (toluene, anisole) to gas phase semi-continuous flow operations for the chlorination of activated and deactivated

[293] a) Tsubogo, T.; Oyamada, H.; Kobayashi, S. *Nature* **2015**, *520*, 329. b) Gemoets, H. P. L.; Su, Y.; Shang, M.; Hessel, V.; Luque, R.; Noël, T. *Chem. Soc. Rev.* **2015**. c) Gutmann, B.; Cantillo, D.; Kappe, C. O. *Angew. Chem. Int. Ed.* **2015**, *54*, 6688. d) Jumde, R. P.; Evangelisti, C.; Mandoli, A.; Scotti, N.; Psaro, R. *J. Catal.* **2015**, *324*, 25.
[294] Degnan Jr., T.F. *Top. Catal*. **2000**, *3,* 349.
[295] a) Weitkamp, J. *Solid State Ionics,* **2000***, 131,* 175. b) Chen, N.Y.; Garwood, W.E.; Dwyer, F.G. *Shape Selective Catalysis in Industrial Applications* **1989**, pp. 203–204. Marcel Dekker, New York, Basel,
[296] a) Jacobs, P. A.; Dusselier, M.; Sels, B. F. *Angew. Chem., Int. Ed.* **2014**, *53*, 8621. b) Dusselier, M.; Wouwe, P. Van; Dewaele, A.; Jacobs, P. A.; Sels, B. F. *Science* **2015**, *349*, 78–80.
[297] Smith, K.; El-Hiti, G. A. *Green Chem.* **2011**, *13*, 1579–1608.

arenes (toluene, chlorobenzene and nitrobenzene).[298] An interesting conclusion of this work was the correlation between the zeolite pore topologies and their ability to convert variously substituted aromatics. Indeed, an optimal activity for the following couples has been reported: H-USY - nitrobenzene, H-ZSM-5 - chlorobenzene and H-ZSM-5 - toluene.[298] Although this process already avoids the use of toxic or volatile solvents and gaseous chlorine, we have to state the remaining downsides consisting in a generally low productivity and relatively high reaction temperatures. Furthermore, the sole fact that the operation was in a semi-continuous mode further hampers the process viability. Nevertheless, these pioneering studies are pointing towards the way to design a truly eco-compatible and competitive halogenation process (**Figure 4-24**, step 5).

In the present work, we report the screening of heterogeneous catalysts for converting iodobenzene into monochlorinated chloroiodobenzenes using trichloroisocyanuric acid (TCCA) as chlorination agent. This reaction was chosen as a benchmark reaction for the optimisation of reaction conditions. Nevertheless, its intrinsic interest is not negligible, because chloroiodobenzenes (High value added chemicals cf. **Table 4-14**) are used in polymer chemistry,[299] and in stepwise C-C coupling reactions.[300] However, the latter molecules are still produced with gaseous chlorine over $AlCl_3$, $FeCl_3$ or $SbCl_5$ catalysts.[301,302] Then, once optimised conditions could be set up towards an eco-compatible halogenation of variously substituted arenes in a batch reactor. Ultimately, we report a transposition attempt to develop a continuous flow liquid-solid process.

4.4.2. From the first Results to the Optimisation

Commercial catalysts were evaluated in the benchmark chlorination reaction of iodobenzene in order to find an optimal heterogeneous catalyst. Those catalysts are characterised in Table 1 (general screening).

In the general screening, various acid site densities, pore sizes and topologies as well as crystal sizes were compared (**Table 4-8**). *BEA zeolite (entry 11, **Table 4-9**) appeared as the most promising candidate, leading to a 71% iodobenzene conversion and extremely high 97%

[298] a) Boltz, M.; Mattos, M. C. S. De; Esteves, P. M.; Pale, P.; Louis, B. *Appl. Catal. A, Gen.* **2012**, *449*, 1. b) Boltz, M.; Losch, P.; Louis, B.; Rioland, G.; Tzanis, L.; Daou, T. J. *RSC Adv.* **2014**, *4*, 27242. c) Daou, T. J.; Boltz, M.; Tzanis, L.; Michelin, L.; Louis, B. *Catal. Commun.* **2013**, *39*, 10. d) Losch, P.; Pascual, A. M.; Boltz, M.; Ivanova, S.; Louis, B.; Montilla, F.; Odriozola, J. A. *Comptes Rendus Chim.* **2015**, *18*, 324. e) Mendonça, G. F.; Bastos, A. R.; Boltz, M.; Louis, B.; Pale, P.; Esteves, P. M.; de Mattos, M. C. S. *Appl. Catal. A Gen.* **2013**, *460-461*, 46.

[299] Kuran, W. *Coordination Polycondensation, in Principles of Coordination Polymerisation: Heterogeneous and Homogeneous Catalysis in Polymer Chemistry - Polymerisation of Hydrocarbon, Heterocyclic and Heterounsaturated Monomers*, John Wiley & Sons, Ltd, Chichester, UK. **2002**.

[300] Miyaura, N.; Suzuki, A. *Chem. Rev.* **1995**, *95,* 2457.

[301] Singh, A.P.; Kumar, S. B. *Catal. Lett.* **1994,** *27,* 171.

[302] Singh, A.P.; Kumar, S. B. *Appl. Catal. A* **1995**, *126,* 27.

selectivity in monochlorination products. Therefore, as it will be presented below, different kinds of *BEA zeolites were prepared and compared for this reaction.

Table 4-8. Characterisation of the different commercially available solid acid catalysts.

Entry	Catalyst	Si/Al	n(H^+) [mmol(H^+).g_{cat}^{-1}][a]	S_{BET} [$m^2.g^{-1}$]	Pore size [Å]	Crystal size [nm]
1	ZSM-5 (Zeolyst CBV2314)	13	1.48	425	5.5	< 100
2	ZSM-5 (Zeolyst CBV5524)	25	0.86	425	5.5	< 100
3	MOR (Zeolyst)	10	1.90	550	7	1000 - 1500
4	USY (Zeolyst)	3.6	3.80	750	12	500-700
5	Y (Aldrich)	2.2	5.37	710	12	500-800
6	EMT (UOP)	6.5	2.38	631	12	2000
7	$Cs_2HPW_{12}O_{40}$	-	0.32	123	-	1000-2000
8	*BEA (Zeochem)	14	1.07	620	6[b]	100 - 400

a: Acid site densities are obtained by H/D-isotope exchange.
b: Precise pore dimensions for *BEA micropores: 6.6 x 6.7 and 5.6 x 5.6 Å.

Table 4-9. Screening of the catalysts. Data obtained after 1h of reaction at 80°C.

Entry	Catalyst	Conversion [%]	S(Mono-chlorinated products) [%]	S(*para*-product) [%]	S(*ortho*-product) [%]
1	-	2	0	0	0
2	$AlCl_3$	28	84	46	38
3	H_2SO_4	80	88	44	44
4	H-ZSM-5 (13)	20	68	42	26
5	H-ZSM-5 (25)	11	71	53	18
6	H-MOR (Zeolyst)	21	89	50	39
7	H-USY (Zeolyst)	72	92	49	43
8	H-Y (Aldrich)	66	92	52	40
9	H-EMT (UOP)	49	86	49	37
10	$Cs_2HPW_{12}O_{40}$	4	84	45	39
11	H-*BEA (Zeochem)	71	97	58	39

Reaction conditions: 1 mmol iodobenzene, 0.33 mmol TCCA, 100 mg zeolite at 80°C, 1h, 5 mL DCE. Conversions were calculated based on the disappearance of the reactant. Selectivities are determined after corresponding calibration.

It is worthy to mention that in the absence of catalyst almost no reaction occurred (entry 1). In contrast, homogeneous Lewis and Brønsted acids led to medium and high iodobenzene conversions (entries 2-3). Especially, sulphuric acid efficiently catalysed this chlorination reaction (80% conversion with a 88% selectivity). This result is in agreement with earlier studies.[290,291] However, no special regioselectivity can be observed as a 1 to 1 *ortho*- *para*-chloroiodobenzene mixture was produced (entry 3). This result corresponds to the thermodynamical product distribution in the absence of any zeolite related shape selectivity. Brønsted solid acids led to significant variations in conversions and selectivities, which is obviously linked to their intrinsic properties: acid site density, pore topology, crystal size and specific surface area (entries 4-9).

$Cs_2HPW_{12}O_{40}$ heteropolyacid with a high S_{BET} of 123 $m^2.g^{-1}$ remains almost inactive (entry 10) indicating that a dispersed Brønsted acidity is not sufficient to perform the halogenation. Medium-pore sized ZSM-5 zeolites led to conversions in the 11-20% range, proportional to the acid site density. Interestingly, the selectivity in monochlorination products

seems to be independent from the conversion. Larger pore zeolites (entries 7-9) allowed to achieve higher conversions, *i.e.;* 72, 66 and 49 % for H-USY, H-Y and H-EMT, respectively. These results are in agreement with former studies which highlighted a better performance of USY and EMT zeolites for nitrobenzene chlorination.[298a,c,e] Surprisingly, only 21% conversion could be achieved over H-MOR which may also indicate a fast deactivation in 1D zeolite pores (entry 6).

Interestingly, the highest selectivity towards targeted products was achieved over commercial *BEA zeolite. This interesting result led us to focus on series of rationally designed *BEA zeolites (**Table 4-10**). According to the characterisation studies, those data show that the three different zeolites obtained exhibit similar Si/Al ratios but significantly differ in crystal size. Consequently, major differences are observed in terms of textural properties: external surface areas (S_{BET} ranging from 560 to 977 $m^2.g^{-1}$ in entries 1 and 4 in **Table 4-10**), porosities, which may *a priori* impact the diffusion of the reactants and products throughout the zeolite frame.

Table 4-10. Characterisation of *BEA zeolites.

Entry	Catalyst	Si/Al Global[a]	Si/Al Framework[b]	n(H^+) [mmol(H^+).g_{cat}^{-1}][c]		S_{BET} [$m^2.g^{-1}$]	V_μ [$cm^3.g^{-1}$]	V_{meso} [$cm^3.g^{-1}$]	Crystal size [nm]
				Brønsted	Lewis				
1	*BEA	13	-	0.50[d]	0.51[d]	560[d]	0.24[d]	-	100-400
2	*BEA NC	15	23	0.44	0.34	726	0.24	0.71	40
3	*BEA MC	14	23	0.62	0.11	626	0.23	0.05	5000
4	*BEA NS	17	22	0.13	0.18	977	0.30	0.74	< 50

a: measured by XRF.
b: drawn from T-O-T band at 1080-1200 cm^{-1} using the correlation given in [303].
c: Acid sites determined by integrating and normalizing Py-absorption bands at 1540 and 1455 cm^{-1}.
d: Values taken from[304].

It is important to note that the commercial zeolite *BEA is very similar to the **NC** sample which will be confirmed below by the characterisation but as well in the catalytic behaviour. As-prepared *BEA zeolites: micro-crystal (**MC**), nano-crystal (**NC**) and nano-sponge (**NS**) samples were thoroughly characterised by XRD, XRF, N_2 adsorption, SEM, TEM and FTIR. Their main features are summarised in **Figure 4-25** and **Table 4-10**. Additional characterisation of these materials can be found in the recent study dealing with their use in the ethanol-to-hydrocarbons reaction.[305]

SEM images for the three samples are given in Fig.4. SEM micrograph of **MC** crystals prepared in the presence of TEAOH exhibits the characteristic truncated bipyramidal shape of beta zeolite with crystal sizes ranging from 6 to 10 μm.[306] Pseudo-spherical crystals with an

[303] Coutanceau, C.; da Silva, J. M.; Alvarez, M. F.; Ribeiro, F. R.; Guisnet, M. *J. Chim. Phys.* **1997,** *94,* 765.
[304] Sad, M. E.; Padró, C. L.; Apesteguía, C. R. *Appl. Catal. A Gen.* **2008**, *342*, 40–48.
[305] Astafan, A.; Benghalem, M. A.; Pouilloux, Y.; Patarin, J.; Bats, N.; Bouchy, C.; Daou, T. J.; Pinard, L. *J. Catal.* **2016**, *336*, 1.
[306] Larlus, O.; Valtchev, V. *Microporous Mesoporous Mater.* **2006**, *93,* 55.

average size of 40 nm are observed for the **NC** sample. *BEA NS sample, synthesised from a poly-quaternary ammonium surfactant ($N_{4\text{-phe}}$), exhibits a sponge-like morphology with nano-sized zeolite particles (**Figure 4-25c**). TEM micrographs demonstrated a somewhat ordered inter-crystallite mesoporosity for **NS** sample as compared to the **NC** sample.[305]

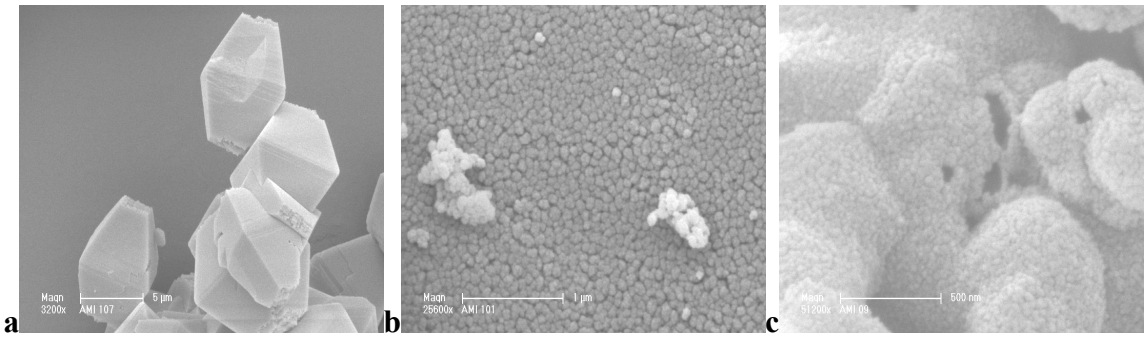

Figure 4-25. SEM micrographs of different *BEA zeolites a) **MC**, b) **NC** and c) **NS**.

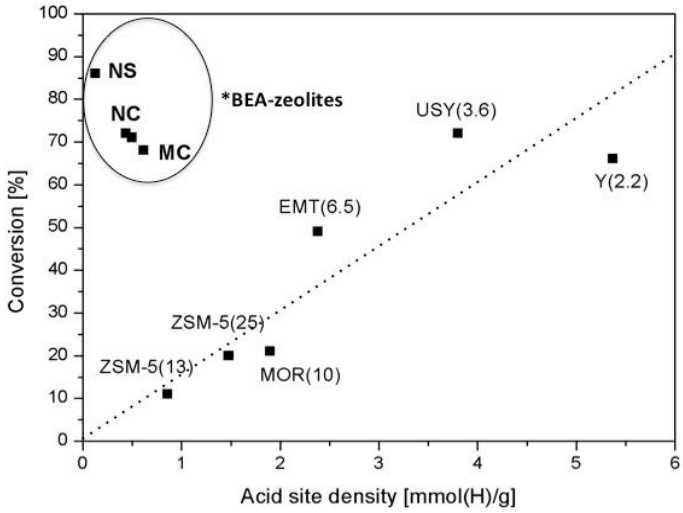

Figure 4-26. The conversion of the benchmark reaction seems to be related to the acid site density, except for the different *BEA-zeolites.

Figure 4-26 presents the conversion of iodobenzene, which seems to be related to the acid site density, except for the investigated *BEA-zeolites. Indeed, the *BEA framework topology may provide a peculiar spatial arrangment, where an optimum can be found. Indeed, this seems to be achieved between a molecular diffusion inside the porous network and the acid site density.

As the studied reaction is an electrophilic aromatic substitution analogous to Friedel Crafts acylations, for which *BEA zeolites are reportedly very competitive catalysts, [307] it is reasonable to observe a correlation between the solid catalyst acid site density and the conversion. However, and quite surprisingly, *BEA zeolites exhibit a peculiar behaviour with a high conversion despite a low acid site density.

[307] Sartori, G.; Maggi, R. *Chem. Rev.* **2006**, *106,* 1077.

When looking at the *o*/*p*-ratio as a function of the zeolite crystal sizes (**Figure 4-27**), it turns out that sizes play a key role. Indeed, small crystal sizes and medium sized pores favor the production of para-substituted aromatics, while large crystal and pore sizes lead to the production of the thermodynamically favored 1/1 *p*/*o*-mixture. This is also true for the *BEA zeolites investigated. Such effect could be due to residence times, the longer favoring equilibration, as well as the pore size, the largest allowing to accommodate the largest compound, i.e. the ortho-product.

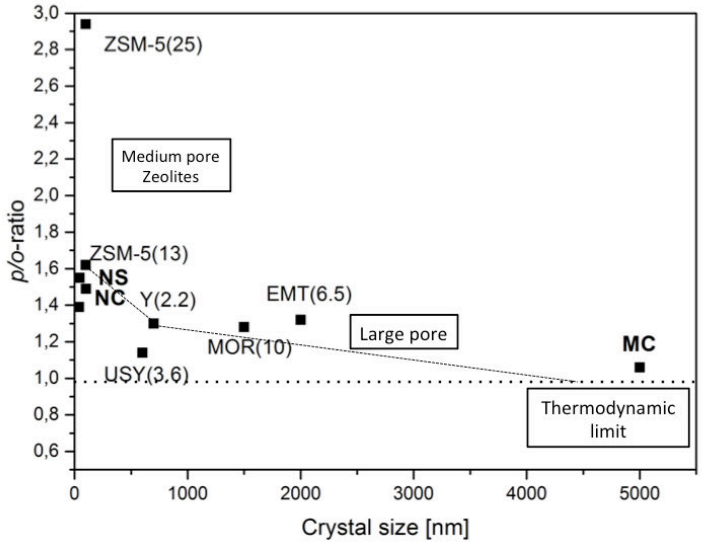

Figure 4-27. The *p*/*o*-ratio as a function of the crystal size, large crystals exhibit long residence times which favour the production of thermodynamically favoured 1/1 *p*/*o*-mixture.

Nevertheless, *BEA zeolites offer a specific behaviour, which can be due to their framework topology. *BEA zeolite displays two types of 12 membered-ring channels having 0.66 x 0.67 and 0.56 x 0.56 nm, respectively. As shown in Chapter 3, molecular diffusion can exhibit an optimum related to the porous network and the acid site density. Indeed, iodobenzene exhibits a C_{2v} symmetry with a C-I bond length of 0.21 nm,[308] while the size of the aromatic ring (~ 0.5 nm) fits well in the [001] channels (0.56 nm). Furthermore, a non-flat diffusion is also possible at the channel intersections or in the ~ 0.7 nm-sized [100] channels.

Similar spatial confinement has already been reported for bromination reactions in single-wall carbon nanotubes having a diameter of 0.7 nm.[309]

[308] Brunvoll, J.; Samdal, S.; Thomassen, H.; Vilkov, LV.; Volden, H.V. *Acta Chem. Scand.* **1990,** *44,* 23-30.
[309] Miners, S.A.; Rance, G.A.; Khlobystov, A.N. *Chem. Commun.* **2013**, *49*, 5586

Table 4-11. Catalytic data collected for *BEA-zeolites in the chlorination of iodobenzene.

Entry	Catalyst	Conversion [%]	S(mono-chlorination) [%]	S(*para*) [%]	S(*ortho*) [%]	TOF [$mol_{PhI\ conv.}$.(mol (H^+).h)$^{-1}$][a]
1	H-*BEA	71	98	58	39	15.2
2	H-*BEA MC	72	97	50	47	11.6
3	H-*BEA NC	68	98	57	41	15.5
4	H-*BEA NS	86	97	59	38	66.2

Reaction conditions: 1 mmol iodobenzene, 0.33 mmol TCCA, 100 mg zeolite at 80°C, 1h, 5 mL DCE. Conversions were calculated based on the disappearance of the reactant. Selectivities were determined after corresponding calibration. a: TOF were calculated after 60 min of reaction.

Table 4-11 shows the performances of these different *BEA zeolites. The design of *BEA zeolites is indeed possible since one can observe an improvement in conversion after 60 min reaction time (from 68 up to 86%). Likewise, a strong impact on TOF values could be evidenced *i.e.;* up to 9 times higher over the nanosponge beta zeolite compared with the commercial zeolite. The general trend for these TOF values is the following: *BEA **NS** > **NC** = commercial *BEA > **MC** (**Table 4-11**) which is a sound indication of a positive impact of hierarchical ordered porosity on the catalytic properties of *BEA zeolites. This is supported by the fact that *BEA NC and NS zeolites exhibit high external S_{BET} values with respect to *BEA MC sample.

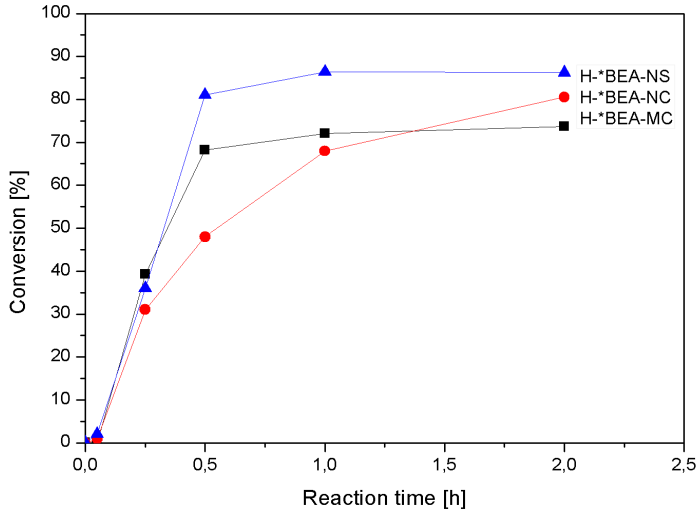

Figure 4-28. Reaction profile versus time of the batch chlorination of iodobenzene over different as-synthesised *BEA zeolites.

The change in crystal sizes further impacted the catalyst activity (**Figure 4-28**), where a conversion limit of about 70% was achieved over MC sample, whereas nanosized samples further converted iodobenzene suggesting that mass transfer limitations could hamper the reaction paths in *BEA MC zeolite and favour deactivation due to pore blocking.

After studying these different beta zeolites and evidencing the huge potential of tailor-made zeolites for improvement in this reaction if used at larger scale, our main goal now was to optimise the catalytic reaction in order to set-up an eco-compatible process. Based on the results

and characterisation data, it is worthy to try to propose a "greener" halogenation process. In the following part, the cheapest (commercial zeolite) was chosen for an optimisation of the reaction conditions: solvent, scope of the reaction and lastly the development of a continuous process.

A solvent screening, from apolar aprotic to polar and protic, was undertaken taking into account GSK's expanded solvent selection guide.[310, 311] Interestingly, acetic acid a sustainable and non-toxic solvent has proven to be the most promising for the reaction (**Table 4-12**). Indeed, it allows gaining in catalytic activity while a very high selectivity towards monochlorinated products could be maintained. As a weak Brønsted acid, acetic acid alone did not catalyse the reaction in the absence of a strong heterogeneous Brønsted acid (entry 9, **Table 4-12**). Several other interesting trends could be drawn from this solvent screening. The reaction seems to perform better in protic polar solvents. In the case of toluene (entry 4), the aromatic solvent was chlorinated, while iodobenzene suffered from halogen exchange forming chlorobenzene. The same phenomenon also occurred in 2-propanol and ethyl acetate (entries 4-7). A further set of experiments carried out at room temperature with different carboxylic acids (CF_3COOH, HCOOH and CH_3COOH entries 11-13) underlines the link between the solvents pK_a and the activity of the considered solvent-catalyst system. Interestingly, at stronger acidities the reactions seems to be catalysed by the solvent itself since the *p*/*o*-ratio changes from 1.9 to 1.4 to 1 when comparing acetic acid to formic acid and to trifluoroacetic acid, respectively.

While chlorination reactions of aromatics with chlorine gas in apolar aprotic solvents tend to involve radicals, in acetic acid with a Brønsted acid catalyst the ionic pathway is more plausible (**Figure 4-30**). Depending on the solvent and the zeolite used, we observed an undesired reaction leading to the formation of chlorobenzene (up to 10% in selectivity). The earlier mentioned side reaction of the halogen exchange may occur through the intermediate formation of iodobenzenedichloride, which subsequently decomposes in contact with a zeolite to form chlorobenzene or *ortho*-substituted chloroiodobenzene. Several tests have been performed to support this tentative explanation:

[310] Henderson, R. K.; Jiménez-González, C.; Constable, D. J. C.; Alston, S. R.; Inglis, G. G. a.; Fisher, G.; Sherwood, J.; Binks, S. P.; Curzons, A. D. *Green Chem.* **2011**, *13*, 854.
[311] a) Phadtare, S.B.; Shankarling, G.S. *Green Chem.* **2010**, *12,* 458. b) Prat, D.; Wells, A.; Hayler, J.; Sneddon, H.; McElroy, C. R.; Abou-Shehada, S.; Dunn, P.J. *Green Chem.* **2016**, **18,** 288.

Table 4-12. Screening of solvents for the iodobenzene chlorination reaction.

Entry	Solvent (pK_a)	Conversion [%]	S(Mono-chlorinated products) [%]	S(*para*-product) [%]	S(*ortho*-product) [%]
1	1,2-DCE	48	98	58	38
2	DMF	0	0	0	0
3	MeCN	84	93	45	48
4[a,b]	Toluene	44	0	0	0
5[b]	H_2O (15.7)	85	71	39	31
6[b]	2-propanol (16.5)	43	23	15	7
7[b]	AcOEt	56	54	25	28
8	-	49	97	51	47
9	**AcOH**	**100**	**83**	**47**	**36**
10[c]	AcOH	48	9	4	3
11[d]	TFAOH (0.23)	99	92	43	45
12[d]	HCOOH (3.77)	96	91	53	38
13[d]	AcOH (4.76)	68	96	63	34

Reaction conditions: 1 mmol iodobenzene, 0.33 mmol TCCA, 100 mg H-*BEA corresponding to 0.05 mmol H^+ (5 mol-%) at 80°C, 30 min, 5 mL solvent. Conversions were calculated based on the disappearance of the reactant. Selectivities are determined after corresponding calibration (Fig. S2).
a: Toluene in excess as compared to iodobenzene is chlorinated, iodobenze degradates.
b: Low monochlorination selectivities are due to both iodobenzene degradation for instance to form chlorobenzene or di-/tri-chlorination.
c: Blank experiment without H-*BEA.
d: Same reaction conditions than in entry 9, but to compare the different carboxylic acids these tests have been carried out at room temperature 25°C in order to evidence a link between the pKa of the solvent and the solvent-catalyst activity.

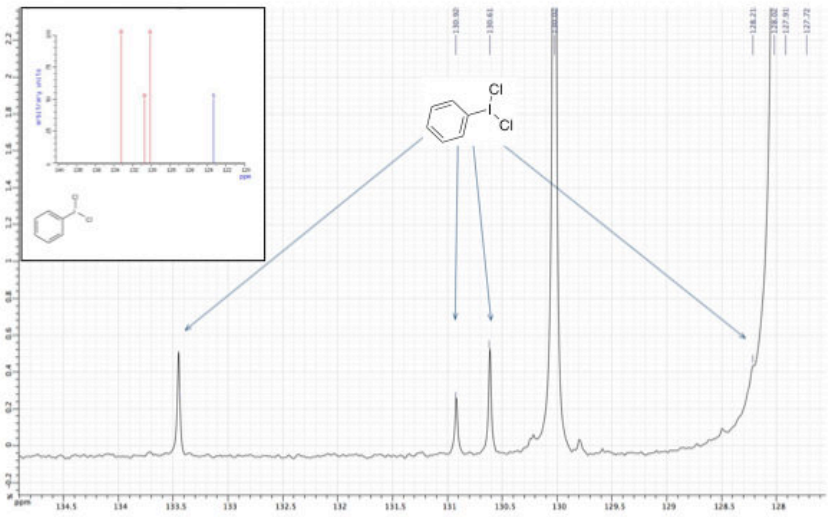

Figure 4-29. ^{13}C-NMR spectrum of $PhICl_2$ in PhI in d_6-benzene. Zoom for the characteristic $PhICl_2$ peaks. With the inset corresponding to reported ^{13}C-NMR for $PhICl_2$.[312]

When iodobenzene was in contact with TCCA with or without zeolite, we were able to detect iodobenzenedichloride by ^{13}C-NMR (**Figure 4-29**). In addition, a yellow colouration of the reaction mixture could be observed suggesting the presence of $PhICl_2$ and ICl. In the case of zeolite-catalysed reaction, chlorobenzene could be detected by gas chromatography. In contrast, for the chlorination of bromobenzene, which is known to do not form bromobenzenedichloride

[312] Wiley subscription services, Inc. (US).

intermediates, the halogen exchange reaction, thus the formation of chlorobenzene could not be observed. Furthermore no colouration of the reaction mixture could be observed.

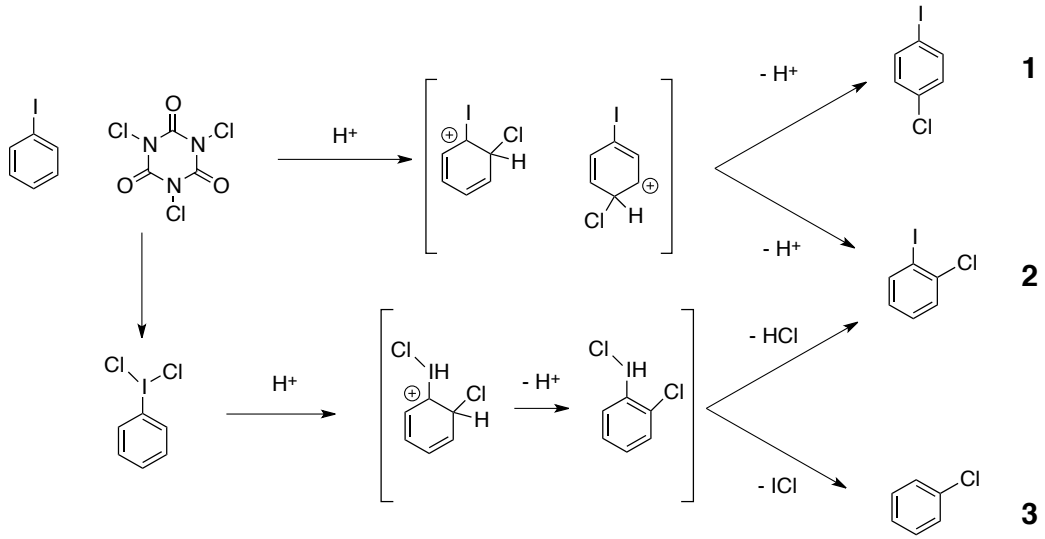

Figure 4-30. Proposed reaction mechanism leading to the observed by-products distribution

After finding optimal reaction conditions for our benchmark reaction, we steered our focus on the extension of the reaction scope. Variously substituted aromatics were submitted to those optimal conditions. For comparison, several other halogenating agents were also investigated (**Table 4-13**). With TCCA, the monochlorination was achieved for all arenes, except for the strongly deactivated nitrobenzene (entry 6). As *'a priori'* expected, a classical trend was observed with the more electron-rich aromatics leading to higher conversions (entries 5, 8 and 9). The unfunctionalised and cheapest aromatic benzene was quite successfully converted to the corresponding iodo-, bromo- or chlorobenzenes (entries 1, 12 and 13). It is of utmost importance to note that these compounds could be obtained very selectively (91-100%) in their mono-halogenated forms and that non converted aromatics may be re-cycled in a continuous flow set up at a larger scale. Rewardingly, the cheaper TCCA is a better chlorinating agent both in terms of activity and selectivity than NCS (entries 1 vs 10 and 5 vs 9). With NBS or NIS as brominating or iodinating agent, the reaction also proceeds at room temperature, but with low to modest conversion (entries 11-15).

Table 4-13. Scope of H-*BEA-catalysed chlorination reaction.

Entry	Reactant 	T [°C}	Halogenating reactant (eqiv.)	Conversion [%]	S(Mono-chlorinated products) [%]	S(*para*-product) [%]	S(*ortho*-product) [%]
1	R= H	80	TCCA (0.33)	44	91	-	-
2	R = Me	80	TCCA (0.33)	66	98	73	25
3	R = Cl	80	TCCA (0.33)	38	100	58	40
4	R = Br	80	TCCA (0.33)	48	100	52	48
5	R = I	80	TCCA (0.33)	100	83	59	39
6	R = NO_2	120	TCCA (0.33)	< 5	100	-	-
7	R = NH_2	80	TCCA (0.33)	61	84	37	59
8	R = OMe	80	TCCA (0.33)	89	100	79	21
9	R = I	80	NCS (1)	56	80	45	35
10	R = H	80	NCS (1)	26	2	-	-
11	R = H	20	NBS (1)	18	100	-	-
12	R = H	80	NBS (1)	40	76	-	-
13	R = H	20	NIS (1)	37	100	-	-
14	R = H	80	NIS (1)	86	89	-	-
15	R = H	20	I_2 (1)	< 5	100	-	-
16	R = H	20	I_2 (1) + TCCA (0.33)	< 5	-	-	-

Reaction conditions: 1 mmol aromatic, 1 equiv. Halogen, 100 mg H-*BEA corresponding to 0.05 mmol H^+ (5 mol-%) at 80°C, 30 min, 5 mL acetic acid. Conversions were calculated based on the disappearance of the reactant. Selectivities are determined after corresponding calibration.

Unfortunately, at higher temperatures the high selectivity towards monohalogenated products decreases (entries 11 vs. 12 and 13 vs. 14), when compared to reactions carried out at room temperature. The reaction with molecular iodine did not lead to significant degree of conversion (entry 15). In further iodination experiments with molecular iodine, entry 16 proved that TCCA a polarizing agent is not improving the conversion or the selectivity.

For large-scale applications, selectivity plays a crucial role whereas conversion limitations can be overcome by recycling unconverted reactant. This is of special interest when applied in a flow process. Therefore, we performed a recyclability test for our system: commercial *BEA zeolite exhibited a limited loss in activity after 10 reaction cycles, whereas *BEA NS zeolite deactivated much faster (**Figure 4-31a**). This might be due to its higher specific surface area, thus adsorbing more water or other detrimental molecules, which cannot be removed between consecutive runs. In addition, the short crystal thickness of *BEA NS zeolite, combined with its low acidity, may limit the growth of coke molecules as well as their accumulation inside micropores. In other reactions, however, in the ethanol-to-gasoline process for instance, the extreme downsizing of zeolite crystal led to an unexpected pore blocking.[305]

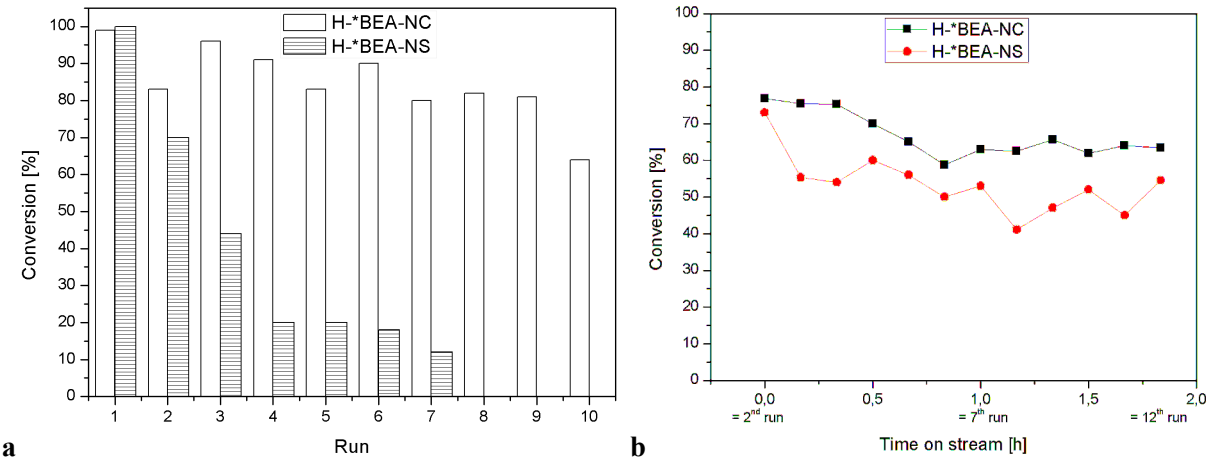

Figure 4-31. a) Recycling experiment with commercial *BEA-zeolite: 30 min of reaction. recycling with *BEA-NS-zeolite: 30 min of reaction and b) continuous flow chlorination of iodobenzene corresponding to 12 runs under batch conditions.

It is noteworthy that, after calcination the activity as well as the selectivity could be completely re-established for both catalysts, reinforcing the earlier mentioned hypothesis for deactivation.

Lastly, both promising nano-sized *BEA zeolites were applied to a continuous flow set-up (**Figure 4-31b**). Although *BEA-NS seems to deactivate more rapidly in consecutive batch reactions, it is tolerant and resistant to the flow set-up. Indeed, no different behaviour compared to the *BEA-NC sample could be noticed. The parameters of the continuous flow process were set to feed the same iodobenzene quantity found after 12 consecutive runs under batch conditions. A molar hourly space velocity of 61 mmol(arene).(g(catalyst).h)$^{-1}$ was applied for this optimised reaction. Compared with our early semi-continuous gas-solid set-up exhibiting a molar hourly space velocity 1.7 mmol(arene).(g(catalyst).h)$^{-1}$,[298b] this new continuous liquid-solid process can produce more than 30 times faster a desired halogenated arene. Interestingly, both zeolites seem more resistant toward deactivation under flow operations. Under these conditions, 100 kg iodobenzene may be converted per kg_{cat} in a single day.

Finally, a dependence between the solid acid pore structure, more precisely *BEA textural properties, and activity / selectivity in chlorination reaction could be established. Further studies are under progress to design a cost efficient flow process. Using PFG-NMR as seen in chapter 3 it will also be possible to extract exact diffusion coefficients for different molecules, hence to determine Thiele moduli (ϕ) and Thiele-Weisz-Wagner-Wheeler degrees of utilization (ψ)

4.4.3. Potential Impact and Outlook

Eco-compatible iodobenzene halogenation reaction by trichloroisocyanuric acid has been developed, which allowed a conversion superior to 95%, with nearly 100 kg iodobenzene converted per kg_{cat} in a single day.

H-*BEA zeolites were found the most performant catalysts among several solid acids and zeolite structures. According to thorough characterisation (microscopy, H/D exchange, BET, XRD), structure-activity relationships could be established for various synthetic *BEA zeolites. Nano-sized *BEA zeolites and more specifically nanosponge-like *BEA crystals exhibited the highest catalytic performances with a conversion up to 100%, corresponding to TOF values of 66 h^{-1} and a selectivity in monochlorinated products up to 98 %.

The main outcome of this study relies on the ability to set-up an eco-compatible continuous flow halogenation process catalysed by zeolites (**Figure 4-32**).

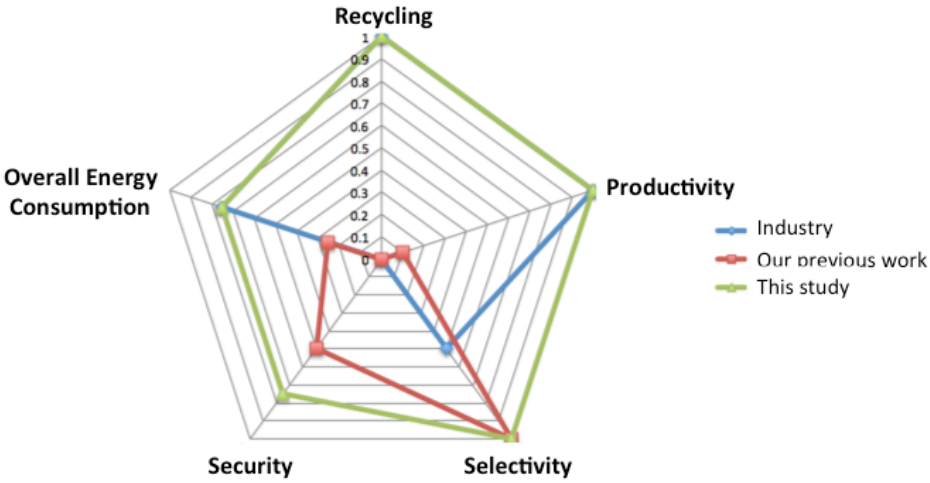

Figure 4-32. Simplified life cycle assessment (LCA) comparing the current industrial processes284 to our previous work[298] and to the present study. Normalised relative values were estimated using our results and available data.

Table 4-14 list the standardised prices per kg of the herein treated and produced products. It seems obvious that the developed continuous flow zeolite *BEA-catalysed halogenation of aromatics represents a huge valorisation in renewable carbon chemistry and is therefore a discrete part of the circular carbon economy.

Table 4-14. Normalised prices for considered chemicals in this study.

Molecule	Price [€.$kg_{product}^{-1}$]	Role
Benzene	80	Starting material from petrochemistry
TCCA	80	Very cheap chlorinating agent: 1/3 eq. needed
Chlorobenzene	120	Value added chemical
1,4-dichlorobenzene	90	Undesired by-product
Bromobenzene	70	Very cheap
2-Chlorobromobenzene	1040	High value added chemical
4-Chlorobromobenzene	400	Value added chemical
Iodobenzene	640	Value added chemical
2-Chloroiodobenzene	3660	High value added chemical
4-Chloroiodobenzene	1600	High value added chemical

4.5. Carbonylation Reactions for Molecular Upgrading with CO from HCOOH

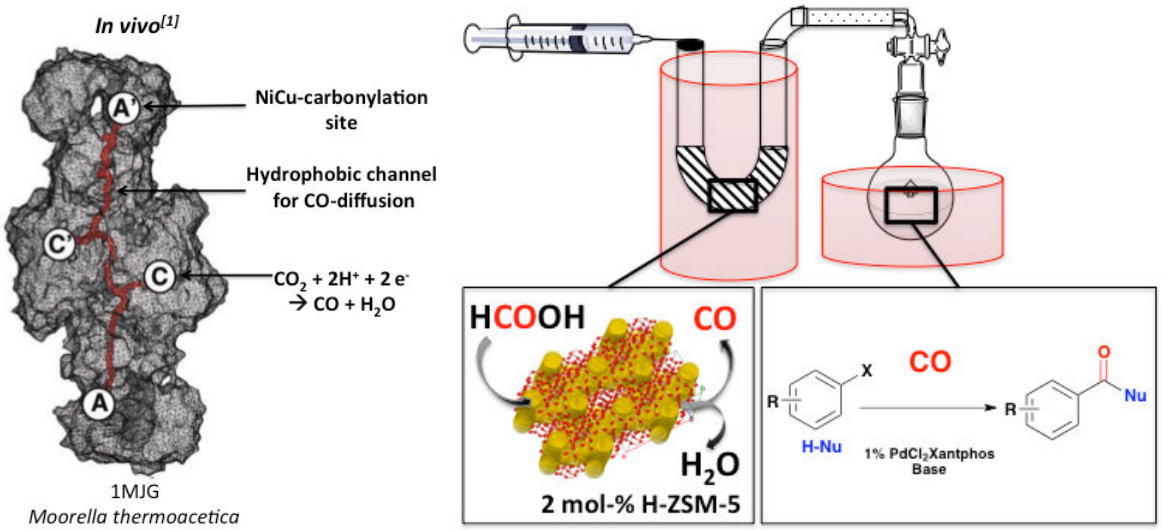

Figure 4-33. ***Sinister***: Inspiration: *Moorella thermoacetica*'s carbon monoxide dehydrogenase acetyl-CoA synthase, in which in a first active site water and CO are produced, the latter molecule is then transported via a hydrophobic channel to a second metal cluster active site where a carbonlative coupling reaction occurs to form acetyl-CoA.[313] ***Rectus***: Our system, in which in a first reactor dehydration of fromic acid occurs on relatively hydrophobic, but acidic zeolite H-ZSM-5 to release carbon monoxide, which is then safely guided to a second reactor containing a Pd-based catalyst where a carbonylative coupling reaction occurs.

4.5.1. The Challenge

The introduction of carbon monoxide onto organic molecules is an essential process, especially in industry,[314] allowing for convergent and rapid access to aldehydes, ketones, carboxylic acids and related compounds.[315] The most important carbonylation is the hydroformylation producing aldehydes from alkenes at scales of multi-million tons/year. Nevertheless, the most versatile and useful of these transformations are the palladium-catalysed carbonylation reactions, in which a variety of carbonylated products can be obtained by simply changing the nature of the nucleophile starting from the same substrate, often aryl halides or related species (**Figure 4-34**).[316] Therefore, various works have been reported dealing with the conception of safe CO-releasing molecules and/or systems targeting a safer and larger use of carbonylative coupling reactions.

[313] Doukov, T. I.; Iverson, T. M.; Seravalli, J.; Ragsdale, S. W.; Drennan, C. L. *Science* **2002**, *298*, 567–572.
[314] a) Kollar, L. *Modern Carbonylation Methods*,Wiley- VCH, Weinheim, **2008**. b) Beller, M. *Catalytic Carbonylation Reaction*,Springer-Verlag, Berlin, **2006**.
[315] a) Skoda-Foldes, R.; Kollar, L. *Curr. Org. Chem.* **2002**, *6*, 1097. b) Wu, X.-F.; Neumann, H.; Beller, M. *Chem. Rev.* **2013,** *113,* 1.
[316] Brennführer, M.; Neumann, H.; Beller, M. *Angew. Chem., Int. Ed.* **2009**, *48*, 4114.

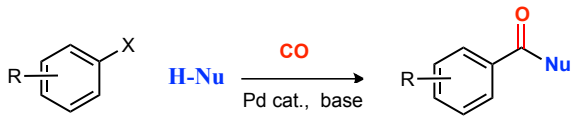

Figure 4-34. Palladium-catalysed carbonylation reaction.

Despite being metal catalysed, direct carbonylation requires harsh conditions, often with high pressure and temperature. This aspect, as well as safety issues associated with handling this toxic but odorless gas, renders this reaction less popular than it should be due to its importance in organic synthesis, especially in academic research. The search for mild and safe alternatives is thus a topic of current high interest.[317]

In this context, carbonylation methods have been developed for the *in situ* generation of CO from a variety of precursors. The most obvious precursors are metal carbonyls such as $Mo(CO)_6$ and $W(CO)_6$,[318] but aldehydes,[319] including formaldehyde, as well as formic acid,[320] formates[321] and formamides,[322] have also been used (**Figure 4-35**, paths A-B). However, these precursors, as well as the reagents required to generate CO, may not be compatible with the chemistry used to trap the liberated CO, especially in metal-catalysed reactions.

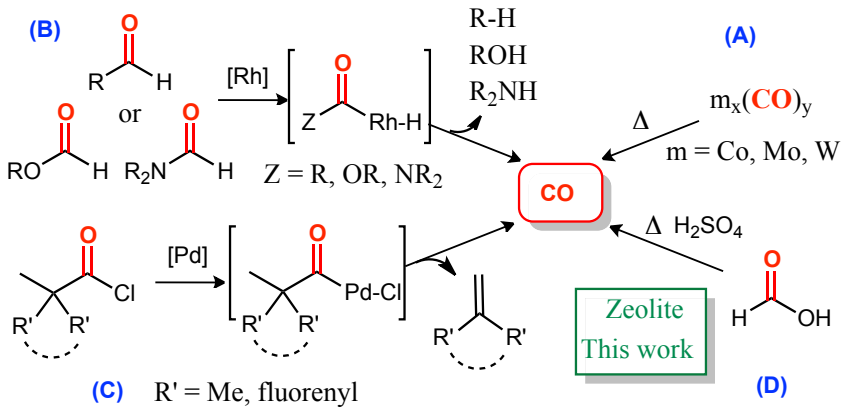

Figure 4-35. Overview of the reported methods for the *in* or *ex situ* generation of carbon monoxide, and the presently developed zeolite-promoted method.

[317] a) Morimoto, T.; Kakiuchi, K. *Angew. Chem., Int. Ed.* **2004**, *43*, 5580. b) Li, H.; Neumann, H.; Beller, M.; Wu, X.-F. *Angew. Chem., Int. Ed.* **2014**, *53*, 6310–6320.
[318] a) Yamazaki, K.; Kondo, K. *J. Comb. Chem.* **2004**, *6*, 121. b) Wieckowska, A.; Fransson, R.; Odell, L.R.; Larhed, M.; *J. Org. Chem.* **2011,** *76*, 978.
[319] a) Morimoto, T.; Fuji, K.; Tsutsumi, K.; Kakiuchi, K. *J. Am. Chem. Soc.* **2002,** *124*, 3806. b) Shibata, T.; Toshida, N.; Takagi, K. *Org. Lett.* **2002,** *4*, 1619.
[320] a) Simonato, J.-P.; Walter, T.; Motivier, P. *J. Mol. Catal. A* **2001**, *171*, 91. b) Mura, M.G.; Luca, L.D.; Giacomelli, G. Porcheddu, A. *Adv. Synth. Catal.* **2012,** *354*, 3180.
[321] Wan, Y.; Alterman, M.; Larhed, M.; Hallberg, A. *J. Org. Chem.* **2002**, *67*, 6232.
[322] Kondo, T.; Okada, T.; Mitsudo, T.-A. *Organometallics* **1999,** *18*, 4123.

To solve this problem, Skrydstrup and co-workers recently described an elegant and practical approach based on the *ex situ* generation of CO in a sealed two-chamber reactor.[323] In one chamber, a CO precursor decomposed and released CO, which was consumed in the other chamber during the carbonylation reaction. These authors developed specific precursors, the most efficient being 9-methylfluorene-9-carbonyl chloride in the presence of palladium (**Figure 4-35**, path C). However, precursors must be synthesised beforehand. Furthermore, all precursors eject a side product and are thus far from sustainable, although recovery and regeneration in two steps have been mentioned.[323e]

Therefore, a truly economical and safe carbonylation system is still highly sought. One of the simplest and cheapest precursors is formic acid and it is well known that in the presence of sulfuric acid and upon heating, CO can be liberated (**Figure 4-35**, path D).[324] This has elegantly been used together with the Skrydstrup reactor and with a tube-in-tube reactor, especially designed for flow chemistry[325] However, this reaction required corrosive pure sulfuric acid, usually in excess. Furthermore, the reaction could also give dihydrogen and carbon dioxide depending on the energy provided and the applied catalyst if any (**Figure 4-36**).[324]

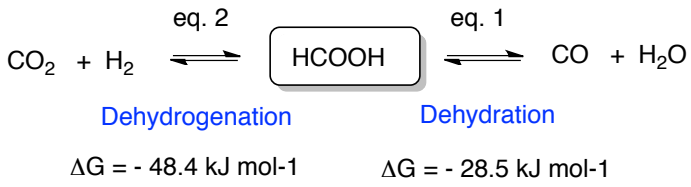

Figure 4-36. The thermal decomposition of formic acid (Morgan reaction).

On the other hand, acidic solids, especially zeolites, are well known as "green" and safe alternatives to strong and corrosive liquid acids.[326] It was thus tempting to use solid acids to produce CO from formic acid and to trap the gas formed in carbonylation reactions. In the present work, we took advantage of our expertise in zeolite-induced chemistry[327] to tune the exclusive formation of CO and to combine it with palladium-catalysed carbonylation reactions in a specifically designed but easy to set up and very cheap two-reactor system.

4.5.2. The Heterogenous Morgan Reaction

Various solid acids were examined for the thermal decomposition of formic acid (**Table 4-15**). Each solid (300 mg) was packed into a hermetically closed U-shaped glass tube placed in

[323] a) Korsager, S.; Nielsen, D. U.; Taaning, R. H.; Lindhardt, A. T.; Skrydstrup, T. *Chem. A Eur. J.* **2013**, *19*, 17687. b) Brancour, C.; Fukuyama, T.; Mukai, Y.; Skrydstrup, T.; Ryu, I. *Org. Lett.* **2013**, *15*, 2794. c) Friis, S.D.; Taaning, R.H.; Lindhardt, A.T.; Skrydstrup, T. *J. Am. Chem. Soc.* **2011**, *133*, 18114. d) Hermange, P.; Lindhardt, A.T.; Taaning, R.H.; Bjerglund, K.; Lupp, D.; Skrydstrup, T. *J. Am. Chem. Soc.* **2011**, *133*, 6061.
[324] a) Showalter, K.; Noyes, R.M. *J. Am. Chem. Soc.* **1978,** *100*, 1042. b) Morgan, J.S. *J. Chem. Soc.* **1916**, *109*, 274.
[325] Brancour, C.; Fukuyama, T.; Mukai, Y.; Skrydstrup, T.; Ryu, I. *Org. Lett.* **2013**, *15*, 2794.
[326] Fraissard, J.; Petrakis, L. *Acidity and Basicity of Solids* Vol. 444, Kluwer Publishers, **1994**.
[327] a) Kuhn, P.; Alix, A.; Kumarraja, M.; Louis, B.; Pale, P.; Sommer, J. *European J. Org. Chem.* **2009**, *2009*, 423–429. b) Louis, B.; Laugel, G.; Pale, P.; Pereira, M. M. *ChemCatChem* **2011**, *3*, 1263–1272.

an oil bath and the amount of CO liberated upon addition of formic acid (10 mmol) was measured by displacing a brine solution from a connected glass flask (**Figure 2-8**, line 1). A preliminary screening, combined with the well known reactivity of formic acid at high temperatures, revealed that the best temperature was 150 °C. At higher temperatures, mixtures of CO, CO_2 and H_2 might be produced (cf. **Figure 4-36**), whereas at lower temperatures, reaction rates were too low to be useful (entries 15-16).

Table 4-15. Heterogneous Morgan reaction over a selection of solid acids.

Entry	Solid acid	Acid site density [mmol(H^+).g^{-1}][b)]	Acid strength [kJ.mol^{-1}][c)]	CO volume [mL][d)]	Conversion [%][e)]	TOF [$mol_{HCOOHconv.}$.(mol(H^+).h)$^{-1}$]
1	-	-	-	5 [d]	0	0
2	SiO_2	0	-	0	0	0
3	amorphous silicoalumina	3.6	-	4	2	0.2
4	$H_6P_2W_{18}O_{62}$ .9 H_2O	0.9	-	43	18	8
5	$Cs_{2.2}H_{0.8}P_2W_{12}O_{40}$. 16 H_2O	0.3	-	23	10	13
6	H-Y	5.3	130	16	7	0.5
7	H-USY	3.2	180	35	15	1.9
8	H-MOR	1.9	165	35	15	2.4
9	H-BEA	1.1	135	15	6	1.4
10	H-ZSM-5 (13) [f]	1.5	140	33	14	3.7
11	H-ZSM-5 (25) [f]	0.8	150	118	49	25
12	H-ZSM-5 (40) [f]	0.5	160	105	44	35
13	H-ZSM-5 (100) [f]	0.2	160	18	8	16
14	H-A	1	95	4	2	0.8
15	H-ZSM-5 (25) [g]	0.8	150	0	0	0
16	H-ZSM-5 (25) [h]	0.8	150	183	76	39

a: Conditions: 300 mg solid acid at 150 °C, 10 mmol formic acid injected over 15 min
b: Acid site densities were estimated using a reported H/D-isotope exchange technique; [328]
c: acid strengths taken from the literature for well-characterised commercial zeolites;[329]
d: *except for entry 1, the thermal expansion due to HCOOH injection (5 ml in entry 1 has been susbstracted from all volumes given;*
e: calculated from $\text{Conversion} = \frac{n(CO)}{n(HCOOH)} * 100$ with $n(CO) = \frac{R*T}{p*V(CO)}$;
f: the numbers correspond to the Si/Al ratio of the corresponding zeolites;
g: performed at 120 °C;
h: performed at 170 °C;
Without acid, no transformation occurred, but a small volume was nevertheless measured corresponding to the thermal expansion due to the injected liquid (entry 1; NB: this expansion volume has been deduced systematically from the measured volumes in all other experiments).

Acid site density and strength within solid acids should be key factors in this dehydration reaction. [330] Therefore, we selected different types of solids, such as silica type solids, polyoxometalates (POMs) and zeolites. Within a series, solids of various acid densities and strengths were tested (entries 2-3, 4-5 and 6-14).

[328] Louis, B.; Walspurger, S.; Sommer, J. *Catal. Lett.* **2004**, *93*, 81–84.
[329] Auroux, A. *Top. Catal.* **2002**, *19*, 205.
[330] For a recent example: Rac, V.; Rakić, V.; Stošić, D.; Otman, O.; Auroux, A. *Microporous Mesoporous Mater.* **2014**, *194*, 126–134.

With silica and related amorphous materials, almost no CO was produced, no matter what the density of acid sites they exhibit (entries 2-3). Polyoxometalates of various acidities induced low CO production, corresponding to conversions lower than 20% (entries 4-5). Nevertheless and in a counter-intuitive way, conversion increased with decreasing acidity (entry 5 vs. 4).

A series of zeolites, exhibiting different characteristics in terms of acid site density, acid strength and porosity, was then evaluated (entries 6-14). The CO formation promoted by these materials was very different (entry 14 vs. 11) and sometimes was also counter-intuitive regarding acidity (e.g. entries 6-7, 10-11). Nevertheless and interestingly, the results showed some trends within three subsets of these zeolites (H-A, H-Y and H-USY; H-BEA and H-MOR; H-ZSM-5 with different Si/Al ratios) (**Figure 4-37**). For H-A, H-Y and H-USY, which exhibit comparable sodalite-type porosities but of different sizes, a higher acid strength of the H-USY led to the highest activity in this series (**Figure 4-37**, left), although the conversion remained low (entries 6, 7 and 14). With the channel-type zeolites H-BEA and H-MOR, a similar but clearer trend was observed with higher activity for the highest acid strength (entry 8 vs. 9 and **Figure 4-37**, middle). In sharp contrast, ZSM-5 zeolites having the same channel shape but with smaller pore sizes (~ 0.5 nm) clearly enhanced the production of CO, but only for certain acidities (entries 10-13). The CO formation was optimum for ZSM-5 having Si/Al ratios of 25 - 40, and the dehydration of formic acid was ten fold higher compared to those of ZSM-5 with lower Si/Al ratio. (entries 11-12 vs. 10 and **Figure 4-37**, right)

These results clearly demonstrated that Brønsted acidity was not the sole factor in this heterogeneous version of the Morgan reaction. High acid site density proved to be more harmful than beneficial, in contrast to what could be expected from the classical homogeneous conditions of the Morgan reaction (entries 3, 6 and 7 vs. entries 11-12). However, some relationship between CO production and acid site strength was observed, depending on zeolite porosities (**Figure 4-37**).

Microporosity was an important factor, with a clear optimum activity for channel-type pores that have the right size (~ 5 Å, ZSM-5, entries 10-13). With such zeolites, acidity played a key role, the lowest and the highest being harmful (entries 10 and 13 vs. 11-12). These results showed that the right combination of interdependent parameters, *i.e.* acid site density and strength, as well as pore size and shape, is required for achieving optimised reaction conditions.

The collected data suggested that relatively dispersed acidity of adequate strength within an appropriate framework represents the key balance for better CO production. For the decomposition of formic acid, the best fit was thus achieved for ZSM-5 having channels of 5.1 × 5.5 and 5.3 × 5.6 Å with a Si/Al ratio of 25. This best solid acid gave a ~ 50 % conversion of formic acid to CO in 15 min.

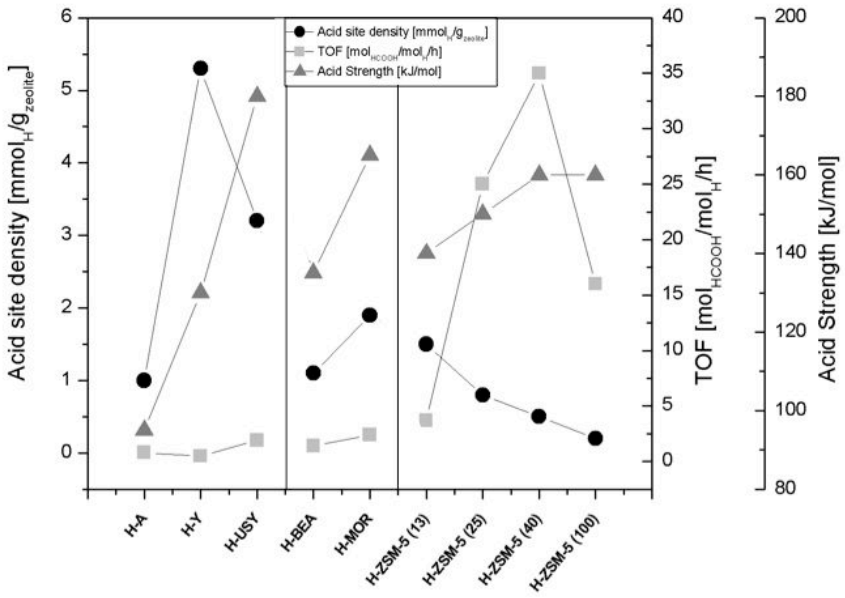

Figure 4-37. Correlation between the zeolite-catalysed formation of CO from HCOOH, expressed in turnover frequency, and the corresponding zeolite acid site density and strength.

This zeolite proved particularly effective because *only 0.2 mmol of solid acid was able to convert 5 mmol of formic acid*. It is thus truly catalytic, which is unprecedented in CO production. In addition, ZSM-5 is readily available and inexpensive, due to its wide use as catalyst in petrochemical and bulk chemical industries. Furthermore, a continuous production of CO could also be achieved with this setup, providing that a continuous addition of formic acid could be performed. Interestingly, the zeolite can be reused at least 10 times without any loss of activity (**Figure 4-38**).

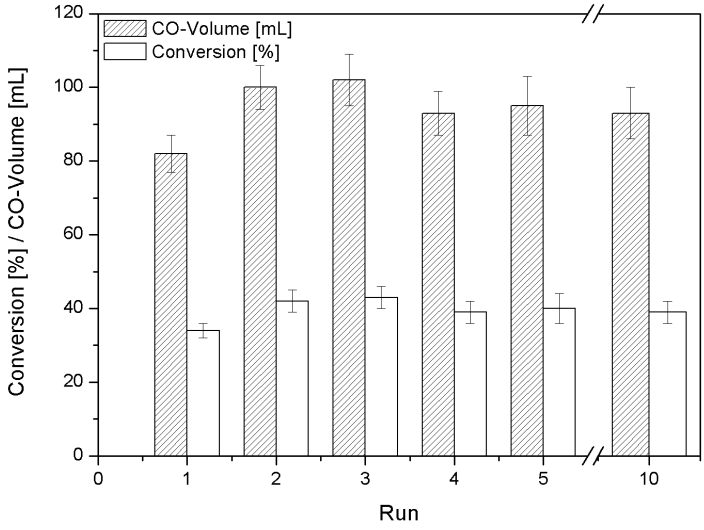

Figure 4-38. Recyclability of the solid acid used (ZSM-5) for the decomposition of HCOOH to CO (error bars represent standard deviation from three experiments).

Although formic acid is not a strong acid, acids are known to be deleterious to silica, alumina and aluminosilicates such as zeolites. Adding formic acid at 150 °C to zeolite could thus alter the zeolite structure. Therefore, the stability of the ZSM-5 framework was examined by looking at the zeolite powder XRD patterns after 5 and 10 runs (**Figure 4-39**). No change could be noticed, confirming the stability of ZSM-5 zeolite under our CO production conditions.

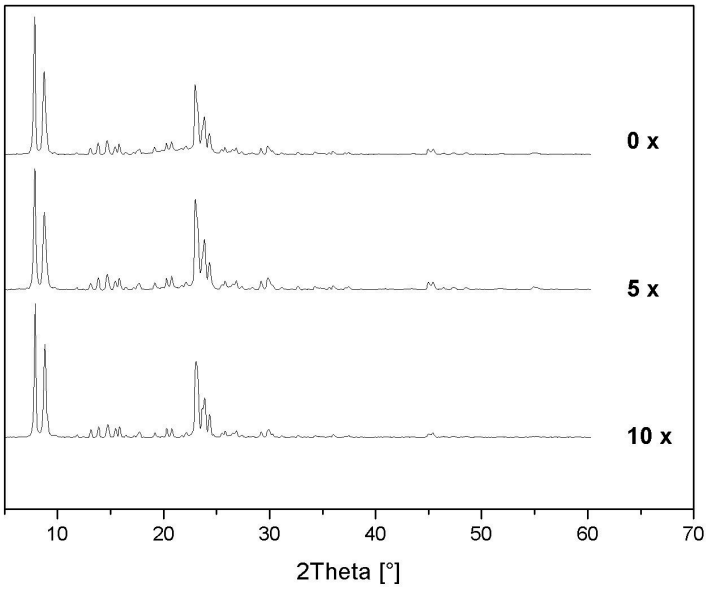

Figure 4-39. XRD-patterns of the ZSM-5 used for the decomposition of HCOOH to CO after 5 and 10 runs.

4.5.3. Palladium catalysed Carbonylation Reactions

Once the safe, controlled and catalytic production of CO was achieved, a two-reactor system was set up, by simply connecting the CO-producing reactor to a flask (**Figure 2-8**, line 2), and representative palladium-catalysed carbonylations were investigated.

We first looked at aminocarbonylation, in which amines are used as nucleophiles toward aryl derivatives in the presence of palladium complex as catalyst under CO (**Figure 4-34**, Nu = NRR'). The reaction of iodobenzene with benzyl amine was used as a model for screening conditions to reach the best catalyst and ligand (**Table 4-16**).

Depending on their nature, ligands are known to strongly influence reaction rates and selectivity. Tetrakis(triphenylphosphine) palladium was first selected as catalyst because it has been successfully applied in carbonylation reactions since 1976.[331] In warm THF, 4 hours were required to reach a full conversion with this catalyst (**Table 4-16**, entry 1). Despite the decoordination of the PPh_3 ligands in solution, the coordinatively saturated nature of this catalyst might be responsible for a slow CO coordination and the decrease of the catalytic rate. We thus

[331] Cassar, L.; Foa, M.; Gardano, A. *J. Organomet. Chem.* **1976**, *121*, C55.

turned to PdL_2 complexes formed *in situ*. The simplest complex obtained by adding two equivalents of triphenylphosphine to $PdCl_2$ indeed was more rapid in fully converting iodobenzene within 3 hours (entry 2).

Table 4-16. The model carbonylation reaction used to set up conditions with our two-reactor system.

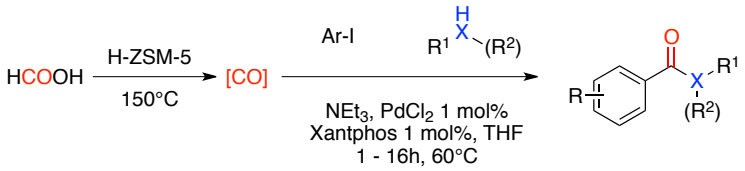

Entry	Pd- source (mol%)	Ligand (mol%)	bite angle (°)[b]	Time (h)	Conversion (%)[c,d]
1	$Pd(PPh_3)_4$ (10)	-	-	4	100
2	$PdCl_2$ (10)	PPh_3(20)	-	3	100
3	$PdCl_2$ (10)	dppm (10)	72	5	20[e]
4	$PdCl_2$ (10)	dppp (10)	91	5	50[e]
5	$PdCl_2$ (10)	dppf (10)	99	5	100
6	$PdCl_2$ (10)	Xantphos (10)	111	1	100
7	$PdCl_2$ (5)	Xantphos (5)	"	1	100
8	$PdCl_2$ (1)	Xantphos (1)	"	1	100 (92)
9	$PdCl_2$ (1)	Xantphos (1)	"	1	8[f]
10	$PdCl_2$ (1)	Xantphos (1)	"	1	3[g]
7	$PdCl_2$ (5)	Xantphos (5)	"	1	100
8	$PdCl_2$ (1)	Xantphos (1)	"	1	100 (92)

[a] Conditions: 1 mmol iodobenzene, 2 mmol benzylamine, 2 mmol NEt_3 in THF (3 mL) at 60 °C starting from 10 mmol formic acid injected over 15 min to 300 mg H-ZSM5(25) at 150°C; [b] taken from [24] ; [c] determined by HPLC; [d] isolated yield in brackets, HPLC monitoring showed the sole formation of the product, yields were thus quantitative at complete conversion; [e] the starting materials were recovered; [f] starting from 5 mmol formic acid; [g] starting from 2 mmol formic acid.

Bidendate ligands were also examined because they are often superior to monodentate ligands due to their greater ability to prevent catalyst poisoning via multiple CO ligation. In our conditions, bidentate ligands indeed favored the carbonylation rate but, interestingly, only when the bidentate ligand exhibits a large bite angle (entries 3-6). [332] Among those examined, Xantphos proved to be the best ligand, probably due to its specific flexibility and the isomerization it could promote upon oxidative addition.[333] The use of this ligand allowed a decrease of the catalyst-ligand loading down to 1 mol% without alteration in reaction rate and conversion (entries 6-8). However, decreasing the amount of formic acid used to generate CO proved harmful, since CO was clearly produced too slowly under such conditions (entries 9-10). The same effect was observed upon decreasing the temperature of the CO formation (**Table 4-15**, entries 15-16).

[332] van Leeuwen, P. W.; Kamer, P. C.; Reek, J. N.; Dierkes, P. *Chem. Rev.* **2000**, *100*, 2741–70.
[333] Martinelli, J.R.; Watson, D.A.; Freckmann, D.M.M.; Barder, T.E.; Buchwald, S.L. *J. Org. Chem.* **2008**, *73*, 7102.

Table 4-17. Scope of the aminocarbonylation using zeolite-catalysed two reactor system.[a]

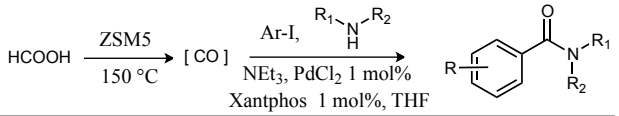

Entry	Amine	ArI	Product	Time (h)	Yield[b] (%)
1	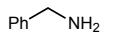	PhI	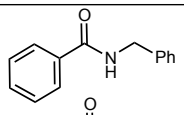	1	92
2	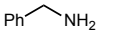	4-MeOPhI	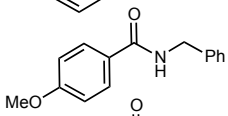	2	95
3	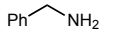	2-MeOPhI	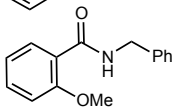	5	88
4	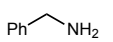	2-MePhI	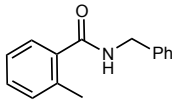	2	97
5	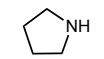	PhI	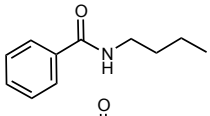	1	85
6		PhI	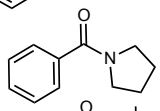	1	80
7	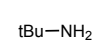	PhI	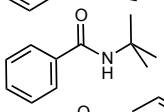	16	56
8	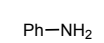	PhI	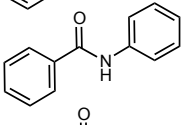	16	76
9	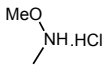	PhI	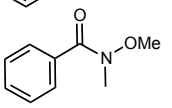	16	59

a: Reaction conditions; 1 mol% $PdCl_2$, 1 mol% Xantphos, 1 mmol ArI, 2 mmol amine, 2 mmol NEt_3 in THF (3 mL) at 60 °C;
b: isolated pure product.

These optimised conditions were then applied to various amines to evaluate the scope of aminocarbonylation in combination with our CO-releasing two-reactor system (**Table 4-17**). Under these conditions, benzyl amine reacted with variously substituted phenyl iodides, giving the corresponding benzamides in very high to almost quantitative yields (entries 1-4). Nevertheless, hindrance at the ortho position could influence reaction rate and yield, but only when a coordinating group is located at that position (entry 3 vs 4). In such cases, the reaction proceeded at a slower rate and led to slightly lower yields (entry 3 vs 2). Like benzyl amines, alkyl amines were quite reactive and were fully converted to the corresponding amides within one hour (entries 5-6 vs 1); however, primary amines gave slightly better results than secondary ones (entry 5 vs 6). Not so surprisingly, bulky amines required longer reaction times and led to lower yields of the corresponding amides (entry 7 vs 5-6). As expected, less nucleophilic amines, such

as aniline, also required prolonged reaction times, but the corresponding benzamide was isolated in reasonable yield (entry 8 vs 5 vs 1). A similar trend was observed starting with *N*-methoxymethanamine under these conditions, to provide a rapid access to the Weinreb amide (entry 9).

Table 4-18. Scope of alkoxycarbonylations using zeolite-catalysed two reactor system.[a]

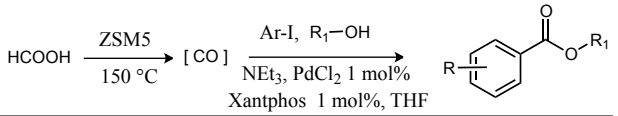

Entry	Alcohol	ArI	Product	Temp. (°C)	Time (h)	Yield[b] (%)
1	MeOH	PhI	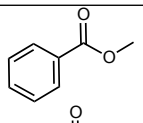	65	2	85
2	*n*BuOH	PhI	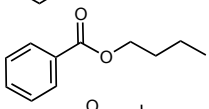	80	16	53
3	*i*PrOH	PhI	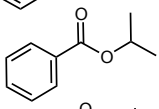	80	16	55
4	*t*BuOH	PhI	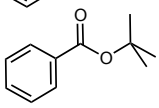	80	16	<10
5		PhI	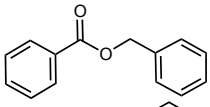	80	16	90
6	PhOH	PhI	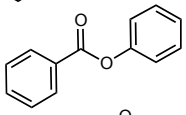	80	16	90
7[c]	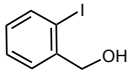		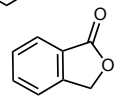	80	4	97

a: Reaction conditions; 1 mol% $PdCl_2$, 1 mol% Xantphos, 1 mmol ArI, 2 mmol NEt_3 in alcohol (3 mL);
b: Isolated pure product;
c: The reaction was performed in toluene.

The second representative palladium-catalysed carbonylation we investigated was the alkoxy-carbonylation (**Table 4-18**), with phenyl iodide as a model. Under the conditions employed for amines (1 mol% $PdCl_2$-Xantphos), the latter cleanly and rapidly reacted with methanol providing the expected methyl benzoate in high yield (entry 1). In contrast, larger aliphatic alcohols, even primary ones, proved less efficient and despite longer reaction times and slightly higher reaction temperatures, moderate yields were obtained (entries 2-3 vs 1). As expected, a tertiary alcohol was even less reactive, giving the corresponding ester only in low yield (entry 4).

The reaction with benzyl alcohol was also slower than the corresponding reaction with benzyl amine (see **Table 4-17**, entry 1 vs **Table 4-18**, entry 5), as expected for a reagent that is

less nucleophilic than amines. The benzyl benzoate ester was nevertheless isolated in high yield. Interestingly, phenol was nucleophilic enough to react under these conditions, leading to phenyl benzoate in high yield (entry 6).

Intramolecular reactions were briefly examined, expecting more facile reaction due to the presence of adjacent hydroxyl group in the acyl palladium intermediate produced upon oxidative addition and carbonylation. Indeed, *ortho*-substituted hydroxymethyl phenyl iodide was rapidly and very efficiently converted under the optimised carbonylation conditions, providing almost quantitatively the corresponding lactone within 4 hours (entry 7).

4.5.4. Impact and Outlook

In summary, we have demonstrated here that the combination of a zeolite-catalysed Morgan reaction and a palladium-catalysed carbonylation reaction provided a novel, safe, mild and efficient way to introduce CO into molecules. The two-reactor system described here can easily be made and handled, allowing the production of carbon monoxide from formic acid and a catalytic amount (1-2 mol%) of heterogeneous and recyclable acidic zeolite, without using an autoclave, specialized safety equipment or specific glassware, like in the Skrydstrup CO-gen system,[323] or in the tube-in-tube flow system.[325] from Fukayama and Skrydstrup. Furthermore, the present system is very practical and inexpensive. Indeed, our CO-reactor system was able to produce 1mmol of gaseous CO for 0.003 € compared to 4.7 € for the now commercially available CO-gen, i.e., more than 1500 times less expensive.[334] Interestingly, Supronowicz *et al.* performed a similar study as ours on the heterogneeous Morgan reaction catalysed by zeolites and published in parallel. [140] They found the same optimum reaction conditions: medium acidic H-ZSM-5 and reaction temperatures from 150 - 200°C without any production of CO_2 (followed by GC-TCD), but their study was more of a fundamental nature since they did not apply their CO in anything useful.

This effectiveness of this method was demonstrated for the direct synthesis of benzamides and various esters from the corresponding aryl iodides by palladium-catalysed carbonylation at atmospheric pressure and with only 1 mol% of catalyst. Furthermore, preliminary results showed that carbonylative Sonogashira and Suzuki-type reactions could also be performed under similar conditions.

In the general frame of this chapter, it is important to mention that the cost efficiency of our process and the controlled release of CO, which is in relation to the injected volume of

[334] Estimated with the following costs: 100 g(zeolite): 70 €, glassware of approx 30 €, COware; 225 € (20 mL flask) or 722 € (100 mL flask); HCOOH: 41 €/L producing 13255 mmol of gaseous CO; chloride producing 103 mmol of gaseous CO. CO-gen: 484 €/25g of 9-methylfluorene-9-carbonyl chloride producing 103 mmol of gaseous CO.

HCOOH may render the commonly avoided, but highly valorising carbonylative coupling reactions a useful tool in organic chemistry.

4.6. Conclusion

In this section various topics have been treated; from the successful synthesis of pure ZSM-5 zeolite from South African coal fly ash, up to the controlled release of CO thanks to the zeolite catalysed dehydration of formic acid and its use in palladium catalysed coupling reactions, via the application and attempt of understanding of *in situ* evolved biosourced secondary templates (BSST's) inducing a controlled mesoporosity and a high aluminum incorporation during ZSM-5 synthesis, and lastly the setting up of a continuous flow zeolite H-*BEA catalysed halogenation reaction of aromatics.

These somehow divergent subjects are cohering through their connection to green chemistry. Furthermore, their link is strengthened by the concept of incremental addition of complexity and value from starting to finite materials, either at the molecular level or in a more passive way by replicating biosourced complexity into inorganic, solid, heterogeneous catalysts. This concept was previously christened as *carbon upgrading*,[335] a broader approach to a global problem.

The future impact of these areas of study is exciting, but as uncertain as the weather of next week in Edinburgh, Scotland. Concerning the economically viable valorisation of South African fly ashes, the company Zeolite Australia[336] was recently quite interested in discussing how it might be possible to valorise extracted alumina for the local aluminum industry. Unfortunately, the intial motivation faded. A similar scenario occurred with the zeolite catalysed halogenation story: as for the scale up collaboration with SATT Connectus and BASF for the outstanding MTP-catalyst, (cf. Section **3.7.**) a scale up project has been submitted and positively evaluated, until its rejection at the last decisive meeting.

Even though no direct industrial collaboration arose from any of the herein presented subjects it will be the future conjunction of policies and economy, which will decide on whether rather the one or the other solution, among the realm of possible alternatives to the *status quo* will be chosen. Henceforth, the above reported diverse subjects constitute distinct parts of this vast ocean of alternatives.

[335] To the best of my knowledge, the herein used term *carbon upgrading* has been used only once as a lucky, unconscient combination in a recent landmark study on the use of macroalgae for the sustainable production of liquid fuels by A. Cole et al. *Energy Environ. Sci.,* **2016**, 9, 1828.
[336] http://www.zeolite.com.au

General Conclusion and Future Prospects

During this Thesis different aspects of heterogeneous catalysis could be approached. Zeolites were synthesised, characterised and applied to various catalytic reactions, from industrial aspects to organic chemistry. The *leitmotif* of this work hence clearly was zeolites. These cheap rationally conceivable aluminosiliceous catalysts could be applied to different Brønsted acid catalysed reactions, even in relatively drastic conditions, thanks to their high hydrothermal stability. An incomparable advantage to use zeolites in heterogeneous catalysis is their shape selectivity, a consequence of their non-flat microporous space of molecular dimensions.

After an introducing **Chapter 1** in which an overview of important concepts was given, either well known to the respective scientific community, or more global concepts, **Chapter 2** exposed the different materials and methods used in this work to obtain the reported results. These two chapters could not possibly be complete, but are detailed enough to enable a proper understanding of the results produced during this PhD that are summarised in the two later chapters.

Chapter 3 disclosed that an industrially competitive catalyst for the methanol to olefins process could be designed by an iterative feedback-looped approach. Indeed, an H-ZSM-5 zeolitic material with large crystallite sizes (50 x 15 x 10 µm) a very disperse acid site density and a high crystalline quality was synthesised in fluoride medium. These catalysts demonstrated a high activity, stability as well as selectivity towards light olefins in the Methanol-To-Olefins (MTO) reaction. By properly controlling the synthesis parameters, ZSM-5 zeolite single crystals exempted from the usually ubiquitous structural defects were obtained. After a thorough characterisation by SEM, HRTEM, CO-FTIR, ^{27}Al and ^{19}F MAS-NMR, Rietveld structure refinement, BET and PFG-NMR techniques, we described its application and proposed a subsequent rationalisation of these ZSM-5F zeolites serving as outstanding MTP (Methanol-To-Propylene) catalysts.

Interestingly, the perfect large crystals (H-ZSM-5FL) behaved in a counter-intuitive manner in catalysis, being very selective towards propylene, very active and the most stable tested catalyst. Exempted from surface defects and exhibiting a perfectly homogeneous acid site distribution, ZSM-5FL catalyst can be used as a model catalyst. Indeed, in the second part of this study, this defect-free zeolite allowed to decipher the importance of diffusion phenomena during MTP catalysis, governing the high propylene selectivity. Lastly, a mathematical-statistical model using Maxwell-Boltzmann diffusion equations was proposed explaining and supporting experimental results.

Thorough investigations of the synthesis of such perfect ZSM-5 zeolites led us to demonstrate an effect of the autoclave and synthesis volume on the quality and size of the resulting crystals, which was tentatively linked to varying nuclei-concentration gradients wether small or large volumes were used.

The future prospect of this project is promising.[188] We currently try to adapt our optimal MTP-catalyst's synthesis to large scale, and initial results have already been obtained concerning the substitution of HF during the synthesis. Furthermore, considering our surprising results such syntheses should avoid the use of large autoclaves in the scale-up process. Downsizing in order to scale-up seems counterintuitive indeed, but this differential approach might allow an eventual transposition of large batch conditions to small multi-vial quasi-continuous conditions.

Chapter 4 related different zeolite related themes in the general frame of *carbon upgrading*, whereby an incremental increase in complexity, either molecular or zeolitic became the central theme.

The overarching concept of *carbon upgrading*, clearly unmagnifies the impact of each of the herein treated topics. Nonetheless, their link is strengthened by this concept of incremental addition of complexity and value from starting to finite materials.

The successful synthesis of pure ZSM-5 zeolite from South African coal fly ash was one part of this chapter. The extraction of alumina from South African fly ash in order to increase the resulting Si/Al-ratio to 100 and thus render it truly useful for the synthesis of MTO-catalysts, while a high amount of valuable alumina is valorised, remains a subject of substantial, commercial impact. Furthermore, during the discussions with our South African collaborators, the introduction of a *fly ash valorisation factor* seemed to become a necessity, for instance:

$$\mathbf{X_{FA}} = \frac{\sum \mathbf{n(Si,\ Al,\ M\ldots)_{valorised}}}{\sum \mathbf{n(Si,\ Al,\ M\ldots)_{FA}}} * \mathbf{100}\ \%$$

Another part of this work consisted in setting up of a continuous flow zeolite H-*BEA catalysed halogenation reaction of aromatics. It would be interesting to translate the developed knowledge and technology for these halogenation reactions, to various other zeolite catalysed liquid-solid reactions. Indeed, it will be exciting to see an implementation of truly continuous flow processes based on liquid-solid zeolite catalysed reactions.

The controlled release of CO, thanks to the zeolite catalysed dehydration of formic acid could be used in palladium catalysed coupling reactions. This *ex situ* and safe zeolite catalysed release of CO from formic acid might once serve as a tool for the controlled insertion of isotopic labelled molecular functionalities. At the moment of this study, ^{11}C- or ^{13}C-formic acid were either too hard to obtain, or simply too expensive and not economically competitive compared with current techniques. However, the formic acid route remains promising. Since carbon isotopes are efficiently introduced to organic molecules by feeding microorganisms with C-isotopes,

labelled CO_2 is easy to access. It is only a matter of time until a controlled and quick hydrogenation technology to form formic acid from labelled CO_2 will be developed. In this near future, it will be interesting to combine a quick hydrogenation of labelled CO_2 and a subsequent quick dehydration to release $^{11/13}CO$ of high value in coupling reactions.

Lastly, the application and attempt of understanding of *in situ* evolved biosourced secondary templates (BSST's) inducing a controlled mesoporosity and a high aluminum incorporation during ZSM-5 synthesis were treated in this chapter. In this context, it will be worth the effort to try other lignocellulosic biomasses, more local such as soft or hard wood stem or waste paper generally exhibiting a similar composition than Brasilian sugar cane bagasse.[337] Further issues I would have liked to tackle concern the crystal growth mechanism. A thorough analysis of the utterly complex evolving BSST's might be interesting, before, during and after the synthesis. An *in situ* liquid state ^{13}C-NMR shall consitute the characterisation tool of choice, since selectively BSST's signals and its interactions with the respective environment can be observed. As it has been evoked in the related chapter, the T-OR affinity might be intermediate between T-OH < T-OR < T-F. It might therefore be interesting to try a synthesis as reported herein, but to use NaF instead of NaCl to adapt the ionic strength in the synthesis gel. A competition between the different actors can hence be expected and might lead to interesting new crystal morphologies.

It should be worth to follow the same approach developed herein with lipids as BSST's. Indeed, lipids are well-known for their self-assembly properties,[338] the phospholipidic self-assembled bilayer being the most vital of examples. For instance, cardanol lipids[338] are the main component in the cashew nutshell liquid (CNSL) a byproduct of cashewnut processing. The cashewnut market represents a 4.4 $Gt.year^{-1}$ market, thus producing large quantities of CNSL.[339] Those biosourced self assembling molecules can hence constitute a valuable cheap amphiphilic secondary structure directing agent in the quest of introducing mesoporosity in a controlled way into high value added zeolite catalysts.

Ultimately, the following thoughts are meant to highlight the importance of the herein presented results and concepts. According to the Global footprint network,[340] the global overshoot day was reached this year the 8th of August, as compared to the 19th of December in 1987. From this day on, our consumptions are qualified as non-sustainable. From a personal point of view, in my home-country Luxembourg the national overshoot day was already attained the 7th of February 2016. Funnily, if Luxembourgers solely populated the planet, we as a small people

[337] Jorgensen, H.; Kristensen, J. B.; Felby, C. *Biofuels, Bioprod. Bioref.* **2007**, *1*, 119.
[338] a) Silverman, J.R.; Samateh, M.; John, G. *Eur. J. Lipid Sci. Technol.* **2016**, *118*, 47. b) Solomons, T.W.G., Fryhle, C.B., Organic Chemistry, Wiley, New York **2000**.
[339] Major Food and Agricultural Commodities and Produces - Countries by Commodity, Fao.org **2013**.
[340] More information on this NGO founded in 2003 (top 100 best NGO's worldwide in 2012 and 2013) can be found on their official website: http://www.footprintnetwork.org/en/index.php/GFN/

would need nine earth-like planets to sustain our lifestyle. This devastating discrepancy between the way of life in developed countries and the *IDEAL* way of life, for instance a circular carbon-based economy with green chemistry as a core part, is an indication for the long way yet to go and the direction towards which we should set sail.

VII) Communications

Peer reviewed publications

- Losch, P.; Pinar, A.B.; Soukup, K.; Willinger, M.; Chavan, S.; Vincent, B.; Pale P.; Louis, B. *J. Catal.* **2016**, *accepted*. "Perfect ZSM-5 Crystal: Structure-Diffusion-Activity Relationship during MTO-Catalysis?"

- Losch, P.; Kolb, J. F.; Astafan, A.; Daou, T. J.; Pinard, L.; Pale, P.; Louis, B. *Green. Chem*. **2016** 10.1039/c6gc00731g. "Eco-Compatible Zeolite Catalysed Continuous Halogenation of Aromatics."

- Louis, B.; Gomes, E.S.; Coelho, T.; Lutzweiler, G.; Losch, P.; Silva, A.V.; da Costa Faro Jr., A.; Romero, T.; Osman, M.B.; Balanqueux, A.; C. Bernardon, M.M. Pereira, *Nanosci. Nanotech. Lett.* **2016**, *8*, 1. "Influence of biomass residues on the metastability of different zeolite structures."

- Messingue, R.N.M.; Losch, P.; Sedres, G.; Musyoka, N.M.; Fatoba, O.O.; Louis, B.; Pale, P.; Petrik, L.F. *CR Chimie* **2016** *in press*. "Transformation of South African coal fly ash into ZSM-5 zeolite and its application as an MTO catalyst."

- Losch, P.; Boltz, M.; Bernardon, C.; Louis, B.; Palcic, A.; Valtchev, V. *Appl. Catal. A Gen.* **2016**, *509*, 30. "Impact of external surface passivation of nano-ZSM-5 zeolites in the Methanol-To-Olefins reaction."

- Losch, P.; Felten, A.-S.; Pale, P. *Adv. Synth. Catal.* **2015**, *357*, 2931. "Easy, Green and Safe Carbonylation Reactions through Zeolite-catalysed CO Production from Formic Acid."

- Losch, P.; Laugel, G.; Martinez-Espin, J.S.; Chavan, S.; Olsbye, U.; Louis, B. *Top Catal.* **2015**, *58*, 826. "Phosphorous modified ZSM-5 zeolites: Impact on methanol conversion into olefins."

- Louis, B. Carvalho Rocha, C.; Balanqueux, B.; Boltz, M.; Losch, P.; Bernardon, C.; Bénéteau, V.; Pale, P.; Maciel Pereira, M. *L'Actualité Chimique*, **2015,** *393*, 2. "Unraveling the Importance of Zeolite Crystal Morphology."

- Losch, P.; Martinez Pascual, A.; Boltz, M.; Ivanova, S.; Louis, B.; Montilla Ramos, F.; Odriozola, J.A. *CR Chimie* **2015**, *18*, 324. "Ionic liquid immobilization on carbon nanofibers and zeolites: catalyst design for the liquid-phase toluene chlorination."

- Losch, P.; Boltz, M.; Louis, B.; Chavan, S.; Olsbye, U. *CR Chimie* **2015**, *18*, 330. "Catalyst optimisation for enhanced propylene formation in the Methanol-To-Olefins reaction."

- Boltz, M.; Losch, P.; Louis, B.; Rioland, G.; Tzanis, L.; Daou, T. J. *RSC Adv.* **2014**, *4*, 27242. "MFI-type zeolite nanosheets for gas-phase aromatics chlorination: a strategy to overcome mass transfer limitations."

- Losch, P.; Boltz, M.; Soukup, K.; Song, I.-H.; Yun, H. S.; Louis, B. *Microporous Mesoporous Mater.* **2014**, *188*, 99. "Binderless zeolite coatings on macroporous-SiC foams."

- Boltz, M.; Losch, P.; Louis B. *Adv. Chem. Lett.* **2013**, *1*, 1. "A General Overview on the Methanol to Olefins reaction: Recent Catalyst Developments."

Conferences: Presenting Author

- Conference at the International Zeolite Conference (18th IZC) **24.06.2016**, Rio de Janeiro, Brasil
Messingue, R.N.M.; Losch, P.; Sedres, G.; Musyoka, N.M.; Fatoba, O.O.; Louis, B.; Pale, P.; Petrik, L.F. "Conversion of South African coal fly ash into high purity ZSM-5 without an additional source of silica and their application as MTO-catalysts."

- Conference at the 1st Students Winter Workshop Hokkaido/Strasbourg **15.03.2016**, Strasbourg, France
Losch P., Pale P., Louis B. "H-ZSM-5 zeolite in MTO-Catalysis."

- Conference at PACIFICHEM **15.12.2015**, Honolulu, United States of America.
Losch P., Pinar A.B., Louis B. "Big or Small ZSM-5 crystals: Does Size really matter?"

- Conference at Journées scientifiques de l'UMR7177 **15.10.2015**, Strasbourg, France.
Losch P., Pale P., Louis B. "Zéolithes: Acides de Brønsted Hétérogènes en Catalyse."

- Conference at ISAMMM6 **15.09.2015**, Pomorie, Bulgaria.
Losch P., Pinar A.B., Louis B. "ZSM-5 crystals for Catalysis: Does Size really matter?"

- Invited talk at InGAP-laboratory **14.06.2014**, Oslo, Norway.
Losch P., Pale P., Louis B. "Methanol-To-Olefins (MTO) Process with large ZSM-5 Crystals."

- Conference at GECat **14.05.2014**, Cluny, France.
Losch P., Louis B. "Methanol-To-Olefins Process with optimised giant ZSM-5 Crystals."

- Invited talk at the Institute of Chemical Process Fundamentals **13.12.2013**, Prague, Czech Republic.
Losch P., Louis B. "Methanol-To-Olefins (MTO) Process with designed ZSM-5 Zeolites."

Posters

- IZC18, **19-25.06.2016**, Rio de Janeiro, Brasil.
P. Losch, B. Louis. "On the utility of high quality large ZSM-5 crystals."

- FCCat, **23-27.05.2016**, Fréjus, France.
P. Losch, B. Louis. "Large or nano-ZSM-5 crystals: How does size matter?"

- GREN2016, **3-6.04.2016**, Berlin, Germany.
P. Losch, P. Pale, B. Louis. "Rational Conception of zeolites and their application in catalysis."

- GECat2015, **26-29.05.2015**, Obernai, France.
P. Losch, M. Boltz, P. Pale, B. Louis. "Perfect ZSM-5 crystals and their behaviour in the MTO-reaction."

- NSC2014, **14-21.06.2014**, Oslo, Norway.
P. Losch, M. Boltz, P. Pale, U. Olsbye, B. Louis. "Toward perfect ZSM-5 crystals and their behaviour in the MTO-reaction."

Pit LOSCH

Synthesis and Characterisation of Zeolites, their Application in Catalysis and subsequent Rationalisation Methanol-To-Olefins (MTO) Process with designed ZSM-5 Zeolites

Résumé

Cette thèse s'articule autour des zéolithes, plus particulièrement leur synthèse, leur caractérisation et leur application comme catalyseurs hétérogènes. Dans certains cas, la compréhension des phénomènes encontrés au cours de ce processus nécessitait un travail de rationalisation. Ce dernier ingrédient permet une réelle amélioration continue, ou une conception sur mesure d'un catalyseur pour une réaction.

Les zéolithes sont des aluminosilicates, microporeux et crystallins, qui se définissent et se différencient de part leur arrangement 3D de tétraèdres (SiO_4 et AlO_4).

Il a été essayé d'utiliser des zéolithes conçues sur mesures en tant que catalyseurs pour des réactions faisant partie d'une chimie renouvelable. Ainsi, ces travaux s'inscrivent dans le cadre des concepts de la chimie verte et de l'addition graduelle de complexité moléculaire.

Au cours de cette thèse, la boucle itéative de l'amélioration continue a mené à deux reprises à un catalyseur très adapté au processus catalytique en question: d'une part l'halogènation d'aromatiques a été effectuée en phase liquide, il s'agit d'un procédé liquide-solide pour lequel le meilleur catalyseur résulte en une zéolithe béta (H-*BEA) avec une porosité hierarchisée. Au contraire, la réaction de la conversion du méthanol en oléfines (MTO) une réaction gas-solide semble avoir comme catalyseur optimal des zéolithes de type ZSM-5 sans porosité hierarchisée, mais ayant des tailles cristallines élevées, une qualité cristalline proche de la perfection (sans défauts) et une densité de sites acides très disperses.

Mots clés: *Zéolithes, ZSM-5, MTO, Catalyse, Carbon Upgrading.*

Résumé en anglais

This work revolved around the synthesis, characterisation and application of zeolites in heterogeneous catalysis. In some cases, counterintuitive observations and results needed a thorough rationalisation, which allowed a truly continuous improvement, or rational design of a catalyst for a given reaction.

Zeolites are crystalline and microporous aluminosilicates, which are defined and differ one from another through their 3D arrangement of tetrahedra (SiO_4 and AlO_4).

It has been aimed to design heterogeneous catalysts for reactions that fit in the concepts of a sustainable chemistry. Thus, this works describes and tried to respect the concepts of green chemistry and carbon upgrading.

Remarkably, during this thesis the feedback looped continuous improvement approach has led twice to adapted catalysts for a catalytic chemical transformation: the liquid-solid continuous flow halogenation of aromatics was best performed with nanosized H-*BEA zeolites exhibiting a hierarchical porosity. In contrast, the gas-solid Methanol-to-Olefins (MTO) process needed an unusual catalyst. Indeed based on our study, large and perfectly crystalline H-ZSM-5 crystals with a disperse Brønsted acidity were the optimum catalyst.

Keywords: *Zeolites, ZSM-5, MTO, Catalysis, Carbon Upgrading.*